Distribution and Properties of Sodium-Dependent Glial Glutamate Transporters in the Mouse Hippocampus

Inaugural-Dissertation

zur Erlangung des Doktorgrades
der Mathematisch-Naturwissenschaftlichen Fakultät
der Heinrich-Heine-Universität Düsseldorf

vorgelegt von

Alexandra Elisabeth Schreiner, geb. Rduch

aus Kattowitz, Polen

Düsseldorf, November 2012

Aus dem Institut für Neurobiologie

der Heinrich-Heine Universität Düsseldorf

Gedruckt mit der Genehmigung der

Mathematisch-Naturwissenschaftlichen Fakultät der

Heinrich-Heine-Universität Düsseldorf

Referent: Prof. Dr. rer. nat. Christine Rose, Heinrich-Heine-Universität Düsseldorf

Korreferent: Prof. Dr. rer. nat. Dieter Willbold, Heinrich-Heine-Universität Düsseldorf

Tag der mündlichen Prüfung:

„Der Fortgang der wissenschaftlichen Entwicklung ist im Endeffekt eine ständige Flucht vor dem Staunen."

ALBERT EINSTEIN (1879-1955)

Zusammenfassung

Die zentralnervöse Informationsverarbeitung von allen komplexen Lebensformen ist vornehmlich vermittelt durch den wichtigsten erregenden Neurotransmitter, Glutamat. Trotz Glutamats Bedeutung für die Signalübermittlung muss seine übermäßige extrazelluläre Akkumulation verhindert werden um Präzision und hohe Auflösung neuronaler Kommunikation zu ermöglichen. Folglich muss seine Wirkung räumlich und zeitlich begrenzt werden, was durch hoch-affine Transporter (EAAT) bewerkstelligt wird. Von diesen sind die Astrozyten-spezifischen Typen GLAST und GLT-1 die häufigsten und maßgeblichsten für die Glutamat Wiederaufnahme. Die einwärts gerichtete Translokation von Glutamat während eines Transportzyklus wird getrieben durch den Einstrom von Na^+ entlang seines elektrochemischen Gradienten. Folglich ist der Transport entscheidend abhängig von $[Na^+]$ und beeinflusst umgekehrt durch seine Aktivität die Na^+-Signalübertragung und -Homöostase. Störung oder Ausfall der Wiederaufnahme haben daher gravierende Folgen für Signalübertragung und Ionen Homöostase des Gehirns.

Die vorliegende Studie untersucht die Reifung und Beeinträchtigung astrozytärer EAATs während der postnatalen Entwicklung bzw. während Schädigung des Maus Hippokampus. Um das Expressionsprofil von GLAST und GLT-1 darzustellen wurden Immunhistochemie und -blot verwandt. Quantitative Fluoreszenzmessungen mit dem Na^+-sensitiven Farbstoff SBFI lieferten funktionelle Daten durch die Visualisierung von EAAT-induzierten intrazellulären Na^+-Signalen. Unsere Studie konnte zeigen, dass das zeitliche, räumliche und zelluläre Expressionsprofil von GLAST und GLT-1 sich stark unterscheidet, während der postnatalen Phase wie auch nach Schädigung. Hochregulation von GLAST folgt entwicklungsbedingtem und pathologischem GFAP Anstieg, dem primären Intermediärfilament in ausgereiften Astrozyten. GLT-1 hingegen, v.a. die monomere Form, steigt erheblich während der Phase synaptische Reifung an, während seine Expression wesentlich durch Deafferenzierung vermindert wird. Zusätzlich zu der engen Interaktion von GLT-1 mit Synapsen konnten wir auch zum ersten Mal zeigen, dass deutliche GLT-1 Cluster an perivaskulären Strukturen zu finden sind und deren Aktivierung beträchtliche $[Na^+]_i$ Erhöhungen auslöst. Schließlich konnten wir ebenfalls konstatieren, dass Schädigungs-induzierte Dysfunktion der Glutamat Wiederaufnahme bei verschiedenen Teilgruppen von reaktiven Astrozyten nicht uniform ausgeprägt ist.

Zusammengenommen weisen diese Ergebnisse darauf hin, dass GLAST und GLT-1 unabhängigen Regulationsmechanismen unterworfen sind, sowohl während der postnatalen Entwicklung wie auch in Folge schwerer Gehirn Schädigung. Astrozytäre EAATs weisen also Heterogenität bezüglich des Subtypen, die räumliche Verteilung, der Multimer-Zusammensetzung und des Zelltypen in dem sie exprimiert werden. All diese Aspekte sind relevant bei der Prüfung des therapeutischen Potentials von astroglialen EAATs.

Abstract

Information processing in the central nervous system of all complex living organisms is primarily mediated by the major excitatory neurotransmitter, glutamate. While glutamate is fundamental for signal transduction, its excessive extracellular accumulation has to be prevented to assure precision and high resolution of neuronal communication. From this it follows that its action has to be spatially and temporally restricted, which is accomplished by high-affinity transporters (EAAT). Of these, the astrocyte-specific types GLAST and GLT-1 are most abundant and particularly responsible for glutamate re-uptake. During a transport cycle, inward-directed translocation of one glutamate is driven by the influx of Na^+ along its electrochemical gradient. Transport is hence critically dependent on $[Na^+]$, and does, vice versa, influence Na^+ signaling and homeostasis by its activity. Thus, impairment or failure of this removal system thus has a devastating effect on signal transduction and ion homeostasis of the brain.

Present study aims to investigate the establishment and impairment of the astrocytic EAATs during postnatal development and injury, respectively, of the murine hippocampus. To portray the expression profile of GLAST and GLT-1 immunohistochemistry and immunoblotting was employed. Quantitative fluorescence imaging with the Na^+-sensitive dye SBFI provided functional data by visualization of EAAT-evoked intracellular Na^+-signals. Our study revealed that the temporal, spatial and cellular expression profile of GLAST and GLT-1 differs considerably during the postnatal period and following injury. GLAST up-regulation parallels developmental and pathological increase in GFAP, the principle intermediate filament in mature astrocytes. On the contrary, GLT-1, in particular the monomeric form, increases most profoundly during the phase of synapse maturation, while its expression declines significantly upon deafferentiation. Besides the close interaction of GLT-1 with synaptic sites we also showed for the first time that prominent GLT-1 cluster are found at perivascular sites and that activation of those evokes substantial $[Na^+]_i$ elevations. Finally, we also establish that injury-mediated dysfunction of the glutamate re-uptake system is non-uniform among defined subsets of reactive astrocytes.

Taken together, these results indicate that GLAST and GLT-1 are subject to independent regulatory mechanisms, both during postnatal development and following severe brain injury. Astrocytic EAATs thus feature heterogeneity by means of subtype, spatial distribution, multimer composition and the cell type they are expressed in. All these aspects have to be taken under consideration when probing the potential of astroglial EAATs as therapeutic targets.

Table of Content

Introduction and Résumé

"What is the function of glial cells in neural centers? The answer is still not known, and the problem is even more serious because it may remain unsolved for many years to come until physiologists find direct methods to attack it."

SANTIAGO RAMÓN Y CAJAL (1852-1934)

In the past years the neuro-centric view has been challenged by numerous studies which diligently demonstrated the critical participation of astrocytes to brain function (Barres, 2008). Nowadays, astrocytes are thought to represent a specialized cell type with a plethora of complex functions based primary on the close interaction with other cell types of the nervous system. It has been discovered that astrocytes can communicate with neurons and modify the signals they send or receive, thus being fundamentally involved in information processing of the brain. Astrocytes exert the most significant influence on synaptic transmission by taking up released neurotransmitters, in particular glutamate.

In the following paragraphs the questions will be addressed why control of external glutamate levels is crucial for brain function, how glutamate removal is accomplished by astrocytes and which physiological consequences arise from from this process. Understanding the relevance of glutamate re-upake in the mature brain is a prerequisite to approach its establishment during development and its role in disease.

1. Glutamate in the Central Nervous System

The amino acid L-glutamate (Glu) serves as brain metabolite (e.g. as an essential substrate for glutamine synthesis; Needergard et al., 2002) and, particularly of importance, as major excitatory neurotransmitter of the mature central nervous system (CNS; Danbolt, 2001). During the embryonic stages and the first two postnatal weeks, network excitation is mainly generated by γ-aminobutyric acid (GABA), the main inhibitory transmitter in the adult brain. This is due to transiently high intracellular chloride concentrations in the neonatal neurons, which remain elevated until the chloride-extruding system becomes operative, and the subsequent maturation of glutamatergic synapses (Ben-Ari, 2001 & 2002). Just after this period, as the number of functional glutamatergic synapses profoundly increases in the course of late postnatal development, glutamate-mediated transmission becomes the principle source of excitation (Li & Sheng, 2003; Dumas, 2005; Ben-Ari, 2001 & 2002).

For adult animals, microdialysis studies *in vivo* determined extracellular glutamate concentrations, $[Glu]_{ex}$, in the range of 1-4 µM (Lerma et al., 1986; Baker et al., 2002; Nyitrai et al., 2006). These values were questioned by a more recent electrophysiological study employing acute hippocampal slices. From this experimental data, a $[Glu]_{ex}$ of 25 nM was calculated, thus a 100-fold smaller value (Herman & Jahr, 2007). Although determined *in situ*, this smaller ambient glutamate concentration seems to be physiologically more reasonable, because a $[Glu]_{ex}$ in the millimolar range would lead to tonic activation of NMDARs (*N*-Methyl-D-aspartic acid receptor), desensitivation of AMPARs (α-amino-3-hydroxy-5-methyl-4-isoxazolepropionic acid receptor) and would argue against the well-established idea of high-affinity glutamate uptake (Danbolt, 2001; Tzingounis & Wadiche, 2007; Eulenburg & Gomeza, 2010). Locally, the extracellular glutamate concentration can even reach peak amplitudes of about 170 µM and of even 1 mM in the synaptic cleft of immature and functional glutamatergic synapses, respectively, following synaptic activation (Clements et al., 1992; Choi et al., 2000).

Under pathophysiological conditions global glutamate levels are elevated in the extracellular space (e.g. up to 30-fold in the epileptogenic brain; Cavus et al., 2005), either caused by excessive glutamate release, impaired transmitter uptake or both (Abele, et al., 1990; Rothstein et al., 1996; Schousboe & Waagepetersen, 2005). The resulting overstimulation of glutamate receptors by its agonist then leads to an increase in intracellular calcium concentration ($[Ca^{2+}]_i$) that can induce cell damage or trigger even apoptotic cascades, a process called excitotoxicity (Ankarcrona et al., 1995; Lau & Tymianski, 2010). Hence, tight control of the ambient glutamate levels is crucial for proper information transfer in the central nervous system.

2. The Glutamatergic Synapse

Glutamatergic transmission is of particular importance in the hippocampus, the brain structure considered to consolidate information from short-term memory to long-term memory and to process spatial positioning (e.g. Eichenbaum, 2000). The hippocampus, comprising the hippocampus proper and the dentate gyrus (DG), is situated, bilateral symmetric, in the medial temporal lobe of each brain hemisphere (Fig. 1A; for detailed anatomical review see Van Strien, 2009). Based on the principle synaptic connections, the hippocampus, together with the subicular complex (SUB) and the entorhinal cortex (EC), composes the hippocampal formation.

The cell bodies of the principle excitatory neurons are organized in two distinct layers, the *stratum pyramidale* (StrP) of the *cornu ammonis* (CA) and the *stratum granulosum* (StrG) of the dentate gyrus. Thereby, based on their stereotypical morphology, two types of glutamatergic neurons can be distinguished. Pyramidal neurons, characterized by a pyramidal-shaped soma and two distinct dendritic trees, are localized in the CA region, which is subdivided into CA1-4 (Fig. 1C;

Spruston et al., 2008). The shorter basal dendrite is found in the *stratum oriens* (StrO), while the apical dendrite spans the *strata radiatum* (StrR) and *lacunosum-moleculare* (StrLM). The dentate granule cells, in contrast, can be found in the *stratum granulosum* and identified by their small
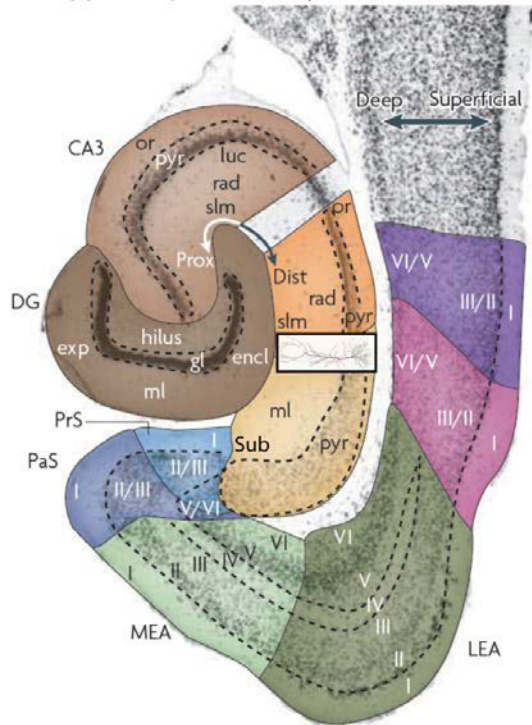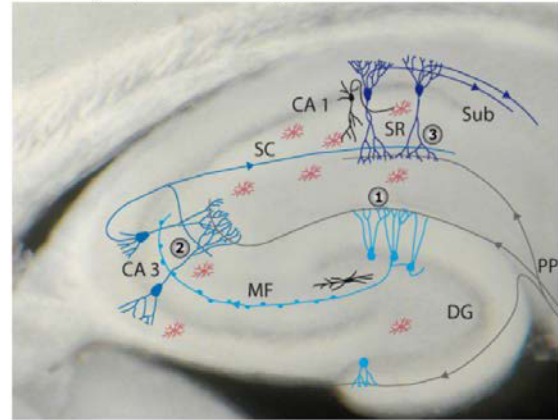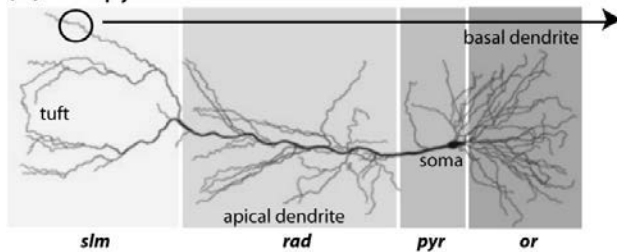
Fig. 1. Glutamatergic synapses in the hippocampus. (A) The hippocampal formation consists of the entorhinal cortex (MEA and LEA), the subicular complex (PaS, PrS and S) and the hippocampus. **(B)** Neuronal excitation in the hippocampus is glutamatergic, organized as so-called tri-synaptic circuitry. **(C)** A typical CA1 pyramidal cell extends an apical, elongated dendrite, directed towards the strata radiatum and lacunosum-moleculare. The short dendrite is situated in the stratum oriens. Axons from CA3 pyramidal cells, termed Schaffer collaterals, project onto CA1 pyramidal neurons via classical glutamate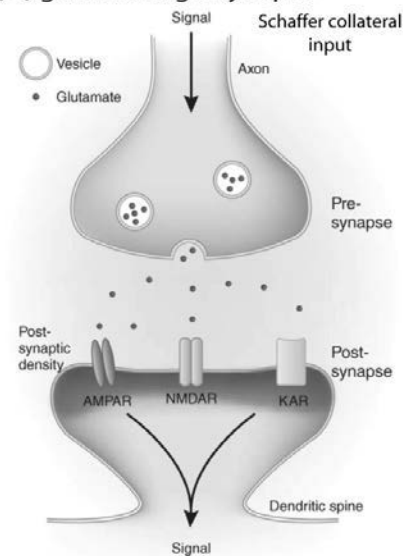rgic transmission as presented in **(D).** Activation of a CA1 pyramidal cell leads to glutamate release via exocytosis at presynaptic sides and subsequent to postsynaptic activation of glutamatergic receptors. *For a more detailed description the reader is kindly referred to the text.*

(A) & **(C)** The Roman numerals indicate cortical layers. *CA*, cornu ammonis; *DG*, dentate gyrus; *exp*, exposed DG blade; *encl*, enclosed DG blade; *ml*, *stratum moleculare*; *gl*, *stratum granulosum*; *ml*, *stratum moleculare*; *slm*, *stratum lacunosum-moleculare*; *rad*, *stratum radiatum*; *luc*, *stratum lucidum*; *pyr*, *stratum pyramidale*; *or*, *stratum oriens*; *PaS*, para-subiculum; *PrS*, pre-subiculum; *Sub*, subiculum; *MEA*, medial entorhinal cortex; *LEA*, lateral entorhinal cortex; *Prox*, proximal; *Dist*, distal; **(B)** *MF*, mossy fibers; *PP*, perforant path; *SC*, Schaffer collaterals; *SR*, *stratum radiatum*; **(D)** *AMPAR*, α-amino-3-hydroxy-5-methyl-4-isoxazolepropionic acid receptor; *NMDAR*, N-methyl-D-aspartate receptor; *KAR*, kainate receptor.

(A) *modified from Van Strien, 2009;* **(B)** *courtesy of Silke Honsek;* **(C)** *modified from Spruston et al., 2008;* **(D)** *from Gécz, 2010*

elliptical soma and their cone-shaped tree of apical dendrites directed towards the *stratum moleculare* (StrM; Amaral et al., 2007).

The hippocampus receives and integrates neuronal input via the trisynaptic circuitry, as described in the following (see e.g. Neves et al., 2008). Initially, axons from the entorhinal cortex project onto dentate granule cells via the perforant path. The axons of these granule cells, in turn, contact pyramidal cells in the CA3 region. Finally, Schaffer collaterals, these are the axons of CA3 pyramidal neurons, form synaptic contacts with the apical dendrites of CA1 pyramidal neurons, whose axons project back to the entorhinal cortex. The synaptic transmission between these different cell types in this tri-synaptic loop is solely glutamatergic (Fig. 1B).

A functional glutamatergic synapse is composed of a presynaptic axonal site where glutamate is released via exocytosis and a postsynaptic terminal equipped with ionotropic and metabotropic glutamate receptors (iGluR and mGluR, respectively), both separated by the synaptic cleft (see Fig. 1D). Briefly, action potential propagation results in calcium influx at the presynaptic site leading to membrane-fusion and release of glutamate-filled vesicles. Released glutamate is then bound postsynaptically by AMPARs or NMDARs, causing neuronal downstream activation (Meldrum, 2000; Lisman et al., 2007).

Upon its release into the extracellular space, glutamate is furthermore efficiently removed by high-affinity, Na^+-dependent glutamate transporters, which are located at neuronal and glial plasma membranes (Danbolt et al., 2001). This rapid uptake mechanism is essential to re-establish low basal $[Glu]_{ex}$, since glutamate is not enzymatically degraded in the synaptic cleft. Missing or insufficient glutamate clearance would otherwise result in extra-synaptic spillover due to neurotransmitter diffusion and tonic overstimulation of glutamate receptors (Voutsinos-Porche et al., 2003; Matsugami et al., 2006).

As neurons are incapable of *de novo* synthesis of glutamate from glucose due to the lack of pyruvate carboxylase and as neuronal re-uptake of glutamate is negligible, glutamatergic neurotransmission also ultimately requires a mechanism that replenishes the pool of releasable glutamate at synaptic terminals (Schousboe et al., 1997). Based on a widely accepted concept, this problem is approached by action of astrocytes. These provide adequate substrate to replenish neuronal glutamate by a cellular compartmentalized sequence of events termed glutamate-glutamine cycle (Daikhin & Yudkoff, 2000; Hertz & Zielke, 2004). In brief, astrocytes take up ambient glutamate by aforementioned glutamate transporters, convert it into non-excitable glutamine via glutamine synthetase (GS) and re-deliver glutamine to neurons, where it can be metabolized into glutamate. Glutamine production by astrocytes, which serves not only glutamate but also GABA

synthesis, is inevitably linked to the ammonia homeostasis: each glutamate or GABA cycled brings about the production of one ammonia molecule by GS (Daikhin & Yudkoff, 2000; Bak et al., 2006).

Glutamate transporter-mediated uptake into astrocytes not only maximizes the synaptic signal-to-noise ratio and prevents excitotoxic injury upon postsynaptic receptor binding, but also provides, as initial step of the glutamate-glutamine cycle, sufficient substrate supply for neuronal glutamate and GABA synthesis. Failure of glutamate removal by astrocytic transporters has therefore tremendous consequences for proper brain function, leading to impaired synaptic function and in some severe cases even to neuronal death due to glutamates´ neurotoxic properties (Camacho & Massieu, 2006).
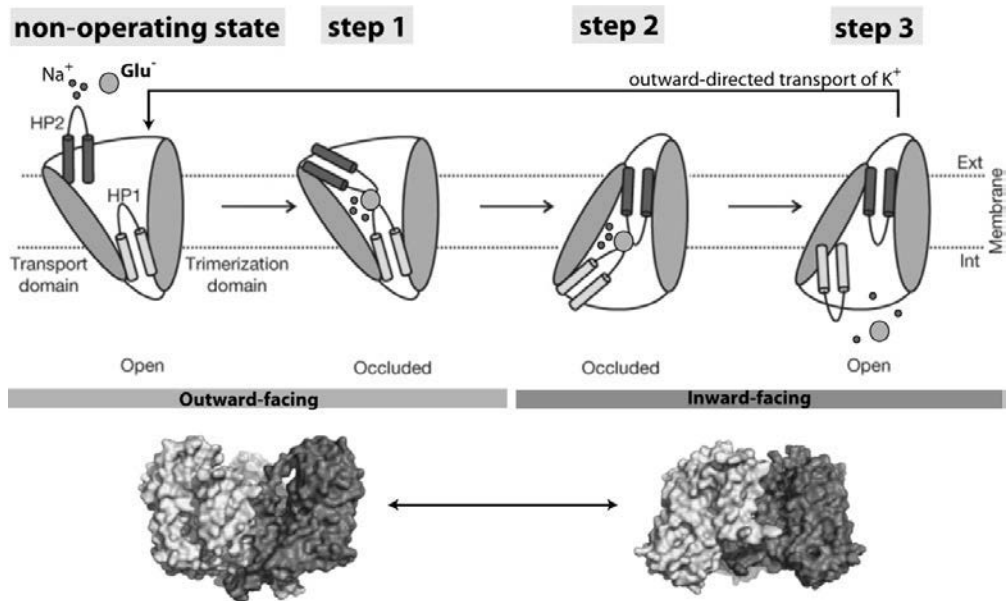
3. Glutamate Transporter

Glutamate transporters, also known as EAATs (excitatory amino-acid transporters), belong to the group of secondary active transporters (SLC; solute carrier family). Five glutamate transporter were identified: GLAST (glutamate-aspartate transporter; rodent homologue of EAAT1), GLT-1 (glutamate transporter 1; rodent homologue of EAAT2), EAAC1 (excitatory amino-acid carrier 1; rodent homologue of EAAT3), EAAT4 and EAAT5 (Storck et al., 1992; Pines et al., 1992; Kanai & Hediger, 1992; Arriza et al., 1994; Fairman et al., 1995). The removal of glutamate from the extracellular space is primarily accomplished by the action of the astrocyte glutamate transporters GLAST and GLT-1 (Rothstein et al., 1996; Matsugami et al., 2006).

Among them GLT-1 (EAAT2) is the most abundant and predominantly expressed transporter in the fully-developed forebrain (Tanaka et al., 1997; Furuta et al., 1997). Glial glutamate uptake leads to a fast decline in the extracellular glutamate concentration, shapes the time course of synaptic conductance, contributes to the input specificity of glutamatergic synapses, and prevents excitotoxicity (Danbolt, 2001; Anderson & Swanson, 2000; Tzingounis & Wadiche, 2007). The uptake has therefore the effect of re-establishing and maintaining low ambient glutamate levels in phases after neuronal activity to assure an appropriate signal-to-noise ratio and also to modulate time course and specificity of synaptic information processing during neuronal activity (Anderson & Swanson, 2000; Tzingounis & Wadiche, 2007).

Protein structure studies along with theoretical considerations lead to the development of a multi-step transport model that will be described in the following (Seal & Amara, 1998; Grunewald & Kanner, 2000; Yernool et al., 2004; Reyes et al., 2009). Glutamate uptake is a secondary-active process harnessing the electrochemical gradient of sodium, which is maintained by the Na^+/K^+-ATPase, to energize the transport cycle. Substrate binding is likewise sodium-dependent (Boudker et al., 2007), which implies that the driving force of the transporter is highly sensitive to fluctuations in adenosine triphosphate (ATP) levels and changes in the sodium concentration (Madl & Burgesser, 1993; Longuemare et al., 1999). In its non-operative state the transporter orientation is directed

(A) model of the transport cycle

non-operating state **step 1** **step 2** **step 3**

Na⁺ Glu⁻

outward-directed transport of K⁺

HP2

HP1

Ext

Membrane

Int

Transport domain   Trimerization domain

Open   Occluded   Occluded   Open

Outward-facing   **Inward-facing**

(B) stoichiometry

Cl⁻

Glu⁻ H⁺ 3Na⁺

K⁺

Cl⁻

Ext

Int

(C) topology model of GLT-1

linker   Ext

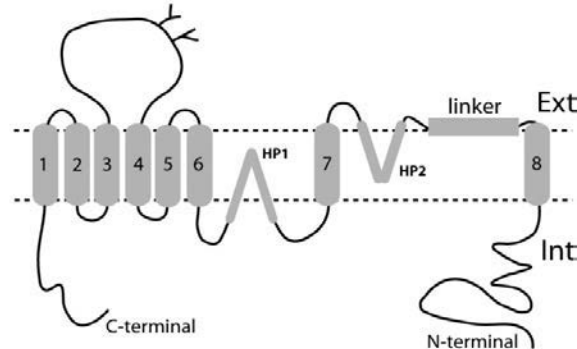1 2 3 4 5 6   HP1   7   HP2   8

Int

C-terminal

N-terminal
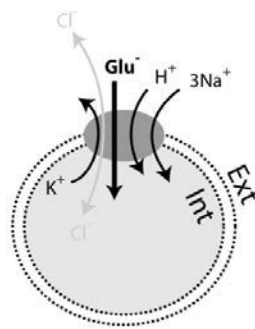
Fig. 2. Astrocytic glutamate transporters. (A) Binding of sodium and glutamate leads to the structural shift of EAATs from outward-facing to inward-facing conformation. The re-establishing of the initial, non-operating state necessitates potassium binding. The translocation of the glutamate binding site across the membrane is accomplished by the operation of two molecular gates (HP2 and HP1, respectively). **(B)** During one complete transport cycle of EAATs 1 glutamate (Glu⁻), 3 Na⁺ and 1 H⁺ enter the cell, while 1 K⁺ is exported. **(C)** GLT-1 possesses eight transmembrane α-helices (1-8), two hairpin loops (HP1 and HP2) and a linker domain. Both, C- and N-terminal are inward-facing. *For a detailed description see text.*

(B) & **(C)** *Ext*, extracellular; *Int*, intracellular;

(A) *top: scheme modified from Reyes et al., 2009; bottom: surface representation taken from Jiang & Amara, 2011*

towards the extracellular space with accessible binding sites for Na⁺ and glutamate, in consequence of the open state of the extracellular gate (HP2; for a transporter topology see Fig. 2C). Both, binding of Na⁺ and glutamate, initiate the change from outward facing to inward facing conformation as first step of the transport cycle (Fig. 2A; step 1 to 2). It is thought that this conformational transformation is coupled to the closure of the extracellular gate (HP2) in addition to the primarily closed intracellular gate (HP1; Reyes et al, 2009; cf. Fig. 2A; non-operative state and step 1). Once transported Na⁺ ions and the substrate have unbound in the inward-facing orientation, the intracellular gate (HP1) opens and the K⁺ binding site becomes accessible. Intracellular K⁺ occupying its binding site then allows re-location of the glutamate transporter to the outside (Fig. 2A; step 3). K⁺

un-binding in the outward-facing orientation finally re-establishes the initial state of the glutamate transporter. Although it is also established that glutamate inward-transport is coupled to net-influx of one proton, it still remains a matter of debate where and at which time point H^+ binds and un-binds in the sequence of substrate binding, translocation and terminal relocation (Anderson & Swanson, 2000; Grewer & Rauen, 2005; Tzingounis & Wadiche, 2007).

Genetic studies showed that substitution of one amino acid (glutamate > glutamine; position 373) in the putative protonation site of the neuronal glutamate transporter EAAC1 does not hinder glutamate translocation but renders the mutant transporter insensitive to changes in extracellular pH (Pines et al., 1995; Grewer et al., 2003). This indicates that H^+ binding might facilitate glutamate uptake, particularly at sites of synaptic release. Finally, several reports demonstrated that the substrate binding to the glutamate transporter is associated, bu not thermodynamically-coupled, with an anion flux (Wadiche et al., 1995; Melzer et al., 2003; Grewer & Rauen, 2005). The observed Cl^--current is however only significant for the neuronal glutamate transporters (EAAT3-5), considered to play a role in the control of neuronal excitability.

Briefly summarized, a complete transport cycle comprises the movement of 1 Glu^-, 3 Na^+ and 1 H^+ into the cell, along with 1 counter-transported K^+. Hence, according its stoichiometry, glutamate transport is electrogenic (Anderson & Swanson, 2000; Danbolt, 2001): two net positive charges are moved into the cell for each completed transport cycle (Fig. 2B).

The efficiency of glutamate uptake is defined by a multitude of regulatory mechanisms which will be described in the following. These allow rapid adaptation to changed environmental conditions as they for instance occur during development or injury.

Studies in the last years indicated that multiple regulatory mechanisms can change glutamate transporter dynamics either on a short- or on a long-term scale. First of all, on transcriptional level, up-regulation of mRNA levels can be accomplished by de-methylation of DNA, which can for instance be induced by neuronal stimulation (Yang et al, 2010). Translational regulation, i.e. control of protein levels synthetized from its mRNA, was shown for GLT-1 *in vitro* and *in vivo* (Tian et al., 2007). Among the substances tested, glutamate inhibited translation, whereas β-lactam antibiotics (e.g. penicillin) stimulated translation of GLT-1 transcript, which reinforced and advanced earlier findings reporting downstream up-regulation of GLT-1 protein levels (Rothstein et al., 2005). Moreover, post-translational modification mechanisms were reported: phosphorylation and glycosylation were both shown to change glutamate transporter protein content and trafficking (Casado et al., 1993; Conradt & Stoffel, 1997; Escartin et al., 2006; Bauer et al., 2010).

Findings of the last years showed that astrocytic glutamate transporters are substantially subjected to alternative splicing (Peacey et al., 2009; Lee & Pow, 2010), which might permit

regulation of glutamate removal on a complex operation level, thereby expanding the response and action pattern of astrocytes. For GLAST, up to now, three splice variants were described: GLAST1a, GLAST1b and GLAST1c. The former variant is expressed by cells of the astroglial lineage like Müller cells and astrocytes (Macnab et al., 2006), while GLAST1b is expressed by a small subset of neurons under physiological conditions (Macnab & Pow, 2007). As GLAST1b protein levels were nominal in the healthy brain and substantially up-regulated after brain injury, it was assumed that expression is generally restricted to aberrant, damaged neurons (Sullivan et al., 2007). A novel splice variant, termed GLAST1c, was discovered just recently by Lee and coworkers (2012) in astroglia and oligodendrocytes. At least for GLAST1a and GLAST1b it was shown by D-aspartate uptake assays that they represent functional transporter variants (Lee et al., 2011). It might be reasonably assumed, that these molecular distinct transporter proteins also differ in features such as topology, which in turn might have an effect on transport function. It was for instance predicted that, based on clipping of exon 3, orientation of the GLAST1a C-terminal in the cell membrane is flipped, which then would reverse glutamate transport (Huggett et al., 2000).

Studies likewise showed the existence of different GLT-1 splice products, referred to as GLT-1a, GLT-1b and GLT-1c, which all feature distinct C-terminal domains (Holmseth et al., 2009; Peacey et al., 2009; Lee & Pow, 2010). Of these, GLT-1a represents the canonical, i.e. prevalent and initially characterized form of GLT-1 (90% of total GLT-1 protein), whereas GLT-1b and GLT-1c only account for 6% and 1% of total GLT-1 protein in hippocampus, respectively (Holmseth et al., 2009). So far, all three isoforms were exclusively found in astroglial cells (Rauen et al., 2004; Holmseth et al., 2009). Functional comparison of those isoforms with variable C-terminal domains revealed that they exhibit no apparent differences in glutamate uptake capacity (Peacey et al., 2009). Two N-terminal splice variants were also detected: GLT1A and GLT1B (Utsunomiya-Tate et al., 1997; Peacey et al., 2009). Similarly to the C-terminal isoforms, transport activity of both was comparable, albeit considerably enhanced when GLT1A and GLT1B were expressed together (Utsunomiya-Tate et al., 1997). These findings point to a mechanism based on isoform interaction that might modify transport according to environmental conditions. Hitherto no information is available on the cellular distribution of these N-terminal isoforms. Although additional N-terminal and numerous internal splice variants have been identified, they are considered dispensable as expression levels are negligible or translated transporter proteins are not functional (Peacey et al., 2009; Lee & Pow, 2010; Scott et al., 2011). Although the function and significance of glutamate transporter splice variants compared to its full-length, canonical protein is still incompletely understood, there is growing evidence that individual isoforms fulfill exceptional tasks. GLAST1b for instance was found to act as negative regulator of GLAST-mediated glutamate uptake (Vallejo-Illarramendi et al., 2005) and presence of GLT-1b was

shown to be indispensable for binding and interaction of GLT-1a with postsynaptic proteins (González-González et al., 2009).

Translation of a certain set of transporter isoforms is not the only mechanism allowing dynamic and diverse regulation of glutamate uptake at cellular membranes. Current data strongly supports the idea that glutamate transporters build structural multimers, i.e. that within one complex each transporter protein subunit has the intrinsic capability of transporting its substrate (Leary et al., 2007; Yernool et al., 2003 & 2004; Koch & Larsson, 2005; Grewer et al., 2005b). Although monomers are capable of independent operation within multimeric assemblies, complex formation may enhance binding and transport rate, respectively (Haugeto et al., 1996). These complexes can be composed of different isoform types, but heteromultimers consisting of different glutamate transporter subtypes like GLAST and GLT appear not to exist (Haugeto et al., 1996; Peacey et al., 2009). Based on freeze-fracture electron microscopy data glutamate transporter assemblies were first assumed to possess a pentameric structure (Eskandari et al., 2000), but molecular and biophysiological findings since then rather indicate a prevalent trimeric structure (Gendreau et al., 2004; Yernool et al., 2003 & 2004; Grewer et al., 2005; Koch & Larsson, 2005). Based on this idea of multimeric transporter complexes it was suggested by Yernool and coworkers (2004) that the bowl-shaped transporter assembly may form an extracellular aqueous basin, which determines substrate access and thus glutamate uptake efficiency.

Finally, the efficiency of extracellular glutamate removal by EAATs is also governed by general biosynthesis rate and cellular trafficking. The pool of available glutamate transporters can be replenished at sites of demand by rapid *de novo* synthesis or by translocation of already synthetized protein. In this respect studies of the last years focused on glutamate transporter mobility, particularly on protein trafficking to or at the plasma membrane, which is processed on a timescale of minutes to hours (*in vitro*: Poitry-Yamate et al., 2002; Zhou & Sutherland, 2004; Nakagawa et al., 2008; *in situ*: Benediktsson et al., 2012). These investigations revealed that EAATs undergo extensive cellular reorganization which manifests itself as clustering of transporter proteins. Induction of such glutamate transporter accumulations is accomplished by glutamate transporter agonists (Glu and D-aspartate [D-Asp]) and inhibition by their antagonists (DL-*threo*-β-Benzyloxyaspartic acid [DL-TBOA] and dihydrokainic acid [DHK]; Nakagawa et al., 2008). GLT-1 clustering was also triggered by a rise of internal $[Na^+]$ and was unaffected by changes in $[Ca^{2+}]_i$ and $[K^+]_i$ (Nakagawa et al., 2008). This process was not solely induced by glutamate transporter activity, as activation of protein kinase C (PKC) by phorbol-12-myristate-13-acetate (PMA) likewise stimulated cluster formation (Zhou & Sutherland, 2004). Just recently, experimental data demonstrated that enhanced neuronal activity can increase the number of glutamate transporter cluster (Benediktsson et al., 2012). Of outstanding interest was here that increased neuronal activation did not lead to global, but to confined recruitment of

glutamate transporters to perisynaptic sites. Given that cluster formation and apposition was facilitated by enhanced neuronal activity, accomplished within minutes and repeatedly inducible, it appears that this mechanism of glutamate transporter reorganization represents a highly dynamic process adapting transporter position to sites, where glutamate removal is required. If and to what extent neural activity regulates the rate of formation, movement, or turnover of GLT-1 clusters has to be addressed by prospective investigations.

To summarize, the dynamic range of glutamate transporters action is defined by elaborated regulatory mechanisms on multiple organization levels that have impact on overall protein content, intrinsic transport properties, isoform composition, degree of multimerization and trafficking. New experimental insight into this fine-tuned, complex interplay will help us understand how astrocytic glutamate transporters adapt to and modulate glutamate-mediated information processing in the brain. Lately it becomes more and more apparent that glutamate transporter regulation is particularly reliant on the intimate spatial and functional interaction of neurons and astrocytes. For this we have to take a look at the basic features of astrocytes first.

4. Astrocytes

4.1 Glia

In the CNS, astrocytes (Fig. 3), along with oligodendrocytes, polydendrocytes and microglia cells are subsumed within the group of glial cells, also known as neuroglia.

Oligodendrocyte´s main assignment is to insulate neuronal axons with lipid-rich membrane protuberances, called myelin sheaths, which thereby speed up the conduction of electrical impulses (Baumann & Pham-Dinh, 2001).

A newly identified glial cell type is the polydendrocyte, also known as NG2-glia. Previously, based on their highly branched morphology, it has been erroneously assumed that polydendrocytes display a special astroglial cell type, referred to as smooth protoplasmatic astrocytes (Levine and Card 1987). However, several studies showed that polydendrocytes differ significantly from classically defined astrocytes in terms of their lack of anatomical association

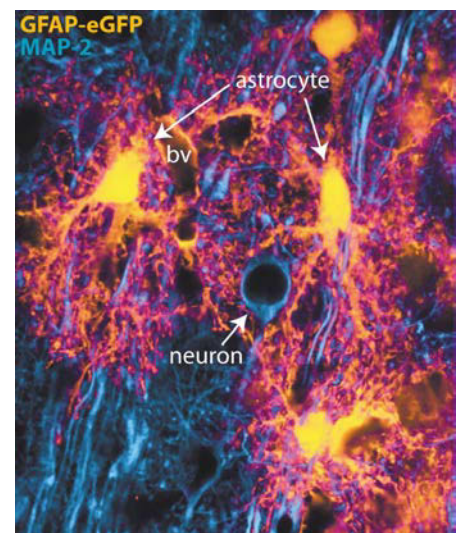**Fig. 3. Spatial organization of astrocytes and neurons in the cortex.** Neurons are labeled with antibody to microtubule-associated protein 2 (MAP-2; blue), whereas astrocytes are genetically labeled with enhanced green-fluorescent protein (eGFP; yellow). Astrocytic processes are closely associated with dendritic structures and blood vessels (BV).

Image taken and modified from Nedergaard et al., 2003

with blood vessels and gap junction coupling, their electrophysiological properties and the absence of glutamate transporters (Bergles et al., 2000; Butt et al., 2002; Peters et al., 2004; Zhou et al., 2006). Nowadays, it is widely accepted that polydendrocytes are progenitor cells of the oligodendrocytic lineage, primarily generating oligodendrocytes in the developing and mature CNS (Nishiyama et al., 2009; Bergles et al., 2010; Trotter et al., 2010). Their additional functions are still incompletely understood, but they were found to form synapse-like contacts with neuronal axons in different brain regions (Bergles et al., 2000; Lin et al., 2005; Kukley et al., 2007; Ziskin et al., 2007). A subpopulation was even found to exhibit substantial voltage-gated Na^+ currents and respond to synaptic input with fast AMPAR- or $GABA_A$R-mediated currents (Jabs et al., 2005; Káradóttir et al., 2008).

In opposition to the aforementioned glial cell types, microglia cells are of mesodermal, not neuroectodermal, origin. These highly motile cells represent the resident innate immune cells in the brain (Kettenmann et al., 2011).
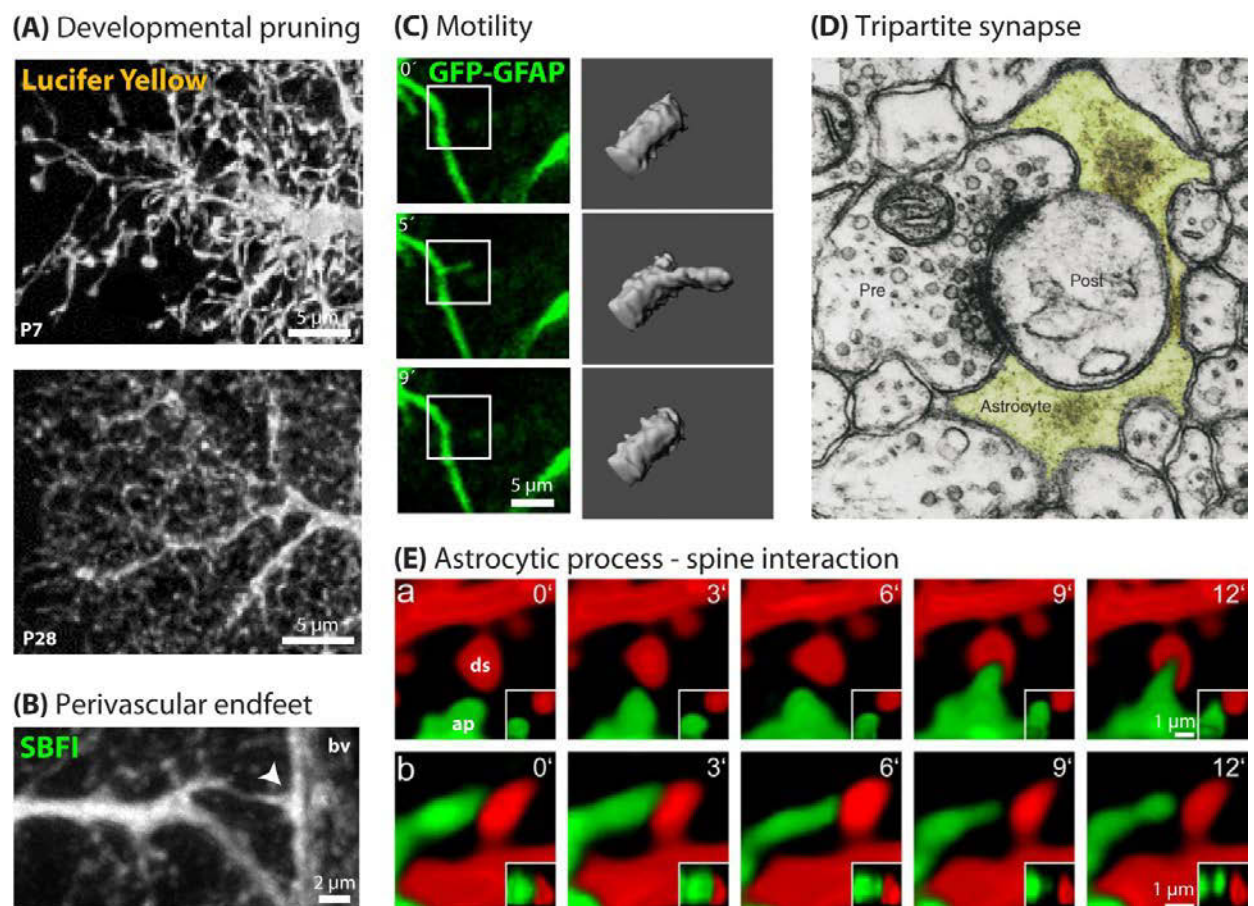
Fig. 4. Morphology and dynamics of astrocytic processes. (A) Structure of perisynaptic processes from P7 (*top*) and P28 murine astrocyte (*bottom*). **(B)** Dye-filled perivascular endfeet contacting a blood vessel. **(C)** GFP-labeled astrocytic process extending upon stimulation and retracting thereafter. **(D)** Electron microscopic picture of the tripartite synapse: synapses are tightly ensheated by perisynaptic astrocytes. **(E)** Structural interplay of an astrocyte perisynaptic process (*ap*) and a dendritic spine (*ds*). *For more details see text.*

 (A) *modified from Bushong et al., 2004*; **(B)** *from Hirrlinger et al.,2004 as reproduced by Reichenbach et al., 2010*; **(C)** *Peters et al, 1991 as reproduced by Halassa et al., 2007*; **(D)** *Haber et al., 2006*; **(E)** *courtesy of Julia Langer.*

4.2 Astrocyte Morphology

Among glial cells, astrocytes are the most diverse group, since they differ in their morphology, developmental origin, gene expression profile, physiological properties, function and response to brain injury (Zhang & Barres, 2010). Although a number of proteins unique to the astroglial lineage have been identified in the last years (e.g. glial fibrillary acidic protein, S100ß, glutamine synthetase; Kimelberg, 2004), none of those does unrestrictedly apply to the entire astrocytic population. To date, Aldh1L1 serves as most specific antigenic marker for astrocytes with a substantially broader pattern of astrocyte expression than traditional astrocyte marker like GFAP (Cahoy et al., 2008; Yang et al., 2011).

Previous and ongoing investigations intend to unequivocally circumscribe the astrocytic population and to define subgroups upon criteria like morphology and physiology (Kimelberg, 2004; Zhang & Barres, 2010). Based on their morphological appearance and their location, astrocytes were initially subdivided into fibrous and protoplasmic types (Matyash & Kettenmann, 2010). Protoplasmic astrocytes are found in grey matter and characterized by numerous branching processes. Their fine distal endings envelop synapses and cover blood vessels (Wang & Bordey, 2008). These specialized structures are termed perisynaptic processes and perivascular endfeet, respectively (Fig. 4A & 4B; Kacem et al., 1998; Reichenbach et al., 2010; Petzold & Murthy, 2011). On the contrary, fibrous (or fibrillary) astrocytes possess distinct, directed processes with little branching. They occupy brain´s white matter, which mostly contains myelinated axon tracts and no neuronal somata, where they enwrap nodes of Ranvier and blood vessels (Wang & Bordey, 2008).

Furthermore, several morphologically distinct astrocytic subtypes have been identified in certain nervous system structures, such as Müller cells of the retina and Bergmann glia cells of the cerebellum (Reichenbach et al., 2010). More recently, mitotic cells of the astrocytic lineage were found in spatially restricted zones of the adult CNS, e.g. radial glial cells in the hippocampus (e.g. Hartfuss et al., 2001; Alvarez-Buylla et al., 2001). These special precursor cells share
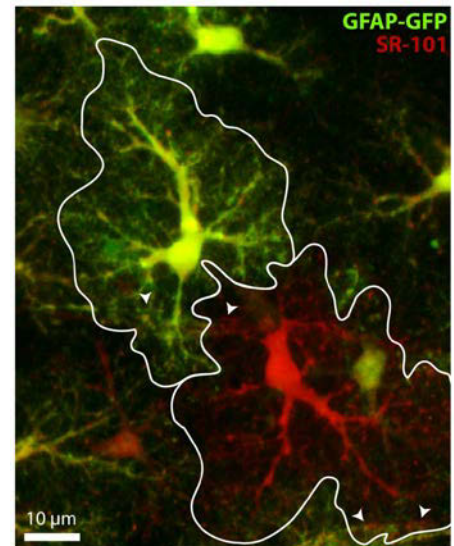
Fig. 5. SR-101-positive astrocytes in the hippocampus of a GFP-GFAP transgenic mouse. Maximum intensity projection of a confocal z-stack with 15 slices, each step 1 μm, are presented. Hippocampal sections obtained from a FVB/N-Tg[GFAPGFP]14Mes/J transgenic mouse (P15), expressing green-fluorescent protein (GFP; green) under the GFAP promotor, were incubated with sulforhodamine 101 (SR-101; red). At P15, the vast majority of SR101-labeled cells is positive for the astrocytic marker GFAP. Employing both, the genetic and chemical approach to label astrocyte allows the distinction of non-overlapping astrocytic domains. White edging of both cells accentuates their individually occupied territories. Arrowheads indicate astrocyte endfeet contacting blood vessels.

antigenic and functional features with mature astrocytes, but are distinct with respect to their multi-potent stem cell competence and their elongated, barely ramified morphology (Barres, 2003; Robel et al., 2011).

Morphological refinement of classical, protoplasmatic astrocytes of the hippocampus proceeds not until the third postnatal week (Fig. 4A; Freeman, 2010; Bushong et al., 2004). During this developmental period the degree of process ramification accelerates significantly. Within the hippocampus, mature protoplasmatic astrocytes eventually display a complex organization, with clearly defined primary and secondary processes, from which in turn fine, ramified processes originate (Fig. 4A and Fig. 5; see e.g. Bushong et al., 2002 & 2004). These processes cover almost all neuronal elements within their reach and terminate preferentially either on synaptic or vascular sites (Witcher et al., 2007; Reichenbach et al., 2010; Mathiisen et al., 2010). The fine astrocytic protrusions were shown to be highly motile: Their morphology can change rapidly from loose association with synaptic compartments to narrow coverage of these, sealing synaptic sites completely and thus preventing hetero-synaptic communication (Fig. 4C-4E; Reichenbach et al., 2004; Haber et al., 2006; Witcher et al., 2007). Pruning of astrocytic processes during postnatal development is accompanied by a significant minimization of process overlap between individual astrocytes. Mature astrocytes finally occupy distinct, non-overlapping domains with discrete, cellular boundaries (Fig. 5; Freeman, 2010; Bushong et al., 2004). Within the rodent hippocampus, a single astrocyte with a cell body size of 7–9 μm in diameter then takes up a volume of $66000 - 85000$ μm^3 with its ramified, very fine processes (Bushong et al., 2002; Ogata & Kosaka, 2002). Notably, these domain borders do not represent a physical barrier between astrocytes, as fine processes of individual astrocytes are connected to one another through gap junctions at these boundaries, building one continuous intracellular compartment.

As we have seen, morphological refinement during postnatal development is a well described process. The functional changes accompanying astrocyte maturation are however unadequately understood.

When considering the evolutionary context, it is truly intriguing that the number of astrocytes in relation to the number of neurons has increased substantially with complexity of the organism: the glial-neuron-ratio in the prefrontal cortex has risen from 0.3 in rodents to 1.7 in humans (Sherwood et al., 2006), the astrocyte-neuron-ratio in the somatosensory cortex from 0.3 to 1.4 (Fig 6A; Bass et al., 1971 in Nedergaard et al., 2003). Phylogenetic augmentation of cell number is paralleled by a rise in the protoplasmic astrocyte dimension by approximately 2.5 times and a 27-fold volume increase of their occupied territories, when comparing rodent and human astroglia (Oberheim et al., 2006; Oberheim et al., 2009). Besides the cellular

Fig. 6. Astrocyte evolution. (A) The relative ratio of astrocytes to neurons rises with increasing brain complexity, size and cognitive abilities of a species (data gained from cortex tissue). **(B)** Graphical representation based on GFAP immunostaining of mouse (left) and human (right) cortical astrocytes. Scale bars below illustrate the sizes of human astrocytes relative to the sizes of these cells in mice. Human cortical astrocytes are almost threefold larger, have approximately tenfold more GFAP-positive processes, more highly-branched processes and are more symmetrical than mouse astrocytes. **(A)** *modified from Nedergaard et al., 2003;* **(B)** *modified from Oberheim et al., 2006.*

extension with higher brain complexity, astrocytes exhibit a more sophisticated morphology: human astrocytes have a symmetrical shape, extend 10-fold more GFAP-positive processes, which are highly ramified, and exhibit greater domain overlap than corresponding rodent astrocytes (Fig 6B; Oberheim et al., 2009). Human protoplasmatic astrocytes are thus more numerous, larger and morphologically more complex than their rodent counterparts. As a result of astrocyte evolution, human astrocytes intimately contact about 2 million synapses compared with only 100 000 synapses covered by the processes of a rodent astrocyte (Oberheim et al., 2006; Kettenmann & Verkhratsky, 2008). Thus, phylogenetic advance of astrocytes implies that astrocyte operation may be crucial for higher brain function.
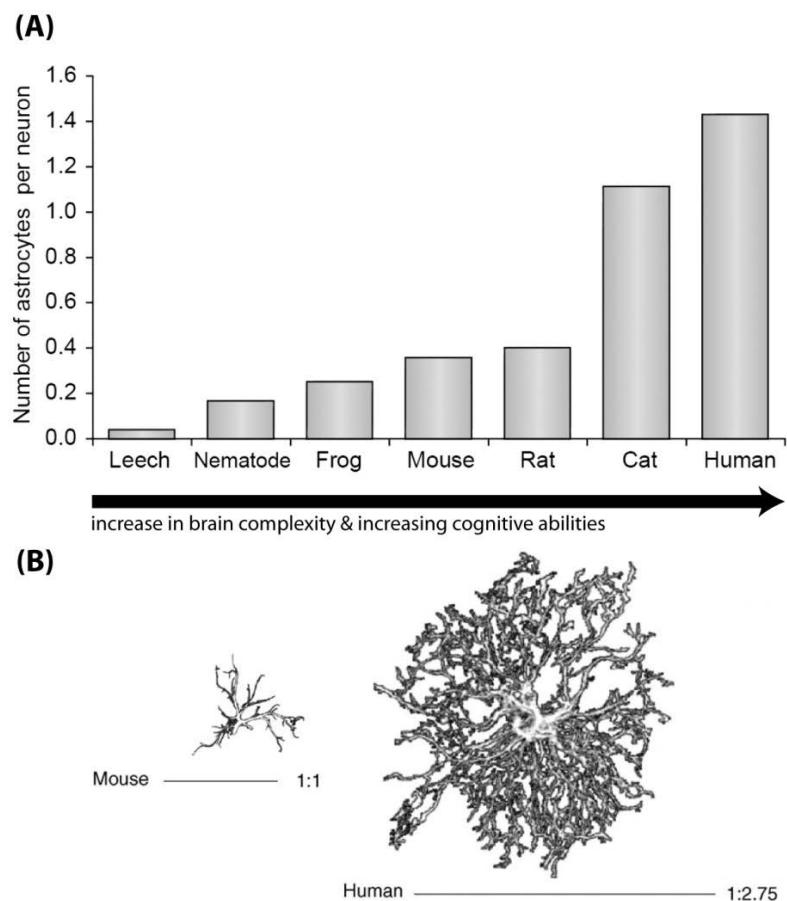
4.3. Astrocyte Function

Besides their above described capacity to monitor extracellular glutamate, maintain it at low levels, metabolize and redeliver it back to neurons glutamine, astrocytes accomplish additional complex and vital tasks in the brain.

First of all, astrocytes do not only sense neuronal activity, but also signal back to them by release of a wide variety of substances (Hassala et al., 2006; Parpura & Zorec, 2010). These so-called gliotransmitters, comprising molecules like glutamate (Parpura et al., 1994), GABA (Angulo et al., 2008), D-Serine (Oliet & Mothet, 2006) and ATP (Coco et al., 2003), are considered to support and synchronize action of neurons (Hassala et al., 2006; Fellin et al., 2004). Moreover, some groups proposed that gliotransmission might represent the basic mechanism to actively modulate basal synaptic transmission. This means that alongside their passive role as maintainers of neuronal homeostasis (Verkhratsky, 2010; Suzuki et al., 2011) they are considered to actually have control over information processing in the brain (Perea & Araque, 2007; Halassa et al., 2007; Panatier et al., 2011). Recent reports even indicate a dependency of long-term potentiation and depression (LTP and LTD, respectively) on astrocytic action (Yang et al., 2003; Henneberger et al., 2010; Navarrete et al., 2012; Chen et al., 2012). Further discoveries substantiating and evolving this idea may have vital implications for the concept of synaptic plasticity, i.e. the cellular and molecular process that underlies learning and memory formation (Gibbs et al., 2008).

As mentioned before, a special feature of astrocytes is their organization into a continuous network, interconnected through gap junctions (Volterra & Meldolesi, 2005; Giaume et al., 2010). This syncytium mediates electrical coupling and, in addition to ions, exchange of small molecules of less than 1.2 kDa (Bennett et al., 2003; Chew et al., 2010), such as glutamate and glucose (Hansson et al., 2000; Dienel & Cruz, 2003). Since gap junction channels are in an open state under physiological conditions, the syncytium thus defines one unified cellular compartment facilitating continuous inter-cellular passage of messengers and metabolites (Chew et al., 2010). These gap junctions channels are composed of underlined connexin (Cx) subtypes Cx43, Cx30 and Cx26 in astrocytes (Scemes et al, 2009). In accordance with astrocyte heterogeneity, diversity of connexin expression is present on the molecular, subcellular and cellular level: (1) among the subtypes is Cx43 most abundantly expressed in the hippocampus (Giaume & McCarthy, 1996; Chew et al., 2010), (2) Cx30 and Cx43 are particularly enriched on perivascular endfeet (Rouach et al., 2008; Ezan et al., 2012) and (3) radial glial cells are only coupled to few neighbouring cells in the mature dentate gyrus (Kunze et al., 2009). Generally, establishment of astrocyte interconnection is initiated in the neonate rodent with considerable variability in extend of individual astrocytic coupling observable during postnatal development, until all astrocytes are ultimately coupled in the adult (Schools et al., 2006)

Considering the close interaction of individual astrocytes with a countless number of neurons, one may speculate that the astroglial coupling facilitates alternative, sophisticated signaling pathways. Assuming this, astrocyte syncytia may serve as integration networks of neuronal signal transmission, which would add another complexity level to brain information processing.

Besides astrocytes´ impact on synapse function, facilitated by the spatial proximity of synaptic compartments and perisynaptic terminals, they also represent an integral part of the blood-brain-barrier (BBB) by their specialized perivascular processes ensheating blood vessels (Fig. 5B; Abbott et al, 2006; Mathiisen et al., 2010; Petzold & Murthy, 2011). Together with endothelial cells, pericytes and vascular smooth muscle cells (VSMC), astrocytes form a functional unit, that provides physical delimitation and control over exchange of substances from blood to brain and vice versa (Petzold & Murthy, 2011).

Hence uniquely positioned between neuronal and vascular sites, astrocytes were found to facilitate adaptation of blood flow to neuronal metabolic demand, a process termed neurovascular coupling (see e.g. Filosa & Blanco, 2007; Koehler et al, 2009; Carmignoto & Gómez-Gonzalo, 2010). It has been known for a long time that neuronal activation is associated with an increase in cerebral blood flow, an observation that was utilized by the functional magnetic resonance imaging technique (fMRI) for over two decades now (Ogawa & Lee, 1990; Figley & Stroman, 2011; Yang et al., 2008). The cellular basis though remained elusive, as it was unpropable that neurons directly mediate vasodilatation and vasoconstriction: Neuronal elements are only rarely found in spatial proximity to VSMCs or pericytes. Vasoactive agents derived from these distant neuronal sites can hardly account for the rapid change of blood flow upon neuronal activity (Zhang et al., 2005; Tsai et al, 2009; McCaslin et al., 2011). It was not until 2002 that experimental data provided evidence for a direct functional relationship between Ca^{2+}-mediated astrocyte activation and diameter change of nearby arterioles (Zonta et al., 2002). This modulation of the cerebrovasculature by astrocytes meets not only brains energy requirements but also its oxygen demand (Gordon et al., 2008 & 2011). Further reports also supported the idea that astrocytes, being positioned in the center of the neurovascular unit, couple neuronal activity and local cerebral blood flow to meet neuronal metabolic requirements (Tanako et al., 2006; Petzold et al., 2008; Girouard et al., 2010). In this context one relevant theory has been established over the last years: The astrocyte–neuron lactate shuttle hypothesis (ANLS; Pellerin et al. 2007; Brown & Ransom, 2007; Pellerin & Magistretti, 2012). This concept attempts to elucidate how neuronal energy demand is met by adequate metabolic supply generated by astrocytic glucose metabolism.

Central to this model was the initial finding that glutamate inward transport by EAATs triggers glucose uptake into astrocytes (Pellerin & Magistretti, 1994). The underlying signaling cascade was found to be initiated by the glutamate transporter-associated Na^+ influx. The substantial rise in $[Na^+]_i$

is counterbalanced by enhanced Na^+/K^+-ATPase activation, an energy-consuming process leading to depletion of cytosolic ATP levels (Chatton et al., 2000). This in turn stimulates enhanced GLUT-1-mediated glucose utilization (glucose transporter 1), facilitated by local increase in cerebral blood flow and activation of aerobic glycolysis in astrocytes (Pellerin et al., 1998; Vannucci et al. 1997; Loaiza et al. 2003; Porras et al., 2008).

After transformation of glucose to pyruvate, it is further anaerobically metabolized to lactate, which is transferred to neurons as metabolic substrate via astrocytic and neuronal monocarboxylate transporters (MCT; Barros & Deitmer, 2010). According to the present model activity-induced glucose utilization is accomplished predominantly, if not exclusively, by astrocytes: They sense the extent of glutamatergic transmission at synaptic sites and induce thereupon a haemodynamic response at vascular sites, which leads to glucose uptake into astrocytes and increased astrocytic metabolism to provide an appropriate energy supply to neurons (Brown & Ransom, 2007; Pellerin & Magistretti, 2012). Upon exceptionally strong or long-lasting stimulation, astrocytes can additionally mobilize their glycogen stores to provide necessary metabolic supply even under conditions when glucose utilization is insufficient in terms of immediate energy requirements (Pellerin et al. 2007; Brown & Ransom, 2007). Moreover, the astrocytic network allows diffusion of energy metabolites, a feature that is positively regulated by AMPA-R activation and that might improve metabolite delivery to sites of high neuronal demand distant from blood vessels. Intracellular transfer of metabolites within the syncytium was considered particularly relevant for sustained neuronal supply during periods of abnormally enhanced synaptic activity (Rouach et al., 2008).

Just like the astrocytic network allows for diffusion of metabolites, it also functions as siphoning structure for ions and absorbed toxins, thereby mediating ion homeostasis and detoxification of brain tissue. The former was for instance shown by the observation that potassium, taken up by astrocytes, is distributed through the gap junction coupled syncytium and finally discharged into capillaries, a process that was termed "spatial K^+ buffering" (Holthoff & Witte, 2000; Walz, 2000; Kofuji & Newman, 2004). Furthermore, propagation of calcium within the intracellular network represents one of the basic signaling mechanisms in astrocytes (Scemes & Giaume, 2006; Kuga et al., 2011; Verkhratsky et al., 2012). Apart from that, astrocytes have been ascribed a pivotal role in several detoxification pathways of the CNS. They have for instance an important antioxidant function by neutralizing reactive oxygen species that are generated by high rates of oxidative metabolic activity, a process termed oxidative stress (Drukarch et al., 1998; Dringen et al., 1999; Tanaka et al., 1999; Bélanger et al., 2011). Equally important, aforementioned detoxification of ammonium is exclusively mediated by astrocyte-specific glutamine synthase, catalyzing the condensation of glutamate and ammonia to glutamine (Daikhin & Yudkoff, 2000; Hawkins et al., 2002; Rao et al, 2005).

But not only ion homeostasis is monitored and adjusted by astrocytes, there is also increasing evidence that astrocytes play a key role in maintaining water homeostasis in the brain (Simard & Nedergaard, 2004; Zelenina, 2010). Interestingly, it was reported that water permeability, mediated by AQP4 (aquaporin-4) channels, increases upon neuronal glutamate release (Gunnarson et al., 2008).

Water homeostasis is not only controlled by glutamate uptake, but can vice versa modify the astrocytic glutamate uptake system (Djukic et al., 2007), which was alike shown for potassium homeostasis (Zeng et al., 2008). These water pores together with glutamate transporter GLT-1 and Kir4.1, the inward rectifier-type potassium channel primarily assumed to mediate spatial buffering (Olsen & Sontheimer, 2008), were proposed to build a supra-molecular complex at the cell membrane (Nagelhus et al., 2004; Zeng et al., 2007). This elaborate interaction seems reasonable, as concentration gradients have to be rapidly re-established after neuronal activity to sustain processing capability. Action potential generation results in excessive extracellular K^+ efflux by delayed voltage-activated potassium channels. $[K^+]_o$ becomes even further elevated by glutamate transporter-mediated K^+ release. Excess ambient potassium is removed by action of astrocytic Kir4.1 channels and dispersed by efficient spatial buffering. Even short-term accumulation of potassium leads to electro-osmotic swelling if not counterbalanced by regulation of water homeostasis (Meeks & Mennerick, 2007, Østby et al., 2009). Hence, homeostasis of neurotransmitters, ions and water in the brain is maintained by an astrocytic interface meeting these vital requirements by spatial arrangement and complex interaction of proteins.

Based on this multitude of experimental data approaching the interaction of astrocytes and neurons, the concept of the "tripartite synapse" was stated (Araque et al., 1999; Haydon & Carmignoto, 2006; Perea et al. 2009). The term "tripartite synapse" refers to the idea that synapses, structurally and functionally, not only consist of the classical synaptic elements, namely the pre- and postsynaptic terminal, but also of perisynaptic processes of astrocytes. Astrocytic cells are on that note considered as active participants in information processing, transfer and storage of the brain (Haydon 2001; Halassa et al., 2007 & 2009; Perea & Araque, 2010). Since astrocytes are equipped with this highly elaborated functional repertoire presented here, it is apparent that even partial dysfunction of these cells upon brain injury has multiple consequences.

4.4. Astrocyte Impairment

Although great progress has been made to understand astrocyte function under physiological conditions most aspects of many vital and dynamic features of astrocytes under pathophysiological conditions remain elusive and fragmented. In general, brain insults trigger a specific astroglial reaction, also referred to as reactive astrogliosis (Sofroniew, 2009; Buffo et al., 2010). A hallmark of

reactive astrogliosis, regardless of its origin and the brain region affected, is the increased expression of the major astrocytic intermediate filament glial fibrillary acidic protein (GFAP; Eng & Ghirnikar, 1994; Eng et al., 2000; Middledorp & Hol, 2011).

Upon traumatic brain injury a severe astrogliotic response is triggered, which is characterized by general hypertrophy of astrocyte cell bodies and processes and strongly enhanced GFAP levels. Adjacent to the lesion site glial scar formation is observable featuring pronounced domain overlap of individual astrocytes, substantial proliferation and recruitment of other glial cells like microglial cells (Sofroniew, 2009; Sofroniew & Vinters., 2010). It generally depends on the severity of the brain injury to which extent tissue re-organization, impairment of cellular connectivity, morphological alterations and proliferation proceed.

Reactive astrocytes exhibit stereotypical alterations of their normal morphology. Particularly the increased density of diverse intermediate filaments (GFAP, vimentin, nestin and synemin; Jing et al., 2007; Robel et al., 2011) results in hypertrophy, i.e. the enlargement of cellular compartments based on a raised protein synthesis rate, and alterations of the viscoelastic properties (Wilhelmsson et al., 2004; Lu et al., 2011). The cellular stiffness of astrocytic processes primarily determines the rigidity of the glial scars and may thus affect motility dynamics and protein trafficking due to impaired cytoskeleton scaffolding (Lu et al., 2011). The number of stem and higher-degree processes is significantly increased upon pathological activation and cellular processes become elongated, mainly directed towards the lesion site (Wilhelmsson et al., 2004 & 2006).

To date, many studies showed that expression of a multitude of genes and downstream proteins in reactive astrocytes are altered, the functional consequences of this molecular transformation remain albeit very incompletely understood (Eddleston & Mucke, 1993; Ridet et al., 1997; Zamanian et al., 2012). Not unexpectedly, reactive astrocytes alike healthy astroglia do not comprise a uniform cell population, but it was not until 1994 that heterogeneity among astrocytes in reactive gliosis was assessed (Höke & Silver, 1994; Zhang & Barres, 2010). Owing initially to their diverse molecular profile and their distance from the primary lesion, two distinct subpopulations were defined: proximal (anisomorphic) and distal (isomorphic) reactive astrocytes (Ridet et al., 1997). It is meanwhile established that at least these two reactive astrocyte subtypes are immunohistochemically, electrophysiologically and morphologically distinct (Chvátal et al., 2008; Malhotra & Shnitka, 2001 and references therein). Proximal reactive astrocytes (PRA) are found in the direct vicinity of the lesion site, i.e. within a distance of approximately 100 μm. Within this area tissue architecture is completely distorted, with astrocyte processes arrayed in a palisade-like manner and directed towards the lesion site (Oberheim et al., 2008). Distal reactive astrocytes (DRAs) are detected more distant from the primary lesion (> 100 μm) retaining their basic structural organization within individual, non-overlapping territories (Wilhelmsson et al., 2006).

They undergo, unlike scar-forming proximal reactive astrocytes, only moderate changes of their healthy astrocyte phenotype and apparently fully recover their normal morphological and functional features after several weeks. While distal astrocytes are nestin(-), do not proliferate and show a temporal up-regulation of K_{IR} currents, proximal astrocytes undergo significant and persistent changes of their functional features. They exhibit on the contrary K_{DR} currents, label positive for nestin, GFAP and BrdU (Chvátal et al., 2008). This particular subpopulation undergoes de-differentiation, regaining juvenile features and re-entering the cell cycle (Buffo et al., 2008; Simon et al., 2011; Robel et al., 2011). In line with this data, gap junction coupling of astrocytes, as shown by Cx43 distribution, seems to be disrupted exclusively in proximal reactive astrocytes situated in the lesion focus (Theriault et al., 1997).

Taking all these findings together, they may suggest that PRAs primarily participate in the forming of a dense structural barrier to isolate the focal injury core, while DRAs presumably retain their functional repertoire to promote the surrounding tissue.

Knowledge, by which signals these (at least) two diverse phenotypes are triggered and to which extend they differ functionally, is for the most part unavailable. Thus, to consider astrocytes as therapeutic target, a coherent theory has to be established of how astrocytes operate on a temporal and spatial basis and whether their actions have to be considered as destructive or compensatory.

In order to better understand how this plethora of highly complex and diverse tasks is accomplished by astrocytes during development, adulthood and injury, it is essential to look closer at the fundamental interrelationship and coordination of signaling events. As this study focuses on glutamate transporter (dys-)function the following paragraphs will address in particular sodium signaling in astrocytes.

5. Sodium Signaling in Astrocytes

Astrocytes, unlike neurons, do not generate action potentials as response to electrical stimulation, but there is good evidence that they process information by changes in intracellular ion concentrations.

Contemporary, the concept of calcium acting as important intracellular messenger in astrocytes is generally accepted (Fiacco & McCarthy, 2006; Nedergaard et al., 2010). Astrocytes display spontaneous calcium fluctuations ranging from random profiles to rhythmic oscillations (Hirase et al., 2004; Honsek et al., 2012). The latter coordinated Ca^{2+} events are exogenously inducible and capable of propagation among several astrocytes within the syncytium (intracellular calcium waves). In astrocytes, these Ca^{2+} waves are assumed to display the principle mechanism of information processing and communication within the cellular network (Scemes & Giaume, 2006). In order to

provide fast and efficient signal transduction, a 20000-fold gradient is maintained between the intracellular and extracellular compartment ($[Ca^{2+}]_i$= 0.1 µM; $[Ca^{2+}]_o$=~1 mM; Clapham, 2007; Nedergaard et al., 2010). This is realized by the action of the plasma membrane calcium ATPase (PMCA) and the sarcoendoplasmic calcium ATPase (SERCA) transporting calcium into the extracellular space or into internal stores of the endoplasmatic reticulum (ER), respectively (Fresu et al., 1999; Grimaldi, 2006). The spatiotemporal signaling properties of calcium are governed by cytoplasmatic calcium binding proteins that provide a buffer capacity which can locally restricts calcium signals to so-called microdomains.

Analogue to the commonly accepted idea that calcium serves a signaling purpose, there is emerging evidence that this may also be true for sodium (Rose, 1997; Deitmer & Rose, 2010; Kirischuk et al., 2012). In this respect great progress has been made in the last few years in understanding the homeostatic and dynamic role of sodium in CNS function, as will be described in the following.

Conservation of energy in form of a sustained Na^+ gradient over the plasma membrane is a principle consistently found in virtually all organisms. The steep inward-directed electrochemical Na^+ gradient across the plasma membrane is provided by the ATP-consuming action of the Na^+/K^+-ATPase, serving in turn as energy source for numerous secondary-active transport systems. Worthy of note is here that intracellular Ca^{2+} and pH homeostasis are directly dependent on changes in $[Na^+]_i$ since most of the involved transport processes are in fact driven by the Na^+ gradient (Deitmer & Rose, 2010; Kirischuk et al., 2012).

Signal transduction mediated by Ca^{2+} is intimately coupled to sodium concentration by the Na^+/Ca^{2+}-exchanger (NCX), which operates in the forward-mode with the stoichiometry of exchange being $3Na^+_{influx}$:$1Ca^{2+}_{efflux}$ (Clapham, 2007). Interdigitation of Ca^{2+} and Na^+ signaling thus implies that sodium fluctuations may trigger internal calcium elevations. Those in turn can initiate intracellular signaling cascades or provoke gliotransmitter release, thus facilitating communication within the astrocytic network and between astrocytes and neurons, respectively.

The sodium gradient alike governs pH homeostasis. The physiological pH buffering system is determined by the cellular ratio of bicarbonate (HCO_3^-) and hydrogen ions (H^+) and linked to the sodium gradient via Na^+/H^+-exchanger (NHE; $1Na^+_{influx}$/$1H^+_{efflux}$) and Na^+/ HCO_3^--cotransporter (NBC; $1Na^+_{influx}$/$2HCO_3^-_{influx}$), respectively (Deitmer & Rose, 2010). In the first place, these two transporters are responsible for maintenance of a physiological pH by extruding metabolically generated acid, which would otherwise lead to intracellular acidification. Lactate transfer from astrocytes to neurons by MTCs is likewise proton-linked, hence indirectly modulated by the intracellular sodium concentration (Halestrap & Price, 1999). In conclusion, cytosolic sodium elevations will ultimately

lead to a reduction in the driving force for sodium-dependent transporters and thus substantially affect pH and Ca^{2+} homeostasis.

As was already stated above, each glutamate molecule taken up by EAATs is accompanied by the co-transport of three sodium ions. Likewise, transmission of GABA is terminated by action of astrocytic high-affinity, sodium-dependent transporters, termed GATs (Eulenburg & Gomeza, 2010). They take up one GABA molecule along with two co-transported Na^+ and one counter-transported Cl^-. The stoichiometry of both transporter types, EAATs and GATs, suggests that elevated extracellular glutamate or GABA concentrations might introduce a significant quantity of sodium ions into the cell. And it was indeed demonstrated *in vitro* that endogenous administration of glutamate and GABA elicits substantial sodium transients in astrocytes (Rose & Ransom, 1996; Chatton et al., 2000; Chatton et al., 2003). First evidence for the existence of synaptically-induced, EAAT-mediated $[Na^+]_i$ elevations in intact tissue was provided by a study analyzing Bergmann Glia cells in the cerebellum (Kirischuk et al., 2007).

These findings were elaborately confirmed, refined and extended by successively acquired experimental data by Christine Roses´ laboratory. Initially, Bennay and coworkers (2008) demonstrated that these synaptically-induced sodium transients do not only occur in cellular bodies but also in processes of cerebellar Bergmann glia cells. Analogous findings were provided for classical protoplasmatic astrocytes of the hippocampus (Langer & Rose, 2009). In acute hippocampal slices, sodium signals were moreover shown to propagate to neighbouring cells in a gap junction mediated manner (Langer et al., 2012). It was proposed that the generation of such intracellular "Na^+ waves" might serve neurometabolic coupling (Bernardinelli et al., 2004). As mentioned before, the workload of the Na^+/K^+-ATPase following glutamate uptake triggers glucose utilization, which may represents a sodium-mediated signaling pathway coupling synaptic activity and metabolic supply (Pellerin & Magistretti, 2012). It was indeed shown that besides its dependence on Na^+/K^+-ATPase, stimulation of GLUT-1 necessitates coincidental induction of Na^+ and Ca^{2+} signals (Bernardinelli et al., 2004; Porras et al., 2008). The spatiotemporal coordination of both ions seems thus to be of vital importance for activity-adapted neuronal supply. Besides these interaction events, Na^+ and Ca^{2+} signaling pathways are also capable of independent operation, which means that Ca^{2+} transients are not always accompanied by Na^+ elevations and vice versa (see e.g. Bernardinelli et al., 2004; Langer et al., 2012).

Lately a study showed that $[Na^+]_i$ in cortical astrocytes even modulates the plasticity of glutamate transporter-mediated currents on a short-term scale (Unichenko et al., 2012). For that, neuronal fibers were activated by focal, double-pulse electrical stimulation and astrocytic synaptically activated, transporter mediated currents were measured. This experimental procedure, since only astrocytes were analyzed, did not allow deciding whether this effect was directly caused by the

influence of sodium on astrocytic glutamate transporters or rather by altered glutamate uptake due to changed neuronal glutamate release. Interestingly, it was also shown that activation of GAT by exogenous GABA can elicit such $[Na^+]_i$ elevations and thus influence glutamate transporter function, indicating that astrocytes may serve as link between GABAergic and glutamatergic transmission pathways.

Concluding, these studies demonstrated that sodium signals in astrocytes, induced upon neuronal activity, exhibit conformity in their amplitude and spatial profile with strength and site of synaptic activation. Their manifestation comprises delicate, locally restricted transients up to robust sodium waved propagating from one cell to another within the astrocytic network. Gradual recruitment of cellular compartments or even of neighboring cells by sodium might represent a signal mechanism coupling increased metabolic need due to prior neuronal activity and glucose utilization. As these local and global sodium signals alter the gradient over the plasma membrane in a certain spatiotemporal manner, they are expected to have multitudinous consequences for associated transport systems, which reciprocally determined modality of Na^+ action. All these sodium-dependent pathways, that are central for brain physiology, illustrate the particular importance to understand the complex interplay of sodium homeostasis and signaling.

6. Aim of the Study and Methods

As the introduction points out, the hippocampus is a well-defined brain structure in terms of its anatomy and inherent glutamate-mediated neuronal connectivity. The cortical organization is fairly simple, the neuronal circuitry is unidirectional and synaptic contacts are restricted to specific tissue layers, which altogether renders the hippocampus the best-studied structure in the brain (Förster et al., 2006; Neves et al., 2008; van Strien et al., 2009). In contrast to the multitude of publications regarding the development and function of neurons in the hippocampus, adequate knowledge about astrocyte participation in brain maturation and information processing is still missing. Especially during postnatal development, when formation and maturation of glutamatergic synapses proceeds, little information exists about the operation of the astrocytic glutamate re-uptake system (Pfrieger, 2002; Ullian et al., 2004). Just like we have an inaccurate understanding of the role of astrocytic glutamate transporters during brain development, knowledge regarding glutamate transporter operation during brain injury is mostly lacking. As was highlighted in a recent review (Kirischuk et al., 2012), little is especially known about alterations of sodium homeostasis and signaling dynamics in pathophysiological states, not to mention the unadequate understanding of the functional heterogeneity of reactive astrocytes in this regard.

The purpose of this study was to acquire fundamental knowledge about the role of astrocyte EAATs and the associated intracellular sodium signaling during establishment and dysfunction of the re-uptake system in the hippocampus.

Accordingly, present investigation examined astrocytic EAAT distribution and function during postnatal ontogenesis and brain injury with a particular focus on transporter subtype composition and cell type heterogeneity.

To picture the expression profile of the astrocytic glutamate transporters GLAST and GLT-1 on different organizational levels during development and injury, fluorescence-based immunocytochemistry and protein immunoblotting were employed. High-resolution microscopy, namely confocal and STED (stimulated emission depletion) microscopy, provided clear cellular resolution of antibody-labeled preparations. In order to quantify GLAST and GLT-1 protein levels, western blot analysis was performed. This technique even allowed the detailed portray of the developmental and pathological changes in multimer composition.

To gain functional data, optical probing of intracellular sodium was accomplished by the sodium imaging technique (Meier et al., 2006; Lamy & Chatton, 2011; Schreiner & Rose, 2012) and the selective stimulation of EAATs by the agonist D-aspartate. Here, the AM-ester of the ratiometric indicator sodium-binding benzofuran isophthalate (SBFI; Minta & Tsien, 1989) was employed in order to vizualize EAAT-mediated sodium transients in cell bodies of reactive astrocytes *in situ* in a hippocampal slice culture lesion model. A comprehensive review addressing quantitative sodium imaging is enclosed here ([1] Schreiner & Rose, 2012). SBFI delivered by the patch pipette was further enabled sodium imaging in delicate perivascular endfeet structures on blood vessels *in situ*. These sodium transients were elicited in astrocytes in acutely prepared tissue slices of hippocampus either by electrical stimulation or by EAAT agonist application. Quantative data was obtained by ratiometric, epifluorescence measurements while high spatial and temporal resolution was facilitated by two-photon imaging.

8. Summary of Results and Discussion

The experimental results presented in this study suggest that both glutamate transporter subtypes expressed by astrocytes, namely GLAST and GLT-1, are differentially regulated during development as well as during brain injury ([2] Schreiner et al., *under review* and [3] Schreiner et al., *in preparation*).

We found that GLAST and GLT-1 are independently up-regulated during postnatal hippocampal development ([2] Schreiner et al., under review). Their temporal, spatial and cellular expression profile differed considerably. GLAST was foremost expressed by radial glial cells and juvenile

astrocytes and temporal up-regulation paralleled the increase in GFAP content, the principle astrocytic intermediate filament. Onset of GLT-1 protein up-regulation proceeded not until the second postnatal week, with a sequential rise in multimeric and monomeric form of the protein, respectively. Unlike GLAST, GLT-1 was particularly detected on distal astrocytic structures such as perisynaptic and perivascular processes, whereby prominent GLT-1 accumulations were found on the latter. Functionally, we demonstrated for the first time that EAAT-mediated sodium signals can indeed originate at perivascular endfeet, invade these and propagate between endfeet of adjacent astrocytes ([4] Langer et al., in preparation).

This study not only established that the astroglial EAATs are differentially regulated during development, but also during pathophysiological conditions ([3] Schreiner et al., in preparation). Following severe brain injury discrete modifications of GLAST and GLT-1 expression and non-uniform alterations of glutamate re-uptake capacity in defined subsets of reactive astrocytes are triggered. Upon brain injury multimeric GLAST protein content increased, accompanying the pathological up-regulation of GFAP, while GLT-1 monomeric protein quantity declined.

The postnatal stage represents a critical period of brain development regarding neuronal and astrocytic commissioning. Hippocampal neurons, which are already generated during the embryonic phase, begin to establish synaptic connections shortly after birth. Synapse formation and maturation then proceeds for the following two postnatal weeks (Ben-Ari, 2001). Just after these two postnatal weeks myelination commences and isn´t complete until P60 (Meier et al., 2004). Neuronal changes are paralleled by vigorous changes of astrocytic cells during postnatal ontogeny of the hippocampus. In contrast to neurogenesis, gliogenesis peaks early postnatal (Sauvageot & Stiles, 2002). Thereafter, fundamental astrocytic functions are established: (I) defined cellular domains are formed, (II) fine processes are highly-dynamically reorganized (Bushong et al., 2004), (III) electrophysiological properties change (Zhou et al., 2006; Kafitz et al., 2008), (IV) changes in protein expression occur (Kimelberg, 2010) and (V) the gap junction network interconnecting astrocytes is build (Schools et al., 2006). The process of astroglial maturation appears to be inevitable for promotion of synapse formation and maturation (Pfrieger, 2002; Ullian et al., 2004; Faissner et al., 2010; Eroglu & Barres, 2010). Additionally to their important homeostatic and regulatory function in the mature brain, glutamate transporters are thought to fulfill important duties during brain development by regulating neuronal migration (Shibata et al., 1997; Matsugami et al., 2006), proliferation (Gilley & Kernie, 2011) and synaptogenesis (Matsugami et al., 2006).

Present research revealed that during this critical developmental period both glutamate transporters are dramatically upregulated, although in a distinct spatio-temperal manner. Immunohistochemistry and western blot analysis showed that GLT-1 protein content in the

hippocampus substantially started to increase after the first postnatal week. On the contrary, considerable amounts of GLAST protein were already expressed before GLT-1 onset and gradually increased postnatally. On a laminar and cellular level GLT-1 was found to be particularly associated with perisynaptic and perivascular astrocyte structures, while GLAST expression could be especially ascribed to juvenile astrocytes and astrocyte procursors like radial glial cells. Hence, although both astrocytic glutamate transporters share 55 % protein identity and exhibit similar functional features (e.g. stoichiometry, topology, K_M values), both seem to fulfill specialized tasks in the developing brain (Gegelashvili & Schousboe, 1997; Danbolt, 2001; Anderson & Swanson, 2000).

Studies utilizing knockout (KO) animals impressively showed the indispensability of both astrocyte glutamate transporters to brain development and normal brain function (Matsugami et al., 2006). Primarily of note, GLAST/GLT-1 double-KO resulted in perinatal mortality between embryonic day 17-18 (Matsugami et al., 2006). Prior transgenic animals exhibited abnormal brain development manifesting itself as structural disorganization as well as impairment of proliferation, radial glia migration and neuronal differentiation. Neither individual GLAST nor GLT-1 ablation featured such general anatomical alterations (Tanaka et al., 1997; Watase et al., 1998). Genetic inactivation of GLAST only lead to minor synaptic impairment and more general to slight dysfunction of motor coordination, while single GLT-1 KO mice showed significantly elevated ambient glutamate concentrations, developed spontaneous seizures and had an increased susceptibility to acute cortical injury, hence only 50 % of the animals survived until the sixth week (Tanaka et al., 1997; Watase et al., 1998; Mitani & Tanaka, 2003). Under pathological conditions however, failure of GLAST-mediated glutamate re-uptake profoundly worsened the outcome of brain injury (Watase et al., 1998). KO of GLT-1 did not alter GLAST expression and vice versa, which indicates that no compensatory mechanism among astrocytic glutamate transporters does exist (Voutsinos-Porche et al., 2003b; Harada et al., 1998; Ueda et al., 2002). These findings provide good evidence that both glutamate transporters are indespensible for proper brain development and function in the mature animal.

Interestingly, exactly during the developmental shift from GABA- to glutamate-mediated excitation, GLT-1 takes over and remains the prevalent and most abundant glutamate transporter in the brain (Lujàn et al., 2005; Ben-Ari, 2001 & 2002). Thus, GLT-1, but not GLAST, seems to be particularly dependent on interaction with glutamatergic neurons, since it was shown that GLT-1 protein expression ceases in primary culture without supplement of neuronal factors (Schlag et al., 1998; Gegelashvili et al., 2000), its expression is reduced when synapses are lost following removal of glutamatergic afferents (Ginsberg et al., 1995 & 1996; Yang et al., 2009) and it is enhanced when synaptic activity increases (Genoud et al., 2006; Benediktsson et al., 2012). This is supported by the finding that GLT-1 interacts with proteins of the postsynaptic terminal like PSD-95 or NMDARs (González-González et al., 2008 & 2009). Postnatal up-regulation glutamate dehydrogenase (GDH)

and of GS also parallels increasing GLT-1 expression starting after P5 (Voutsinos-Porche et al., 2003b; Kugler & Schleyer, 2004). Thus, the data obtained here is in good accordance with earlier published data implicating a tight functional dependence of GLT-1, and not GLAST, on synaptic activity.

GLAST on the other hand seems to be merely uninfluenced by the maturation of the glutatergic network, as up-regulation proceeds steadily during postnatal development. This is supported by the finding that GLAST is already robustly expressed by radial glial cells during embryogenesis (Shibata et al., 1997; Hartfuss et al., 2001). This implicates that other regulatory mechanisms trigger upregulation and functional membrane integration of GLAST. Unfortunately, the explicit role of GLAST in the forebrain is still not fully unraveled. It was proposed that GLAST-mediated glutamate binding competes with mGluRs expressed by interneurons, thereby regulating inhibition in the hippocampus (Huang et al., 2004).

Several studies demonstrated that both GLAST and GLT-1 co-compartmentalize and thus intimately interact with proteins involved in energy metabolism (Rose et al., 2009; Genda et al., 2011; Bauer et al., 2012). Among these particular importance was attributed to the functional and structural cooperation of EAATs with the Na^+/K^+-ATPase, which were considered to operate as a functional unit (Cholet et al., 2002; Rose et al., 2009). This interaction seems useful as a significant part of the energy by astrocyte metabolism is used to restore the sodium gradient as a consequence of its reduction by the action of the neurotransmitter coupled transporter systems (Genda et al., 2011).

Surprisingly, it was in particularly GLT-1 that was found on perivascular endfeet during postnatal development, which might indicate a specialized function of this glutamate transporter subtype. The remarkable high glutamate transporter density at perivascular endfeet structures lead to the question whether sodium signals can be actually elicited these specialized astrocytic compartments, as would be expected from the foregoing observation in perivascular endfeet. And indeed, we found that sodium signals caused by EAAT activation can invade perivascular endfeet, originate at these specialized structures and even propagate between endfeet of adjacent astrocytes ([3] Langer et al., *in preparation*). As described before, concurrent Na^+ and Ca^{2+} signals are needed to stimulate glucose utilization from the blood (Bernardinelli et al., 2004; Porras et al., 2008), it is thus tempting to speculate that EAAT-mediated sodium signals in perivascular endfeet might serve an exceptional function for neuronal metabolic supply.

The research data presented here thus indicates that protein expression and spatial distribution of GLAST and GLT-1 are independently regulated and that both transporters occupy distinct functional niches in the developing brain as suggested e.g. by the appearance and operation of GLT-1 at perivascular structures.

Whether regulation of astrocytic glutamate transporters is also variously changed under pathophysiological conditions was addressed by another investigation enclosed. This examination demonstrated for the first time that glutamate transporter distribution and function is indeed differentially impaired in specific subtypes of reactive astrocytes *in situ* ([3] Schreiner et al., *in preparation*). As we have seen before, several studies indicated that heterogeneity among reactive astrocytes exists. Research presented here approves this idea, as we have found two distinct subpopulations of reactive astrocytes showing differential impairment of the astrocytic glutamate transporter uptake system. On the one hand, severe astrogliosis adjacent to the lesion site induced strong glutamate clustering and severe reduction in astroglial glutamate re-uptake of PRAs. Mild to moderate astrogliosis in the periphery of a mechanical lesion on the other hand was not accompanied by an apparent change in cellular distribution and glutamate uptake capacity in DRAs. PRAs within a distance of approximately 100µm surprisingly also ceased to accept the astrocyte-specific vital dye SR-101 as it was already shown for neonate astrocytes (Kafitz et al., 2008). This thus further supports the idea that reactive astrocytes partially regain juvenile feature (Robel et al., 2011). It was already firmly established in recent years that astrocytes in the cortex and the hippocampus selectively incorporate the fluorescence dye SR-101 and its fixable analogue Texas Red *in situ* and *in vivo* (Nimmerjahn et al., 2004; Kafitz et al., 2008; Nimmerjahn & Helmchen, 2012). Even though the precise uptake mechanism is still unknown, SR-101 has become a widely used and appreciated tool to identify astrocytes. Since number of astrocytes taking up SR-101 increases not until the postnatal period (Kafitz et al., 2008) and since, as shown here, induction of a severe astrogliosis results in the inability of a subpopulation of reactive astrocytes adjacent to the lesion core to label for SR-101, the use of this vital dye seems unfortunately to be limited. Thus, it would be of particular interest whether neonate astrocytes and those reactive astrocytes ceasing SR-101 acceptance might take up sulforhodamin B (SRB) or sulforhodamin G (SRG). These are newly investigated compounds of the sulforhodamine family that are specifically taken up by astrocytes and additionally by specialized cells of the astroglial lineage, e.g. Bergman glia cells (Appaix et al., 2012). If applicable the slightly shifted fluorescence spectra of SR-101 and the new compounds would then allow e.g. the distinction between immature and mature astrocytic cells as well as between proximal and distal reactive astrocytes with an easy performable approach.

The present research shows for the first time that EAAT-mediated sodium signaling in proximal and distal reactive astrocytes is dissimilar impaired. Beforehand only general down-regulation of glutamate transporter expression and overall reduction of glutamate uptake activity was reported (Chen et al., 2005; Morretto et al., 2005; van Landeghem et al., 2006). Several studies have even found glutamate transporter reversal under pathological conditions like ischemia (Gemba et al., 1994; Seki et al. 1999; Phillis et al., 2000; Rossi et al. 2000), we however couldn´t observe uptake

reversal by EAATs. Our results thus suggest that at least one week after the initial lesion raised external glutamate concentrations as they are found following traumatic brain injury (TBI) might be due to impaired, but not reversed glutamate re-uptake and other glutamate release mechanisms, respectively. It can however not be excluded that glutamate transporter reversal leads to extracellular glutamate accumulation and neuronal cell death during the acute injury phase. Some groups indeed provided experimental evidence that pointed towards a phase-dependent modification of glutamate transporter operation (QUELLEN; Grewer et al., 2008). Whether these EAAT changes in upon brain injury are causal or consequential remains unfortunately unresolved and will be an assignment of prospective research. Intriguingly, this study also showed for the first time that the multimeric composition of both astrocytic glutamate transporters is differentially altered following severe brain injury. Thus, heterogeneity of glutamate transporter does not only occur with reference to different astrocytic subpopulations, but also to the individual glutamate transporter subtypes.

To recapitulate, this composition of studies provided good evidence that astroglial glutamate re-uptake is accomplished by a differential regulation of both astrocytic glutamate transporters during development and disease. All in all, our data demonstrates that heterogeneity among astrocytes and their glutamate transporters is still a widely ill-adresses issue. Diversity exists by means of glutamate transporter subtype composition as well as multimeric complexation. The heterogeneity not only concerns the protein equipment, but also the astrocyte subtype under investigation. Although protoplasmatic astrocytes apparently act stereotypically in the healty brain, this seems not to be the case in brain injury. It thus seems that only flexible phenotypic response behavior among astrocytes can meet brains complex requirements. Glutamate transport into astrocytes is always accompanied by a profound sodium influx and thus massive changes in sodium balance. Intriguing, sodium signaling *per se* seems to be based on fundamental biological principles like compartimentalization, diffusion and coincidence detection to encode and transduce information. It might thus provide a mechanism to sense neuronal activity and respond to the consequential energy demand.

Publications

1. Schreiner & Rose, *in press* (accepted July 2012, will be published December 2012)

Quantitative Imaging of Intracellular Sodium

Alexandra E. Schreiner, Christine R. Rose

invited contribution in: CURRENT MICROSCOPY CONTRIBUTIONS TO ADVANCES IN SCIENCE AND TECHNOLOGY (2012), MÉNDEZ-VILAS A (ED.), BADAJOZ, SPAIN.

I wrote

- the first version of the manuscript

I contributed to

- drafting and revision of figures and manuscript

Quantitative Imaging of Intracellular Sodium

A. E. Schreiner[1] and **C. R. Rose**[1]

[1] Institute of Neurobiology, Heinrich-Heine-University Duesseldorf, Universitaetsstrasse 1, Duesseldorf, Germany.

A fundamental functional principle of animal cells is their ability to store energy across the plasma membrane in form of ion gradients. This is mainly realized by the activity of the Na^+/K^+-ATPase, which consumes ATP to establish an inwardly directed gradient for sodium ions. In the brain, the sodium gradient not only drives many transport processes across the plasma membrane, but also provides the basis for electrical signaling. Any change in intracellular sodium and any reduction in the sodium gradient will thus influence a multitude of processes, and breakdown of the sodium gradient during pathological conditions can have fatal consequences. Knowledge about intracellular sodium concentration and its alterations under different conditions is thus indispensable. The study of the temporal and spatial dynamics of $[Na^+]_i$ can be accomplished by fluorescence-based intracellular sodium imaging, which also enables measurements in small microdomains such as dendrites and spines or fine glial processes. In this chapter, we review the properties and application range of sodium-sensitive fluorescent indicator dyes. Furthermore, the principles of ratiometric imaging, which allows the reliable measurement of intracellular sodium concentrations, are presented. While focusing our experimental description on neurons and glial cells in brain slices, the reader will be provided with basic instructions and information on how to perform quantitative intracellular sodium imaging applicable also to other cells and tissues.

1. Introduction

1.1 Physiological Role of Sodium

For the majority of mammalian cells, the concentration of intracellular free sodium ($[Na^+]_i$) is in the range of 10-20 mM, whereas the extracellular sodium concentration ($[Na^+]_e$) is considerably higher (approximately 150 mM). This, in combination with the negative membrane potential, results in a steep inwardly directed electrochemical gradient for sodium ions. The sodium gradient is established by the permanent activity of the Na^+/K^+-ATPase, which represents the major energy consumer in cells: in the central nervous system it uses at least $^2/_3$ of the cells' energy expenditure [1]. It thereby regulates many physiological functions, providing the driving force for a multitude of transport processes across the plasma membrane. For instance, sodium is central to the homeostasis of other ions (e.g. through Na^+/H^+- or Na^+/Ca^{2+}-exchange), for osmoregulation, the uptake of nutrients or the re-uptake of transmitters in the brain (via EAATs and GATs). Furthermore, sodium serves an important signaling role, mediating action potential generation and fast excitatory transmission in neurons. It was also proposed that activity-induced astrocytic sodium transients [2, 3] represent a key signal for coupling glial metabolism to neuronal activity [4, 5].

Because of the particular importance of sodium, knowledge about intracellular sodium homeostasis and signaling is indispensable. Measurement of extra- and intracellular sodium in invertebrate preparations using ion-selective microelectrodes was already commenced in the early sixties [6], but the large tip diameter of these electrodes excluded measurement in small mammalian cells. In 1989, imaging of intracellular sodium was first reported using the newly developed fluorescent indicator sodium-binding benzofuran isophthalate (SBFI) [7], and since then, several other sodium indicators were designed [8-11]. Because these dyes (as other synthetic fluorescent indicators dyes) distribute in the entire cytosol, they not only enable measurement in the somata of small cells, but may also be used to monitor the spatial distribution of $[Na^+]$ changes in subcellular compartments. For further reading on the role of sodium in neuronal cells and neuroglia the reader is kindly referred to earlier reviews [12-15].

1.2 Basics of Ion Imaging and Sodium Indicators

The sodium imaging technique takes advantage of the so-called fluorescent sodium indicator dyes, molecules that change their spectral properties in response to the binding of sodium ions. These are composed of an ion-binding site and a fluorophore unit, which translates the conformational change of the molecule upon sodium binding into an optical signal.

Important aspects when considering the application of an indicator dye are the specificity, the affinity, the fluorescence properties and the general chemical properties of the employed molecule. First of all, a reliable sodium indicator should be highly specific for sodium over other ions. This is especially critical for K^+, the

intracellular concentration of which is more than 10-fold higher than that of sodium, and could hence impair the measurement. The indicator should also exert negligible sensitivity to changes in pH. The dissociation constant (K_d), a measure for the affinity of the ligand (sodium) to the receptor (the sodium indicator), should be in the range of the expected sodium concentration and changes thereof. As a rule of thumb, indicators are useful for measurement of ions concentrations ranging from 0.1 to 10 times of their K_d values.

Sodium binding (or unbinding) to the indicator should result in a significant change of the fluorescence emission. Furthermore, excitation and emission spectra should exert only a minimal overlap. The quantum yield, that is the emission efficacy of the fluorophore, should be as high as possible to allow for short exposure times and low indicator concentrations, thus minimizing cellular stress. On the molecular level, enough polar groups should be present to render the dye water soluble and to allow for uniform dispersion in the cytoplasm. Modified forms of sodium indicators are available, in which the polar groups are temporally masked (e.g. by acetoxymethyl esters) to enable the dyes' passage across the cell membrane. Cytoplasmic cleavage of these masking moieties then traps the indicator inside the cell by hindering its exit across the membrane.

The number of commercially available sodium indicators is still quite small (see Table 1) when compared to the wide range of calcium indicator dyes with different spectral properties, K_d, or molecular weight. In addition to SBFI, the first sodium indicator available, commonly used sodium indicator dyes include Sodium Green and the CoroNa indicators. Recently, a new sodium dye, Asante Natrium, has been developed.

Sodium Green (Molecular Probes, Invitrogen, Eugene, OR) is an indicator that has been used in a variety of imaging studies [18-20]. The Sodium Green indicator (MW 1667.6 g/mol) shows high selectivity for Na^+ over K^+ (41-fold) and a relatively high quantum yield (0.2) in sodium-containing solutions. The dissociation constant of Sodium Green is approximately 21 mM in saline, thus making it well-suited for investigation of cytosolic sodium concentrations (which is in the range of 10-20 mM). Sodium Green is excited by visible light (ex λ = 507 nm) that enables efficient excitation at 488 nm by conventional argon lasers. It exhibits an increase in fluorescence emission (em λ = 532 nm) with increasing sodium concentration. Because neither fluorescence excitation nor emission spectra shift upon sodium binding, a conventional ratiometric approach (see paragraph 1.3) is not applicable. Sodium Green can, however, be used in fluorescence lifetime imaging microscopy (FLIM) studies [21-23]. Contrary to conventional, intensity-based sodium imaging, FLIM takes advantage of a change in the exponential decay rate of the fluorescence signal (fluorescence lifetime) with changing sodium concentration. In contrast to Sodium Green, neither SBFI [24] nor CoroNa Green exhibit sodium-dependent changes in the exponential decay time and are thus not suitable for FLIM measurements (Kleinhans, Schreiner and Rose, unpublished observations).

The **CoroNa dyes** are a group of recently developed sodium indicators with quite different characteristics, consisting of the fluorescent probes CoroNa Green and CoroNa Red. The properties of **CoroNa Green** (Molecular Probes, Invitrogen, Eugene, OR) were described in detail by earlier studies [10, 25]. The selectivity of Na^+ versus K^+ binding is about 4-fold for CoroNa Green [25], thus considerably lower than that of Sodium Green. CoroNa Green (MW 585.6 g/mol) exhibits a relatively high sodium dissociation constant (K_d of 82 mM; [25]), making it well suitable for measurement of very large Na^+ transients or Na^+ changes upon a high background Na^+ concentration. As described for Sodium Green, CoroNa Green is excited by visible light and exhibits an increase in fluorescence emission intensity upon binding of Na^+ (ex λ /em λ = 492/516 nm) with just little shift in wavelength. The absorbance maximum of CoroNa Green, as for Sodium Green, is near 488 nm, which enables excitation by argon lasers commonly used in confocal microscopy. A disadvantage of CoroNa Green is that it is not well suited for AM-ester loading because it tends to leak out of the cells due to its small molecular size [10]. Dye loading via a patch-pipette ensures permanent delivery and stable intracellular dye concentrations [10]. In a promising novel approach, Lamy and coworkers encapsulated CoroNa Green in a PAMAM dendrimer-nanocontainer to counteract permanent dye extrusion [26]. The second CoroNa derivate, **CoroNa Red** (Molecular Probes, Invitrogen, Eugene, OR) is very lipophilic and allows the direct loading into cells without any modifications, such as using an AM ester precursor, needed. The dye exhibits a net positive charge leading to its accumulation in mitochondria. It undergoes a 15-fold increase of the fluorescence emission upon Na^+ binding and has a low sodium-binding affinity (K_d = 200 mM). These special properties make it suitable for investigation of mitochondrial sodium signals in intact cells [9, 27-28].

Lately, a novel sodium indicator, **Asante NaTrium Green 1 (ANG-1)**, was described [11, 17]. According to the manufacturer (TEFLabs Inc., Austin, TX), another Asante derivate, Asante NaTrium Green 2 (ANG-2), does even show improved fluorescence properties, but up to now, no publications with this dye exist. Examination of the selectivity revealed that ANG-1 exhibits a 14-fold selectivity for Na^+ over K^+, which is an intermediate value between Sodium Green and CoroNa Green (41-fold and 4-fold, respectively). ANG-1 shows a dissociation constant that is higher than the physiological baseline $[Na^+]_i$ (K_d = 39 mM), and will probably thus enable detection of a higher concentration range compared to Sodium Green and SBFI (see Table 1). Maximum ex λ and em λ are 532 nm and 550 nm, and sodium binding induces an increase in fluorescence intensity [11, 17].

Despite these new developments, the dye most commonly used for sodium imaging is still SBFI, first described in 1989 ([7]; available e.g. from Molecular Probes, Eugene, OR). It is an UV-excited dye similar in structure to the well-known calcium sensitive dye Fura-2 and has since been employed for one- and two-photon

Na$^+$ imaging in many cell types and preparations [2, 29-33]. Because of its widespread application and superior suitability for quantitative sodium imaging, it will be described in the following paragraph in detail.
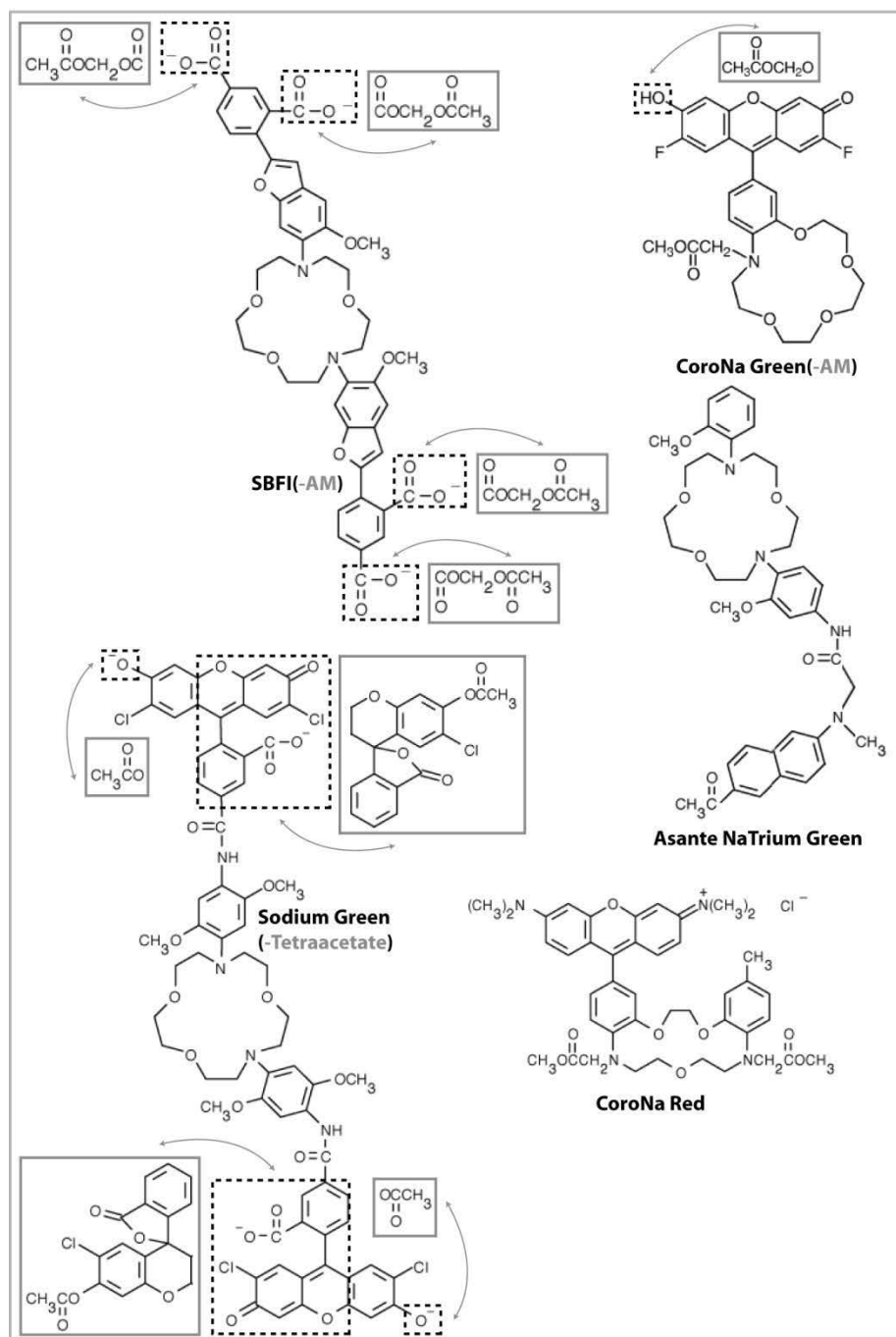
Figure 1. Chemical structure of the sodium indicators SBFI, Sodium Green, CoroNa Green, CoroNa Red and Asante NaTrium Green. The grey boxes show the masked AM- and tetraacetate moieties, respectively. The chemical structures are taken and modified from [16] and [17].

Table 1. Commercially available sodium indicators.

sodium indicator	SBFI	Sodium Green	CoroNa Green	CoroNaRed	ANG-1	ANG-2
ex λ [nm]	340/380[1]	507	492	560	517	517

em λ [nm]	505	532	516	578	540	540
K_d *in situ* [mM]	18[7]; 26[32]; 22[10]	21	82	200	39[11]; 20[17]	20 [*in vitro*]
selectivity Na+ > K+ *in vitro*	18-fold	41-fold	4-fold	ND	14-fold	n.d.
quantum yield	0.08	0.2	ND	ND	0.65	n.d.
ratiometric	yes[2]	no	no	no	no	no
laser λ CLSM [nm]	UV	488	488	488	488/514	n.d.
2hν-applicable	yes	yes	yes	yes	yes	n.d.
references	[7]; [32]; [10]	[8]	[25]; [10]	[9]	[11]; [17]	Teflabs Inc. (Austin, TX)

[1] = low Na+ sensitivity (near isosbestic point)/ high Na+ sensitivity; [2] = dual-excitation (& dual-emission) ratiometric mode applicable; ex = excitation; em= emission; CLSM = confocal laser scanning microscopy; 2hν = two-photon; SBFI = sodium-binding benzofuran isophthalate; ANG = Asante NaTrium Green; n.d. = not determined.

1.3 Ratiometric Imaging with SBFI

Ratiometric fluorescence imaging refers to a procedure, in which the intensity changes of a fluorophore are recorded after alternate use of either two different excitation wavelengths (for "dual excitation" indicators shifting their excitation spectra with ion binding) or by detection at two different emission wavelengths ("dual-emission" indicators), and a quotient ("ratio *R*") is calculated from these two values. In case of SFBI, as for other classical UV-excitable ratiometric dyes such as Fura-2, one can take advantage of the fact that the fluorescence emission is not only dependent on ion binding, but also changes with the excitation wavelength. For these dyes, a so-called "isosbestic" wavelength exists, at which absorption is independent from the ion concentration. Emission when excited at this wavelength is dependent on other factors such as dye concentration, and can serve as a "reference". Such ratiometric dyes are alternately excited at the isosbestic point and at a wavelength, where emission is maximally dependent on ion binding ("ion-sensitive" wavelength). The use of the ratio thus makes the measurement independent from confounding factors, such as variable dye concentration (e.g. bleaching) and cell thickness.

To date only one sodium-sensitive indicator, namely SBFI, exhibits the necessary prerequisites for dual excitation/emission ratiometric measurements [7]. The other aforementioned sodium indicators can only be employed for single-wavelength measurements, because they respond to sodium binding with a rise in fluorescence intensity without showing a spectral shift utilizable for the ratiometric dual-wavelength mode. Thus, a "pseudo-ratio" must be employed using a second dye (e. g. [34]), which, however, is less reliable because both dyes can exert different rates of bleaching, diffusion, or export from the cell. SBFI allows for measurements in the dual-excitation as well as in the dual-emission mode, though usually excitation with two alternating wavelengths is performed. SBFI binds sodium with a 1:1 stoichiometry and *in situ* K_d of 18-26 mM have been reported [16, 32, 35], making it well-suited to detect sodium concentrations and changes thereof that occur in the cell under physiological conditions. As reported for other ion-sensitive dyes, the properties of SBFI fluorescence and its selectivity change in intracellular environments, probably because of an increased viscosity. This includes K_d (*in vitro* K_d: 11 mM) and SBFI fluorescence absorption spectra, which show a significant shift to the left when loaded inside cells [2, 36]. The same is true for selectivity of Na+ over K+, reported to be 18-fold *in vitro*. When loaded inside cells, a significantly lower apparent K+-sensitivity of SBFI has been found [10, 31].

Upon sodium binding, the excitation maximum of SBFI (em λ = 507 nm) shifts to shorter wavelengths accompanied by an enhancement of the quantum yield and a narrowing of the excitation maximum. Hence, SBFI is usually excited near the isosbestic wavelength (ex_1 λ = 340 nm) and at a sodium-sensitive wavelength (ex_2 λ = 380 nm). *In situ*, excitation spectra indicated an isosbestic point of SBFI slightly below 340 nm [2, 36]. However, with conventional imaging systems, excitation below 340 nm is not feasible. As described above, calculating the ratio *R* (ΔF at 340nm/ΔF at 380nm) makes the measurement independent from cell size, photobleaching, non-uniform indicator distribution or dye loss from the cell. It also allows to cancel out possible movement artefacts that may arise in tissue or in cultured cells. These factors have an identical effect on both wavelengths and are therefore eliminated while the ratio is calculated. The ratiometric approach thus enables direct comparison between different experiments and quantitative measurement of signals.

SBFI can also be employed in the emission ratio mode [37]. Here, cells are excited at a single wavelength (340 nm) and fluorescence emission is collected at both 410 nm (em_2 λ; sodium-sensitive wavelength) and 590 nm (em_1 λ; virtually sodium-insensitive wavelength). Hence, the use of special UV-lasers enables high resolution ratiometric measurements with a confocal laser scanning system.

2. Sodium Imaging Techniques

2.1 Loading of Sodium Sensitive Dyes

Cell loading procedures for soluble sodium indicators can be divided into two categories. First, bulk loading procedures can be applied, which result in the staining of several cells. Second, cells can be filled individually. Loading of cell populations is most commonly achieved by employing acetoxymethyl ester (AM-) derivates of fluorescence indicators. Single cell loading is performed by delivery of the cell-impermeable salt via a sharp microelectrode, a patch-pipette or by electroporation, respectively.

The AM-ester form (in case of Sodium Green the tetraacetate form) is lipophilic and has therefore the ability to pass the cell membrane. Once inside the cell, non-specific cytosolic esterases remove the lipophilic moiety, and the polar dye is unable to passively cross the plasma membrane again. AM-loading is a well feasible and basically non-invasive method to stain dissociated cells grown in culture as well as cells in tissue slices. For brain tissue slices the so-called "bolus injection" is recommendable for AM ester loading (see [38]). For loading of sodium dyes, the procedure is described in detail by earlier publications from our laboratory (e. g. [10], [3]). In brief, the sodium indicator (final concentration in the pipette ~150μM) is repeatedly pressure-injected into the tissue through a fine-tipped glass microelectrode. After some time needed for de-esterification of the dye (~30 min), both neurons and glial cells in brain slices show acceptable staining (Figure 2). It is of note, that AM-loading works best at room temperature. Higher temperature (for instance when loading in the incubator at 37° Cel.) increase compartmentalization of the indicator in cellular organelles. Furthermore, in the absence of a perfusion system tissue degeneration is promoted, probably due to accumulation of toxic by-products that are generated during the de-esterification (formaldehyde and acetic acid).

Using AM-ester loading, many cells can thus be stained at the same time. Dead or damaged cells do not stain since dye de-esterification is necessary. Because AM-ester loading results in a high background label, bulk loading of ion indicators can only be used for detection of ion signals from the cell body and thick processes. If signals are to be recorded from fine cellular compartments and with low background, single-cell loading has to be employed [40].

To introduce the sodium indicator into single cells by the patch-clamp technique (described in detail by [2, 10, 32, 41]), or by electroporation (see [42, 43] for details, respectively), the membrane-impermeable acid salt of the sodium indicator is used. Compared to bulk loading, single-cell loading results in a superior signal-to-noise ratio with low background. Of note, relatively high indicator concentrations have to be used in the patch-pipette (0.5–2 mM) to result in acceptable fluorescence emission. Depending on the cell size and morphology, dye diffusion from the cell body to the most distal parts takes several minutes to up to one hour. When using a patch-pipette for loading, imaging can either be performed with the patch-pipette attached, which allows continuous monitoring of electrical signals in the cell, but also inherits all disadvantages brought about by the dilution of the cell with the intracellular saline and wash-out of intracellular molecules, respectively. Alternatively, if electrical signals must not be recorded, the patch-pipette can be carefully withdrawn after several minutes and the cell be allowed to reseal (see [3]).

For electroporation, the pipette containing the sodium indicator has to be positioned close or in direct contact to a chosen cell. By application of an electric field, the cell membrane permeability is temporary enhanced, thus allowing for dye diffusion into the cell. The parameters of the electric current pulse have to be determined for each cell type and the cell size separately and great care has to be taken to ensure viability of the electroporated cell (see [44]).
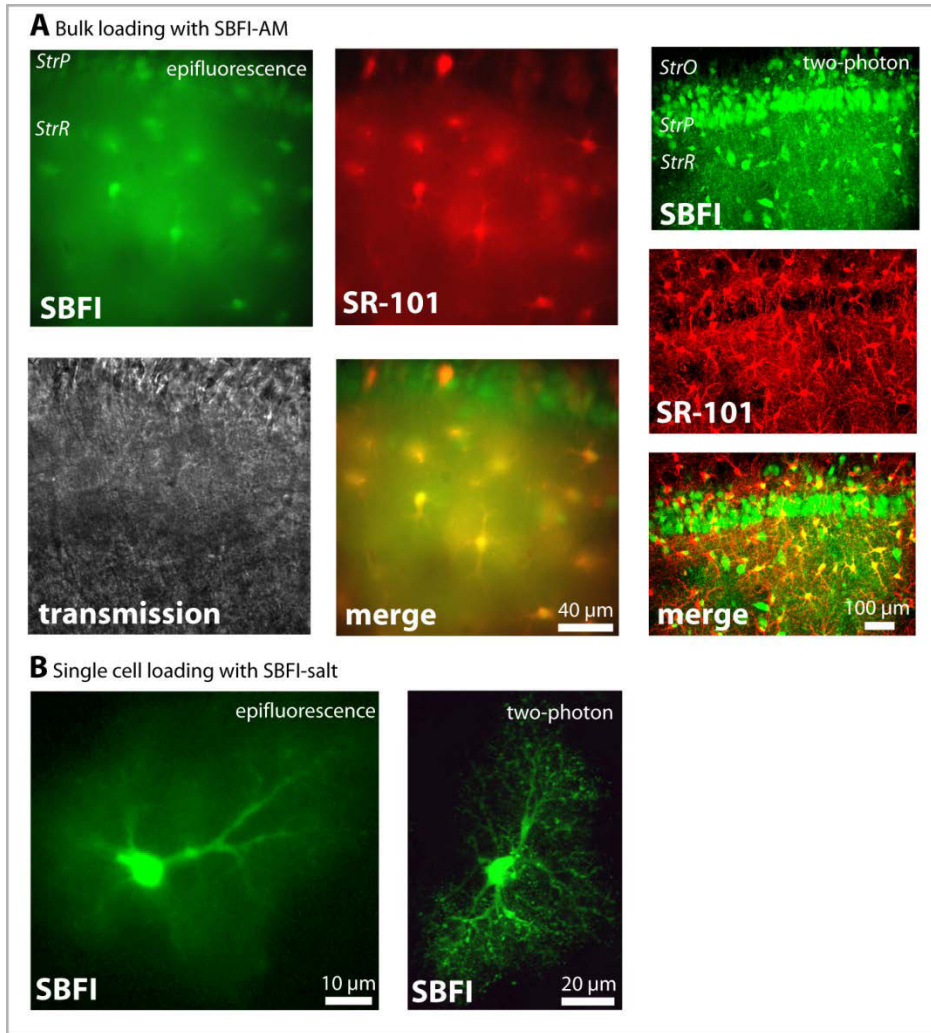
Figure 2. (A) *Top left:* epifluorescence images of the labeling pattern of SBFI (green) after AM bulk loading of a hippocampal acute slice. *Top centre*: astrocytes were co-stained with SR-101 (red; see [39]). *Bottom left and centre:* the transmitted light image and the merge of both fluorescence channels. *Right*: SBFI-AM and SR-101 staining as well as the corresponding merge of a hippocampal slice taken with a two-photon laser-scanning microscope. **(B)** Epifluorescence *(left)* and two-photon *(right)* image of a SBFI-filled hippocampal astrocyte (excited with 380 and 790 nm, respectively). The dye was in both cases introduced via patch-pipette. **(A, right)** Assembled and reproduced, with permission, from [39]; **(B, right)** courtesy of Julia Langer. All other images: A. E. Schreiner, unpublished.

2.2 Calibration of SBFI fluorescence

When employing a ratiometric, selective indicator, $[Na^+]_i$ is not measured directly. It is, however, possible to calibrate the fluorescence signals and to construct calibration curves which then allow to convert the fluorescence signals into $[Na^+]_i$. Thus, a calibration procedure is recommended, which basically consists of recording fluorescence signals in response to defined and known changes in $[Na^+]_i$. The calibration of the absolute $[Na^+]_i$ values *in situ* can be either performed after each physiological experiment or in separate experiments.

As described above, the basic properties of SBFI strongly differ *in vitro* and inside the cell, and it is thus necessary to perform calibrations *in situ* to obtain realistic values. For *in situ* calibration of intracellular SBFI fluorescence, either bulk-loaded or dialyzed cells are perfused with calibration solutions containing different sodium concentrations as well as ionophores (3 μM gramicidin D, 10 μM monensin) to equilibrate extra- and intracellular sodium concentrations (Fig. 3). Gramicidin D equilibrates Na^+, K^+, H^+ and monensin adjusts the controlled external Na^+, H^+ concentration to the ion concentration within the cell. Additionally, 100 μM ouabain may be added to the calibration solutions to block Na^+/K^+-ATPase activity and to promote equilibrium.

The first step to induce the equilibrium of sodium across the plasma membrane is the perfusion of the cells with a Na^+-free extracellular saline (0Na) containing the ionophores and ouabain. Once a stable fluorescence emission in the 0Na solution is reached, calibration solutions of different Na^+ concentrations are successively administered (e.g. 10, 20, 30, 40, 50 and 100 mM Na^+). For the chosen sodium concentrations the sequential arrangement should be altered randomly in different calibration experiments in order to avoid time-dependent artefacts. As illustrated in Fig. 3, stepwise changes in sodium concentration lead to stepwise changes in the

monitored ratio fluorescence intensity in the presence of ionophores. Plotting the ratio against the sodium concentration reveals a virtually linear relationship between $[Na^+]_i$ and the ratio in the range of 10 and 40 mM Na^+. Hence, calibration of SBFI can be reliably employed to convert relative fluorescence intensity values into absolute sodium concentrations, based on the linear correlation of both factors within this range.
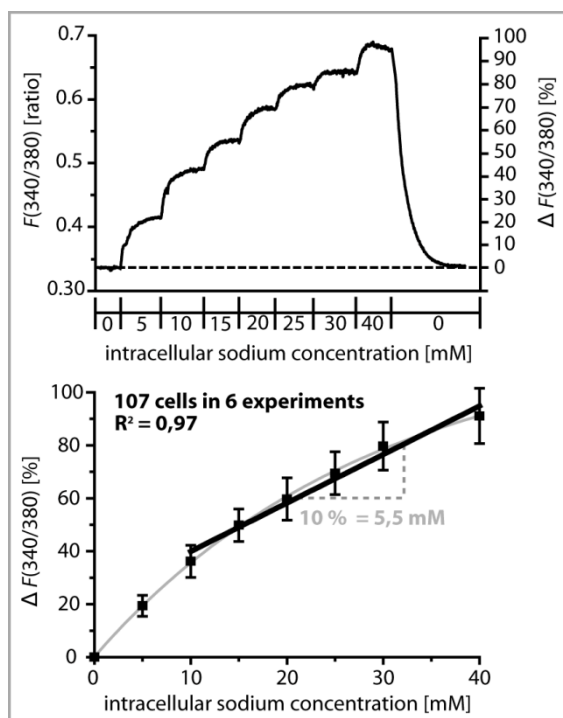

Figure 3. Calibration of SBFI fluorescence signals in astrocytes in organotypic mouse hippocampus slices. Cells were bolus-loaded and then subjected to calibration solutions with defined sodium concentrations, supplemented with ouabain and ionophores for equilibration of extra- and intracellular sodium. The upper graph demonstrates that stepwise changes in the extracellular sodium concentration from 0 to 40 mM result in stepwise changes in the fluorescence ratio of SBFI $F(340/380)$. In the lower graph, the relationship between changes in fluorescence ratio $\Delta F(340/380)$ and $[Na^+]_i$ is plotted and normalized to the ratio in sodium-free calibration saline. Shown are mean values ± S.E.M. ($n = 107$). The fit reveals a virtually linear relationship between 10 and 40 mM sodium. Within this range (and in the employed imaging system, see below), a 10% change in fluorescence emission corresponds to a change of about 5.5 mM sodium (Schreiner and Rose, unpublished).

2.3 Equipment and Technical Aspects

Dynamic wide-field fluorescence imaging can be utilized to perform quantitative sodium imaging. Fig. 4 shows a conventional imaging rig as it is used in many laboratories. Most commonly, a variable scan digital system is used (e.g. distributed by TILL Photonics). This assembly consists of (I) a monochromator as light source, i.e. an optical device that generates light of a selected wavelength at a given instant, (II) a microscope that is equipped with a suitable dichroic mirror, emission filter sets and objectives, (III) a charge coupled device (CCD) photon detector, for detection of fluorescence intensity changes, (IV) a control device for exact synchronization of the requested computer commands and the monochromator and (V) a computer with an imaging software for data digitalization and storage. The monochromator provides excitation light of a given wavelength and allows the rapid change between excitation wavelengths. With ratiometric imaging and conventional cameras working at video rates, acquisition rates of up to 15 Hz are possible.
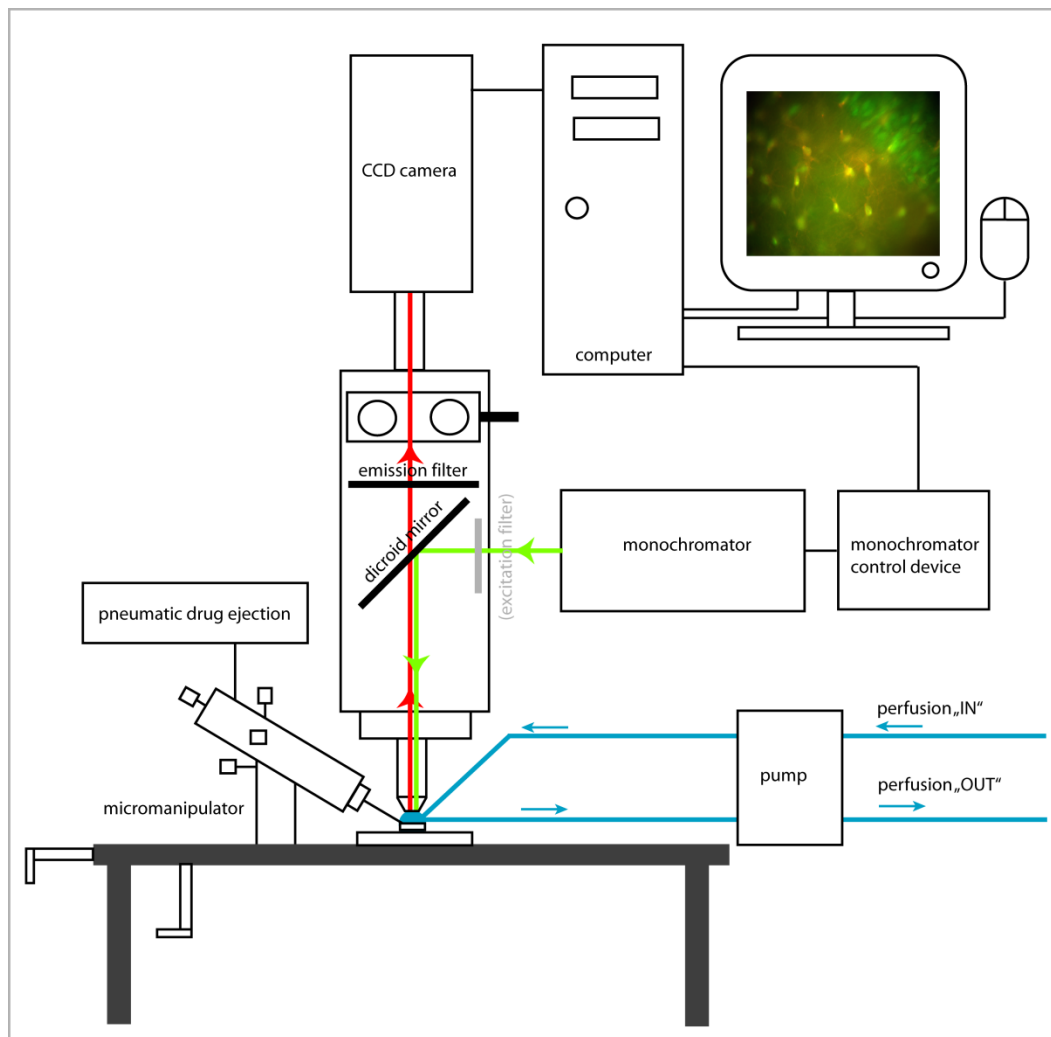
Figure 4. Setup for quantitative sodium imaging experiments, as used for sodium imaging in hippocampal brain slices in the author's laboratory. The pump provides constant perfusion with saline to ensure viability of the tissue. Pneumatic drug ejection is used for bolus loading and for application of drugs.

2.4 Quantitative Sodium Imaging Experiments

For sodium imaging, as for all experiments using fluorescence, great care has to be taken to minimize excitation and to prevent phototoxicity which can occur as by-products of photobleaching. Another important point to consider is that the maximal amplitude of sodium signals that can be obtained in cells is about 140 mM (corresponding to the complete equilibration of extra- and intracellular sodium), which is only about the 10-fold the intracellular sodium concentration at rest. Such equilibration, however, probably never occurs under physiological conditions. Sodium signals in spines of hippocampal neurons induced by short-burst activity amounted to maximally 30 mM [41], while sodium transients in astrocytes are in the low mM range [2]. This is fundamentally different from calcium signals, which arise from a background of 50-100 nM and may amount to several μM. Given the relatively low quantum efficacy of SBFI and other sodium dyes as compared to available calcium dyes, it becomes clear that sodium imaging necessitates optimal imaging conditions including maximum care to optimize the signal-to-noise ratio. To prevent cell damage by the energy-rich UV illumination, the detector sensitivity should first be maximized within the limits resolution permits, before enhancement of the excitation light. Increases in $[Na^+]_i$ are reflected by decreases in the fluorescence emission of SBFI at 380 nm excitation, thus, the baseline fluorescence emission may not be set too low.

Figure 5 shows an example of sodium imaging in an organotypic slice culture of the mouse hippocampus (Schreiner and Rose, unpublished), which was bulk-loaded with SBFI-AM after labeling of astroglial cells with sulforhodamine-101 (SR-101; Fig. 2A & 4A; see [39, 45]). SR-101 enables to reliably identify astrocytes, whereas SBFI is taken up by virtually all cell types in the brain. Three regions of interest (ROIs) were defined for fluorescence emission collection at 340 and 380 nm, specifying a background region, a neuronal and an astrocytic cell body, respectively. To induce a sodium signal in both cell types, 1 mM D-aspartate was applied by local pressure injection. This causes influx into neurons by activating ionotropic glutamate receptors of the NMDA type, and in astrocytes by activating sodium-dependent glutamate uptake (see [2]).

Application of D-aspartate caused a slight decline in fluorescence emission intensity at ex λ 340 and a large one at ex λ 380 nm of both, the astrocytic and the neuronal soma region. At the same time, virtually no change is detectable in fluorescence emission intensity of the background region at both excitation wavelengths (Fig. 5B). The fluorescence emission change recorded at ex λ 340, the weakly sodium-sensitive wavelength, can partly be ascribed to the higher absorbance of the locally applied D-aspartate diluted in HEPES- buffered ACSF (artificial cerebrospinal fluid) compared to the bicarbonate buffered ACSF with which the slices are constantly perfused (not shown). This artefact, though, influences the emission at both wavelengths in an identical manner and is overcome by ratio calculation (see paragraph 2.5).
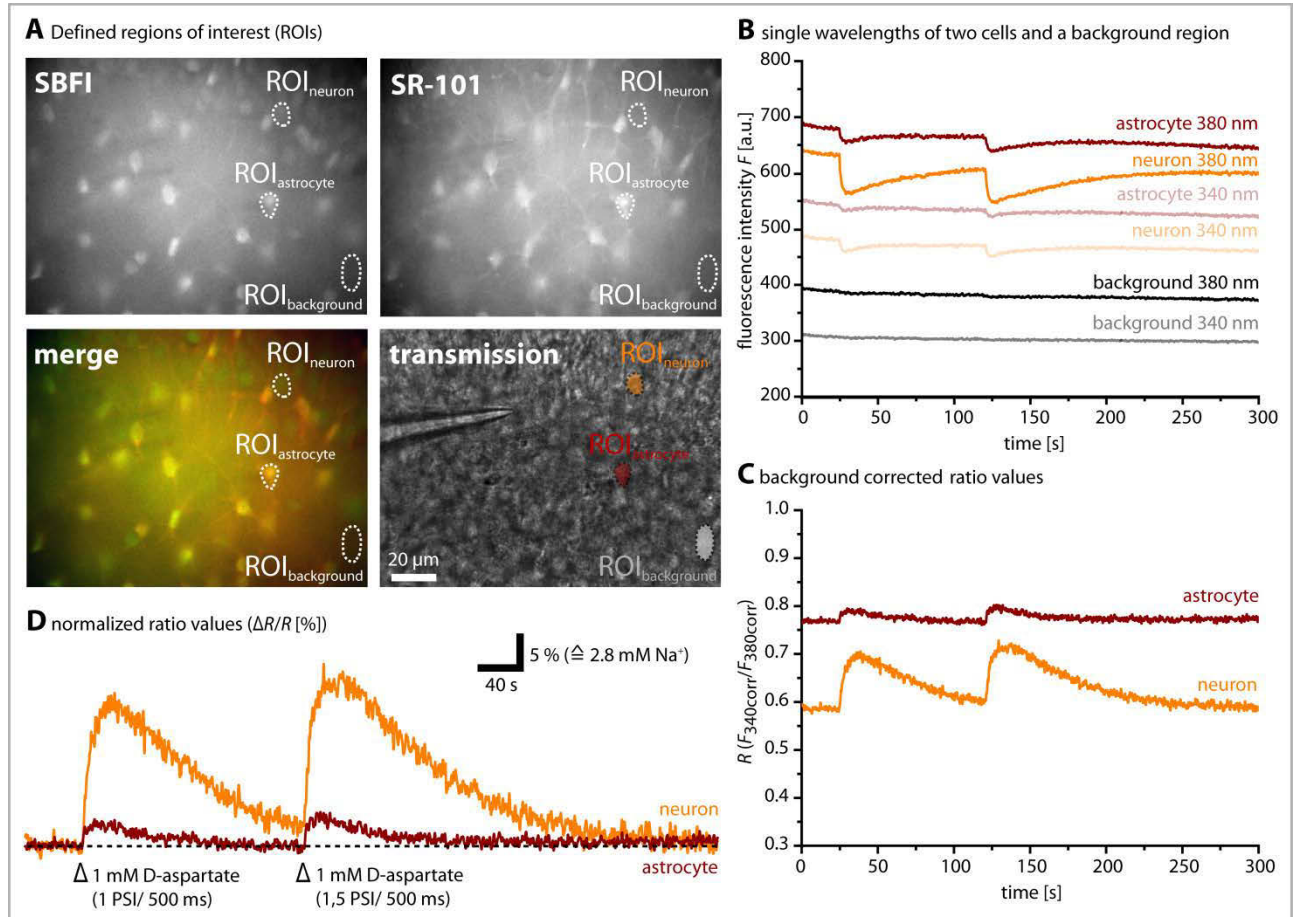

Figure 5. Sodium imaging with the sodium indicator SBFI using wide-field, ratiometric approach. Local puff application of 1 mM D-aspartate resulted in a rise in the intracellular sodium concentration of both, neurons and astrocytes in the hippocampal CA1 subregion. **(A)** shows a SBFI labeling after AM bulk loading, the corresponding labeling of astrocytes with SR-101, the merge of both fluorescence channels, and the transmitted light image in which the application pipette can be seen on the left. Fluorescence intensities were collected from the selected regions of interest (ROIs) indicated in **(A)**. **(B)** illustrates the single fluorescence intensities collected from each ROI at 340 and 380 nm. **(C)** Background corrected ratio values R. **(D)** Normalized ratio values $\Delta R/R$, which can be translated into sodium concentrations after determination of the conversion factor by calibration (Schreiner and Rose, unpublished).

Subsequent to sodium imaging experiments, data post-processing is accomplished. The considerations stated in the following apply in particular to measurements in the intact tissue. First of all one has to consider background fluorescence (F_{bg}) as interfering factor, because it may distort intracellular measurements. One component of background fluorescence is autofluorescence, that is the light emission of endogenous fluorophores in the tissue. In case of SBFI excitation, autofluorescence is in large part due to NADH/NADPH fluorescence (ex λ 290/340 nm) which, because of its low intensity (10% of basal SBFI fluorescence), is however, largely negligible [2].

A second component of background fluorescence consists of dye in the extracellular space that sticks on membranes. This is especially critical when using bulk-loading, where the dye is injected into the tissue at a high concentration. Because the background fluorescence may change during an experiment (e.g. due to photobleaching or diffusion of the dye in the extracellular space), a dynamic, rather than a static background correction should be performed. This can be done by selecting a region of interest (ROI) which is free of clearly visible cellular structures and in which fluorescence emission is then recorded continuously and in parallel to the

ROIs positioned on cellular structures. Importantly, determined background levels must be subtracted from the cellular fluorescence intensities before ratio calculation for each excitation wavelength (e. g. for SBFI: F_{340}-F_{bg340}=$F_{340corr}$ and F_{380}-F_{bg380}=$F_{380corr}$, see Fig. 5c).

After calculation of the ratio R, the values can be further processed by normalization to baseline values, thus yielding $\Delta R/R$ (Fig. 5d). Translation of the relative $\Delta R/R$ values into sodium concentrations can be accomplished after SBFI calibration was performed (see paragraph 2.2).

3. Limitations of Ratiometric Sodium Imaging

In contrast to the large toolbox of fluorescence-based calcium indicators, only few sodium indicators are available. Also, no genetically-encoded sodium indicators do exist to date. As mentioned above, sodium indicators exhibit a relatively low quantum yield and the changes in fluorescence upon Na^+ binding are quite low (rarely exceeding 10-20%, compare Fig. 3) with a consequential unfavourable signal-to-noise ratio. Although reliable quantitative ratiometric sodium imaging is feasible with SBFI, several other drawbacks of this technique exist. While SBFI *per se* is not toxic and there haven´t been any pharmacological effects of the indicator demonstrated yet, it is excited with high-energetic UV light which may cause formation of radicals and cellular damage. In addition, UV excitation is suboptimal for imaging deep in tissues due to strong scattering of short-wavelength light and an enhanced interference from sample autofluorescence. This drawback can, however, be circumvented using 2-photon excitation [32, 41].

Unlike for calcium, the possibilities for controlled experimental manipulation of intracellular sodium concentrations are restricted. No caged-compounds for sodium are available to date, and no experimentally applicable sodium chelators or buffers do exist. Furthermore, for none of the fluorescent sodium indicators, high-molecular weight dextran-compounds (e. g. 10.000 MW) are accessible, which would enable a direct comparison between "stationary" (that is non-diffusible) dye and low molecular weight indicators (< 1.000 MW). In this context, it is also important to keep in mind, that experimental manipulation of intracellular sodium concentrations is not trivial, because sodium ions are central cellular charge carriers and the sodium concentration is intimately related to the potassium concentration via the Na^+/K^+-ATPase. Thus, manipulation of sodium has fundamental consequences on the electrophysiological properties of neurons.

Compared to the sophisticated procedures necessary for calibration of intracellular calcium signals, calibration of SBFI is fairly simple and straightforward in respect to the determination of the K_d value and the conversion of relative fluorescence to concentration values, because calibration solutions with different sodium concentrations in the mM range can reliably and easily be prepared.

References

[1] Rose EM, Koo JC, Antflick JE, Achmed SM, Angers S, Hampson DR. Glutamate Transporter Coupling to Na,K-ATPase. *Journal of Neuroscience*. 2009;29(25):8143-55.

[2] Langer J, Rose CR. Synaptically Induced Sodium Signals in Hippocampal Astrocytes *In Situ*. *Journal of Physiology*. 2009;589(24):5859-77.

[3] Langer J, Stephan J, Theis M, Rose CR. Gap Junctions Mediate Intracellular Spread of Sodium Between Hippocampal Astrocytes In Situ. *Glia*. 2012;60(2):239-52.

[4] Pellerin L, Magistretti PJ. Glutamate Uptake into Astrocytes Stimulates Aerobic Glycolysis; A Mechanism Coupling Neuronal Activity To Glucose Utilization. *Proceedings of the National Academy of Science*. 1994;91(22):10625-9.

[5] Deitmer JW, Rose CR. Ion Changes and Signaling in Perisynaptic Glia. *Brain Research Review*. 2010;63(1-2):113-29.

[6] Hinke JA. The Measurement of Sodium and Potassium Activities in the Squid axon by Means of Cation-Selective Glass Micro-Electrodes.*Journal of Physiology*. 1961;156:314-35.

[7] Minta A, Tsien RY. Fluorescence Indicators for Cytosolic Sodium. Journal of Biological Chemistry. 1989;264(32):19449-57.

[8] Amorino GP, Fox MH. Intracellular Na^+ Measurements Using Sodium Green Tetraacetate with Flow Cytometry.*Cytometry*. 1995;21(3):248-56.

[9] Bernardinelli Y, Azarias G, Chatton JY. In Situ Fluorescence Imaging of Glutamate-Evoked Mitochondrial Na^+ Responses in Astrocytes.*Glia*. 2006;54(5):460-70.

[10] Meier SD, Kovalchuk Y, Rose CR. Properties of the New Fluorescent Na^+ indicator CoroNa Green: Comparism with SBFI and Confocal Na^+ imaging. *Journal of Neuroscience Methods*.2006;155(2):251-9.

[11] Lamy CM, Chatton JY. Optical Probing of Sodium Dynamics in Neurons and Astrocytes.*Neuroimage*. 2011;58(2):572-8.

[12] Rose CR. Intracellular Na^+ Regulation in Neurons and Glia: Functional Implications. *The Neuroscientist.* 1997;3(2):85-8.

[13] Kirischuk S, Parpura V, Verkhratsky A. Sodium Dynamics: Another Key to Astroglial Excitability? *Trends in Neuroscience.* 2012; *in press.*

[14] Bhattacharjee A, Kaczmarek LK. For K^+ channels, Na^+ is the new Ca^{2+}. *Trends in Neuroscience.* 2005;28(8):422-8.

[15] Allaman I, Bélanger M, Magristretti PJ. Astrocyte-Neuron Metabolic Relationship: For Better and for Worse. *Trends in Neuroscience.* 2011;34(2):76-87.

[16] Johnson I, Spence MTZ, eds. The Molecular Probes Handbook – A Guide to Fluorescent Probes and Labeling Technologies. New York, NY (USA): *Life Technologies*; 2010.

[17] Kim MK, Lim CS, Hong JT, Han JH, Jang HY, Kim HM, Cho BR. Sodium-Ion-Selective Two-Photon Fluorescent Probe for In Vivo Imaging. *Angewandte Chemie* (int. edition). 2010;49(2):364-7.

[18] Friedman JE, Haddad GG. Anoxia Induces an Increase in Intracellular Sodium in Rat Central Neurons In Vitro. *Brain Research*. 1994;663(2):329-34.

[19] Senatorov VV, Stys PK, Hu B. Regulation of Na^+K^+-ATPase by Persistent Sodium Accumulation in Adult Rat Thalamic Neurons. *Journal of Physiology*. 2000;525(2):343-53.

[20] Winslow JL, Cooper RL, Atwood HL. Intracellular Ionic Concentration by Calibration from Fluorescence Indicator Emission Spectra, its Relationship to the K_d, F_{min}, F_{max} Formula, and Use with Na-Green for Presynaptic Sodium. *Journal of Neuroscience Methods*. 2002;118(2):163-75.

[21] Szmacinski H, Lakowicz JR, Johnson ML. Fluorescence Lifetime Imaging Microscopy: Homodyne Technique Using High-Speed Gated Image Intensifier. *Methods in Enzymology*. 1994;240:723-48.

[22] Szmacinski H &Lakowicz JR. Sodium Green As a Potential Probe For Intracellular Sodium Imaging Based on Fluorescence Lifetime. *Analytical Biochemistry*. 1997;250(2):131-8.

[23] Despa S, Vecer J, Steels P, Ameloot M. Fluorescence Lifetime Microscopy of the Na+ Indicator Sodium Green in HeLa Cells. *Analytical Biochemistry*. 2000;281(2):159-75.

[24] Despa S, Steels P, Ameloot M. Fluorescence Lifetime Microscopy of the Sodium Indicator Sodium-Binding BenzofuranIsophthalate in HeLa Cells. *Analytical Biochemistry*. 2000;280(2):227-41.

[25] Martin VV, Rothe A, Gee KR. Fluorescent Metal Ion Indicators Based on Benzoannelated Crown Systems: A Green Fluorescent Indicator for Intracellular Sodium Ion. *Bioorganic&Medicinal Chemistry Letters*.2005; 15(7):1851-5.

[26] Lamy CM, Sallin O, Loussert C, Chatton JY. Sodium Sensing in Neurons with a Dendrimer-Based Nanoprobe.*ACS Nano*. 2012;6 (2):1176-87.

[27] Baron S, Caplanusi A, van de Ven M, Radu M, Despa S, Lambrichts I, Ameloot M, Steels P, Smets I. Role of Mitochondrial Na^+ Concentration, Measured by CoroNa Red, in the Protection of Metabolically Inhibited MDCK Cells. *Journal of the American Society of Nephrology*. 2005;16(12):3490-7.

[28] Azarias G, Van de Ville D, Unser M, Chatton JY. Spontanous Na^+ Transients in Individual Mitochondria of Intact Astrocytes.*Glia*. 2008;56(3):342-53.

[29] Harootunian AT, Kao JP, Eckert BK, Tsien RY. Fluorescence Ratio Imaging of Cytosolic Free Na^+ in Individual Fibroblasts and Lymphocytes. *Journal of Biological Chemistry*. 1989;264(32):19458-67.

[30] Levi AJ, Lee CO, Brooksby P. Properties of the Fluorescent Sodium Indicator "SBFI" in Rat and Rabbit Cardiac Myocytes.*Journal of Cardiovascular Electrophysiology*. 1994;5(3):241-57.

[31] Rose CR, Ransom BR. Intracellular Sodium Homeostasis in Rat Hippocampal Astrocytes. *Journal of Physiology*. 1996;491(2):291-305.

[32] Rose CR, Kovalchuk Y, Eilers J, Konnerth A. Two-photon Na^+ Imaging in Spines and Fine Dendrites of Central Neurons.*European Journal of Physiology*. 1999;439:201-7.

[33] Bennay M, Langer J, Meier SD, Kafitz KW, Rose CR. Sodium Signals in Cerebellar Purkinje Neurons and Bergmann Glia Cells Evoked by Glutamatergic Synaptic Transmission. *Glia*. 2005;56(10):1138-49.

[34] Honsek SD, Walz C, Kafitz KW, Rose CR. Astrocyte Calcium Signals at Schaffer Collateral to CA1 Pyramidal cell Synapses Correlate with the Number of Activated Synapses but not with Synaptic Strength.*Hippocampus*. 2010;22(1):29-42.

[35] Diarra A, Sheldon C, Church J. In Situ Calibration and $[H^+]$ Sensitivity of the Fluorescent Na^+ indicator SBFI.American Journal of Physiology: *Cell Physiology*. 2001;280(6):C1623-33.

[36] Borzak S, Reers M, Arruda J, Sharma VK, Sheu SS, Smith TW, Marsh JD. Na+ Efflux Mechanism in Ventricular Myocytes: Measurement of $[Na^+]i$ with Na^+-Binding BenzofuranIsophalate. *American Journal of Physiology*.1992;263(3Pt2):H866-74.

[37] Baartscheer A, Schumacher CA, Fiolet JW. Small Changes of Sodium in Rat Ventricular Myocytes Measured in Emission Ratio Mode. *Journal of Molecular and Cellular Cardiology*. 1997;29(12):3375-83.

[38] Stosiek C, Garaschuk O, Holthoff K, Konnerth A. In Vivo Two-Photon Calcium Imaging of Neuronal Networks.*Proceedings of the National Academy of Science*. 2003;100(12):7319-24.

[39] Kafitz KW, Meier SD, Stephan J, Rose CR. Developmental Profile and Properties of Sulforhodamine 101-Labeled Glial Cells in Acute brain slices of rat hippocampus. *Journal of Neuroscience Methods*.2008;169(1):84-92.

[40] Reeves AM, Shigetomi E, Khakh BS. Bulk Loading of Calcium Indicator Dyes to Study Astrocyte Physiology: Key Limitations and Improvements Using Morphological Maps. *Journal of Neuroscience*. 2011;31(25):9353-8.

[41] Rose CR, Konnerth A. NMDA Receptor-Mediated Na^+ Signals in Spines and Dendrites. *Journal of Neuroscience*. 2001;21(12):4207-14.

[42] Molleman A. Patch Clamping: An Introductory Guide to Patch Clamp Electrophysiology.Chichester, WS (UK): John Wiley and Sons; 2003.

[43] Tsong TY. Electroporation of Cell Membranes.*Biophysiological Journal*. 1991;60(2):297-306.

[44] Nevian T, Helmchen F. Calcium Indicator Loading of Neurons Using Single-Cell Electroporation. *PflügersArchiev*. 2007;454(4):675-88.

[45] Nimmerjahn A, Kirchhoff F, Kerr JN, Helmchen F. Sulforhodamine 101 as a Specific Marker of Astroglia in the NeocortexIn Vivo. *Nature Methods*. 2004;1(1):31-7.

2. Schreiner et al., *submitted* (submitted October 2012, *under review*)

Heterogeneity of GLAST and GLT-1 in the Developing Postnatal Hippocampus

Alexandra E. Schreiner, Martin C. Stock, Christine R. Rose, U. Rüther, Karl W. Kafitz

JOURNAL OF COMPARATIVE NEUROLOGY

Impact factor [2011]: 3.808

I performed

- about 80% of experiments and data analysis

I contributed to

- the experimental design

- interpretation of data

- drafting and revision of figures and manuscript

3. Schreiner et al., *manuscript* (*in preparation*)

Heterogeneous Alterations of Glutamate Transporter Expression in Proximal and Distal Reactive Astrocytes

Alexandra E. Schreiner, Martin C. Stock, J. Langer, Karl W. Kafitz, Christine R. Rose

This manuscript will be submitted in spring 2013.

I performed

- about 80% of experiments and data analysis

I contributed to

- the experimental design

- interpretation of data

- drafting and revision of figures and manuscript

LAMINAR AND SUBCELLULAR HETEROGENEITY OF GLAST AND GLT-1 IMMUNOREACTIVITY IN THE DEVELOPING POSTNATAL MOUSE HIPPOCAMPUS

SCHOLARONE™
Manuscripts

Graphical Abstract

The glial glutamate transporters GLAST and GLT-1 are essential for the maintenance of low extracellular glutamate levels. Performing a comparative analysis using immunohistochemistry, western blotting and high-resolution fluorescence microscopy, we uncover a remarkable subcellular heterogeneity of their laminar and subcellular expression profile in the developing postnatal mouse hippocampus. While GLAST is distributed rather homogeneously, GLT-1 is clustered at perisynaptic processes and astrocyte endfeet, indicating that it might serve a specialized role during formation of the hippocampal network.
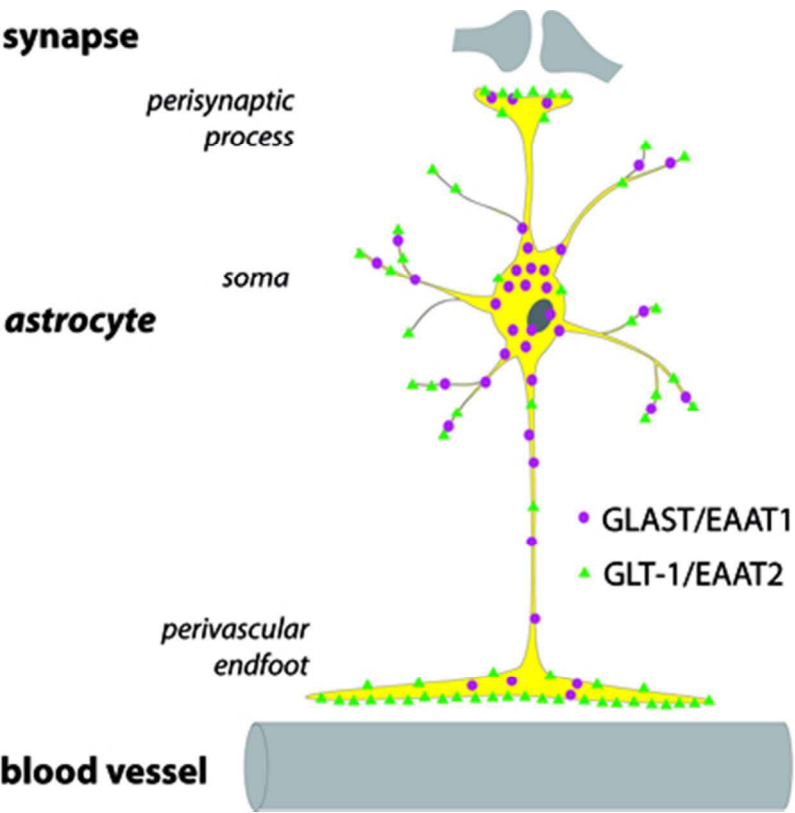
140x141mm (72 x 72 DPI)

LAMINAR AND SUBCELLULAR HETEROGENEITY OF GLAST AND GLT-1 IMMUNOREACTIVITY IN THE DEVELOPING POSTNATAL MOUSE HIPPOCAMPUS

Alexandra E. Schreiner[1], Martin C. Stock[2], Ulrich Rüther[2], Christine R. Rose[1]*

& Karl W. Kafitz[1]

[1]Institute of Neurobiology and [2]Institute for Animal Developmental and Molecular Biology, Heinrich Heine University Duesseldorf, Universitaetsstrasse 1, 40225 Duesseldorf, Germany.

Running head: Heterogeneity of glutamate transporters

Associate Editor: Dr. Kathleen S. Rockland

Key Words: astrocyte, GFAP, S100ß, perivascular endfeet

*Corresponding author: Institute of Neurobiology, Heinrich Heine University Duesseldorf, Universitaetsstrasse 1, Building 26.02.00, 40225 Duesseldorf, Germany.

Tel.: +49 (0)211 81-13416, Fax: +49 (0)211 81-13415.

E-mail: rose@uni-duesseldorf.de

Abstract

Astrocytes express two sodium-coupled transporters, GLAST and GLT-1, which are essential for the maintenance of low extracellular glutamate levels. Here, we performed a comparative analysis of the laminar and subcellular expression profile of GLAST and GLT-1 in the developing postnatal mouse hippocampus using immunohistochemistry and western blotting and employing high-resolution fluorescence microscopy. Astrocytes were identified by co-staining with GFAP or S100ß. In CA1, the density of GFAP-positive cells and GFAP expression rose during the first two weeks after birth, paralleled by a steady increase in GLAST immunoreactivity. Up-regulation of GLT-1 was completed only at postnatal days (P) P20-25 and thus delayed by about ten days. Western blots further revealed a differential up-regulation of multimeric and monomeric forms of GLAST and GLT-1 during this period. GLAST staining was highest along *stratum pyramidale* and was preferentially expressed in astrocytes at P3-5. GLAST immunoreactivity showed no preferential localization to a specific cellular compartment. GLT-1 exhibited a laminar expression pattern from P10-15 on, with highest immunoreactivity in the *stratum lacunosum-moleculare*. At the cellular level, we found that GLT-1 immunoreactivity did not entirely cover astrocyte somata and exhibited clusters at perisynaptic processes. In juvenile animals, discrete clusters of GLT-1 were also detected at perivascular endfeet. Our results thus uncover a hitherto unnoticed and remarkable subcellular heterogeneity of GLAST and GLT-1 expression in the developing hippocampus. The clustering of GLT-1 at astrocyte endfeet indicates that it might serve a specialized functional role at the blood-brain barrier during formation of the hippocampal network.

Introduction

Glutamate is the major excitatory neurotransmitter of the central nervous system. Upon its release into the extracellular space, it is efficiently removed by high-affinity, sodium-dependent glutamate transporters, located at neuronal and glial plasma membranes (Danbolt, 2001; Rothstein et al., 1994). Astrocytes, which express the glutamate transporters GLAST/EAAT1 (glutamate-aspartate transporter/excitatory amino acid transporter 1; Storck et al., 1992) and GLT-1/EAAT2 (glutamate transporter 1/ excitatory amino acid transporter 2; Pines et al., 1992), account for the majority of the glutamate uptake activity in the brain (Danbolt et al., 1992; Matsugami et al., 2006). Glial glutamate uptake results in a fast decline in the extracellular glutamate concentration, shapes the time course of synaptic conductance, contributes to the input specificity of glutamatergic synapses, and prevents excitotoxicity (Danbolt, 2001). Furthermore, Na^+ signals accompanying glutamate uptake have been proposed to serve a central role in coupling glial to neuronal metabolism (Allaman et al., 2011; Deitmer and Rose, 2010).

In addition to their function at established synapses, glutamate transporters have also been assigned a critical role during development and maturation of neuronal networks (Kudryashov et al., 2001; Nosyreva and Huber, 2005), by regulating neuronal migration (Matsugami et al., 2006; Shibata et al., 1997), proliferation (Gilley and Kernie, 2011), and synapse formation and function (Matsugami et al., 2006). In the hippocampus proper, as in most brain regions, neurogenesis is largely completed at birth, while gliogenesis and astrocytic maturation are still in progress and parallel dendritic growth and synaptic maturation (Freeman, 2010; Ming and Song, 2005; Pfrieger, 2002). Astrocyte differentiation comprises reorganization of fine processes and formation of defined cellular domains (Bushong et al., 2004), formation of the gap junctional network (Schools et al., 2006), as well

4

as alterations in ion channel and transporter expression (Bordey and Sontheimer, 1997; Seifert et al., 2009).

The general expression pattern of astrocytic glutamate transporters has been the focus of several investigations (Danbolt, 2001). Earlier studies employing immunohistochemistry at the ultrastructural level showed that in the rat hippocampus and cerebellum both, GLAST and GLT-1 transporters are located close to synapses and at a lower level at perivascular astrocyte endfeet (Chaudhry et al., 1995; Lehre and Danbolt, 1998; Lehre et al., 1995). Immunohistochemistry on the light microscopic level and immunoblotting further revealed significant differences between different brain regions and established a general increase in glutamate transporter expression from birth to adulthood (e.g. Furuta et al., 1997; Rothstein et al., 1994; Ullensvang et al., 1997). In addition, it was found that GLAST is predominately expressed by radial glial cells and immature astrocytes, while GLT-1 is regarded as the major transporter of mature astrocytes (Hartfuss et al., 2001; Yang et al., 2009).

Because astrocytes are decidedly polarized cells, with delicate perisynaptic processes contacting synapses on one side and highly specialized endfeet contacting blood vessels on the other (Mathiisen et al., 2010; Reichenbach et al., 2010), glutamate transporter expression might be heterogeneous not only in respect to development, but also at the cellular and subcellular level. In the present study, we therefore characterized the laminar and subcellular protein expression profile of GLAST and GLT-1 hippocampus of mice during postnatal development using immunohistochemistry, western blot analysis and high-resolution fluorescence microscopy.

Materials and Methods

Animals and tissue preparation

All experiments were carried out in accordance with the institutional guidelines of the Heinrich Heine University Duesseldorf as well as the European Communities Council Directive (86/609/EEC). Balb/c mice (*mus musculus*) of both genders at different postnatal stages (P3-P5; P10-P15; P20-P25; adults (P60-P70)) were used for this study. Animals older than postnatal day 10 (P10) were decapitated following CO_2 anesthesia, which was omitted in younger animals. Brains were quickly removed and immersion-fixed for two to three days at 4°C in 4% paraformaldehyde (PFA) in phosphate buffered saline (PBS). The tissue was stored in PBS for at least one day at 4°C until it was sliced at a vibratome (Campden Instruments Ltd., Leicester, UK). Transversal hippocampus sections (30 μm) were used for immunohistochemical processing. For stimulated emission depletion (STED) microscopy, slices of P15 animals were prepared at a HM 650 V vibratome (8 μm, Thermo Scientific, Germany).

All chemicals were purchased from Sigma-Aldrich Chemical (Germany) if not stated otherwise.

Antibody characterization

All antibodies employed in this study are listed in table 1. The following antisera, representing well established, commercially available standard markers, were utilized in this study: guinea-pig GLT-1 antiserum directed against the C-terminus of rat GLT-1 (Millipore Corp., Ireland; e.g. Benediktsson et al., 2012), guinea-pig GLAST antiserum directed against the C-terminus of rat GLAST (Millipore Corp., Ireland; e.g. Zhou et al., 2006). Beyond previous studies showing validation of these antibodies (Suaréz et al., 2000; Zhu et al., 2008; Brunne et al., 2010) a detailed characterization of both is provided by the present study.

For specific identification and morphological characterization of astrocytic cells, polyclonal rabbit antibodies against GFAP (GFAP-pAb; Dako Cytomation, Denmark; Wu et al., 2005; Brunne et al., 2010) and S100ß (Abcam, United Kingdom; Magavi et al., 2012) were employed. As the specific epitope(/s) of GFAP-pAb was (/were) not determined, we compared the gained staining pattern with results obtained with a monoclonal mouse antibody detecting GFAP (GFAP-mAb) (Sigma Aldrich, Germany; Olabarria et al., 2010; Brunne et al., 2010).

Initial control experiments employing double-labeling with antibodies for neuronal structures and the antibodies used in the present study never showed colocalization, suggesting that the labeling presented here is of pure glial nature.

According to manufacturer, the GFAP-mAb epitope amino acid sequence is: LQSLTCDVESLRGTNESLERQMREQEERHAREAASYQEALTRLEEEGQSLKDEMARH LQEYQELLNVKLALDIEIATY. The database UniProt-KnowledgeBase revealed that this sequence corresponds to a part of the coil IIb structure of the rod domain. Both, GFAP-mAb and –pAb labeled the same cells and subcellular compartments, however more structures were visualized by GFAP-pAb. All three antibodies (S100ß, GFAP-mAb and –pAb) reliably stained cells that could be either identified by prior SR-101 incorporation, which is a vital dye exclusively taken up by astrocytes, or cells expressing GFP under the GFAP promoter (data not shown). Thus these antibodies can be considered specifically recognizing their supposed target. Moreover, virtually all S100ß positive cells stained positive for GFAP (data not shown).

Standard fluorochrome-conjugated antibodies (AlexaFluor, Invitrogen) were used as secondary antibodies for immunohistochemistry. To visualize immunoblots, HPR-conjugated antibodies were used (for details see table 1).

All antibodies used for immunohistochemistry were employed for western blot analysis. To assure comparability, the investigated specimen was in both cases murine

hippocampal tissue. For all antibodies used, pattern of bands and their molecular weight was comparable with calculated (e.g. utilizing the ExPASy compute pl/Mw tool) and experimental data published by other groups (e.g. Haugeto et al., 1996; Suaréz et al., 2000; Brunne et al., 2010).

Immunohistochemistry

Hippocampal sections were permeabilized and blocked in PBS containing 0.25% triton-X100(TX) and 2% normal goat serum (NGS, Invitrogen; blocking reagent) for 90 min at 4°C followed by incubation with rabbit-anti-GFAP (1:1000) or rabbit-anti-S100ß (1:100, in blocking reagent) over night at 4°C. After 5 washes (2x brief, 3x 15 min), sections were incubated either with guinea pig-anti-GLAST or with guinea pig- anti-GLT-1 (both 1:1000, 4 hrs. at room temperature; RT). All following working steps were likewise performed at RT. Excess primary antibody was removed with 5 washes (2x short, 3x 15 min) using 2%NGS in PBS. Anti-rabbit-AlexaFluor594 and anti-guinea pig-AlexaFluor488 were used for visualization of antibody binding (both 1:100, 2%NGS/PBS, 2 hrs.). Following 6 washes in PBS (10 min each), a DAPI (Invitrogen) counterstain was performed. The slices were washed for another 3 times (10 min) and mounted on glass slides with mowiol/DABCO (Calbiochem, Fluka). For super-resolution microscopy, biotinylated anti-guinea pig (1:50, 2%NGS/PBS, 2 hrs.; Biozol, Germany) together with streptavidin-conjugated Atto 647N (1:100, 2%NGS/PBS, 2 hrs.); Atto Tec, Germany) and Chromeo 494 (Active Motive, Germany) were employed as secondary antibodies (1:100, 2%NGS/PBS, 2 hrs.). Labeling patterns were identical to those found with the Alexa fluorophores.

Identical conditions in tissue processing were employed in all individually performed stainings. Negative controls were run in parallel to each staining by either omitting all or one of the primary antibodies. Control stainings omitting one of the primary antibodies exhibited identical labeling patterns for the remaining antibody as for the doublestainings. Excluding

both primary antibodies never resulted in a staining. This was equally true for tissue processed for confocal and for STED microscopy.

Changes in the number of GFAP-immunopositive cells in the hippocampal CA1 subregions (*strata oriens*, *pyramidale* and *radiatum)* of the different age groups were assessed utilizing maximum projections of whole frame confocal z-stacks (159.84 x 119.84 μm, 30 μm thick Z-stack, 30 optical sections each 1 μm). Independent measurements were performed for each age cohort. Densities of GFAP(+) cell bodies were calculated per volume tissue, on the basis of the field of analysis and the thickness of the tissue probe imaged. All GFAP(+) cell bodies depicted in a given frame were treated as a count. Data on the experimental groups were expressed as the mean number of cells ± standard error of the mean (S.E.M.).

Western blotting

For western blotting, whole hippocampi or the hippocampal CA1 subfield including the *strata oriens*, *pyramidale* and *radiatum* were excised, frozen in liquid nitrogen and homogenized at 4°C in RIPA (radio-immunoprecipitation assay) buffer containing 1% deoxycholic acid (NP-40), 0.25% sodium deoxycholate, protease inhibitors (CompleteMini, Roche, Germany), 150 mM NaCl and 50 mM Tris-HCl adjusted to a pH of 7.4. The homogenate was centrifuged at 13.000 *g* for 10 min and 4x Laemmli sample buffer (5% sodium dodecyl sulfate (SDS), 43.5% glycerol, 100mM DL-dithiothreitol (DTT), 0.02% bromphenol blue, 20% 2-mercaptoethanol, 125 mM Tris-HCl adjusted to a pH of 6.8) was added to the supernatant. Proteins were electrophoretically separated on 10% gels by sodium dodecyl sulfate-polyacrylamide gel electrophoresis (SDS-PAGE). Subsequently, the proteins were transferred electrophoretically to PVDF membranes (Polyvinylidene fluoride). Strips of the PVDF membranes were pre-incubated in PBS containing 0.1% tween and 5% milk powder over night at 4°C. To this blocking solution, either guinea pig-anti-GLAST, guinea pig-anti-GLT-1 or rabbit-anti-GFAP were added in a 1:2000 dilution and applied to the PVDF membrane for 1

hour (RT). Bound immunoglobulins were visualized using horseradish peroxidase-conjugated goat anti-rabbit or goat anti-guinea pig IgG in a 1:2000 dilution (incubated for 30 min at RT) and the enhanced luminol chemiluminescence technique (ECL-kit, Amersham, Germany). In parallel, a detection of the relative protein content of every probe was performed using an antibody against α-actin. The resulting chemiluminescence was detected using the luminescent image analyzer LAS-4000 (Fujifilm Europe GmbH, Germany).

For standardization of the probes, an α-actin alignment was performed. Since many proteins change in their expression quantity during postnatal development, leading to incorrect standardization, we additionally performed a GAPDH and α-tubulin alignment of the α-actin alignment (Suppl. Fig. 1). This control experiment demonstrated no difference between α-actin and the housekeeping protein GAPDH, but an increase in α-tubulin protein levels. These results are in line with findings showing that the expression of the α1 and α2 isoform remains constant during the postnatal period, whereupon other α-tubulin isoforms exhibit an increase in protein levels during development. Thus, pan-detection of α-tubulin was not suitable for normalization of protein contents of different age stages during the first postnatal weeks and α-actin was used instead in this study.

Western blot data were quantified using Axiovision software (Zeiss, Germany). Background-corrected grey values of the given protein were divided by the α-actin grey value. All resulting data were normalized to the value determined for the adult animals.

Confocal and STED microscopy and image processing

Immunofluorescence was analyzed by a confocal laser scanning system at an Olympus BX51WI microscope (FV300, Olympus, Germany). Images were collected with either a 20x/0.50 (UMPlanFl, Olympus), a 40x/0.80 (LUMPlan, Olympus) water immersion or a 60x/1.40 (PlanApoVC, Nikon, Germany) oil immersion objective. A Kalman filter 4 was applied for every scan. Fluorescent images labeled with AlexaFluor488 and AlexaFluor594

were collected using an excitation wavelength of 488 (multiline argon ion laser) and 543 nm, respectively (helium neon laser; both Melles Griot, Germany). Simultaneous or sequential scanning of both fluorophores revealed no difference in their staining pattern, indicating no cross-excitation or spectral bleed-through. Stacks of optical sections (1 μm) were taken. Extended focus images are shown as indicated in the figure legend and were calculated from z-stacks of optical sections using ImageJ software (NIH, USA). Images were overlaid or inverted employing Adobe Photoshop CS2 (Adobe Systems, CA). The PMT settings and the image processing were kept constant when comparing the different age groups.

To improve spatial resolution, documentation of sets (n=5) of immunofluorescence-labeled tissue slices was further performed by taking advantage of super-resolution microscopy employing a Leica TCS SP5 STED (stimulated emission depletion; Leica Instruments, Mannheim; Germany) with a 100x /1,4 NA STED oil objective (Leica Instruments, Mannheim; Germany). Fluorophores were excited by pulsed lasers (excitation wavelengths: 531 nm and 635 nm; Pico Quant, Berlin, Germany). Depletion was achieved by a MaiTai HP BB laser (SpectraPhysics, Darmstadt, Germany) at 750 nm. Every image underwent 2D deconvolution using LASAF software (Leica Instruments, Mannheim; Germany). Color coding and slight adjustments in brightness of the final figures were done with Adobe Photoshop CS2. For adjustment in brightness, all images were corrected with the identical settings.

Statistics

Unless specified otherwise, data are expressed as means ± S.E.M.. Data were analyzed using an unpaired student´s t-test. In all cases, a *p* value < 0.05 expressed a significant difference (* *p* < 0.05; ** *p* < 0.01; *** *p* < 0.001). "n" represents the number of slices and "N" the number of individuals, if not stated otherwise.

Results

GFAP expression in the developing hippocampal CA1 region

For identification of astrocytes, we used GFAP, a well-characterized and widely used marker for mature astrocytes including at least a subset of radial glial cells (Brunne et al., 2010; Middeldorp and Hol, 2011). We first established the time course of GFAP expression as well as the number of GFAP-positive cells during postnatal development in our preparation by immunohistochemistry and western blot analysis. To this end, we employed a polyclonal antibody against GFAP, which exhibited favorable properties compared to a monoclonal antibody tested for this study. Preliminary tests revealed that GFAP-pAb binds to more astrocytic structures, particularly in neonate astrocytes and radial glial cells, and that extra protein bands are detected in western blots, the molecular weight of which matches well the specific GFAP isoforms (not shown; Middeldorp and Hol, 2011). Thus, we employed GFAP-pAb for our study as astrocytic pan-marker, as proposed earlier (Brunne et al., 2010).

Labeling the hippocampal CA1 region for GFAP revealed considerable changes in the density and the distribution of GFAP-immunoreactive structures during postnatal development (Fig. 1A). From P3-5 to P10-15, the density of GFAP-immunoreactive structures exhibiting astroglial morphology increased especially within the *strata oriens* and *radiatum*. In parallel, the volume of the hippocampal layers increased. Afterwards, these parameters remained stable until adulthood. Morphological analysis at the cellular level revealed that the structure, which was labeled by GFAP immunoreactivity, changed its intracellular organization during the first postnatal weeks (Fig. 1B). In general, the GFAP-immunoreactivity in the neonate hippocampus at P3-5 appeared frayed and rough (Fig. 1B). Later on, the GFAP-immunoreactive structures became more and more evenly shaped and homogenously distributed (Fig. 1B) pointing to a rearrangement and modification of the intracellular GFAP network.

Cell counting in the CA1 region of the hippocampus revealed that the number of GFAP-immunoreactive cells per μm^3 triplicated from P3-P5 to P10-P15 (3.3 ± 0.2 and 10.8 ± 0.4 GFAP-positive cells per 100,000 μm^3, respectively; Fig. 1C). Thereafter, a stable value of approximately 7 GFAP-positive cells per 100,000 μm^3 was found for the juvenile and adult (7.8 ± 0.3 and 7.4 ± 0.3 per 100,000 μm^3). In aged animals (18 months), this value was maintained (6.7 ± 0.2 per 100,000 μm^3; data not shown). In summary, our results show a strong increase in the density of GFAP(+)-astrocytes in the second postnatal week. Between P10-15 and P20-25, cell density declined again, probably due to increasing tissue volume during this period.

To quantitatively determine the relative GFAP expression levels, we performed a western blot analysis of the hippocampal CA1 subregion including the *strata oriens, pyramidale, radiatum and lacunosum-moleculare*. The 50 kDa GFAP protein content detected in the CA1 homogenates increased abruptly between P3-P5 and P10-15 (3.1-fold; p < 0.01) and remained constant thereafter (P20-P25 and adult tissue; Fig. 1D and 1E).

Taken together, our results confirm that overall GFAP expression, the number and the morphology of GFAP-immunoreactive cells in the hippocampal CA1 region undergo substantial changes during postnatal development.

Distribution of GLAST-immunoreactivity in CA1

To visualize astroglial glutamate transporter expression, we performed double stainings detecting either GLAST or GLT-1 together with GFAP in neonate (P3-P5), early postnatal (P10-P15), juvenile (P20-25) and adult mice (P60-P70). In the neonate hippocampus (P3-P5), prominent GLAST-immunoreactivity (IR) was observed in the CA1 region, particularly in the radially elongated GFAP-positve processes that traverse the *strata oriens* and *pyramidale*. GLAST-immunoreactive (IR) cells without GFAP labeling were only found in exceptional cases (Fig. 2A-C). In the *stratum radiatum,* mainly astrocytic cell bodies were labeled for

GLAST (cf. Fig. 5). Both, the GFAP as well as the GLAST-labeling pattern in this layer exhibited a narrow stellate morphology.

At P10-P15, some of the astrocytes traversing the pyramidal cell layer showed an intense immunoreactivity alike the unipolar radial processes observed in the neonate (Fig. 2D-F). Compared to earlier developmental stages, these cells showed a more branched morphology. At P10-15, a characteristic labeling of fine fibers (approximately 0.5 μm in diameter) crossing almost the entire hippocampal subregion appeared for the first time in the *strata radiatum* and *oriens* (Fig. 2D-F). The strongest GLAST immunofluorescence was still observed in the *stratum pyramidale*. Additional punctate GLAST-positive labeling of variable intensities and densities was found in close association with neuronal somata during all stages investigated.

The P20-P25 and adult hippocampi showed quite similar labeling patterns for GLAST (Fig. 2G-L). In the adult, however, fewer astrocytic processes were distinctively labeled by GLAST and a more homogenous subcellular GLAST distribution was detected. Furthermore, GLAST-IR puncta, arranged like beads on a chain, passed through the *stratum radiatum* perpendicular to the pyramidal cell layer in hippocampi from adult animals.

Distribution of GLT-1-immunoreactivity in CA1

In contrast to GLAST (cf. Fig. 2), GLT-1 showed no differential laminar label at P3-P5 (Fig. 3A-C). Only a few detached GLT-1-IR-cells located either in the *strata oriens or lacunosum-moleculare* were detectable. In these cells, GLT-1 was highly accumulated adjacent to presumptive astrocytic cell bodies (Fig. 3A-C). At P10-15, the GLT-1-IR increased significantly with the weakest protein levels detected throughout the *stratum pyramidale* (Fig. 3D-F). Almost all GFAP-positive cells showed immunoreactivity for GLT-1 that was especially arranged at the proximal, primary processes and dispersed towards the distal processes.

At P20-P25, GLT-1 was distributed over a larger surface of a given astrocyte and strongly co-localized with GFAP (Fig. 3G-I). In contrast to the inhomogeneous staining pattern of GLT-1 seen during the first three weeks of postnatal development, a rather uniform protein distribution was seen in the adult mouse CA1 (Fig. 3J-L). All hippocampal subregions expect the *stratum pyramidale* exhibited similar high expression levels. This homogenous staining pattern might result from the high density of transporter label at GFAP-negative peripheral astrocytic processes.

In conclusion, a laminar distribution of GLAST and GLT-1 is established during postnatal development. Both glutamate transporters are expressed in a basically complementary fashion with GLAST localized predominantly in the *s. pyramidale* and predominant GLT-1 localization in other regions of the hippocampus, exhibiting lower levels in the *s. pyramidale*. Furthermore, both GLAST and GLT-1 immunoreactivity increase during postnatal development, though GLT-1 exhibits a delayed rise in labeling as compared to GLAST.

Developmental changes in GLAST and GLT-1 protein levels

To quantify the relative overall expression levels of both GLAST and GLT-1 in the CA1 region during postnatal development, we performed western blots (Fig. 4). In CA1 homogenates, several bands were detected (Fig. 4A and 4B) that presumably correspond to the monomeric and the oligomeric forms of the transporters, known to exist as homomultimers (Haugeto et al., 1996; Peacey et al., 2009). The experimentally determined molecular weights of the monomeric forms of GLAST (~60 kDa) and GLT-1 (~65 kDa) are in agreement with calculations using the ExPASy compute pl/Mw tool for murine GLAST (59.6 kDa) and GLT-1 (62.1 kDa).

For GLAST, two additional forms were present: a dominant dimeric (120 kDa) and a trimeric form (180 kDa; Fig. 4A). Throughout postnatal development until adulthood, the

dimeric GLAST assembly exhibited the largest protein quantity (Fig. 4A). Both oligomeric GLAST forms, dimer and trimer, increased from P3-5 to P10-15 (with an initial value of 48.5% and 25.7%, respectively), and remained unchanged thereafter, whereas the monomeric form increased until P20-P25 (6.5-fold increase from P3-P5 to P20-P25; $p < 0.001$; Fig. 4C). The three GLAST complexation types exhibited different protein contents in the adult mouse: dimeric > trimeric > monomeric form (Fig. 4C).

For GLT-1, the presumed monomeric (~65 kDa), trimeric (~190 kDa) and tetrameric (>200 kDa) forms increased between P3-P5 and P20-25 (Fig. 4B, D). Both oligomeric GLT-1 forms escalated after P3-P5 (from 5.5% to 41.8% of adult values), the monomeric GLT-1 delayed after P10-P15 (from 12.3% to 94.9% of adult values; Fig. 4D). Both multimeric forms showed an equal protein content in the adult mouse, the monomeric half of it (Fig. 4B).

Numerical summation of the intensity of the different bands revealed that the overall GLAST protein content doubled from P3-P5 to P10-P15 (37.6% to 70.3% of adult protein content; Fig. 4E). Total GLT-1 content did not reach detectable relative protein values until P10-P15 (35.1% of adult protein content). The protein content more than doubled until P20-P25 (76.2% of adult protein content; Fig. 4E).

In summary, we found that both GLAST and GLT-1 protein content increase time-delayed during the first two-three weeks of postnatal development in the CA1 region of the mouse hippocampus. Furthermore, and as described before, GLAST and GLT-1 visualize as several bands, representing multimeric assemblies, on SDS-PAGE. These complexation forms show a differential temporal up-regulation during postnatal development.

Subcellular expression pattern of GLAST and GLT-1

High spatial resolution analysis of immunostainings was performed to reveal the subcellular distribution of the two glutamate transporter subtypes. To this end, co-staining with S100ß, a glial-specific cytosolic calcium binding protein (Raponi et al., 2007), was carried out to better

delineate the morphology of the astrocytic cell bodies and processes. This double staining showed a rather homogeneous GLAST labeling at astrocyte somata as well as on processes (Fig. 5A). GLT-1, in contrast, showed explicit labeling of processes with only sparse labeling of the cell body (Fig. 5B).

To further elucidate the subcellular distribution of GLT-1 immunoreactivity in astrocytes, we employed super-resolution microscopy using dual-color STED-imaging (stimulated emission depletion microscopy, Meyer et al., 2008; Willig et al., 2006), providing a spatial resolution of less than 50 nm for fluorescent beads (not shown). Dual-color STED-imaging resolved clusters of GLT-1 immunofluorescence on astrocyte processes and somata that were closely associated with intracellular filament structures of GFAP (Fig. 6). Here, GFAP was labelled with Chromeo 494 (green) and GLT-1 was labelled with Atto 647N (magenta). The direct comparison with images taken in the conventional confocal mode of the laser scanning system (Fig. 6) furthermore revealed that STED microscopy resolved GLT-1 clusters as well as GFAP structures that were not detected with confocal imaging.

Analysis of astrocyte endfeet on blood vessels revealed another, rather unexpected heterogeneity in the subcellular staining pattern of the two transporter subtypes. Already at P3-P5, a time period when GLT-1 expression was generally very low (cf. Figs. 3 and 4), pronounced GLT-1 protein clusters were detectable at perivascular endfeet (Fig. 7A). At both P10-P15 (Fig. 7B) and P25 (Fig. 7A), a labeling of distinct and dense clusters of GLT-1 was observed on most endfeet. Interestingly, this pattern disappeared almost completely in tissue derived from adult mice (Fig. 7A). In contrast to this, GLAST was never found to show a comparable concentration of clusters on astrocytic endfeet (Fig. 7A).

In general, clusters of GLT-1 on astrocyte endfeet seemed to preferentially co-localize with GFAP (Fig. 7B). A close spatial interrelationship between GLT-1 clusters and GFAP on perivascular endfeet was confirmed using STED microscopy (Fig. 8). Documentation of defined sub-resolution multicolor beads revealed a spatial resolution of 40-50 nm. Again,

STED microscopy enabled resolution of single clusters of GLT-1 that were not visible in the confocal mode.

In summary, our data reveal a differential expression pattern of the two glutamate transporters on the cellular level and throughout the postnatal development of the hippocampus. While GLAST immunoreactivity showed no preferential localization to a specific cellular compartment, GLT-1 is particularly found in fine astrocytes processes, with only sparse labeling of the cell bodies. In juvenile animals, distinct GLT-1 clusters were detected at perivascular endfeet, and these clusters seem to preferentially co-localize with GFAP.

Discussion

Our study shows that the density of GFAP-positive cells and GFAP expression increase during the first two weeks after birth in the CA1 area of the mouse hippocampus, paralleled by an increase in overall GLAST expression. Up-regulation of GLT-1 protein levels is delayed by about 1 week. Western blots revealed a differential temporal up-regulation of multimeric and monomeric forms of GLAST and GLT-1 during this period. In addition, our data show that GLAST increased steadily with highest transporter density in neuronal cell body layers and was preferentially expressed in astrocytes at P3-5 and by radial glia. GLAST immunoreactivity was distributed rather homogenously with no preferential localization to a specific cellular compartment. GLT-1 expression was especially prominent in adult tissue. Starting at P10-15, GLT-1 exhibited a laminar expression pattern, with highest immunoreactivity in the *stratum lacunosum-moleculare*. GLT-1 was only sparsely located at astrocyte somata, whereas it exhibited discrete clusters at perisynaptic processes and at endfeet on blood vessels, where they seem to preferentially co-localize with GFAP.

Postnatal changes in the levels and cellular organization of GFAP

GFAP, the principal intermediate filament in mature astrocytes, is a widely used marker to identify cells of the astroglial lineage including radial glial (Liu et al., 2006; Raponi et al., 2007; Shibata et al., 1997). We found a strong increase in the density of GFAP-positve cells from P3-5 to P10-15 in the CA1 area, followed by a reduction of cell density to a stable value from P20-25 on. The observed initial increase in the number of GFAP expressing cells as well as the decline after P10-P15 are in agreement with earlier results (Kimoto et al., 2009; Nixdorf-Bergweiler et al., 1994). These data are also in line with reports showing that GFAP transcript levels increase until P15 after which they decline again (Riol et al., 1992).

At the cellular level, the GFAP network resembles a rough, fibrous mesh extending from the cell body which is progressively straightened during maturation and limited to the proximal processes (Nixdorf-Bergweiler et al., 1994). Because, under certain conditions, bundles of GFAP filaments can dissociate and expose more epitopes leading to an artificial increase in antibody-coupled fluorescence, we performed western blots to quantify changes in protein levels. These demonstrate that canonic GFAP increases within the first two weeks of postnatal development, confirming results reported earlier (Kim et al., 2011).

GFAP not only controls astrocytic motility and shape by providing structural stability (Rodnight et al., 1997), but also serves as a scaffold to anchor proteins at the plasma membrane (Middeldorp and Hol, 2011). Indeed, Sullivan and coworkers showed that GFAP serves as a cytoskeleton anchor for GLAST (Sullivan et al., 2007a). GFAP knock-out mice exhibit a reduction in glutamate transport activity, a decrease in GLAST protein expression and compromised trafficking of GLT-1 to the plasma membrane (Hughes et al., 2004). In addition, GLAST expression and its functionality are prerequisites for proper function of glutamine synthetase and of transmitter clearance in Müller cells of the retina (Derouiche and Rauen, 1995; Ishikawa et al., 2011). In astrocytes, it has been demonstrated that decreasing GFAP levels are accompanied by a rise in glutamine synthetase activity and vice versa (Lieth et al., 1998; Pekny et al., 1999; Weir and Thomas, 1984). These findings strongly indicate that changes in the expression and structural organization of GFAP during postnatal development will also affect the trafficking of glutamate transporters to the plasma membrane and the functionality of the glutamate-glutamine cycle.

Temporal changes in protein content and multimer composition of GLAST and GLT-1

For analysis of temporal changes in the protein levels of GLAST and GLT-1, we employed western blots using two antibodies against GLAST and GLT-1. The anti-GLAST was raised against a synthetic peptide (KPYQLIAQDNEPEKPVADSETKM) corresponding to the

carboxy-terminus of rat glutamate transporter GLAST. It does not discriminate between GLAST-1a and GLAST-1b (Vallejo-Illarramendi et al., 2005), two splice variants of GLAST (Lee and Pow, 2010). The anti-GLT-1 was raised against a synthetic peptide (AANGKSADCSVEEEPWKREK) corresponding to the carboxy-terminus of rat glutamate transporter GLT-1. Several splice variants of GLT-1 have been described (Holmseth et al., 2009; Lee and Pow, 2010), which form homomeric and heteromeric assemblies (Peacey et al., 2009). Based on the location of the splice sites, it can be assumed that the antibody used here recognized GLT-1a, but did not label the C-terminal splice variants GLT-1b or GLT-1c.

Our study now shows that the temporal profile of the overall postnatal up-regulation of the two glutamate transporters differs: while total GLAST already reached adult protein levels at P10-15; GLT-1 protein content rose until P20-25. This differs from results obtained for other regions in the rat brain (i.e. cerebellum, striatum, cortex and spinal cord), where GLAST expression was basically unaltered from P5 to P16, while GLT-1 expression increased steadily (Furuta et al., 1997). The increase in total GLAST protein levels in the mouse CA1 region thereby essentially parallels the rise in GFAP protein, whereas GLT-1 protein expression does not necessarily closely follows up-regulation of GFAP levels.

Our data confirmed that GLT-1 and GLAST proteins migrate as monomeric bands, but also form multimers on SDS-PAGE. While it is generally accepted that glutamate transporters form multimers (Danbolt, 2001; Haugeto et al., 1996; Peacey et al., 2009), we now report evidence for a differential up-regulation of the monomeric versus the multimeric forms during postnatal development. Whereas the relative expression of oligomeric GLAST seems to be maximal already at P10-15, the expression level of its monomeric form continued to rise until P20-25. Furthermore, the expression of monomeric GLT-1 surges between P10-15 and P20-25 (increase by 80%), while the relative expression levels of the multimeric forms increase more steadily.

Our study thus suggests that protein up-regulation and protein multimerization of glutamate transporters seem to be independently regulated during development. The physiological relevance of such differential regulation is unclear. Notwithstanding, homomultimers are assumed to be stabilized by noncovalent bonds *in vivo* and to play a role in functional glutamate uptake (Haugeto et al., 1996; Jiang and Amara, 2011; Peacey et al., 2009). Indeed, the degree of complexation strongly amplifies the activity of the glutamate transporters, indicating that their assembly could allow a rapid, activity-dependent adaptation of glutamate transport efficacy (Haugeto et al., 1996).

Laminar and subcellular profile of GLAST and GLT-1 immunoreactivity

Analysis of immunohistochemical stainings using confocal microscopy revealed that GLAST and GLT-1 exhibit changes in their laminar and subcellular expression pattern in the hippocampus. In general, an overall increase in the labeling intensity for both transporters during postnatal development was observed, which is in line with earlier studies (Furuta et al., 1997; Kugler and Schleyer, 2004), and complements the results obtained from our western blots. Our stainings also confirm the view that GLAST is the predominant glutamate transporter early in postnatal development and in immature astrocytes and radial glial cells (Raponi et al., 2007; Shibata et al., 1997).

Our data, moreover, also clearly indicate that GLAST expression is not restricted to immature and radial glial cells, but that during maturation virtually all astrocytes up-regulate GLAST to moderate levels (Furuta et al., 1997). The labeling for GLAST also exhibited a punctate signal in the *strata pyramidale*. As mentioned before, the antibody employed here was directed against a motive of the antigenic binding site that is found in both isoforms, GLAST1a and GLAST1b. GLAST1b, contrary to the astrocyte-specific GLAST1a isoform, is found to be especially located in neuronal cell bodies (Sullivan et al., 2007b). It is still under debate whether GLAST1b represents a functional isoform (Vallejo-Illarramendi et al., 2005).

22

GLAST-labeling was also specifically found on cell bodies of S100ß-positive astrocytes, as well as on their processes. In contrast to GLT-1, GLAST immunoreactivity was rather homogeneously distributed, and we never observed a specific clustering on GFAP-positive endfeet. Thus, even though GFAP has been proposed to enhance glutamate uptake activity and to serve as a cytoskeleton anchor for GLAST (Sullivan et al., 2007a), GLAST is apparently not generally co-localized with GFAP nor specifically targeted to a subcellular compartment.

GLT-1 immunoreactivity increased most discernably between P3-5 and P10-15, which also matches the most prominent increase in the multimer forms as revealed by western blots. Interestingly, and as pointed out above, the relative expression levels of the monomeric form only surged between P10-15 and P20-25. The strong increase in GLT-1 protein content and immunolabeling during the first three weeks of postnatal development parallels the phase of major synaptogenesis and synapse maturation in the hippocampus (Ullian et al., 2004). Such a coincidental progression was already described for other brain regions by Furuta and co-workers (1997). Indeed, glutamate uptake through GLT-1 is an important functional element of mature hippocampal synapses (Arnth-Jensen et al., 2002; Verbich et al., 2012), and it was recently shown that GLT-1 protein up-regulation during postnatal development is correlated to the frequency of transmitter release at excitatory synaptic sites (Benediktsson et al., 2012).

Our data demonstrate that GLT-1 is not homogeneously distributed throughout all cellular domains. They show explicit immunolabeling of processes with only sparse labeling of the cell body, the latter preferentially co-localized with GFAP-fibers. Furthermore, they confirm the presence of GLT-1 clusters at fine perisynaptic astrocyte processes (Zhou & Sutherland, 2004; Nakagawa et al., 2008). GLT-1 expression is highly dependent on and sensitive to fast excitatory synaptic transmission (Bergles et al., 2002; Nakagawa et al., 2008; Schlag et al., 1998; Seifert et al., 2009). On the other hand, GLT-1 is vital for synapse establishment (Benediktsson et al., 2012; Verbich et al., 2012). Earlier work has found evidence that sodium signals, which arise following Na^+-dependent glutamate uptake in

astrocyte processes (Langer and Rose, 2009), might be a critical modulator in the formation of clusters of GLT-1 at synapses (Nakagawa et al., 2008). Interestingly, perisynaptic astroglial processes are devoid of GFAP, but are characterized by restricted localization of the actin-binding protein ezrin (Derouiche et al., 2002). The interrelationship between ezrin and glutamate transporters, has, to our knowledge, not been studied so far.

Unexpectedly, we found a distinct clustering of GLT-1 on GFAP-positive perivascular endfeet during the first three weeks of development, but not in adult tissue. In contrast to this, GLAST was never found to show comparable clustering on astrocytic endfeet. Electron microscopic studies have detected both GLAST and GLT-1 at endfeet (Chaudhry et al., 1995; Lehre and Danbolt, 1998; Lehre et al., 1995). Our study now shows for the first time a discrete and pronounced clustering of GLT-1 at most endfeet in juvenile animals, already at a time point, where GLT-1 expression is generally very low and no such clusters are seen at perisynaptic processes.

The functional role of clusters of GLT-1 at astrocyte endfeet and the blood-brain barrier is unclear. A recent study on co-cultures of endothelial cells and astrocytes provided evidence for an active transport of glutamate in the abluminal-to-luminal direction (Helms et al., 2012). The possible existence of a glutamate "siphoning" mechanism from the brain to the blood is also indicated by studies showing that glutamate entry into the brain is either very slow or virtually not present (Hawkins et al., 1995; Vina et al., 1997). Such a pathway would help to clear the brain tissue from glutamate and might serve a protective role by preventing excitotoxicity. On the other hand side, specific clustering of GLT-1 on endfeet could also promote uptake of glutamate and enable rapid detoxification of blood-derived ammonia, which freely diffuses over the blood-brain barrier, in the glutamate/glutamine cycle (Allaman et al., 2011). Indeed, earlier studies demonstrated that a substantial part of the ammonia/ammonium circulating in brain blood vessels passes the blood-brain barrier and becomes incorporated into glutamine through astroglial glutamine synthetase (Cooper et al.

1979 & 1987). Glial glutamate transporters on perivascular endfeet might thus serve either one of these processes, glutamate siphoning or ammonia detoxification, depending on the electrochemical driving forces and resulting direction of glutamate transport (Danbolt, 2001).

Acknowledgments

Conflict of interest statement

The authors declare that there is no known or potential conflict of interest including any financial, personal or other relationships.

Author contributions

All authors had full access to all the data in the study and take responsibility for the integrity of the data and the accuracy of the data analysis.

A. E. Schreiner: immunohistochemistry and western blot experiments, data analysis and interpretation, experimental design and manuscript writing

M. C. Stock: western blot experiments, revision of manuscript

U. Rüther: western blot analysis, revision of manuscript

C. R. Rose: project initiation and experimental design, data interpretation and manuscript writing

K. W. Kafitz: project design, experimental design, STED microscopy, data interpretation and manuscript writing

26

References

Allaman I, Belanger M, Magistretti PJ. 2011. Astrocyte-neuron metabolic relationships: for better and for worse. Trends Neurosci 34(2):76-87.

Arnth-Jensen N, Jabaudon D, Scanziani M. 2002. Cooperation between independent hippocampal synapses is controlled by glutamate uptake. Nature Neuroscience 5(4):325-331.

Benediktsson AM, Marrs GS, Tu JC, Worley PF, Rothstein JD, Bergles DE, Dailey ME. 2012. Neuronal activity regulates glutamate transporter dynamics in developing astrocytes. Glia 60(2):175-188.

Bergles DE, Tzingounis AV, Jahr CE. 2002. Comparison of coupled and uncoupled currents during glutamate uptake by GLT-1 transporters. J Neurosci 22(23):10153-10162.

Bordey A, Sontheimer H. 1997. Postnatal development of ionic currents in rat hippocampal astrocytes in situ. J Neurophysiol 78(1):461-477.

Brunne B, Zhao S, Derouiche A, Herz J, May P, Frotscher M, Bock HH. 2010. Origin, maturation, and astroglial transformation of secondary radial glial cells in the developing dentate gyrus. Glia 58(13):1553-1569.

Bushong EA, Martone ME, Ellisman MH. 2004. Maturation of astrocyte morphology and the establishment of astrocyte domains during postnatal hippocampal development. Int J Dev Neurosci 22(2):73-86.

Chaudhry FA, Lehre KP, van Lookeren Campagne M, Ottersen OP, Danbolt NC, Storm-Mathisen J. 1995. Glutamate transporters in glial plasma membranes: highly differentiated localizations revealed by quantitative ultrastructural immunocytochemistry. Neuron 15(3):711-720.

Cooper AJ, Lai JC. 1987. Cerebral ammonia metabolism in normal and hyperammonemic rats. Neurochemical Pathology 6(1-2):67-95.

Cooper AJ, McDonald JM, Gelbard AS, Gledhill RF, Duffy TE. 1979. The metabolic fate of 13N-labeled ammonia in rat brain. The Journal of Biological Chemistry 254(12):4982-4992.

Danbolt NC. 2001. Glutamate uptake. Prog Neurobiol 65(1):1-105.

Danbolt NC, Storm-Mathisen J, Kanner BI. 1992. An [Na$^+$ + K$^+$]coupled L-glutamate transporter purified from rat brain is located in glial cell processes. Neuroscience 51(2):295-310.

Deitmer JW, Rose CR. 2010. Ion changes and signalling in perisynaptic glia. Brain Res Rev 63(1-2):113-129.

Derouiche A, Anlauf E, Aumann G, Muhlstadt B, Lavialle M. 2002. Anatomical aspects of glia-synapse interaction: the perisynaptic glial sheath consists of a specialized astrocyte compartment. Journal of physiology, Paris 96(3-4):177-182.

Derouiche A, Rauen T. 1995. Coincidence of L-glutamate/L-aspartate transporter (GLAST) and glutamine synthetase (GS) immunoreactions in retinal glia: evidence for coupling of GLAST and GS in transmitter clearance. Journal of neuroscience research 42(1):131-143.

Freeman MR. 2010. Specification and morphogenesis of astrocytes. Science 330(6005):774-778.

Furuta A, Rothstein JD, Martin LJ. 1997. Glutamate transporter protein subtypes are expressed differentially during rat CNS development. J Neurosci 17(21):8363-8375.

Gegelashvili G, Schousboe A. 1998. Cellular distribution and kinetic properties of high-affinity glutamate transporters. Brain Res Bull 45(3):233-238.

Gilley JA, Kernie SG. 2011. Excitatory amino acid transporter 2 and excitatory amino acid transporter 1 negatively regulate calcium-dependent proliferation of hippocampal neural progenitor cells and are persistently upregulated after injury. Eur J Neurosci 34(11):1712-1723.

Hartfuss E, Galli R, Heins N, Gotz M. 2001. Characterization of CNS precursor subtypes and radial glia. Dev Biol 229(1):15-30.

Haugeto O, Ullensvang K, Levy LM, Chaudhry FA, Honore T, Nielsen M, Lehre KP, Danbolt NC. 1996. Brain glutamate transporter proteins form homomultimers. The Journal of biological chemistry 271(44):27715-27722.

Hawkins RA, DeJoseph MR, Hawkins PA. 1995. Regional brain glutamate transport in rats at normal and raised concentrations of circulating glutamate. Cell and Tissue Research 281(2):207-214.

Helms HC, Madelung R, Waagepetersen HS, Nielsen CU, Brodin B. 2012. In vitro evidence for the brain glutamate efflux hypothesis: Brain endothelial cells cocultured with astrocytes display a polarized brain-to-blood transport of glutamate. Glia.

Holmseth S, Scott HA, Real K, Lehre KP, Leergaard TB, Bjaalie JG, Danbolt NC. 2009. The concentrations and distributions of three C-terminal variants of the GLT1 (EAAT2; slc1a2) glutamate transporter protein in rat brain tissue suggest differential regulation. Neuroscience 162(4):1055-1071.

Huang YH, Bergles DE. 2004. Glutamate transporters bring competition to the synapse. Curr Opin Neurobiol 14(3):346-352.

Hughes EG, Maguire JL, McMinn MT, Scholz RE, Sutherland ML. 2004. Loss of glial fibrillary acidic protein results in decreased glutamate transport and inhibition of PKA-induced EAAT2 cell surface trafficking. Brain Res Mol Brain Res 124(2):114-123.

Ishikawa M, Yoshitomi T, Zorumski CF, Izumi Y. 2011. Downregulation of glutamine synthetase via GLAST suppression induces retinal axonal swelling in a rat ex vivo hydrostatic pressure model. Investigative ophthalmology & visual science 52(9):6604-6616.

Jiang J, Amara SG. 2011. New views of glutamate transporter structure and function: advances and challenges. Neuropharmacology 60(1):172-181.

Kim JS, Kim J, Kim Y, Yang M, Jang H, Kang S, Kim JC, Kim SH, Shin T, Moon C. 2011. Differential patterns of nestin and glial fibrillary acidic protein expression in mouse hippocampus during postnatal development. J Vet Sci 12(1):1-6.

Kimoto H, Eto R, Abe M, Kato H, Araki T. 2009. Alterations of glial cells in the mouse hippocampus during postnatal development. Cell Mol Neurobiol 29(8):1181-1189.

Kudryashov IE, Onufriev MV, Kudryashova IV, Gulyaeva NV. 2001. Periods of postnatal maturation of hippocampus: synaptic modifications and neuronal disconnection. Brain Res 132(2):113-120.

Kugler P, Schleyer V. 2004. Developmental expression of glutamate transporters and glutamate dehydrogenase in astrocytes of the postnatal rat hippocampus. Hippocampus 14(8):975-985.

Langer J, Rose CR. 2009. Synaptically induced sodium signals in hippocampal astrocytes in situ. J Physiol 587(Pt 24):5859-5877.

Lee A, Pow DV. 2010. Astrocytes: Glutamate transport and alternate splicing of transporters. Int J Biochem Cell Biol 42(12):1901-1906.

Lehre KP, Danbolt NC. 1998. The number of glutamate transporter subtype molecules at glutamatergic synapses: chemical and stereological quantification in young adult rat brain. J Neurosci 18(21):8751-8757.

Lehre KP, Levy LM, Ottersen OP, Storm-Mathisen J, Danbolt NC. 1995. Differential expression of two glial glutamate transporters in the rat brain: quantitative and immunocytochemical observations. J Neurosci 15(3 Pt 1):1835-1853.

Lieth E, Barber AJ, Xu B, Dice C, Ratz MJ, Tanase D, Strother JM. 1998. Glial reactivity and impaired glutamate metabolism in short-term experimental diabetic retinopathy. Penn State Retina Research Group. Diabetes 47(5):815-820.

Liu X, Bolteus AJ, Balkin DM, Henschel O, Bordey A. 2006. GFAP-expressing cells in the postnatal subventricular zone display a unique glial phenotype intermediate between radial glia and astrocytes. Glia 54(5):394-410.

Magavi S, Friedmann D, Banks G, Stolfi A, Lois C. 2012. Coincident generation of pyramidal neurons and protoplasmic astrocytes in neocortical columns. The Journal of Neuroscience 32(14):4762-4772.

Mathiisen TM, Lehre KP, Danbolt NC, Ottersen OP. 2010. The perivascular astroglial sheath provides a complete covering of the brain microvessels: an electron microscopic 3D reconstruction. Glia 58(9):1094-1103.

Matsugami TR, Tanemura K, Mieda M, Nakatomi R, Yamada K, Kondo T, Ogawa M, Obata K, Watanabe M, Hashikawa T, Tanaka K. 2006. From the Cover: Indispensability of the glutamate transporters GLAST and GLT1 to brain development. Proc Natl Acad Sci U S A 103(32):12161-12166.

Meyer L, Wildanger D, Medda R, Punge A, Rizzoli SO, Donnert G, Hell SW. 2008. Dual-color STED microscopy at 30-nm focal-plane resolution. Small 4(8):1095-1100.

Middeldorp J, Hol EM. 2011. GFAP in health and disease. Prog Neurobiol 93(3):421-443.

Ming GL, Song H. 2005. Adult neurogenesis in the mammalian central nervous system. Ann Rev Neurosci 28:223-250.

Nakagawa T, Otsubo Y, Yatani Y, Shirakawa H, Kaneko S. 2008. Mechanisms of substrate transport-induced clustering of a glial glutamate transporter GLT-1 in astroglial-neuronal cultures. Eur J Neurosci 28(9):1719-1730.

Nixdorf-Bergweiler BE, Albrecht D, Heinemann U. 1994. Developmental changes in the number, size, and orientation of GFAP-positive cells in the CA1 region of rat hippocampus. Glia 12(3):180-195.

Nosyreva ED, Huber KM. 2005. Developmental switch in synaptic mechanisms of hippocampal metabotropic glutamate receptor-dependent long-term depression. J Neurosc 25(11):2992-3001.

Olabarria M, Noristani HN, Verkhratsky A, Rodriguez JJ. 2010. Concomitant astroglial atrophy and astrogliosis in a triple transgenic animal model of Alzheimer's disease. Glia 58(7):831-838.

Peacey E, Miller CC, Dunlop J, Rattray M. 2009. The four major N- and C-terminal splice variants of the excitatory amino acid transporter GLT-1 form cell surface homomeric and heteromeric assemblies. Mol Pharm 75(5):1062-1073.

Pekny M, Eliasson C, Siushansian R, Ding M, Dixon SJ, Pekna M, Wilson JX, Hamberger A. 1999. The impact of genetic removal of GFAP and/or vimentin on glutamine levels and transport of glucose and ascorbate in astrocytes. Neurochem Res 24(11):1357-1362.

Pfrieger FW. 2002. Role of glia in synapse development. Curr Opinion Neurobiol 12(5):486-490.

Pines G, Danbolt NC, Bjoras M, Zhang Y, Bendahan A, Eide L, Koepsell H, Storm-Mathisen J, Seeberg E, Kanner BI. 1992. Cloning and expression of a rat brain L-glutamate transporter. Nature 360(6403):464-467.

Raponi E, Agenes F, Delphin C, Assard N, Baudier J, Legraverend C, Deloulme JC. 2007. S100B expression defines a state in which GFAP-expressing cells lose their neural stem cell potential and acquire a more mature developmental stage. Glia 55(2):165-177.

Reichenbach A, Derouiche A, Kirchhoff F. 2010. Morphology and dynamics of perisynaptic glia. Brain Res Rev 63(1-2):11-25.

Riol H, Fages C, Tardy M. 1992. Transcriptional regulation of glial fibrillary acidic protein (GFAP)-mRNA expression during postnatal development of mouse brain. J Neurosci Res 32(1):79-85.

Rodnight R, Goncalves CA, Wofchuk ST, Leal R. 1997. Control of the phosphorylation of the astrocyte marker glial fibrillary acidic protein (GFAP) in the immature rat hippocampus by glutamate and calcium ions: possible key factor in astrocytic plasticity. Braz J Med Biol Res 30(3):325-338.

Rothstein JD, Martin L, Levey AI, Dykes-Hoberg M, Jin L, Wu D, Nash N, Kuncl RW. 1994. Localization of neuronal and glial glutamate transporters. Neuron 13(3):713-725.

Schlag BD, Vondrasek JR, Munir M, Kalandadze A, Zelenaia OA, Rothstein JD, Robinson MB. 1998. Regulation of the glial Na+-dependent glutamate transporters by cyclic AMP analogs and neurons. Mol Pharmacol 53(3):355-369.

Schools GP, Zhou M, Kimelberg HK. 2006. Development of gap junctions in hippocampal astrocytes: evidence that whole cell electrophysiological phenotype is an intrinsic property of the individual cell. J Neurophysiol 96(3):1383-1392.

Seifert G, Huttmann K, Binder DK, Hartmann C, Wyczynski A, Neusch C, Steinhauser C. 2009. Analysis of astroglial K+ channel expression in the developing hippocampus reveals a predominant role of the Kir4.1 subunit. J Neurosci 29(23):7474-7488.

Shibata T, Yamada K, Watanabe M, Ikenaka K, Wada K, Tanaka K, Inoue Y. 1997. Glutamate transporter GLAST is expressed in the radial glia-astrocyte lineage of developing mouse spinal cord. J Neurosci 17(23):9212-9219.

Storck T, Schulte S, Hofmann K, Stoffel W. 1992. Structure, expression, and functional analysis of a Na(+)-dependent glutamate/aspartate transporter from rat brain. Proceedings of the National Academy of Sciences of the United States of America 89(22):10955-10959.

Suarez I, Bodega G, Fernandez B. 2000. Modulation of glutamate transporters (GLAST, GLT-1 and EAAC1) in the rat cerebellum following portocaval anastomosis. Brain Research 859(2):293-302.

Sullivan SM, Lee A, Bjorkman ST, Miller SM, Sullivan RK, Poronnik P, Colditz PB, Pow DV. 2007a. Cytoskeletal anchoring of GLAST determines susceptibility to brain damage: an identified role for GFAP. J Biol Chem 282(40):29414-29423.

Sullivan SM, Macnab LT, Bjorkman ST, Colditz PB, Pow DV. 2007b. GLAST1b, the exon-9 skipping form of the glutamate-aspartate transporter EAAT1 is a sensitive marker of neuronal dysfunction in the hypoxic brain. Neuroscience 149(2):434-445.

Ullensvang K, Lehre KP, Storm-Mathisen J, Danbolt NC. 1997. Differential developmental expression of the two rat brain glutamate transporter proteins GLAST and GLT. Eur J Neurosci 9(8):1646-1655.

Ullian EM, Christopherson KS, Barres BA. 2004. Role for glia in synaptogenesis. Glia 47(3):209-216.

Vallejo-Illarramendi A, Domercq M, Matute C. 2005. A novel alternative splicing form of excitatory amino acid transporter 1 is a negative regulator of glutamate uptake. J Neurochem 95(2):341-348.

Verbich D, Prenosil GA, Chang PK, Murai KK, McKinney RA. 2012. Glial glutamate transport modulates dendritic spine head protrusions in the hippocampus. Glia 60(7):1067-1077.

Vina JR, DeJoseph MR, Hawkins PA, Hawkins RA. 1997. Penetration of glutamate into brain of 7-day-old rats. Metabolic Brain Disease 12(3):219-227.

Weir MD, Thomas DG. 1984. Effect of dexamethasone on glutamine synthetase and glial fibrillary acidic protein in normal and transformed astrocytes. Clin Neuropharm 7(4):303-306.

Willig KI, Kellner RR, Medda R, Hein B, Jakobs S, Hell SW. 2006. Nanoscale resolution in GFP-based microscopy. Nat Methods 3(9):721-723.

Wu Y, Zhang AQ, Yew DT. 2005. Age related changes of various markers of astrocytes in senescence-accelerated mice hippocampus. Neurochemistry International 46(7):565-574.

Yang Y, Gozen O, Watkins A, Lorenzini I, Lepore A, Gao Y, Vidensky S, Brennan J, Poulsen D, Won Park J, Li Jeon N, Robinson MB, Rothstein JD. 2009. Presynaptic regulation of astroglial excitatory neurotransmitter transporter GLT1. Neuron 61(6):880-894.

Zhou J, Sutherland ML. 2004. Glutamate transporter cluster formation in astrocytic processes regulates glutamate uptake activity. The Journal of Neuroscience 24(28):6301-6306.

Zhou M, Schools GP, Kimelberg HK. 2006. Development of GLAST(+) astrocytes and NG2(+) glia in rat hippocampus CA1: mature astrocytes are electrophysiologically passive. Journal of Neurophysiology 95(1):134-143.

Zhu X, Bergles DE, Nishiyama A. 2008. NG2 cells generate both oligodendrocytes and gray matter astrocytes. Development 135(1):145-157.

Figure Legends

Fig. 1. GFAP expression during postnatal development. Immunohistochemical labeling for GFAP of transverse sections of the mouse hippocampus at the indicated developmental stage. (**A**) Overviews of the CA1 area representing extended focus images from stacks of 15 serial Z-sections of 1 μm. The boxes delineate the areas in which GFAP-positive astrocytes were counted (see C). (**B**) Morphology of GFAP-positive astrocytes at the indicated developmental stages. (**C**) Histogram showing the number of GFAP-positive cells (astrocytes) per 100,000 μm^3. Cells were counted in one image section through the depth of the slice, corresponding to 30 μm (P3-P5: n=22, N=11; P10-P15: n=28, N=14; P20-P25: n=35, N=15; adults (P60-P70): n=24, N=4). (**D**) Representative western blot and western blot-based analysis of relative GFAP expression (**E**) at indicated developmental stages (N=3 for each age-group). Shown are mean values ± S.E.M.; *** $p<0.001$; ** $p<0.01$; * $p<0.05$. StrO, *stratum oriens*; StrP, *stratum pyramidale*; StrR, *stratum radiatum*; StrLM, *stratum lacunosum-moleculare*, StrM, *stratum moleculare*. Scale bar: 20 μm and 50 μm, respectively.

Fig. 2. GLAST expression in CA1. Images derived from single optical slices of 1 μm of the hippocampal CA1-region at the indicated developmental stages, immunohistochemically labeled with antibodies directed against GLAST (**A**, **D**, **G**, **J**) and GFAP (**B**, **E**, **H**, **K**). (**C**, **F**, **I**, **L**) show the overlay of both channels. (**A-C**): In the neonate mouse, robust GLAST expression is found in elongated GFAP-positive astrocytic processes traversing the *strata oriens and pyramidale*. The arrowhead indicates the rare case of a GLAST-positive, but GFAP-negative process. (**D-F**): At P10-15, a punctate GLAST labeling pattern around neuronal cell bodies in the *stratum pyramidale* is established. Robust GLAST expression was found in more branched cells at this developmental stage. Arrowheads point to a thin (~0.5 μm) structure labeled for GLAST that crosses several astrocytic domains. (**G-L**): At P20-25

and in adult mice, a laminar distribution is established with highest GLAST expression around neurons of the pyramidal cell layer. (**J-L**). Scale bar: 20 µm. Al= *alveus*; StrO, *stratum oriens*; StrP, *stratum pyramidale*; StrR, *stratum radiatum*.

Fig. 3. GLT-1 expression in CA1. Images derived from single optical slices of 1 µm of the hippocampal CA1-region at the indicated developmental stages, immunohistochemically labeled with antibodies directed against GLT-1 (**A**, **D**, **G**, **J**) and GFAP (**B**, **E**, **H**, **K**). (**C**, **F**, **I**, **L**) show the overlay of both channels. (**A-C**): In the neonate, only few GLT-1 positive cells are detectable in the *strata oriens* and *radiatum*. (**D-F**): GLT-1 protein levels as well as the number of distinctly labeled cells increase by P10-P15. (**G-L**): At P20-25, GLT-1 highly co-localizes with GFAP. (**J-L**): GLT-1 labeling in the adult. Arrowheads indicate GLT-1- as well as GFAP-positive astrocytes. Scale bar: 20 µm. Al= *alveus*; StrO, *stratum oriens*; StrP, *stratum pyramidale*; StrR, *stratum radiatum.*

Fig. 4. Complexation grade of GLAST and GLT-1 in CA1. Western blots of CA1 homogenates developed against GLAST (**A**) and GLT-1 (**B**) with the corresponding analysis of the different bands in (**C**) and (**D**), respectively. Note that the different protein bands, which presumably correspond to multimerization forms of the glutamate transporters, are differentially up-regulated during postnatal development. (**E**) Quantification of total protein content, determined by the numeric summation of the individual bands, for GLAST and GLT-1, respectively. Shown are mean values ± S.E.M. (3 animals in each age cohort).

Fig. 5. Cellular distribution of GLAST and GLT-1 in CA1. Astrocytes at P3-P5 (upper row) and P20-P25 (lower row) labeled with GLAST (**A**) or GLT-1 (**B**), (AlexaFluor488-coupled, left column), and with S100ß (AlexaFluor594-coupled, middle column). The right column

represents the overlay of the two channels. The arrows point to the cell body, which is densely labeled with GLAST (A), but virtually avoid of GLT-1 (B). Scale bars: 20 µm.

Fig. 6: Localization of GLT-1 at a GFAP-labelled astrocyte. Confocal and super-resolution images of a GFAP-positive astrocyte (Chromeo 494, green) in the *stratum radiatum* of the mouse hippocampus at P15 and the sub-cellular localization of the labelling for the glial glutamate transporter GLT-1 (Atto 647N, magenta). The images in the left column are taken at a conventional CLSM (Leica SP5). Images taken at the STED microscope are presented in the right column. All images except of the images presented in the first row (raw-images) were processed for xy-deconvolution and post-productionally handled absolutely identical. Note the drastically increased resolution (< 50nm) in the images taken at the STED microscope compared to the images taken at the CLSM. All images represent a maximum projection of 12 optical sections.

Fig. 7. GLAST and GLT-1 labeling pattern at perivascular endfeet. Image of the immunohistochemical staining of GLAST or GLT-1 (visualized with AlexaFluor488), co-labeled with GFAP (visualized with AlexaFluor594), in the *stratum radiatum* during postnatal development. (**A**, two left columns): GLAST was not localized on astrocytic endfeet (**A**, two right columns): already at P3-P5, a time period GLT-1 expression in general was very low, GLT-1 protein clusters were detectable at scattered perivascular endfeet. Between P10 and P25 a pronounced labeling of perivascular endfeet was observed that disappeared in the adult. (**B**) GLT-1 labeling of a P15 hippocampus. Arrows point to astrocytic endfeet identified by GFAP. Scale bars, 20 µm.

Fig. 8: Clusters of GLT-1 at GFAP-labelled astrocyte endfeet. The figure shows the lining of a blood vessel (BV) in the mouse hippocampus at P15 by GFAP-positive astroglial processes (Chromeo 494, green) and the localization of the labelling for the glial glutamate transporter GLT-1 (Atto 647N, magenta). The images in the left column are taken at a conventional CLSM (Leica SP5). Super-resolution images taken at a STED microscope are presented in the right column. All images were processed for xy-deconvolution and post-productionally handled absolutely identical. All images represent a maximum projection of 10 optical sections.

.

Table 1. Antibody List.

Primary antibodies									
antibody	structure of the immuno-gen	manufacturer	Order no.	Lot no.	species	type	dilution	application	listed
GLAST (EAAT1)	KPYQLIAQDNEPEKPVADSETKM	Chemicon/ Millipore	AB1782*	LV1395302; JC1615843; JC1658217	Guinea Pig IgG	polyclonal	1:1000	IHC	yes
GLAST (EAAT1)	KPYQLIAQDNEPEKPVADSETKM	Tocris Bioscience	2064	1	Rabbit IgG	polyclonal	1:2000	WB	no
GLT-1 (EAAT2)	AANGKSADCSVEEEPWKREK	Chemicon/ Millipore	AB1783	LV1377592; LV1547805; LV1688372	Guinea Pig IgG	polyclonal	1:1000/ 1:2000	IHC/ WB	yes
GFAP	n.s. (full-length protein from cow spinal cord)	Dako Cytomation	Z 0334	00036063	Rabbit IgG	polyclonal	1:1000 / 1:2000	IHC/ WB	yes
GFAP	clone G-A-5 (LQSLTCDVESLRGTNESLERQMREQEERHAREAASYQEALTRLEEEGQSLKDEMARHLQEYQELLNVKLALDIEIATY)	Sigma-Aldrich	G3893	078K4830	Mouse IgG	monoclonal	1:1000/ 1:2000	IHC/ WB	yes
S100ß	n.s. (recombinant full-length cow protein)	Abcam	ab868	877135; 200026	Rabbit IgG	polyclonal	1:100	IHC	no
α-actin	SGPSIVHRKCF	Sigma-Aldrich	A2066	090M4758	Rabbit IgG	polyclonal	1:2000	WB	yes
α-tubulin	clone 6-11B-1	Santa Cruz Biotechnology	sc-23950	B0711	Mouse IgG	monoclonal	1:2000	WB	no
GAPDH	clone 71.1	Sigma-Aldrich	G8795	080M4806	Mouse IgM	monoclonal	1:20000	WB	yes
Mouse IgG	AF488 conjugated	Invitrogen (Life Technologies)	A11029	56881A	Goat	-	1:100	IHC	yes
Mouse IgG	AF633 conjugated	Invitrogen (Life Technologies)	A21050	690316; 796022	Goat	-	1:100	IHC	no
Rabbit IgG	AF594 conjugated	Invitrogen (Life Technologies)	A11012	47098A; 695244	Goat	-	1:100	IHC	no
Guinea Pig IgG	AF488 conjugated	Invitrogen (Life Technologies)	A11073	400881; 629114; 753761	Goat	-	1:100	IHC	yes
Mouse IgG	HPR conjugated	Dako Cytomation	P0260	00039217	Rabbit	-	1:2000	WB	no
Rabbit IgG	HPR conjugated	Dako Cytomation	P0448	00041782	Goat	-	1:2000	WB	no
Guinea Pig IgG	HPR conjugated	Sigma-Aldrich	A5545	089K4858	Rabbit	-	1:2000	WB	no
Rabbit IgG	Cromeo-494 conjugated	Active Motif	15042	1	Goat	-	1:100	IHC	no
-	Atto647N streptavidin conjugated	ATTO-TEC	AD647N-61	1	-	-	1:50	IHC	no
Guinea Pig IgG	Biotinylated	Biozol	BA-7000	V0615	Goat	-	1:100	IHC	no

GLAST, glutamate aspartate transporter; GLT-1, glutamate transporter 1; GFAP, glial fibrillary protein; AF, AlexaFluor; GAPDH, glycerinaldehyd-3-phosphat-dehydrogenase; IHC, immunohistochemistry; WB, western blot; n.s. = not specified

*, Unfortunately, the manufacturer has lately stopped the sale and distribution of the GLAST antibody used here.

A GFAP staining of the hippocampal CA1 subregion

B GFAP positive cells of the *StrR*

C GFAP(+) cell counting in the CA1 region

E relative GFAP expression in the CA1 region

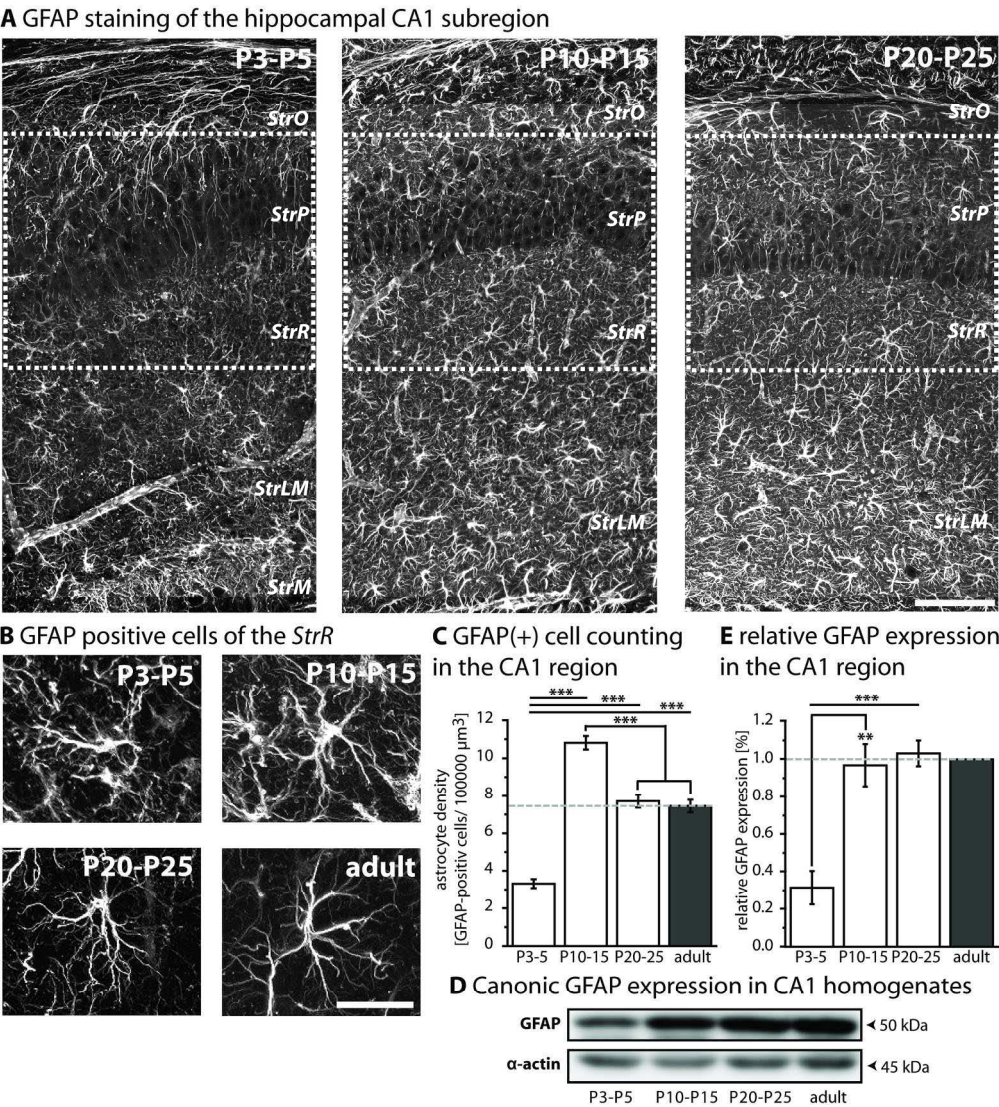**D** Canonic GFAP expression in CA1 homogenates

Figure 1. Schreiner, Stock, Rüther, Rose & Kafitz
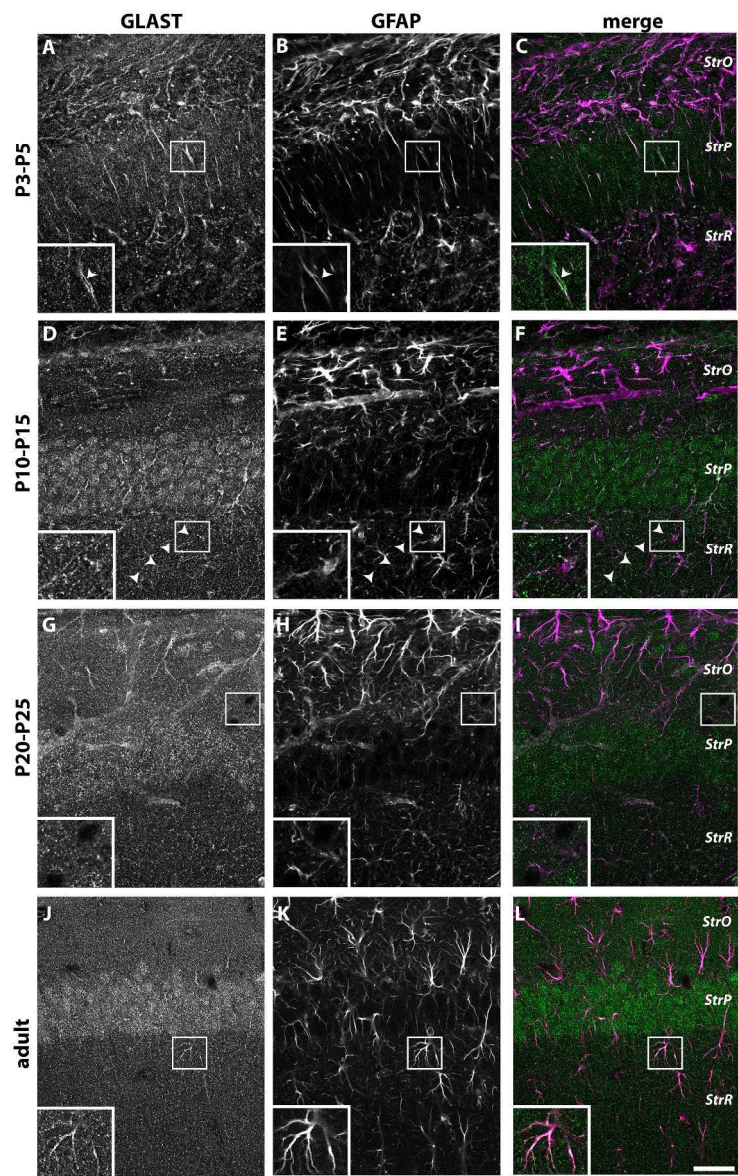
194x230mm (300 x 300 DPI)

Figure 2. Schreiner, Stock, Rüther, Rose & Kafitz
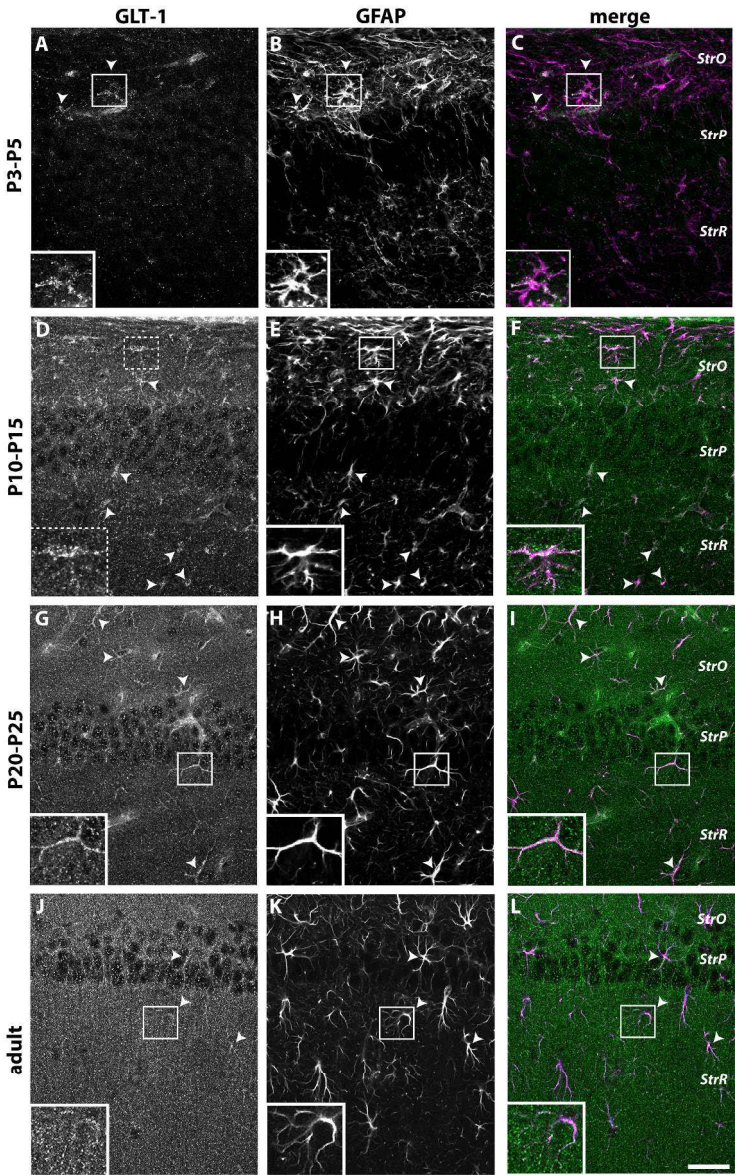
280x462mm (300 x 300 DPI)

Figure 3. Schreiner, Stock, Rüther, Rose & Kafitz

279x458mm (300 x 300 DPI)

Figure 4. Schreiner, Stock, Rüther, Rose & Kafitz

251x429mm (300 x 300 DPI)

Figure 5. Schreiner, Stock, Rüther, Rose & Kafitz

209x384mm (300 x 300 DPI)

Figure 6. Schreiner, Stock, Rüther, Rose & Kafitz

228x283mm (300 x 300 DPI)

A GLAST and GLT-1 on perivascular endfeet during postnatal development

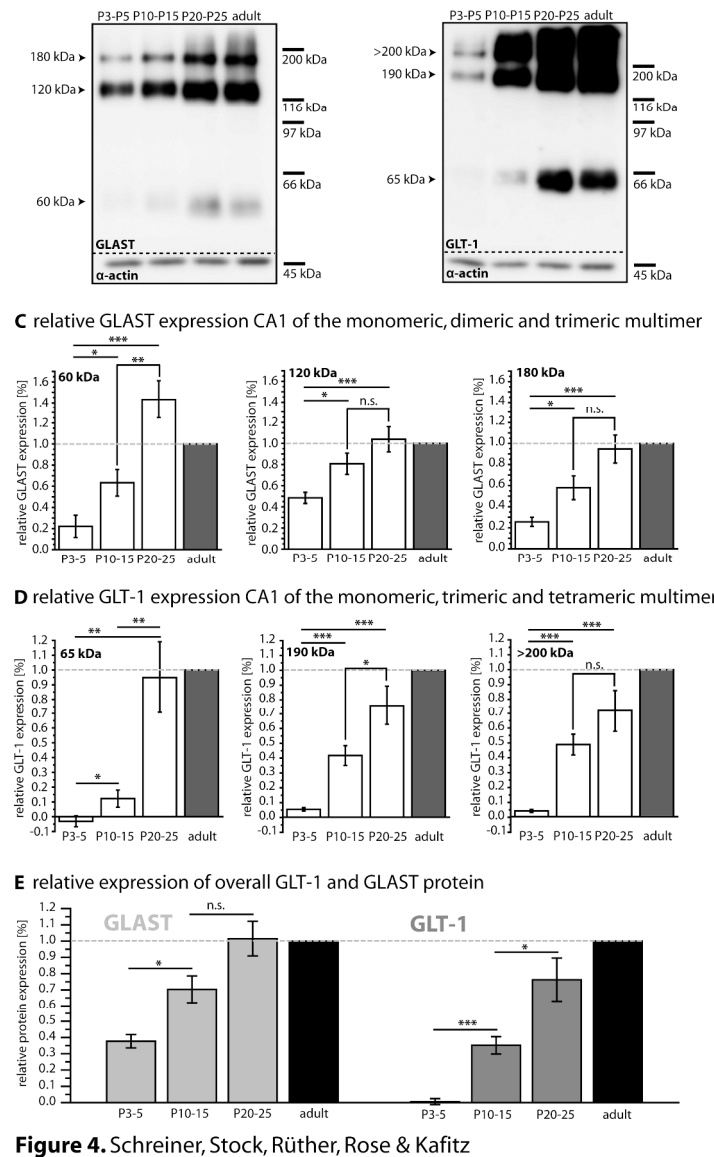**B** Distinct localization of GLT-1 at perivascular endfeet
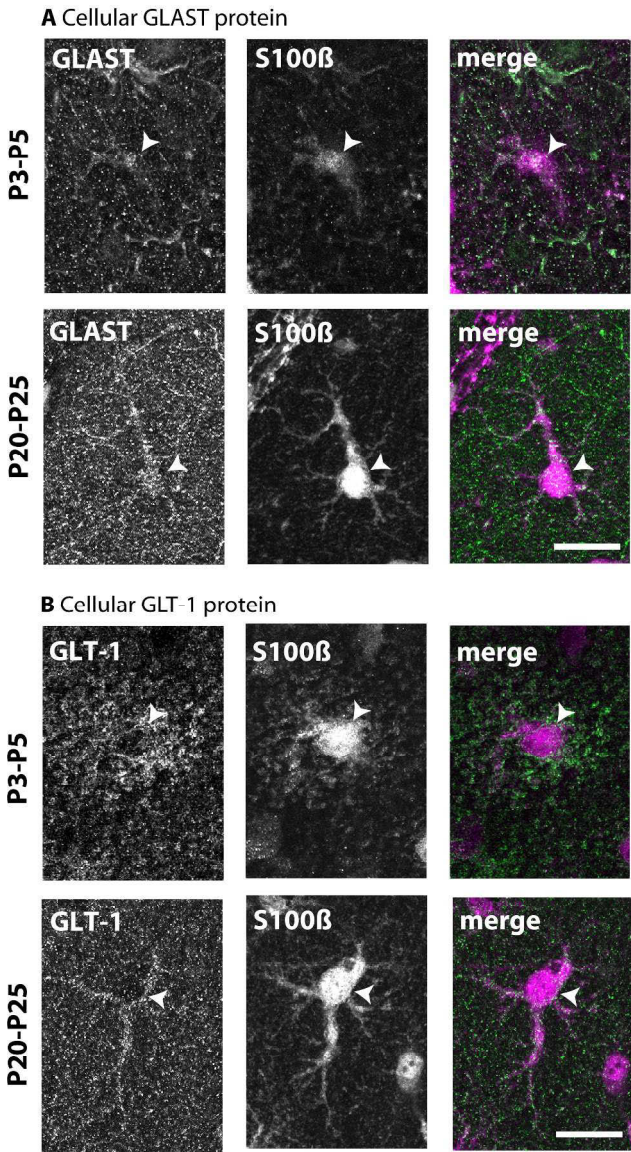
Figure 7. Schreiner, Stock, Rüther, Rose & Kafitz

251x378mm (300 x 300 DPI)

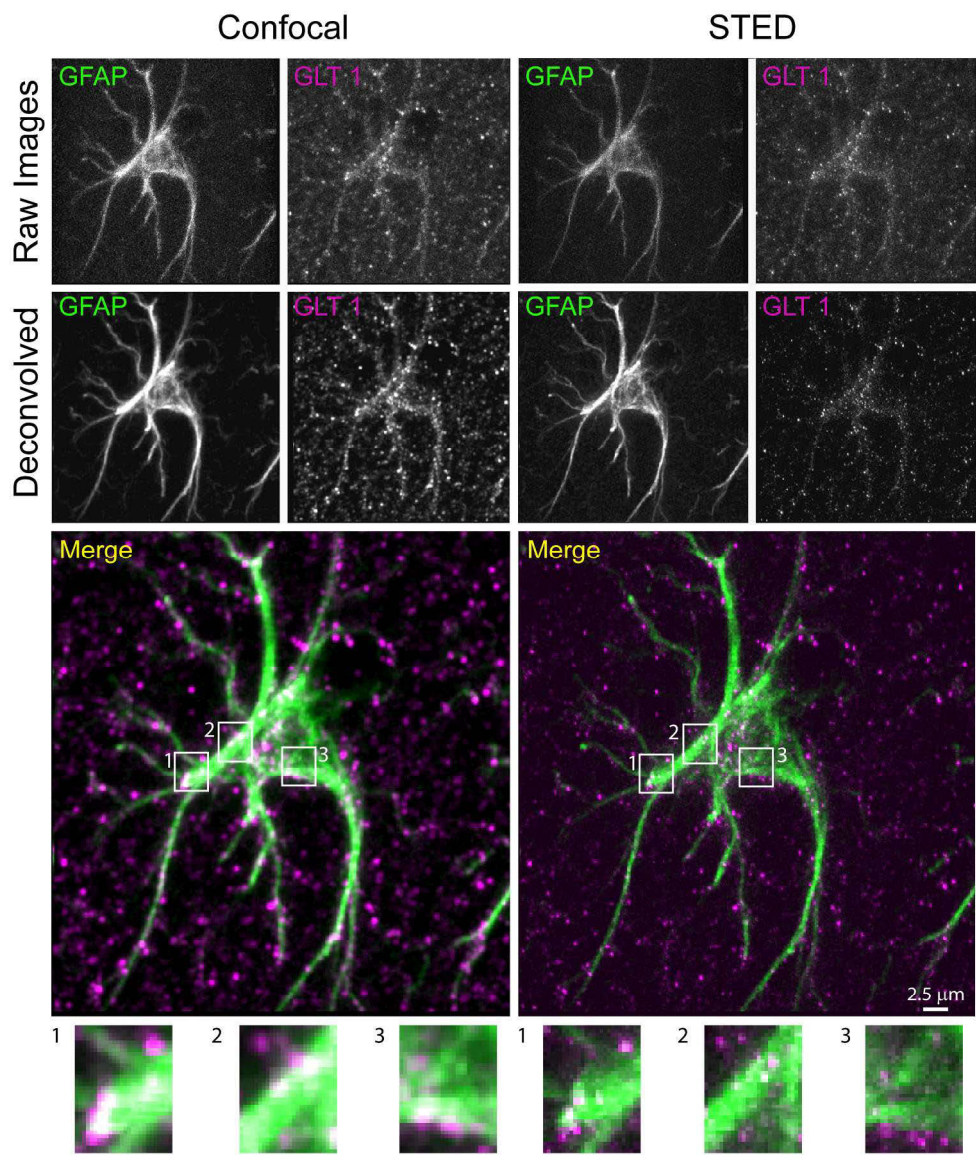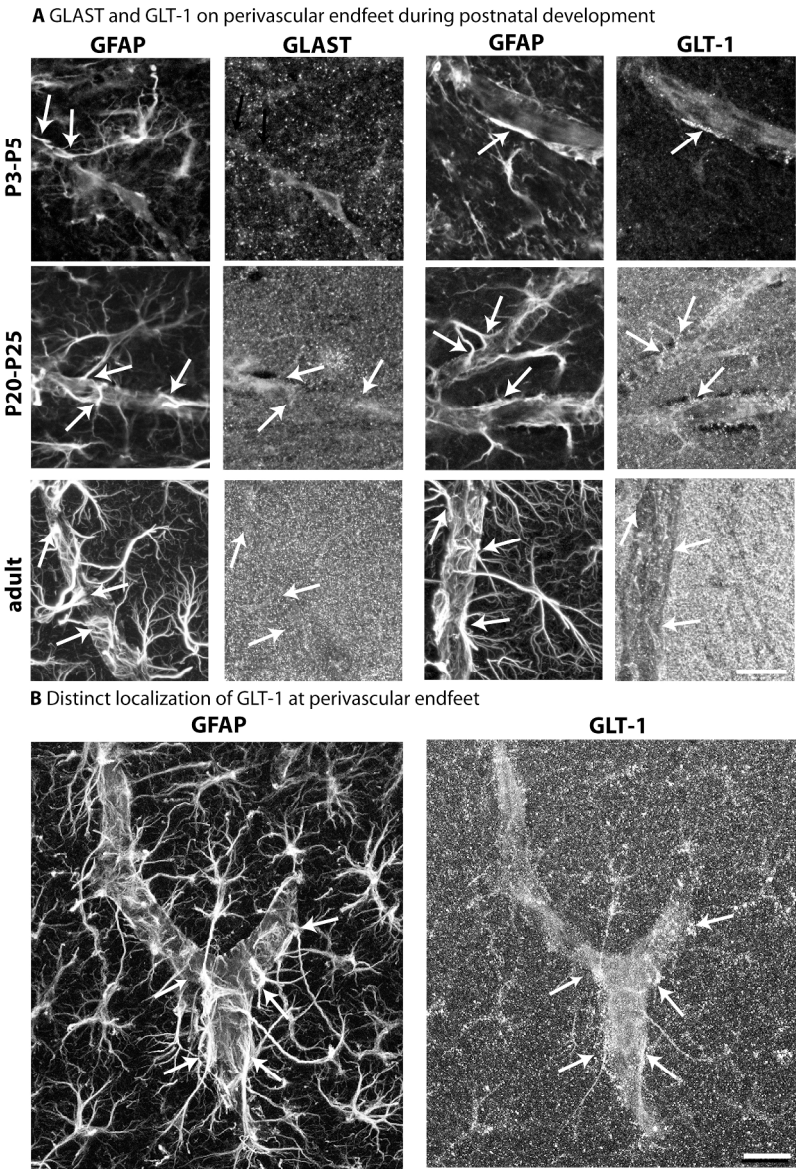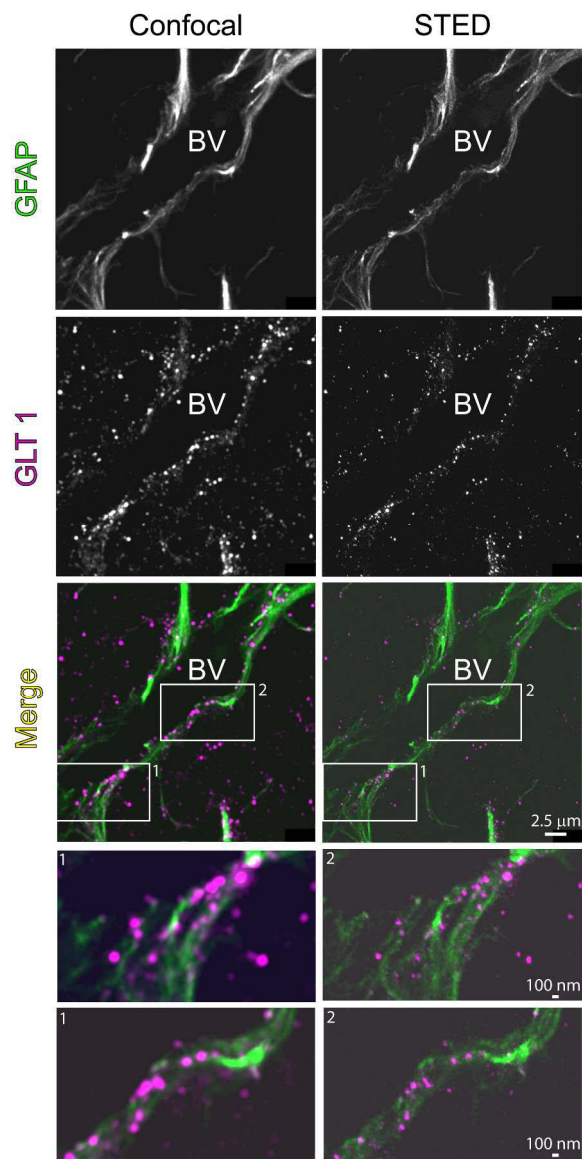**Figure 8.** Schreiner, Stock, Rüther, Rose & Kafitz

262x551mm (300 x 300 DPI)

4. Langer, Schreiner et al., *in preparation*

Sodium Signals in Endfeet of Hippocampal Astrocytes in Situ.

Julia Langer, <u>Alexandra E. Schreiner</u>, Christine R. Rose

Manuscript will be submitted in spring 2013.

I performed

- about 20% of experiments and data analysis

I contributed to

- the experimental design

- interpretation of data

5. Reddy-Vangoor, Schreiner et al., *in preparation*

Overexpression of CPEB3 Induces Astrocyte Dysfunction.

V. Reddy-Vangoor, <u>A.E. Schreiner</u>, C.R. Rose & M. Theis

Manuscript will be presumably submitted in early 2013.

I performed

- about 50% of experiments and data analysis

I contributed to

- the experimental design

- interpretation of data

Distinct Alterations of Glutamate Transporter Expression in Proximal and Distal Reactive Astrocytes

Alexandra E. Schreiner[1], Martin C. Stock[2], Julia Langer[1], Karl. W. Kafitz[1] & Christine R. Rose[1]*

[1]Institute of Neurobiology and [2]Institute for Animal Developmental and Molecular Biology, Heinrich Heine University Duesseldorf, Universitaetsstrasse 1, 40225 Duesseldorf, Germany.

Running Head: GLAST & GLT in Reactive Astrocytes

Associate Editor: Dr. Kathleen S. Rockland

Key Words: reactive astrogliosis, glutamate transporter, hippocampus

***Corresponding author**: Institute of Neurobiology, Heinrich Heine University Duesseldorf, Universitaetsstrasse 1, Building 26.02.00, 40225 Duesseldorf, Germany.
Tel.: +49 (0)211 81-13416, Fax: +49 (0)211 81-13415.
E-mail: rose@uni-duesseldorf.de

Graphical Abstract

Proper function of astroglial glutamate uptake is crucial for termination of synaptic transmission and prevention of extracellular glutamate accumulation, eventually causing excitotoxicity. Previous studies demonstrated that astrocytic glutamate transporters are generally down-regulated and cease function following brain injury (Ginsberg et al., 1995; van Landeghem et al., 2006).

By employing protein-based analysis and sodium imaging as functional assay, we actually found that astrocyte glutamate transporters are not uniformly affected upon severe pathological activation. We identified two subpopulations of reactive astrocytes that show diverging alterations in terms of SR101 uptake, a vital dye specifically taken up by astrocytes, glutamate transporter distribution and uptake capacity following mechanical injury. In direct spatial proximity to the lesion site glutamate transporters were clustered and astrocytic glutamate uptake was severely impaired, while more distally only moderate alterations were detected in terms of glutamate transporter expression and function. Among both only distal reactive astrocytes included SR101, indicating profoundly altered membrane properties of proximal reactive astrocytes.

This data indicates that the astrocytic response following severe injury is non-uniform and that distinct subsets of reactive astrocytes may undertake unique tasks in the retrieval phase.
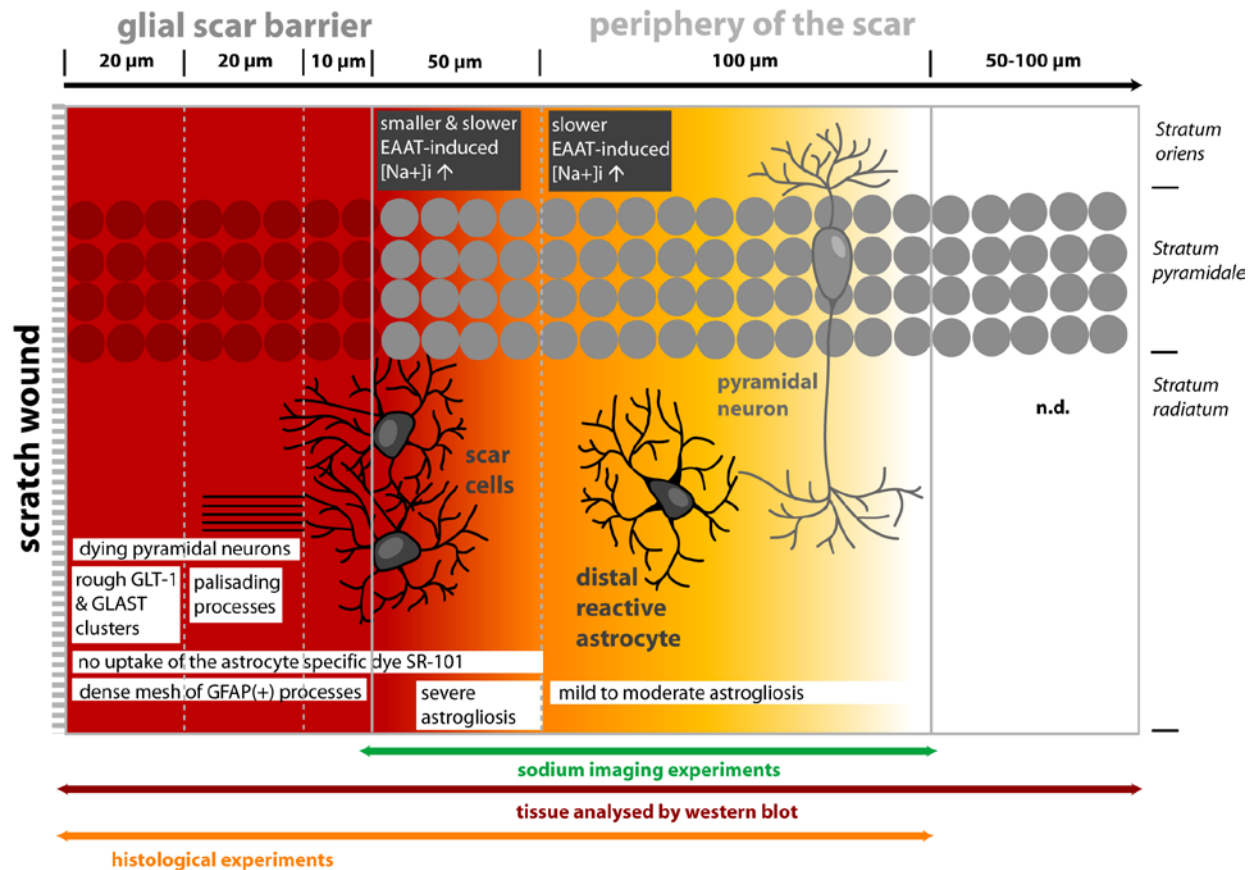
Figure 0. Schematic depiction of alterations astrocytes undergo in dependence on the distance from a lesion site in case of severe reactive astrogliosis. The histological experiments revealed that in the direct vicinity of the cell neuronal damage and death takes place (up to ~100 μm from the lesion site). In this district a dense mesh of astrocytic GFAP-positive processes was observable, which had a characteristic palisade-like organization directed towards the lesion site some in a distance of about 30 μm. Up to 30 μm rough glutamate transporter clusters were detectable near expiring processes, overall a decline in the predominant astrocytic glutamate transporter GLT-1 was observed by immunohistochemistry and western blot analysis. 100-150 μm from the lesion site no SR-101 uptake was accomplished by astrocytes, which was accompanied by smaller Na$^+$ responses with slower kinetics to the glutamate transporter agonist D-aspartate. These cells, named "scar cells" in this study, furthermore exhibited a massive cytoplasmic cell volume and a decline in sodium baseline values. Based on our experimental data it is tempting to assume that severe astrogliosis takes place in this area that ends approximately 150 μm from the lesion site in our preparation and the present scratch wound assay. More distant astrocytes stain for SR-101, showing prolonged sodium transients after D-aspartate stimulation, though unaltered peak amplitude. All SR-101 positive cells exhibited no change in basal sodium concentration, but were also found to be swollen. In this peripheral area in some distance from the lesion site it can be supposed that mild to moderate astrogliosis takes place.

Abstract

The extracellular glutamate concentration is ultimately terminated by the action of the astroglial glutamate re-uptake system consisting of the sodium-driven transporters GLAST and GLT-1. Their action ensures an optimal signal-to-noise-ratio for synaptic transmission and prevents toxic glutamate accumulation in the synaptic cleft. Upon severe brain injury ambient glutamate levels are profoundly raised, which might be counteracted by at least preserved glutamate transporter operation.

Here we addressed the question whether and how traumatic brain injury (TBI) affects the expression and function of GLAST and GLT-1 in the hippocampus by employing an experimental scratch wound assay *in situ*. Mechanical lesion triggered massive cell death and astrogliosis manifested by elevated expression of GFAP and significant hypertrophy. Furthermore, a compact glial scar formed adjacent to the lesion site. We found that in contrast to distal reactive astrocytes (DRA), proximal reactive astrocytes (PRA) situated within a distance of ~100 µm from the lesion site were not capable of SR101-uptake, a vital dye specifically taken up by astrocytes. To compare GLAST and GLT-1 distribution and quantity in control and lesioned slices, we employed immunohistochemistry and western blot analysis. Additionally, quantitative sodium imaging with the sodium-sensitive fluorescent indicator dye SBFI served as functional read-out of glutamate uptake capacity by recording intracellular sodium transients evoked by the glutamate transporter antagonist D-aspartate. Following mechanical lesion we detected prominent glutamate transporter clusters, in particular of GLAST, along with a severe functional reduction in astroglial glutamate re-uptake in PRA. DRA on the contrary displayed only negligible changes referring to glutamate transporter expression and function upon injury. Immunoblotting further revealed that solely GLAST multimer content was up-regulated, while, opposed to that, only GLT-1 monomer declined.

This data points to discrete alterations of GLAST and GLT expression and non-uniform impairment of glutamate re-uptake capacity in defined subsets of reactive astrocytes following brain trauma.

Introduction

Traumatic brain injury (TBI) occurs when an external physical force causes damage to the brain. Although TBI represents one of the major causes of death and disability worldwide, the neurochemical mechanisms underlying this complex and irreversible medical condition are still insufficiently determined (Werner and Engelhard, 2007). It is well established that two phases characterize the pathophysiological progress of TBI: The primary injury is immediately triggered by the initial trauma, while the secondary injury proceeds delayed, probably mediated by a slow-acting cascade of cellular processes (Borgens and Liu-Snyder, 2012). As ambient glutamate concentrations were shown to be significantly increased post-traumatically, glutamate(Glu)-mediated excitotoxicity was proposed to primarily mediate secondary brain damage (Nilsson et al., 1990; Katoh et al., 1997; Koizumi et al., 1997).

In the intact central nervous system (CNS), glutamate reuptake represents the principle mechanism to inactivate glutamate released at synaptic sites, and thus to prevent excitotoxicity (Danbolt, 2001). Efficient and rapid glutamate removal is mainly accomplished by astrocytic glutamate transporters (EAATs; excitatory amino acid transporters), namely GLAST (glutamate/aspartate-transporter) and GLT-1 (glutamate-transporter-1; rodent analogues of EAAT1 and EAAT2, respectively; Rothstein et al., 1996; Matsugami et al., 2006). The inward-transport of glutamate is energized by the sodium gradient over the plasma membrane, which is in turn maintained by the ATP(adenosine triphosphate)-consuming activity of the Na^+/K^+-ATPase. A complete transport cycle comprises the movement of 1 Glu^-, 3 Na^+ and 1 H^+ into the cell, along with 1 counter-transported K^+, which means that operation of EAATs is electrogenic (Anderson and Swanson, 2000). Their activation causes fast termination of the postsynaptic response, which assures a high signal-to-noise-ratio of glutamatergic transmission and shapes the time course of synaptic conductance (Tzingounis and Wadiche, 2007).

Causal or consequential dysfunction of these astrocyte-specific glutamate transporters in the course of TBI might lead to accelerated accumulation of extracellular glutamate and thus enhanced excitotoxic neuronal death due to over-excitation of postsynaptic receptors (Yi and Hazell, 2006). Given that ionotropic glutamate receptor (iGluR) antagonists failed to prove useful as drugs for clinical TBI intervention treatment, EAATs are considered as most promising prospective therapeutic target (Ikonomidou and Turski, 2002; Arundine and Tymianski, 2004; Beschorner et al., 2007; Laird et al., 2008). In order to develop new therapeutic strategies, we need, in the first instance, to gain more profound knowledge about the fundamental process of excitotoxicity, including the function and the regulation of EAATs in pathophysiological conditions.

Brain insults in general trigger a specific astroglial reaction, also referred to as reactive astrogliosis (Pekny and Nilsson, 2005; Sofroniew, 2009; Sofroniew and Vinters, 2010). A hallmark of reactive astrogliosis, regardless of its origin and the brain region affected, is a significant increased expression of the major astrocytic intermediate filament glial fibrillary acidic protein (GFAP). GFAP up-regulation, which represents the most commonly used indication in research and clinical diagnostics, is a highly sensitive process, however unspecific, because the protein is expressed in most mature astrocytes and miscellaneous progenitor cells of the astrocytic lineage (Middeldorp and Hol, 2011). Enhanced synthesis rate

of structural proteins such as GFAP and related cytoskeleton elements like vimentin, nestin and synemin in response to brain injury leads to a considerable hypertrophy of the astrocyte cell body and processes (Jing et al., 2007; Robel et al., 2011). Further morphological changes include alterations of the viscoelastic membrane properties as well as elongation and raised number of stem and higher-order processes (Wilhelmsson et al., 2004; Wilhelmsson et al., 2006; Lu et al., 2011). Brain injury of profound severity like TBI even leads the formation of a dense glial scar adjacent to the lesion centre, resulting in complete distortion of tissue organization, impairment of cellular connectivity and reduction of the extracellular space volume, e.g. due to astrocytic cell volume increase and proliferation (Sofroniew, 2009; Sofroniew and Vinters, 2010; Kawano et al., 2012).

In the intact CNS tissue, astrocytes play a decisive role in many vital functions, including neuronal metabolic supply by neurovascular coupling (Barros and Deitmer, 2010), blood-brain-barrier (BBB) function and integrity (Abbott et al., 2006; Zacchigna et al., 2008), detoxification (Norenberg, 1998), homeostasis of ions (Deitmer and Rose, 2010) and of neurotransmitters (Eulenburg and Gomeza, 2010). Astrocytes thus contribute to information processing at the synapse (Perea et al., 2009), which includes processes like neurotransmitter inactivation by reuptake, recycling and redelivery of precursor molecules to neuronal cells.

Upon brain injury at least a subpopulation of reactive astrocytes undergoes de-differentiation, meaning that they regain juvenile features and re-enter cell cycle (Buffo et al., 2008; Robel et al., 2011; Simon et al., 2011), which, as a matter of course, goes with massive alterations of functional properties. Astrogliosis further leads to a general impairment of astrocyte gap junction coupling, which might have severe consequences for ion regulation by astrocytes and energy provision over great distances (Rouach et al., 2002; Chew et al., 2010). Aforementioned alterations in amount and distribution of the major intermediate filament also affect astrocyte function, as GFAP not only provides structural stability to astrocytic processes, but also serves as scaffold to anchor proteins, which determine the position of multiple transmembrane proteins (Middeldorp and Hol, 2011). This has for instance functional implications for the glutamate-glutamine cycle, as it was demonstrated that a decline in GFAP levels is accompanied by a rise in glutamine synthetase activity in astrocytes and vice versa (Weir and Thomas, 1984; Lieth et al., 1998; Pekny et al., 1999). Impairment of the astrocyte functional repertoire following brain injury will consequently result in discontinuous supply of neurons and an altered performance of synaptic transmission. Along this line, partial dysfunction or failure of the astrocytic glutamate uptake system would have tremendous effect on excitatory transmission and thus on information processing in the brain.

In response to brain injury most studies so far demonstrated overall protein down-regulation of both astrocytic glutamate transporters, GLAST and GLT-1 in the rodent and human brain (e.g. Ginsberg et al., 1995; Rao et al., 1998; Chen et al., 2005; van Landeghem et al., 2006). A corresponding reduction of glutamate uptake activity was reported (Levy et al., 1995; Springer et al., 1997; Moretto et al., 2005). Interestingly, it was proposed that astrocyte EAATS can, under certain pathophysiological conditions, even change the orientation of operation, i.e. transport in the reverse mode (Li et al., 1999; Kosugi and Kawahara, 2006; Grewer et al., 2008). The increase in ambient glutamate levels following TBI might therefore be crucially determined by the operation of glutamate transporters. Regulatory enhancement of EAATs might hence extenuate progress of secondary injury and improve outcome of disease. That this might be indeed the case was indicated by a study showing that beta-lactam

antibiotics exert a neuroprotective effect in a rat model of TBI, which were shown before to enhance EAAT uptake efficiency (Rothstein et al., 2005; Wei et al., 2012).

It unfortunately remained un-addressed whether or how the described impact on glutamate transporter is diverse, as some studies might imply, regarding the temporal sequence, response severity and distance from a lesion core (Vermeiren et al., 2005; Frizzo et al., 2007). In order to investigate the expression and functional profile of astrocytic EAATs in pathophysiology, we established here a hippocampal TBI model *in situ.* By performing a standard scratch wound assay severe reactive astrogliosis was reliably trigger, which was throughout accompanied by glial scar formation alongside the lesion site. GLAST and GLT-1 protein levels were determined by immunohistochemistry and western blot analysis, while ratiometric sodium imaging was employed as functional assay for astrocytic glutamate transporter.

Methods

All experiments in this study were carried out in accordance with the institutional guidelines of the Heinrich-Heine-University Duesseldorf as well as the European Communities Council Directive (86/609/EEC).

Materials

All chemical were purchased from Sigma-Aldrich Chemical (Germany) unless stated otherwise.

Acute Hippocampal Slices

Acute slices of the hippocampus were prepared from Balb/c mice (*mus musculus*) of both genders at postnatal days 7 to 8 (P7-P8) using standard procedures. Briefly, mice were decapitated, brains quickly excised and hemisected in ice-cold artificial cerebrospinal fluid (ACSF) composed of (in mM): 125 NaCl, 2.5 KCl, 2 CaCl$_2$, 1 MgCl$_2$, 1.25 NaH$_2$PO$_4$, 26 NaHCO$_3$, and 20 glucose, bubbled with 95% O$_2$ and 5% CO$_2$, adjusted to a pH of 7.4. Hemisections were trimmed and transverse slices (200 μm) comprising the entorhinal cortex, hippocampus, fimbria and thalamus were prepared using a microtome (Microm HM650V, Thermo Fischer Scientific, Walldorf, Germany). Slices were transferred for 30 min to ACSF at 35°C.

Transgenic animals (FVB/N-Tg[GFAPGFP]14Mes/J) expressing green fluorescence protein (GFP) under GFAP promoter were obtained from the Jackson Laboratory (Harbor, USA).

Organotypic Hippocampal Tissue Slice Cultures and Mechanical Lesion

Organotypic hippocampal slice cultures were prepared and cultured according to the protocol of Stoppini et al. (1991) with minor modifications as follows (Stoppini et al., 1991). In brief, acute hippocampal slices (see above) were transferred to a Millicell culture insert (PICM ORG 50, hydrophilized PTFE, pore size 0.4 μm, Merck Millipore, USA) and maintained at the interface of a serum-based culture medium in a humidified incubator atmosphere of 5% CO$_2$ at 37°C. The culture medium was composed of: 30 % sterile filtered normal horse serum (NHS; GIBCO/Life Technologies), 30% dulbecco's modified eagle medium (DMEM; GIBCO/Life Technologies), 40% hanks balanced salt solution (HBSS; GIBCO/Life Technologies) supplemented with 38 mM glucose (pH adjusted to 7.3-7.4). No antibiotics were used as these may lead to epileptiform discharges (Schneiderman, 1997; Tian et al., 2005) as well as changes in glutamate transporter function and expression (Rothstein et al., 2005). The medium was changed three times a week and the insert surface was washed with medium once a week to guarantee sufficient supply of nutrients and to remove cell debris, respectively.

After at least 12 days in culture ("dic"), a mechanical lesion was performed using a scalpel. The lesion was positioned in the CA1 area perpendicular to the *stratum pyramidale*, included the *strata oriens*, *pyramidale*, *radiatum* and *lacunosum-moleculare* and spanned the entire depth of the slice (cf. Fig. 2). Afterwards, slices were maintained in culture for another 6-7 (designated as 6-7 days post lesion; 6-7 dpl). Unlesioned control slices were cultured for a corresponding number of days (19-25 dic).

SR101-Loading and Sodium Imaging

For selective vital staining of astrocytes (Nimmerjahn et al., 2004; Kafitz et al., 2008), acute or organotypic slices were incubated in ACSF containing 2.5 μM sulforhodamine 101 (SR101) for 30 min at 37°C. Slices were maintained in ACSF at room temperature (RT; 19–22°C) until they were used for experiments, which were also performed at RT. Organotypic cultures were excised from the Millicell inserts and transferred to fresh ACSF after carefully excising the glial sheath, that is a monolayer consisting of diverse glial cells that forms as top layer of the tissue during the culture period. Therefore the cover layer is tightened with two cannulas in order to split it off at one side. For sodium imaging, slices were additionally bulk-loaded with the membrane permeable form of the sodium-sensitive fluorescent dye SBFI (SBFI-AM; sodium-binding benzofuran isophthalate-acetoxymethyl ester; Molecular Probes/Life Technologies) as described earlier (Meier et al., 2006; Langer and Rose, 2009).

Wide-field fluorescence imaging was performed using a variable scan digital imaging system (TILL Photonics, Martinsried, Germany) attached to an upright microscope (BX51Wi, Olympus Europe, Hamburg, Germany) and a CCD camera (TILL Imago VGA, Till Photonics). Images were collected with an Achroplan 40x objective (water immersion, N.A. 0.8, Zeiss). SR101 was excited at 575 nm, emission was collected above 590 nm. Excitation wavelength for detection of GFP was 488 nm, emission was collected above 510 nm.

Ratiometric sodium imaging was performed as previously described (Rose and Ransom, 1996; Langer and Rose, 2009). SBFI was alternately excited at 4 Hz at 340 nm, at which its emission is only weakly sodium sensitive ("isosbestic" wavelength), and at 380 nm, at which SBFI is strongly sodium sensitive. Emission (>440 nm) was collected defined regions of interest (ROI) representing SBFI-filled somata. Standard dynamic background correction was performed as described earlier in detail (Langer and Rose, 2009; Langer et al., 2012). After background correction, the fluorescence ratio (F_{340}/F_{380}) was calculated for the individual ROIs and analyzed off-line using OriginPro 8G Software (OriginLab Corporation, Northhampton, MA). Changes in SBFI fluorescence ratio were expressed as changes in sodium concentration based on *in situ* calibrations as reported before (Rose and Ransom, 1996; Meier et al., 2006; Langer and Rose, 2009). To equilibrate extra- and intracellular Na^+-concentration, SBFI-loaded organotypic slice cultures were perfused with saline containing ionophores (3 μM gramicidin D, 100 μM monensin) and the Na^+/K^+-ATPase blocker ouabain (100 μM),a s well as different concentrations of Na^+. These calibrations revealed a virtually linear increase in SBFI-fluorescence ratio for Na^+ concentrations between 10 and 40 mM (n=107; N=6, Fig. 6). Within this range, a 10% change in the fluorescence ratio corresponded to a change in the intracellular sodium concentration by 5.5 mM.

The glutamate transporter agonist D-aspartate was applied by a pressure application device (PDES-02D, NPI Electronic GmbH, Tamm, Germany) coupled to standard micropipettes (Hilgenberg, Waldkappel, Germany) placed 20–100 μm from cell bodies of selected cells in the presence of 0.5 μM tetrodotoxin.

Antibody Characterization

All antibodies employed in this study are listed in table 1. The following antisera were utilized in this study, which represent well established, commercially available standard markers: guinea-pig GLT-1 antiserum directed against the C-terminus of rat GLT-1 (Millipore Corp., Ireland; e.g. Benediktsson et al., 2012), guinea-pig GLAST antiserum directed against the C-terminus of rat GLAST (Millipore Corp., Ireland; e.g. Zhou et al., 2006). Validation and

a detailed characterization of both antibodies were provided before (Suarez et al., 2000; Zhu et al., 2008; Brunne et al., 2010). + Schreiner et al., 2012

For specific identification and morphological characterization of astrocytic cells polyclonal rabbit antibodies against GFAP (GFAP-pAb; Dako Cytomation, Denmark; Wu et al., 2005; Brunne et al., 2010) and S100ß (Abcam, United Kingdom; Magavi et al., 2012) were employed. When double staining with the latter antibody was performed, a monoclonal mouse antibody detecting GFAP was used (GFAP-mAb; Sigma Aldrich, Germany; Brunne et al., 2010; Olabarria et al., 2010). All three antibodies (S100ß, GFAP-mAb and –pAb) reliably stained cells that could be either identified by prior SR101 incorporation or cells expressing GFP under the GFAP promoter (data not shown). Thus these antibodies can be considered specifically recognizing their supposed target. Moreover, virtually all S100ß positive cells stained positive for GFAP (data not shown).

Standard Fluorochrome-conjugated antibodies (AlexaFluor, Invitrogen) were employed as secondary antibodies for immunohistochemistry. To visualize immunoblots, HPR-conjugated antibodies were used (for details see table 1).

All antibodies used for immunohistochemistry were notwithstanding employed for western blot analysis. To assure comparability, the investigated specimen was in both cases murine hippocampal tissue. For all antibodies used, pattern of bands and their molecular weight was comparable with calculated (e.g. utilizing the ExPASy compute pl/Mw tool) and experimental data published by other groups (e.g. Haugeto et al., 1996; Suarez et al., 2000; Brunne et al., 2010).

Table 1. antibody list.

Primary antibodies									
antibody	structure of the immuno-gen	manufracturer	Order no.	Lot no.	species	type	dilution	application	listed
GLAST (EAAT1)	KPYQLIAQD NEPEKPVAD SETKM	Chemicon/ Millipore	AB1782*	LV139 5302; JC1615 843; JC1658 217	Guinea Pig IgG	polyclonal	1:1000	IHC	yes
GLAST (EAAT1)	KPYQLIAQD NEPEKPVAD SETKM	Tocris Bioscience	2064	1	Rabbit IgG	polyclonal	1:2000	WB	no
GLT-1 (EAAT2)	AANGKSAD CSVEEEPW KREK	Chemicon/ Millipore	AB1783	LV137 7592; LV154 7805; LV168 8372	Guinea Pig IgG	polyclonal	1:1000/ 1:2000	IHC/ WB	yes
GFAP	n.s. (full-length protein from cow spinal cord)	Dako Cytomation	Z 0334	000360 63	Rabbit IgG	polyclonal	1:1000 / 1:2000	IHC/ WB	yes
GFAP	clone G-A-5 (LQSLTCDV ESLRGTNES LERQMREQ EERHAREA ASYQEALT RLEEEGQSL KDEMARHL QEYQELLN	Sigma-Aldrich	G3893	078K4 830	Mouse IgG	monoclonal	1:1000/ 1:2000	IHC/ WB	yes

	VKLALDIEI ATY)								
S100ß	n.s. (recombinant full-length cow protein)	Abcam	ab868	877135; 200026	Rabbit IgG	polyclonal	1:100	IHC	no
α-actin	SGPSIVHRK CF	Sigma-Aldrich	A2066	090M4758	Rabbit IgG	polyclonal	1:2000	WB	yes

Secondary antibodies

antibody	conjugation	manufracturer	Order no.	Lot no.	species	type	dilution	application	listed
Mouse IgG	AF488 conjugated	Invitrogen (Life Technologies)	A11029	56881 A	Goat	-	1:100	IHC	yes
Rabbit IgG	AF594 conjugated	Invitrogen (Life Technologies)	A11012	47098 A; 695244	Goat	-	1:100	IHC	no
Guinea Pig IgG	AF488 conjugated	Invitrogen (Life Technologies)	A11073	629114; 753761	Goat	-	1:100	IHC	yes
Mouse IgG	HPR conjugated	Dako Cytomation	P0260	00039217	Rabbit	-	1:2000	WB	no
Rabbit IgG	HPR conjugated	Dako Cytomation	P0448	00041782	Goat	-	1:2000	WB	no
Guinea Pig IgG	HPR conjugated	Sigma-Aldrich	A5545	089K4858	Rabbit	-	1:2000	WB	no

GLAST, glutamate aspartate transporter; GLT-1, glutamate transporter 1; GFAP, glial fibrillary protein; AF, AlexaFluor; IHC, immunohistochemistry; WB, western blot; n.s. = not specified

*, Unfortunately, the manufacturer has lately stopped the sale and distribution of the GLAST antibody used here.

Immunohistochemistry

Prior to immunohistochemical processing, organotypic slices were immersion-fixed for 30 min at RT in 4% paraformaldehyde (PFA) in phosphate buffered saline (PBS) following three washes every 30 min with PBS. Cell membranes were permeabilized and unspecific binding sites were blocked in PBS containing 0.25% triton-X100 (TX) and 2% normal goat serum (NGS; GIBCO/Life Technologies) for 90 min at 4°C followed by incubation with the primary antibody GFAP-pAb (1:1000, Dako Cytomation, Denmark), diluted in the same solution over night at 4°C. In case of S100ß/GFAP double stainings, slices were incubated with a mixture of the primary antibodies GFAP-mAb (1:1000, Dako Cytomation, Denmark) and rabbit-S100ß (1:100, Abcam, United Kingdom). After 5 washes in PBS containing 0.25% TX and 2% NGS, slices were incubated either with guinea pig- anti-GLAST or with guinea pig- anti-GLT-1 (both 1:1000, diluted in) for 4 hrs at RT. Excess primary antibody was removed with five washes using 2% NGS/PBS. Anti-rabbit-AlexaFluor594 and anti-guinea pig-AlexaFluor488 or anti-mouse-AlexaFluor488 (1:100 in blocking solution) were used for visualization of antibody binding and incubated for 2 hrs at RT. The slices were subjected to DAPI staining (4',6-diamidino-2-phenylindole; 0.5 μm; Invitrogen) washed for three times and mounted on a glass slide with mowiol/DABCO (Calbiochem, Fluka).

Identical conditions were applied to all individually performed stainings regarding tissue processing and the staining procedure. Negative controls were run in parallel to each staining by either omitting all or just one of the primary antibodies. Control stainings in which one of the primary antibodies was omitted showed the identical labeling pattern for the remaining antibody as in the double-stainings. Omitting both primary antibodies never resulted in a staining.

As specified in the text, documentation of immunofluorescence was either performed with the Eclipse Nikon 90i (epifluorescence microscopy) or the Olympus Fluoview300 microscopy system (confocal microscopy). Immunofluorescence documentation was on the one hand realized with the Eclipse Nikon 90i microscopy system (Nikon, Germany), equipped with a standard DAPI (EX 340-380; DM 400; BA 435-485) FITC (EX 465-495; DM 505; BA 515-555) and TRITC (EX 540/25; DM 365; BA 605/55) filter set. Illumination was provided by an Intensilight fiber lamp (C-GHFI; Nikon) and emission was detected with a monochrome digital camera (DS-Qi1Mc; Nikon). Images were collected with either a 20x/0.75 (PlanApoVC, Nikon, Germany) air objective or a 60x/1.40 (PlanApoVC, Nikon) oil immersion objective. NIS-Elements software (Nikon) was used for image acquisition. Immunofluorescence was otherwise analyzed at an Olympus BX51WI microscope coupled to a confocal laser scanning system (FV300, Olympus, Germany) equipped with an multi-line argon laser (488 nm) and a helium-neon laser (543 nm, both Melles Griot, Germany). Images were collected with either a 20x/0.50 (UMPlanFl, Olympus), a 40x/0.80 (LUMPlan, Olympus) water immersion or a 60x/1.40 (PlanApoVC, Nikon) oil immersion objective. A Kalman filter 4 was applied for every scan. Simultaneous or sequential scanning of both fluorophores revealed no difference in the staining pattern of both fluorophores, indicating no cross-excitation or spectral bleed-through. The thickness of Z-plane sections was 1 μm with differing numbers of optical sections depending on the figure. Extended focus images are shown as indicated in the figure legend and were calculated from Z-stacks of optical sections using ImageJ software (NIH, USA). Images were overlaid or inverted employing Adobe Photoshop CS2 (Adobe Systems, CA).

Immunoblotting

Western blot analysis was performed as described previously with little modifications regarding tissue preparation (Schreiner et al., 2012). In brief, a tissue sample extending longitudinal from the *stratum oriens* to the *stratum lacunosum-moleculare* of the CA1 region (~400 μm; 700 μm width; in case of a lesion, identical distance from the scratch wound to both sides) was dissected from a slice culture. All tissue samples of one hemisphere were pooled and quickly frozen in liquid nitrogen. Per preparation two litter mates were prepared: one individual served as control and one was subject to mechanical lesion (see above). The tissue was homogenized at 4°C in RIPA buffer containing 1% deoxycholic acid (NP-40), 0.25% Na-Deoxycholat, protease inhibitors (CompleteMini, Roche, Germany), 150 mM NaCl and 50 mM Tris-HCl adjusted to a pH of 7.4. Homogenates were centrifuged at 13.000 g for 10 min and 4x laemmli buffer (5% sodium dodecyl sulfate (SDS), 43.5% glycerol, 100mM DL-dithiothreitol (DTT), 0.02% bromphenol blue, 20% 2-mercaptoethanol, 125 mM Tris-HCl adjusted to a pH of 6.8) was added to the supernatant. Proteins were electrophoretically separated on 10% gels by sodium dodecyl sulfate-polyacrylamide gel electrophoresis (SDS-PAGE). Subsequently, proteins were transferred electrophoretically to PVDF membranes. Strips of the PVDF membranes were preincubated in PBS containing 0.1% tween and 5% skimmed milk over night at 4°C in order to block unspecific binding sites. To the blocking solution, either rabbit-anti-GLAST, guinea pig- anti-GLT-1 or rabbit-anti-GFAP (both 1:2000, Dako Cytomation, Denmark) was added in an 1:2000 dilution and applied to the PVDF membrane for 1 hours (RT). Bound immunoglobulins were visualized using horseradish peroxidase-conjugated goat anti-rabbit or goat anti-guinea pig IgG in a 1:2000 dilution (incubated for 30 min at RT) and the enhanced luminol chemiluminescence technique (ECL-

kit, Amersham, Germany). In parallel, a detection of the relative protein content of every probe was performed using an antibody against α-actin. The resulting chemiluminescence was detected using the luminescent image analyser LAS-4000 (Fujifilm Europe GmbH, Germany).

Axiovision software (Zeiss, Germany) was used for the quantification of the western blot data. After background correction the grey value of the protein under examination was divided by the α-actin grey value. All values were normalized to the value determined for the control tissue from each corresponding litter mate.

Propidium Iodide Assay

To visualize dead cells in organtypic slice culture, ACSF that contained 0.5 μg/ml propidium iodide (PI) was applied to the slice surface and incubated for 3 hours at 37°C and 5% CO_2, followed by a wash with ACSF (N=3). Lesioned slice cultures were compared to unlesioned (negative control) and 1 mM H_2O_2(hydrogen peroxide)-treated cultured slices (positive control), respectively. Documentation was either accomplished with the aforementioned Eclipse Nikon 90i epifluorescence or the Olympus Fluoview300 laser scanning microscopy system.

Statistics

Unless otherwise specified, data are expressed as means ± S.E.M. Western blot data was statistically analyzed by Chi^2-test, for all statistical evaluations Student´s t-test was employed. In all cases, a p value < 0.05 was considered significant (* $p < 0.05$; ** $p < 0.01$; *** $p < 0.001$). If not stated otherwise, n represents the number of analyzed cells and N the number of experiments. Each set of experiment was performed on at least three different individuals.

Results

In this study we addressed the question whether a severe mechanical injury, which results in reactive astrogliosis, leads to changes in EAAT-mediated glutamate uptake. For this purpose we established a scratch wound assay that was applied to murine hippocampal organotypic slice cultures.

Hippocampal organotypic slice cultures

The membrane-interface tissue culture technique, introduced by Stoppini et al. (1991), features major advantages over explant or dissociated cell culture with regard to a preserved spatial tissue organization, astrocytic morphology and protein expression. In contrast to astrocytes kept in primary cell culture, those in organotypic slice culture maintain a more complex morphology and do, for instance, not cease to express GLT-1 over time (Gegelashvili et al., 1997; Schlag et al., 1998; Gegelashvili et al., 2000). Our organotypic slice culture protocol resulted in a well-preserved cytoarchitecture of the hippocampus and only few damaged cells were identified after 19-25 d.i.c. by propidium iodide assay. It is noteworthy, that the majority of these dead cells was located in the *stratum lacunosum-moleculare* and that these were aligned like pearls on a chain, probably corresponding to degenerated blood vessels (3 ± 0.6 cells CA1 subfield; 18 ± 3.4 entire hippocampus; 6 slices; N=3; data not shown). Organotypic slice cultures treated with 1 mM H_2O_2 thereby served as positive control for the propidium iodide assay, thus as reference of maximal cell damage. After the culturing period of 19-25 d.i.c. hippocampal slices flattened to a thickness of 40-50 μm and were composed of 3 to 4 cell layers. Immunohistochemistry revealed that nearly all GFAP-expressing cells labeled positive for S100ß, an astrocyte marker defining a more mature developmental stage (Raponi et al., 2007; Fig. 2). Surprisingly, hippocampal slice cultures also exhibited a good receptiveness for SR101 (see Fig. 1), a vital dye which is selectively taken up by astrocytes *in vivo* and in acute tissue slices (Nimmerjahn et al., 2004; Kafitz et al., 2008; Nimmerjahn and Helmchen, 2012), but not by astrocytes *in vitro* (data not shown). When SR101 was applied to hippocampal slice cultures of transgenic mice (FVB/N-Tg[GFAPGFP]) in which the GFAP promoter controls GFP expression, the vast majority of GFAP-expressing cells incorporate SR101, resembling the *in situ* situation (approximately 95%; see Fig. 1A). All cells that showed endogenous GFP expression but no SR-101 uptake exhibited an immature morphology with few if any processes and smaller cell bodies compared to GFP(+)SR101(+)-cells.

To conclude, since preliminary testing revealed no significant cell degeneration, a well-preserved tissue organization and good SR101 acceptance, we assigned this culturing system well feasible to study astrocytic activation following lesion induction.

Mechanical lesion induced severe reactive astrogliosis

To investigate severe astrogliosis in our culture system, that is an astrocytic reaction to injury comprised of different gradations of reactive gliosis and glial scar formation, we have triggered this glial response via a scratch wound through the hippocampal CA1-region. After induction of this mechanical lesion (see Material and Methods for the detailed procedure; see also Fig. 2A) a considerable overall increase in GFAP expression was visualized by immunohistochemistry and western blot analysis 6-7 dpl (67% increase compared to control levels; $p < 0.001$; Fig. 2B and 2C). It is of note that due to the *in vitro* situation already unlesioned slice cultures showed an increase in GFAP content compared to adult (P60-P70)

mouse tissue (data not shown). Nevertheless, a GFAP increase in lesioned compared to control slice cultures was measureable in all paired litter mate probes analyzed (14 probes, 6 sibling pairs). Spatially, the most pronounced enhancement of GFAP immunoreactivity was evident in the direct vicinity of the lesion site (within a distance of 50 μm; Fig. 2C and 2D). In this particular region adjacent to the lesion site the mostly "palisading" GFAP(+)-fibers formed a dense meshwork. The numerous GFAP labeled processes were considerably thickened compared to those more distal from the lesion site. Mild to moderate GFAP hypertrophy, however, was found in the entire hippocampus. Cellular inspection revealed that activated astrocytes generally bore more and longer GFAP-immunoreactive processes (Fig. 2E). Compared to control astrocytes, they displayed a more fibrous and frayed structure. The GFAP filaments extended less bundled and wavy from the astrocytic cell body, indicating alterations in proper organization of the astrocyte intermediate filament. These structural changes became more pronounced with proximity to the lesion site.

The territory next to the lesion was not only characterized by a prominent GFAP meshwork, but also by intense S100ß accumulation (Fig. 2D). Unlike more distant from the lesion, S100ß immunoreactivity couldn´t be exclusively assigned to intracellular compartments. Unexpectedly, our investigation further revealed that those reactive astrocytes alongside the scratch wound, which were identified by their GFAP expression, ceased to accept SR101 (Fig. 3). As stated before, under control conditions almost all GFAP-expressing cells, thus identifying them as cells of the astrocytic lineage, incorporated SR-101 (Fig. 3B). This bordering area free of SR101(+)-astrocytes had a mean width of 111 ± 3 μm (values ranging between about 86-146 μm) in the *strata pyramidale* and *radiatum* ($N = 5$; cf. Fig.3). Both, the inability to either take up SR101 or to prevent dye leakage and the extracellular S100ß presence suggest that membrane properties of astrocytes change upon activation. To determine the amount of SR101(+)-cells on the total number of cells in the *stratum radiatum* in controls versus lesioned slices, we performed double-labeling with SR101 and the ester form of sodium-binding benzofuran isophthalate (SBFI), a conventional Na^+-selective fluorescent dye that exhibits similar properties as Fura-2 (Minta and Tsien, 1989; Meier et al., 2006; Langer and Rose, 2009). As aforementioned, no SR101 uptake was accomplished by astrocytes found in the narrow region next to the lesion site. But SR-101 incorporation also seemed to be impaired more peripheral, as the proportion of SR101(+)-cells in the *stratum radiatum* significantly declined from approximately 91% to 55 % of all SBFI-labeled cells (control: $n = 274$; $N = 16$; lesion: $n = 123$; $N = 7$; data not shown). The percentage of cells found in control slices compares favorably with values previously obtained for acute slices at P15 (Kafitz et al., 2008). In order to further evaluate the apparent heterogeneity between proximal reactive astrocytes (PRA) and distal reactive astrocytes (DRA), we determined the cytoplasmic cell volume based on the size of SBFI-labeled cell bodies found in the focal plane. Analysis revealed that somata sizes of both, PRAs and DRAs were considerably enlarged (Fig.4). Compared to control astrocytes, the soma size of DRAs was 12 % larger, while cell body size of PRAs was even increased by 16 % (control: 133.7 ± 1.4 μm^2; DRA: 150.4 ± 2.6 μm^2; PRA: 155.4 ± 5.3 μm^2; $p < 0.001$; $n = 442, 152$ and 41, respectively; Fig. 4B). As illustrated by figure 4A, enlargement of the cell bodies was moreover accompanied by pronounced thickening of the primary processes.

Despite these findings, no significant change in neuronal cell size were observed (control: 150.5 ± 1.7 μm^2; lesion: 153.7 ± 3.5 μm^2; $n = 329$ and 77, respectively; data not shown).

However, propidium iodide assay revealed that massive cell death in the *stratum pyramidale* adjacent to the lesion side was triggered one week after lesion induction within an average distance of 100 ± 14 μm ($N = 3$), that was confined to the CA1 subregion (53 ± 8.5 PI(+)-cells CA1 subfield; $N = 4$; data not shown). Based on the particular layer propidium iodide uptake was limited to, which almost exclusively consists of neuronal cells and based on the known susceptibility of CA1 neurons to under-provision (McCullers et al., 2002; Ouyang et al., 2007), death cell was assigned particularly to pyramidal neurons.

All observations presented so far show that the lesion model utilized here is well suitable to investigate severe astrogliosis with compact glial scar formation. Upon mechanical injury delayed neuronal cell death and astrocytic activation are triggered in the hippocampal CA1 subregion: astrocytes significantly up-regulate GFAP, undergo massive morphological changes and become hypertrophied. A subset of reactive astrocytes within a distance of approximately 100 μm from the lesion site, named PRA, even decline acceptance of SR101, suggesting heterogeneity among the astrocytic response in dependence on the severity of tissue damage.

Astroglial glutamate transporter protein levels are changed one week after mechanical injury

In the sequel, this mechanical lesion model was employed to investigate whether severe reactive astrogliosis leads to alterations in astrocytic glutamate transporter expression. To determine spatial and overall protein levels of the astrocytic glutamate transporters, GLAST and GLT-1, we utilized immunohistochemistry as well as western blot analysis (Fig. 5 and 6). Immunhistochemical visualization of both glutamate transporters revealed that accumulations of immunopositive GLT-1 and GLAST puncta were preferentially localized at the distal end of processes that were directed towards the lesion site (see arrowheads in Fig. 5A and 5B). These were particularly pronounced when it comes to GLAST. As component of the dense glial scar these processes exhibited the highest GFAP immunoreactivity in lesioned preparations. Besides these dense cluster regions GLAST immunoreactivity remained basically unaltered, whereas GLT-1 immunoreactivity generally declined graduated with distance from the wound (as far as 250 μm from the lesion site). As results gained with immunohistochemistry can be influenced by factors like the ability of the antibody to penetrate tissue (e.g. to dense scar tissue) and as quantification is difficult to perform we subsequently performed immunoblots. For this we used the same probes that were earlier tested for GFAP enhancement. Induction of a mechanical lesion resulted in opposed changes in total GLT-1 and GLAST protein content as ascertained by western blot analysis (Fig. 6). Compared to GLT-1, which protein content did not change significantly, GLAST protein content increased by 15% in lesioned compared to control slice cultures ($p < 0.001$; 12 probes, 6 sibling pairs). To give consideration to the multimerization of both glutamate transporter (see Haugeto et al., 1996; Peacey et al., 2009) we also analyzed the monomeric and the multimeric forms of both transporters. Several bands were detected in organotypic slice culture homogenates (Fig. 6B and 6C) that most likely correspond to the monomeric and the oligomeric forms of both glutamate transporters. The experimentally determined molecular weights of the monomeric forms of GLAST (~60 kDa) and GLT-1 (~65 kDa) are in good agreement with calculations using the ExPASy compute pl/Mw tool for murine GLAST (59.6 kDa) and GLT-1 (62.1 kDa). For GLT-1, two additional multimerization types were present: a trimeric and a tetrameric form (Fig. 6B). An additional dimeric (120 kDa) and a

trimeric form (180 kDa) can be observed for GLAST (Fig. 6C). In order to perform quantification of both monomeric and multimeric protein content within the dynamic signal range, exposure latitudes were recorded. For GLT-1 the monomeric form (65 kDa) showed a considerable decline in protein content (14.3%; $p < 0.05$), while trimeric form (190 kDa) and tetrameric form (> 200 kDa) showed no difference to control conditions. GLAST on the other hand showed surprisingly no change of the monomeric form, but a substantial up-regulation of both multimeric forms (20.8 and 12.8%, respectively; $p < 0.001$).

Thus, after induction of severe astrogliosis GLAST multimer levels are generally increased, whereas the GLT-1 monomer content is decreased 6-7 dpl. Moreover, spatially restricted accumulations of GLAST and GLT-1 clusters are found at the astrocytic process endings facing the border of the scar.

Changed kinetics of glutamate transporter mediated sodium transients in reactive astrocytes

We then addressed the question how these changes in glutamate transporter composition affects high-affinity glutamate uptake. To evaluate glutamate transporter function in lesioned and control slice cultures we performed sodium imaging experiments with SBFI. First and foremost, to be able to calculate absolute sodium concentrations from the measured relative fluorescence values, SBFI calibration was performed in organotypic slice cultures (Fig. 7D and 7E). For a detailed description on the calibration procedure, the reader is kindly referred to earlier publications (Langer and Rose, 2009) + Schreiner & Rose, 2012). In our model system, a change in fluorescence ratio of 10% in the linear range corresponded to a change of sodium concentration by 5.5 mM ($n = 107$; $N = 6$, Fig. 6), comparable to results obtained in acute hippocampal slices (7.1 mM: Langer & Rose, 2009; 3.8 mM: Langer et al., 2012; Fig. 7D and 7E). Previous studies showed that either bath or local pipette application of D-aspartate activates glutamate transporters in astrocytes *in vitro* and *in situ* (Rose and Ransom, 1996; Langer and Rose, 2009). This process is coupled to an inward-directed transport of sodium and thus results in a measureable increase in the intracellular sodium concentration. Pressure application of 1mM D-aspartate for 500ms was used to induce glutamate uptake in this study (Fig. 7B). Afore performed dose-response analysis showed that 1 mM D-aspartate resulted in intracellular sodium transients of 3.8 ± 0.2 mM, that were still in the dynamic range, but close to transporter saturation (5mM D-aspartate induced $[Na^+]_i$ changes of 4.7 ± 0.5 mM; $n = 19$; $N = 3$; Fig. 7C). Throughout experiments ASCF was supplemented with 0.5 μM tetrodotoxin (TTX) to inhibit neuronal activity. Of the CA1 subregion, all cells positioned in the *stratum pyramidale* were excluded from the data analysis as the vast majority of these cells represent neurons. We subdivided the remaining SBFI-labeled cells of the *stratum radiatum* into two groups, proximal reactive astrocytes (PRA), which were not SR101 labeled within a distance of approximately 100 μm from the lesion site and distal reactive astrocytes (DRA) in the periphery of the lesion (> 100 μm). Our experiments revealed that the peak amplitude of D-aspartate induced sodium transients of control astrocytes and DRA were unaltered (3.8 ± 0.2 mM and 3.8 ± 0.3 mM, respectively; Fig. 8D). However, PRA displayed significant decreased peak amplitudes: the amplitude was about 2.5-fold smaller compared to control astrocytes and DRA, respectively (1.6 ± 0.21 mM; $p < 0.001$; Fig. 8C and 8D). Analysis of the rise rate, determined by the time passed between 10 % and 90 % of baseline to peak (often also referred to as 10%-90% rise time), further revealed that DRA exhibited a significantly prolonged (4.3-times) rise rate as compared to control astrocytes (control: 0.9 ± 0.05 Δ mM/s; DRA: 0.6 ± 0.06 Δ mM/s; $p < 0.001$; Fig. 8E). The rise rate was even more

decelerated in PRA ($0.2 \pm 0.04 \ \Delta$ mM/s). Analogous profound alterations were observed for the decay rate. As observed in earlier studies, the decay phase of intracellular Na^+ transients followed a mono-exponential time course (e.g. Rose et al., 1999; Bennay et al., 2008; Fig. 8B and 8C) Fig. 8B and 8C). Thus, the decay time constant τ (time until $1-1/e \approx 63.2$ % of Na^+ basal levels are re-established) was determined and used to calculate the decay rate. Compared to the decay rate of control astrocyte ($0.03 \pm 0.002 \ \Delta$ mM/s), the decay rate of DRA was 1.7-times smaller, the one of PRA even 4.8-times ($0.02 \pm 0.002 \ \Delta$ mM/s and $0.01 \pm 0.005 \ \Delta$ mM/s, respectively; $p < 0.001$; Fig. 8F).

As we have seen, all cells investigated in mechanically lesioned slice cultures exhibited prolonged kinetics of EAAT-mediated sodium transient as compared to controls. Both, the rise and the decay rate were severely slowed in DRA and PRA, PRA however were most intensely affected. Additionally, the peak amplitude of EAAT-induced sodium transients was exclusively scaled-down in PRA. Thus, the glutamate re-uptake capacity, the time scale of EAAT-induced sodium rise and recovery were severely impaired in PRA. DRA kinetics were likewise affected, however to a minor degree and glutamate re-uptake capacity was apparently unchanged. These findings are suggestive of an impaired function of astrocytic glutamate transporters and, moreover, of different degrees of alterations depending on the distance to the lesion site.

Discussion

Here, we employed hippocampal organotypic slice cultures as model to study the consequences of TBI in intact tissue. Mechanical lesion was followed by substantial up-regulation of GFAP, as demonstrated by immunohistochemistry as well as western blot analysis, and considerable hypertrophic swelling one week post-lesion. In the region bordering the lesion site astrocyte organization was completely distorted. GFAP(+)-processes were corrugated, elongated and partially radially re-arranged towards the lesion site. Astrocytes in this particular region displayed the most pronounced increase in cell body volume. Neuronal cell volume was not affected, delayed cell death of neurons next to the lesion site in the CA1 subregion was however observable. All the aforementioned findings are by all means indicative of severe reactive gliosis with formation of a define glial scar and neuronal degeneration as found in TBI (cf. Di Giovanni et al., 2005; Sofroniew, 2009; Sofroniew and Vinters, 2010). It can thus be confidably assumed that astrocytes become pathologically activate in the present TBI *in situ* model.

The most significant outcome gleaned from this data is that two distinct subtypes of reactive astrocytes could be classified upon criteria such as their distance from the lesion site, their capability to take up SR-101 and their glutamate uptake capacity.

It was already firmly established in recent years that astrocytes in the cortex and the hippocampus selectively incorporate the fluorescence dye SR101 and its fixable analogue Texas Red *in situ* and *in vivo* (Nimmerjahn et al., 2004; Kafitz et al., 2008; Nimmerjahn and Helmchen, 2012). Even though the precise uptake mechanism is still unknown, SR101 has become a widely used and appreciated tool to identify astrocytes. In this study we could show for the first time that induction of severe astrogliosis results in the inability of a subpopulation of reactive astrocytes adjacent to the lesion site to label for SR101. An earlier study already showed that the number of SBFI labeled cells in the *stratum radiatum* and in particular of electrophysiologically passive astrocytes that take up SR-101 increases substantially in the second to third postnatal week (Kafitz et al., 2008). While at P3 only 50 % of the SBFI labeled *stratum radiatum* cells were SR101-positive, the number had increased to 90 % by P15. In good accordance, we have determined a fraction of approximately 91 % SBFI – labeled, SR101-positive in the *stratum radiatum* of un-lesioned slice cultures. Intriguingly, this value declined to 56 % in the periphery of the scar (> 100 μm) one week after mechanical lesion. It can be speculated that PRAs in particular, based on their complete inability to accept SR101, might regain a more juvenile phenotype. That de-differentiation of mature astrocytes actually occurs in reactive gliosis was impressively shown by fate-mapping experiments performed by the group of Magdalena Götz (Buffo et al., 2008; for an review article see ; Robel et al., 2011). However, re-entry of the cell cycle was apparently limited to subset of reactive astrocytes, which were found within a distance of 100 μm from the lesion site, thus probably corresponding to the PRAs investigated here (Lee et al., 2003; Buffo et al., 2008; Barreto et al., 2011). Our results thus give support to earlier work, which already described the existence of two immunohistochemically, electrophysiologically and morphologically distinct subtypes of reactive astrocytes, manifested by the distance from the primary lesion (MacFarlane and Sontheimer, 1997; Chvatal et al., 2008; Barreto et al., 2011). They demonstrated that PRA within a distance of 100 μm exhibited enhanced K_{DR} currents, labeled positive for nestin, GFAP and BrdU, while DRA in the periphery were nestin(-), did not

proliferate and showed a temporal up-regulation of K_{IR} currents ($> 100 \mu$m; Perillan et al., 1999; Perillan et al., 2000). Furthermore, DRA, unlike the scar-forming PRA, undergo only moderate changes of their healthy astrocytic phenotype and show apparently full recovery of their normal morphological and functional features after several weeks (Chvatal et al., 2008). Thus, considering already published and here presented data, it can be assumed that the reactive astrocyte phenotype strongly depends on the type and severity of the inducing injury (Ridet et al., 1997; Chvatal et al., 2008; Barreto et al., 2011).

These two types of reactive astrocytes further exhibited a differentially impaired glutamate transporter distribution and re-uptake capacity. The protein-based analysis of both GLT-1 and GLAST that was performed one week after prime injury provided important insights into changes in protein distribution, quantity and multimer composition of the individual transporters upon severe injury. First of all, immunohistrochemistry showed that pronounced glutamate transporter accumulations, particularly of GLAST, at endings of astrocytic processes are induced at the border of the lesion site. When considering the vicinity of the wound as area of massive glutamate extrusion due to damaged or dead cells, decline in inhibitory projections, excitotoxicity, dendritic sprouting and path finding, the appearance of glutamate transporter clusters seems not to be surprising (Horner and Gage, 2000; Danbolt, 2001; Hinzman et al., 2010). Reversible cluster formation was shown to be inducible by e.g. the EAAT substrates L-glutamate, D-aspartate, ATP and the protein kinase C (PKC-)activator phorbol-12-myristate-13-acetate *in vitro* (PMA; Poitry-Yamate et al., 2002; Zhou and Sutherland, 2004; Nakagawa et al., 2008; Shin et al., 2009). Just currently Benediktsson and coworkers demonstrated that this local EAAT protein redistribution can also be triggered *in situ* (Benediktsson et al., 2012). Cluster formation was inhibited in sodium-free solution and when glutamate transporter blockers like DL-threo-β-benzyloxyaspartic acid (DL-TBOA) and dihydrokainate (DHK) were added (Nakagawa et al., 2008). The authors of the latter study speculated that very high glutamate concentrations would be necessary to induce cluster formation *in vivo*, as they possibly appear under pathological conditions. Along with GLAST clustering we found that multimerized, but not monomeric, GLAST protein content was significant increased. Opposed to this finding, GLT-1 multimer levels were unaltered, while GLT-1 monomer quantity was decreased. Accordingly, immunohistochemistry demonstrated a decline in GLT-1 protein. Reactive astrogliosis thus appears to affect the expression and multimerization of both astrocyte glutamate transporters differentially. Although several studies have acknowledged glutamate transporters congregation, no study has beforehand addressed altered glutamate transporter multimerization in a pathophysiological context (Haugeto et al., 1996; Schlag et al., 1998; Kalandadze et al., 2002; Peacey et al., 2009)

Present research also shows for the first time that EAAT-mediated sodium signaling in proximal and distal reactive astrocytes is dissimilar impaired. The massive changes in astrocytic EAAT protein levels and distribution were accompanied by diverging functional changes in both, PRA and DRA. PRAs in the direct vicinity of the lesion site exhibited significantly reduced Na$^+$ transient amplitudes with slowed dynamics. DRAs, which were localized more distant from the site of wound, showed Na$^+$ responses with unchanged amplitudes, but with compromised rise and decay rates. It thus seems that not only glutamate transporter expression of the two astrocytic subtypes is differentially affected by brain injury, but that glutamate transporter operation is further differentially impaired in different subsets of reactive astrocytes.

This study further revealed that the internal sodium clearance following EAAT activation is delayed. The slowed decay rate of EAAT-mediated sodium transients observed here might indicate that mechanical injury impairs not only EAAT function, but also Na^+/K^+-ATPase activity, since the mono-exponential decay time course of sodium can be mainly ascribed to the pump´s activity (Lima et al., 2008). Reduction in Na^+/K^+-ATPase expression was often found to be associated with pathological conditions (Gusarova et al., 2011). But a slowed clearance of internal sodium might also be due to a reduced pool of membrane-integrated Na^+/K^+-ATPase protein, changes in the composition of the α1- and α2-subunit and hence changes in sodium affinity and disassembly of the heteromeric protein subunits (Xie and Askari, 2002). In recent years it was established that in astrocytes glutamate transporters and the Na^+/K^+-ATPase are both part of the same macromolecular complex and that they operate as a functional unit to regulate glutamatergic transmission (Cholet et al., 2002; Rose et al., 2009). Based on this close interaction, alterations of the glutamate transporters may affect Na^+/K^+-ATPase content and function in a concentration-dependent manner, as suggested by the present research. Furthermore, sodium is not buffered in the cell and travels solely by means of diffusion in the cytoplasm. Hindered diffusion, resulting from increased cytoplasmic protein content or impaired gap junction coupling which both occur upon astrocytic activation, might thus also partially contribute to delayed sodium recovery (Chew et al., 2010; Middeldorp and Hol, 2011).

Conclusion

Present experimental data indicates that the functional response of astrocytes upon pathological activation is diverse, depending on the severity of brain damage. Mild to moderate astrogliosis in the periphery of a mechanical lesion seems not to be accompanied by a significant change in glial glutamate uptake capacity. At the glial scar itself, in proximal reactive astrocytes, a strong clustering of glutamate transporters is observed that apparently goes along with a severe functional reduction in astroglial glutamate uptake. A better understanding of this functional diversity is urgently needed, to develop treatment approaches that specifically target a certain subsets of reactive astrocytes.

Conflict of interest statement

The authors declare that there is no known or potential conflict of interest including any financial, personal or other relationships.

Author contributions

All authors had full access to all the data in the study and take responsibility for the integrity of the data and the accuracy of the data analysis.

A. E. Schreiner: vital and antibody stainings, western blot experiments, sodium imaging, cell death assay, vital staining, picture post-processing, data analysis and interpretation, experimental design and manuscript writing

M. C. Stock: western blot experiments, data interpretation, revision of manuscript

J. Langer: experimental design

K. W. Kafitz: establishment of organotypic slice cultures and scratch wound essay, interpretation of immunohistochemical stainings

C. R. Rose: project initiation and experimental design, data interpretation and manuscript writing

Literature

Abbott NJ, Ronnback L, Hansson E. 2006. Astrocyte-endothelial interactions at the blood-brain barrier. Nature reviews Neuroscience 7(1):41-53.

Anderson CM, Swanson RA. 2000. Astrocyte glutamate transport: review of properties, regulation, and physiological functions. Glia 32(1):1-14.

Arundine M, Tymianski M. 2004. Molecular mechanisms of glutamate-dependent neurodegeneration in ischemia and traumatic brain injury. Cellular and molecular life sciences : CMLS 61(6):657-668.

Barreto GE, Sun X, Xu L, Giffard RG. 2011. Astrocyte proliferation following stroke in the mouse depends on distance from the infarct. PloS one 6(11):e27881.

Barros LF, Deitmer JW. 2010. Glucose and lactate supply to the synapse. Brain research reviews 63(1-2):149-159.

Benediktsson AM, Marrs GS, Tu JC, Worley PF, Rothstein JD, Bergles DE, Dailey ME. 2012. Neuronal activity regulates glutamate transporter dynamics in developing astrocytes. Glia 60(2):175-188.

Bennay M, Langer J, Meier SD, Kafitz KW, Rose CR. 2008. Sodium signals in cerebellar Purkinje neurons and Bergmann glial cells evoked by glutamatergic synaptic transmission. Glia 56(10):1138-1149.

Beschorner R, Dietz K, Schauer N, Mittelbronn M, Schluesener HJ, Trautmann K, Meyermann R, Simon P. 2007. Expression of EAAT1 reflects a possible neuroprotective function of reactive astrocytes and activated microglia following human traumatic brain injury. Histology and histopathology 22(5):515-526.

Borgens RB, Liu-Snyder P. 2012. Understanding secondary injury. The Quarterly review of biology 87(2):89-127.

Brunne B, Zhao S, Derouiche A, Herz J, May P, Frotscher M, Bock HH. 2010. Origin, maturation, and astroglial transformation of secondary radial glial cells in the developing dentate gyrus. Glia 58(13):1553-1569.

Buffo A, Rite I, Tripathi P, Lepier A, Colak D, Horn AP, Mori T, Gotz M. 2008. Origin and progeny of reactive gliosis: A source of multipotent cells in the injured brain. Proceedings of the National Academy of Sciences of the United States of America 105(9):3581-3586.

Chen JC, Hsu-Chou H, Lu JL, Chiang YC, Huang HM, Wang HL, Wu T, Liao JJ, Yeh TS. 2005. Down-regulation of the glial glutamate transporter GLT-1 in rat hippocampus and striatum and its modulation by a group III metabotropic glutamate receptor antagonist following transient global forebrain ischemia. Neuropharmacology 49(5):703-714.

Chew SS, Johnson CS, Green CR, Danesh-Meyer HV. 2010. Role of connexin43 in central nervous system injury. Experimental neurology 225(2):250-261.

Cholet N, Pellerin L, Magistretti PJ, Hamel E. 2002. Similar perisynaptic glial localization for the Na+,K+-ATPase alpha 2 subunit and the glutamate transporters GLAST and GLT-1 in the rat somatosensory cortex. Cereb Cortex 12(5):515-525.

Chvatal A, Anderova M, Neprasova H, Prajerova I, Benesova J, Butenko O, Verkhratsky A. 2008. Pathological potential of astroglia. Physiological research / Academia Scientiarum Bohemoslovaca 57 Suppl 3:S101-110.

Danbolt NC. 2001. Glutamate uptake. Progress in neurobiology 65(1):1-105.

Deitmer JW, Rose CR. 2010. Ion changes and signalling in perisynaptic glia. Brain research reviews 63(1-2):113-129.

Di Giovanni S, Movsesyan V, Ahmed F, Cernak I, Schinelli S, Stoica B, Faden AI. 2005. Cell cycle inhibition provides neuroprotection and reduces glial proliferation and scar formation after traumatic brain injury. Proceedings of the National Academy of Sciences of the United States of America 102(23):8333-8338.

Eulenburg V, Gomeza J. 2010. Neurotransmitter transporters expressed in glial cells as regulators of synapse function. Brain research reviews 63(1-2):103-112.

Frizzo ME, Frizzo JK, Amadio S, Rodrigues JM, Perry ML, Bernardi G, Volonte C. 2007. Extracellular adenosine triphosphate induces glutamate transporter-1 expression in hippocampus. Hippocampus 17(4):305-315.

Gegelashvili G, Danbolt NC, Schousboe A. 1997. Neuronal soluble factors differentially regulate the expression of the GLT1 and GLAST glutamate transporters in cultured astroglia. Journal of neurochemistry 69(6):2612-2615.

Gegelashvili G, Dehnes Y, Danbolt NC, Schousboe A. 2000. The high-affinity glutamate transporters GLT1, GLAST, and EAAT4 are regulated via different signalling mechanisms. Neurochemistry international 37(2-3):163-170.

Ginsberg SD, Martin LJ, Rothstein JD. 1995. Regional deafferentation down-regulates subtypes of glutamate transporter proteins. Journal of neurochemistry 65(6):2800-2803.

Grewer C, Gameiro A, Zhang Z, Tao Z, Braams S, Rauen T. 2008. Glutamate forward and reverse transport: from molecular mechanism to transporter-mediated release after ischemia. IUBMB life 60(9):609-619.

Gusarova GA, Trejo HE, Dada LA, Briva A, Welch LC, Hamanaka RB, Mutlu GM, Chandel NS, Prakriya M, Sznajder JI. 2011. Hypoxia leads to Na,K-ATPase downregulation via Ca(2+) release-activated Ca(2+) channels and AMPK activation. Molecular and cellular biology 31(17):3546-3556.

Haugeto O, Ullensvang K, Levy LM, Chaudhry FA, Honore T, Nielsen M, Lehre KP, Danbolt NC. 1996. Brain glutamate transporter proteins form homomultimers. The Journal of biological chemistry 271(44):27715-27722.

Hinzman JM, Thomas TC, Burmeister JJ, Quintero JE, Huettl P, Pomerleau F, Gerhardt GA, Lifshitz J. 2010. Diffuse brain injury elevates tonic glutamate levels and potassium-evoked glutamate release in discrete brain regions at two days post-injury: an enzyme-based microelectrode array study. Journal of neurotrauma 27(5):889-899.

Horner PJ, Gage FH. 2000. Regenerating the damaged central nervous system. Nature 407(6807):963-970.

Ikonomidou C, Turski L. 2002. Why did NMDA receptor antagonists fail clinical trials for stroke and traumatic brain injury? Lancet neurology 1(6):383-386.

Jing R, Wilhelmsson U, Goodwill W, Li L, Pan Y, Pekny M, Skalli O. 2007. Synemin is expressed in reactive astrocytes in neurotrauma and interacts differentially with vimentin and GFAP intermediate filament networks. Journal of cell science 120(Pt 7):1267-1277.

Kafitz KW, Meier SD, Stephan J, Rose CR. 2008. Developmental profile and properties of sulforhodamine 101--Labeled glial cells in acute brain slices of rat hippocampus. Journal of neuroscience methods 169(1):84-92.

Kalandadze A, Wu Y, Robinson MB. 2002. Protein kinase C activation decreases cell surface expression of the GLT-1 subtype of glutamate transporter. Requirement of a carboxyl-terminal domain and partial dependence on serine 486. The Journal of biological chemistry 277(48):45741-45750.

Katoh H, Sima K, Nawashiro H, Wada K, Chigasaki H. 1997. The effect of MK-801 on extracellular neuroactive amino acids in hippocampus after closed head injury followed by hypoxia in rats. Brain research 758(1-2):153-162.

Kawano H, Kimura-Kuroda J, Komuta Y, Yoshioka N, Li HP, Kawamura K, Li Y, Raisman G. 2012. Role of the lesion scar in the response to damage and repair of the central nervous system. Cell and tissue research 349(1):169-180.

Koizumi H, Fujisawa H, Ito H, Maekawa T, Di X, Bullock R. 1997. Effects of mild hypothermia on cerebral blood flow-independent changes in cortical extracellular levels of amino acids following contusion trauma in the rat. Brain research 747(2):304-312.

Kosugi T, Kawahara K. 2006. Reversed actrocytic GLT-1 during ischemia is crucial to excitotoxic death of neurons, but contributes to the survival of astrocytes themselves. Neurochemical research 31(7):933-943.

Laird MD, Vender JR, Dhandapani KM. 2008. Opposing roles for reactive astrocytes following traumatic brain injury. Neuro-Signals 16(2-3):154-164.

Langer J, Rose CR. 2009. Synaptically induced sodium signals in hippocampal astrocytes in situ. The Journal of physiology 587(Pt 24):5859-5877.

Langer J, Stephan J, Theis M, Rose CR. 2012. Gap junctions mediate intercellular spread of sodium between hippocampal astrocytes in situ. Glia 60(2):239-252.

Lee CY, Pappas GD, Kriho V, Huang BM, Yang HY. 2003. Proliferation of a subpopulation of reactive astrocytes following needle-insertion lesion in rat. Neurological research 25(7):767-776.

Levy LM, Lehre KP, Walaas SI, Storm-Mathisen J, Danbolt NC. 1995. Down-regulation of glial glutamate transporters after glutamatergic denervation in the rat brain. The European journal of neuroscience 7(10):2036-2041.

Li S, Mealing GA, Morley P, Stys PK. 1999. Novel injury mechanism in anoxia and trauma of spinal cord white matter: glutamate release via reverse Na+-dependent glutamate transport. The Journal of neuroscience : the official journal of the Society for Neuroscience 19(14):RC16.

Lieth E, Barber AJ, Xu B, Dice C, Ratz MJ, Tanase D, Strother JM. 1998. Glial reactivity and impaired glutamate metabolism in short-term experimental diabetic retinopathy. Penn State Retina Research Group. Diabetes 47(5):815-820.

Lima FD, Souza MA, Furian AF, Rambo LM, Ribeiro LR, Martignoni FV, Hoffmann MS, Fighera MR, Royes LF, Oliveira MS, de Mello CF. 2008. Na+,K+-ATPase activity impairment after experimental traumatic brain injury: relationship to spatial learning deficits and oxidative stress. Behavioural brain research 193(2):306-310.

Lu YB, Iandiev I, Hollborn M, Korber N, Ulbricht E, Hirrlinger PG, Pannicke T, Wei EQ, Bringmann A, Wolburg H, Wilhelmsson U, Pekny M, Wiedemann P, Reichenbach A, Kas JA. 2011. Reactive glial cells: increased stiffness correlates with increased intermediate filament expression. FASEB journal : official publication of the Federation of American Societies for Experimental Biology 25(2):624-631.

MacFarlane SN, Sontheimer H. 1997. Electrophysiological changes that accompany reactive gliosis in vitro. The Journal of neuroscience : the official journal of the Society for Neuroscience 17(19):7316-7329.

Magavi S, Friedmann D, Banks G, Stolfi A, Lois C. 2012. Coincident generation of pyramidal neurons and protoplasmic astrocytes in neocortical columns. The Journal of neuroscience : the official journal of the Society for Neuroscience 32(14):4762-4772.

Matsugami TR, Tanemura K, Mieda M, Nakatomi R, Yamada K, Kondo T, Ogawa M, Obata K, Watanabe M, Hashikawa T, Tanaka K. 2006. From the Cover: Indispensability of the glutamate transporters GLAST and GLT1 to brain development. Proceedings of the National Academy of Sciences of the United States of America 103(32):12161-12166.

McCullers DL, Sullivan PG, Scheff SW, Herman JP. 2002. Mifepristone protects CA1 hippocampal neurons following traumatic brain injury in rat. Neuroscience 109(2):219-230.

Meier SD, Kovalchuk Y, Rose CR. 2006. Properties of the new fluorescent Na+ indicator CoroNa Green: comparison with SBFI and confocal Na+ imaging. Journal of neuroscience methods 155(2):251-259.

Middeldorp J, Hol EM. 2011. GFAP in health and disease. Progress in neurobiology 93(3):421-443.

Minta A, Tsien RY. 1989. Fluorescent indicators for cytosolic sodium. The Journal of biological chemistry 264(32):19449-19457.

Moretto MB, Arteni NS, Lavinsky D, Netto CA, Rocha JB, Souza DO, Wofchuk S. 2005. Hypoxic-ischemic insult decreases glutamate uptake by hippocampal slices from neonatal rats: prevention by guanosine. Experimental neurology 195(2):400-406.

Nakagawa T, Otsubo Y, Yatani Y, Shirakawa H, Kaneko S. 2008. Mechanisms of substrate transport-induced clustering of a glial glutamate transporter GLT-1 in astroglial-neuronal cultures. The European journal of neuroscience 28(9):1719-1730.

Nilsson P, Hillered L, Ponten U, Ungerstedt U. 1990. Changes in cortical extracellular levels of energy-related metabolites and amino acids following concussive brain injury in rats. Journal of cerebral blood flow and metabolism : official journal of the International Society of Cerebral Blood Flow and Metabolism 10(5):631-637.

Nimmerjahn A, Helmchen F. 2012. In vivo labeling of cortical astrocytes with sulforhodamine 101 (SR101). Cold Spring Harbor protocols 2012(3):326-334.

Nimmerjahn A, Kirchhoff F, Kerr JN, Helmchen F. 2004. Sulforhodamine 101 as a specific marker of astroglia in the neocortex in vivo. Nature methods 1(1):31-37.

Norenberg MD. 1998. Astroglial dysfunction in hepatic encephalopathy. Metabolic brain disease 13(4):319-335.

Olabarria M, Noristani HN, Verkhratsky A, Rodriguez JJ. 2010. Concomitant astroglial atrophy and astrogliosis in a triple transgenic animal model of Alzheimer's disease. Glia 58(7):831-838.

Ouyang YB, Voloboueva LA, Xu LJ, Giffard RG. 2007. Selective dysfunction of hippocampal CA1 astrocytes contributes to delayed neuronal damage after transient forebrain ischemia. The Journal of neuroscience : the official journal of the Society for Neuroscience 27(16):4253-4260.

Peacey E, Miller CC, Dunlop J, Rattray M. 2009. The four major N- and C-terminal splice variants of the excitatory amino acid transporter GLT-1 form cell surface homomeric and heteromeric assemblies. Molecular pharmacology 75(5):1062-1073.

Pekny M, Eliasson C, Siushansian R, Ding M, Dixon SJ, Pekna M, Wilson JX, Hamberger A. 1999. The impact of genetic removal of GFAP and/or vimentin on glutamine levels and transport of glucose and ascorbate in astrocytes. Neurochemical research 24(11):1357-1362.

Pekny M, Nilsson M. 2005. Astrocyte activation and reactive gliosis. Glia 50(4):427-434.

Perea G, Navarrete M, Araque A. 2009. Tripartite synapses: astrocytes process and control synaptic information. Trends in neurosciences 32(8):421-431.

Perillan PR, Li X, Potts EA, Chen M, Bredt DS, Simard JM. 2000. Inward rectifier K(+) channel Kir2.3 (IRK3) in reactive astrocytes from adult rat brain. Glia 31(2):181-192.

Perillan PR, Li X, Simard JM. 1999. K(+) inward rectifier currents in reactive astrocytes from adult rat brain. Glia 27(3):213-225.

Poitry-Yamate CL, Vutskits L, Rauen T. 2002. Neuronal-induced and glutamate-dependent activation of glial glutamate transporter function. Journal of neurochemistry 82(4):987-997.

Rao VL, Baskaya MK, Dogan A, Rothstein JD, Dempsey RJ. 1998. Traumatic brain injury down-regulates glial glutamate transporter (GLT-1 and GLAST) proteins in rat brain. Journal of neurochemistry 70(5):2020-2027.

Raponi E, Agenes F, Delphin C, Assard N, Baudier J, Legraverend C, Deloulme JC. 2007. S100B expression defines a state in which GFAP-expressing cells lose their neural stem cell potential and acquire a more mature developmental stage. Glia 55(2):165-177.

Ridet JL, Malhotra SK, Privat A, Gage FH. 1997. Reactive astrocytes: cellular and molecular cues to biological function. Trends in neurosciences 20(12):570-577.

Robel S, Berninger B, Gotz M. 2011. The stem cell potential of glia: lessons from reactive gliosis. Nature reviews Neuroscience 12(2):88-104.

Rose CR, Kovalchuk Y, Eilers J, Konnerth A. 1999. Two-photon Na+ imaging in spines and fine dendrites of central neurons. Pflugers Archiv : European journal of physiology 439(1-2):201-207.

Rose CR, Ransom BR. 1996. Intracellular sodium homeostasis in rat hippocampal astrocytes. The Journal of physiology 491 (Pt 2):291-305.

Rose EM, Koo JC, Antflick JE, Ahmed SM, Angers S, Hampson DR. 2009. Glutamate transporter coupling to Na,K-ATPase. The Journal of neuroscience : the official journal of the Society for Neuroscience 29(25):8143-8155.

Rothstein JD, Dykes-Hoberg M, Pardo CA, Bristol LA, Jin L, Kuncl RW, Kanai Y, Hediger MA, Wang Y, Schielke JP, Welty DF. 1996. Knockout of glutamate transporters reveals a major role for astroglial transport in excitotoxicity and clearance of glutamate. Neuron 16(3):675-686.

Rothstein JD, Patel S, Regan MR, Haenggeli C, Huang YH, Bergles DE, Jin L, Dykes Hoberg M, Vidensky S, Chung DS, Toan SV, Bruijn LI, Su ZZ, Gupta P, Fisher PB. 2005. Beta-lactam antibiotics offer neuroprotection by increasing glutamate transporter expression. Nature 433(7021):73-77.

Rouach N, Avignone E, Meme W, Koulakoff A, Venance L, Blomstrand F, Giaume C. 2002. Gap junctions and connexin expression in the normal and pathological central nervous system. Biology of the cell / under the auspices of the European Cell Biology Organization 94(7-8):457-475.

Schlag BD, Vondrasek JR, Munir M, Kalandadze A, Zelenaia OA, Rothstein JD, Robinson MB. 1998. Regulation of the glial Na+-dependent glutamate transporters by cyclic AMP analogs and neurons. Molecular pharmacology 53(3):355-369.

Schneiderman JH. 1997. The role of long-term potentiation in persistent epileptiform burst-induced hyperexcitability following GABAA receptor blockade. Neuroscience 81(4):1111-1122.

Shin JW, Nguyen KT, Pow DV, Knight T, Buljan V, Bennett MR, Balcar VJ. 2009. Distribution of glutamate transporter GLAST in membranes of cultured astrocytes in the presence of glutamate transport substrates and ATP. Neurochemical research 34(10):1758-1766.

Simon C, Gotz M, Dimou L. 2011. Progenitors in the adult cerebral cortex: cell cycle properties and regulation by physiological stimuli and injury. Glia 59(6):869-881.

Sofroniew MV. 2009. Molecular dissection of reactive astrogliosis and glial scar formation. Trends in neurosciences 32(12):638-647.

Sofroniew MV, Vinters HV. 2010. Astrocytes: biology and pathology. Acta neuropathologica 119(1):7-35.

Springer JE, Azbill RD, Mark RJ, Begley JG, Waeg G, Mattson MP. 1997. 4-hydroxynonenal, a lipid peroxidation product, rapidly accumulates following traumatic spinal cord injury and inhibits glutamate uptake. Journal of neurochemistry 68(6):2469-2476.

Stoppini L, Buchs PA, Muller D. 1991. A simple method for organotypic cultures of nervous tissue. Journal of neuroscience methods 37(2):173-182.

Suarez I, Bodega G, Fernandez B. 2000. Modulation of glutamate transporters (GLAST, GLT-1 and EAAC1) in the rat cerebellum following portocaval anastomosis. Brain research 859(2):293-302.

Tian GF, Azmi H, Takano T, Xu Q, Peng W, Lin J, Oberheim N, Lou N, Wang X, Zielke HR, Kang J, Nedergaard M. 2005. An astrocytic basis of epilepsy. Nature medicine 11(9):973-981.

Tzingounis AV, Wadiche JI. 2007. Glutamate transporters: confining runaway excitation by shaping synaptic transmission. Nature reviews Neuroscience 8(12):935-947.

van Landeghem FK, Weiss T, Oehmichen M, von Deimling A. 2006. Decreased expression of glutamate transporters in astrocytes after human traumatic brain injury. Journal of neurotrauma 23(10):1518-1528.

Vermeiren C, Najimi M, Vanhoutte N, Tilleux S, de Hemptinne I, Maloteaux JM, Hermans E. 2005. Acute up-regulation of glutamate uptake mediated by mGluR5a in reactive astrocytes. Journal of neurochemistry 94(2):405-416.

Wei J, Pan X, Pei Z, Wang W, Qiu W, Shi Z, Xiao G. 2012. The beta-lactam antibiotic, ceftriaxone, provides neuroprotective potential via anti-excitotoxicity and anti-inflammation response in a rat model of traumatic brain injury. The journal of trauma and acute care surgery.

Weir MD, Thomas DG. 1984. Effect of dexamethasone on glutamine synthetase and glial fibrillary acidic protein in normal and transformed astrocytes. Clinical neuropharmacology 7(4):303-306.

Werner C, Engelhard K. 2007. Pathophysiology of traumatic brain injury. British journal of anaesthesia 99(1):4-9.

Wilhelmsson U, Bushong EA, Price DL, Smarr BL, Phung V, Terada M, Ellisman MH, Pekny M. 2006. Redefining the concept of reactive astrocytes as cells that remain within their unique domains upon reaction to injury. Proceedings of the National Academy of Sciences of the United States of America 103(46):17513-17518.

Wilhelmsson U, Li L, Pekna M, Berthold CH, Blom S, Eliasson C, Renner O, Bushong E, Ellisman M, Morgan TE, Pekny M. 2004. Absence of glial fibrillary acidic protein and vimentin prevents hypertrophy of astrocytic processes and improves post-traumatic regeneration. The Journal of neuroscience : the official journal of the Society for Neuroscience 24(21):5016-5021.

Wu Y, Zhang AQ, Yew DT. 2005. Age related changes of various markers of astrocytes in senescence-accelerated mice hippocampus. Neurochemistry international 46(7):565-574.

Xie Z, Askari A. 2002. Na(+)/K(+)-ATPase as a signal transducer. European journal of biochemistry / FEBS 269(10):2434-2439.

Yi JH, Hazell AS. 2006. Excitotoxic mechanisms and the role of astrocytic glutamate transporters in traumatic brain injury. Neurochemistry international 48(5):394-403.

Zacchigna S, Lambrechts D, Carmeliet P. 2008. Neurovascular signalling defects in neurodegeneration. Nature reviews Neuroscience 9(3):169-181.

Zhou J, Sutherland ML. 2004. Glutamate transporter cluster formation in astrocytic processes regulates glutamate uptake activity. The Journal of neuroscience : the official journal of the Society for Neuroscience 24(28):6301-6306.

Zhou M, Schools GP, Kimelberg HK. 2006. Development of GLAST(+) astrocytes and NG2(+) glia in rat hippocampus CA1: mature astrocytes are electrophysiologically passive. Journal of neurophysiology 95(1):134-143.

Zhu X, Bergles DE, Nishiyama A. 2008. NG2 cells generate both oligodendrocytes and gray matter astrocytes. Development 135(1):145-157.

Figure Legends

Figure 1. Astrocytes in hippocampal organotypic slice cultures after 19-25 days in culture. (A) Morphological comparison of astrocytes in acute slices and organotypic slice cultures of the hippocampus.Shown are SR-101 labeled cells (*left row*) expressing GFP under control of the GFAP promoter (FVB/N-Tg[GFAPGFP]14Mes/J mice; *right row*) in acute slices (*upper column*) and organotypic slice cultures (*lower column*). Almost all SR-101 positive cells in organotypic slice cultures showed detectable GFP levels, identifying them as astrocytes. The ratio of SR-101 labeled and GFP expressing cells in this *in vitro* system is comparable to the in *situ* situation. Asterisks indicate SR-101 labeled cells that do not express GFP and arrowheads GFP(+)/SR-101(-) cells. The dashed line highlights the boundary of the *stratum pyramidale*. Documentation was accomplished by a confocal laser scanning microscope (15 optical slices á 1 μm). **(B)** *Left*: Inverted picture of an SR-101 overview staining in hippocampal organotypic slice cultures (taken with a confocal laser scanning microscope, 20 optical slices á 1 μm). The green marked region accentuates the *stratum pyramidale*, the boxed area indicates the CA1 region this study focused on. *Right*: Immunohistochemical staining detecting the astrocytic marker glial fibrillary acidic protein (GFAP) and S100 calcium binding protein ß (S100ß). DAPI counterstaining was performed to visualize cell nuclei. The upper row shows the individual fluorescence images of GFAP (*left*) and S100ß (*right*), the lower row DAPI counterstaining (*blue; left*) to visualize the pyramidal cell layer, and the merge of the antibody double-staining (GFAP= *green*; S100ß= *magenta*; *right*). The dashed line highlights the boundary of the *strata pyramidal*e and *radiatum*. Documentation was accomplished by widefield epifluorescence microscopy (Nikon 90i). Both, uptake of SR-101 and the expression of GFAP and S100ß demonstrate that astrocytes in hippocampal organotypic slice cultures do not maintain their rather immature phenotype after 19-25 days *in vitro*. DAPI, 4',6-diamidino-2-phenylindole; GFAP = glial fibrillary acidic protein; GFP, green fluorescence protein; S100ß, S100 calcium binding protein; SR-101, sulforhodamine 101; StrO, *stratum oriens*; StrP, *stratum pyramidale*; StrR, *stratum radiatum*; StrLM, *stratum lacunosum-moleculare*; StrM, *stratum moleculare*; Scale bars: **(A)** 50 μm, **(B)** 100 μm (*left*) and 50 μm (*right*), respectively.

Figure 2. Induction of severe reactive gliosis by mechanical injury. The employed scratch wound assay reliably induced reactive gliosis. **(A)** Mechanical lesion model: The scratch wound was positioned in the CA1 area perpendicular to the *stratum pyramidale*, included the *strata oriens*, *pyramidale*, *radiatum* and *lacunosum-moleculare* and spanned the entire depth of the slice. For western blot analysis CA1 tissue pieces with a width of about 700 μm were excised. **(B)** *top*: western blot analysis detecting GFAP in control and lesioned litter mates. *bottom*: quantification of western blot data. Western blot analysis revealed a significantly increased protein content of the canonic GFAP form in lesioned slice cultures compared to control litter mates (50 kDa band; p < 0.001). The data was statistically analysed by Chi^2-test (*** $p < 0.001$; n = 14 probes, N = 5; 6 sibling pairs). **(C)** GFAP antibody visualization in an overview picture of the hippocampus and a corresponding detail of the CA1 region (as indicated by the dashed box) underneath. The dashed line in the right detail indicates the position of the lesion core. GFAP expression substantially increases 6-7 days post lesion, in particular besides the lesion site. **(D)** Staining pattern of GFAP (*top*) and S100ß (*bottom*) adjacent to the lesion site. Particular in the scar region GFAP and S100ß expression are highly up-regulated. **(E)** illustrates the GFAP network of a control astrocyte and of a peripheral reactive astrocyte (DRA) in a distance of approximately 150 μm from the scratch wound. Number and thickness of processes increases and GFAP filaments became undirected. The position of the astrocytic cell bodies is indicated by asterisk. Documentation of (C) was accomplished by widefield epifluorescence microscopy (Nikon 90i), while all other images were taken with a confocal laser scanning microscope (15 optical slices á 1 μm). AL, alveus; EC, entorhinal cortex; GFAP, glial fibrillary acidic protein; StrO, *stratum oriens*; StrP, *stratum pyramidale*; StrR, *stratum radiatum*; StrLM, *stratum lacunosum-moleculare*; Scale bars **(B)** 200 μm and 50 μm, respectively, **(D)** 10 μm, **(E)** 10 μm.

Figure 3. Diminished SR-101 uptake in reactive astrocytes. (A) shows an inverted representation of an SR-101 stained slice cultures of the hippocampus 6-7 days post lesion (the *stratum pyramidale* is highlighted for better orientation). An image with a higher magnification of the lesion area can be found on the right site. In mechanically lesioned slice cultures astrocytes take up less SR-101 or are even completely devoid of labeling in the direct vicinity of the lesion side (indicated by the dashed line). Those SR-101-positive cells, positioned at the

border of this barely labeled area, directed prolonged processes towards the lesion core (asterisk; see magnified astrocyte at the right lower corner). **(B)** Transgenic animals (FVB/N-Tg[GFAPGFP]14Mes/J) expressing green fluorescence protein (GFP) under the GFAP promoter could demonstrate that cells that took up the sodium sensitive dye SBFI, but not SR-101, near the lesion site in the stratum radiatum were indeed astrocytic cells. Shown is the SR-101, GFP-GFAP, SBFI fluorescence and the transmission image of the stratum radiatum (CA1 region) near the lesion site. Documented was accomplished with a widefield epipfluorescence microscope that was alike used for sodium imaging recordings. AL, alveus; EC, entorhinal cortex; GFAP, glial fibrillary acidic protein; GFP, green fluorescence protein; SBFI, sodium binding benzofuran isophthalate; SR-101, sulforhodamine 101; StrO, *stratum oriens*; StrP, *stratum pyramidale*; StrR, *stratum radiatum*; StrLM, *stratum lacunosum-moleculare*; Scale bars: 100 μm (upper left) and 20 μm (other images), respectively.

Figure 4. Impaired cell volume regulation and decreased basal sodium levels. **(A)** Confocal Image of astrocytes that express GFP under the control of the GFAP promotor in lesioned (*top*) and control (*bottom*) hippocampal slice cultures (10 optical slices á 1 μm). Cells marked by arrowheads are presented in a higher magnification on the right side **(A´)**. To accentuate cell body size, somata are framed by a dashed outline. In lesioned slices one proximal reactive astrocyte (PRA) and one distal reactive astrocyte (DRA) is displayed. **(B)** shows the quantification of cell body volume and determined by SBFI fluorescence (not shown). Cytoplasmic cell volume increase was seen in all both reactive astrocyte types under investigation. Compared to control astrocytes DRA soma size was 12 % and PRA soma size 16 % enlarged ($p < 0.001$; control: $n = 442$; DRA: $n = 127$; PRA: $n = 28$ in $N = 19$ and 9, respectively). Data was statistically analyzed by Student's t test (*** $p < 0.001$; *n.s.* > 0.05). GFAP, glial fibrillary acidic protein; GFP, green fluorescence protein; SBFI, sodium binding benzofuran isophthalate; StrP, *stratum pyramidale*; StrR, *stratum radiatum*; StrLM, *stratum lacunosum-moleculare*; Scale bar: 10 μm

Figure 5. Spatial glutamate transporter distribution after mechanical injury. (A) represents inverted images of immunohistochemical stainings detecting the glutamate transporters GLT-1 (*top row*) and the astrocytic intermediate filament GFAP (*bottom row*) as counterstaining in control (*left column*) and lesioned slice cultures (*right bottom*). **(B)** shows a corresponding GLAST (top row) and GFAP doublelabeling of a mechanically lesioned slice culture. After mechanical lesion induction, concentrated glutamate transporter immunoreactive puncta are found accumulated in the direct vicinity of the lesion site (arrowheads). GLT-1 immunoreactivity generally declined while GLAST immunoreactivity was basically unaltered disregarding the dense GLAST cluster. GFAP, glial fibrillary acidic protein; GLAST, glutamate aspartate transporter; GLT-1, glutamate-transporter-1; StrO, *stratum oriens*; StrP, *stratum pyramidale*; StrR, *stratum radiatum*; StrLM, *stratum lacunosum-moleculare*; Scale bars: (A) 40 μm, (B) 20 μm.

Figure 6. Changed glutamate transporter expression and multimer composition following mechanical injury. Western blot analysis revealed that 6-7 days post lesion total GLT-1 and GLAST protein content show converse changes. **(A)** Comparison of overall GLT-1 and GLAST protein content showed that GLT-1 expression was basically unaltered (*left*), while GLAST content (*right*) was significantly increased in lesioned slice cultures compared to controls (15 %; $p < 0.001$). Exemplary detection of GLT-1 and GLAST protein, respectively, on western blots can be gathered from **(B)** and **(C)**. Western blot revealed several bands corresponding to the different monomeric and multimeric forms of the respective glutamate transporter. **(B)** Quantitative analysis of the complex composition of GLT-1 demonstrated that only the monomeric form was significantly altered exhibiting 5 % lower protein levels after mechanical lesion compared to control conditions ($p < 0.05$). **(C)** GLAST on the other hand showed an increase of both multimers, the dimeric and the tetrameric complex form, but not of the monomeric form ($p < 0.001$; GLT-1: $n = 38$ probes, 6 sibling pairs; $N = 5$; GLAST: $n = 48$ probes, 6 sibling; $N = 5$.). Data was statistically analyzed by Chi^2-test (* $p < 0.05$; *** $p < 0.001$; *n.s.* > 0.05).

Figure 7. SBFI imaging in hippocampal organotypic slice cultures. (A) *Left*: image of SR-101 fluorescence in which astrocytes are labeled in red. *Middle left*: Image of the SBFI fluorescence taken from the same area with neuronal and glial cells stained in green. Cell bodies of CA1 pyramidal neurons can be recognized in the *stratum pyramidale* (StrP). *Middle right*: overlay of both fluorescence channels in which SBFI-loaded, SR101-positive astrocytes appear in yellow. *Right*: transmitted light image of this particular detail of the hippocampal CA1 region. **(B)** illustrates sodium transients typically elicited by local application of 1 mM D-aspartate. **(C)** Dose-

response analysis showed that stimulation with 1 mM D-aspartate resulted in intracellular sodium transients of 3.8 ± 0.2 mM, thus still in the dynamic response range, but close to transporter saturation (about 5 mM). **(D)** *Left*: calibration of the sodium sensitivity of SBFI in astrocytes. Cells were bolus-loaded with the membrane-permeable form SBFI-AM and then subjected to calibration solution containing ionophores and ouabain for accelerated equilibration. Stepwise changes in the extracellular sodium concentration from 0 to 40 mM and back caused stepwise changes in the fluorescence ratio of SBFI ($F340/F380$). *Right*: relationship between changes in fluorescence ratio ($\Delta F340/F380$) and intracellular sodium concentration, normalized to the ratio in sodium-free calibration saline. Shown are mean values $\pm$ S.E.M. ($n = 107$ cells; $N = 6$). The fit reveals a virtually linear relationship between 10 and 40 mM sodium. Within this range, a 10% change in fluorescence emission corresponds to a change of about 5.5 mM sodium. SBFI, sodium binding benzofuran isophthalate; SR-101, sulforhodamine 101; StrP, *stratum pyramidale*; StrR, *stratum radiatum*; Scale bar: 20 μm.

Figure 8. Altered glutamate transporter-mediated sodium transients in reactive astrocytes. (A) images of the SBFI fluorescence (*left*) and of the SR101 fluorescence (*right*) taken from the hippocampal CA1 area of double labeled control (*upper row*) and lesioned (*bottom row*) hippocampal organotypic slice cultures. The transmission picture visualizes the position of the stimulation pipette. Circles indicate the regions of interest analyzed in the experiment depicted in **(C)**. The lesion site is indicated by the dashed line. **(B)** D-aspartate mediated activation of EAATs resulted in sodium transients with distinct signal kinetic in distal (DRA) and proximal reactive astrocytes (PRA). **(C)** The rise rate of somatic sodium transients is considerably prolonged in DRA (*2*) and PRA (*3*) compared to control astrocytes (*1*), thereby PRA showed the slowest slope ($p < 0.001$). The quantification of this observation can be found in **(E)**. **(D)** The mean peak amplitude of sodium signals in DRA was not different from the one in control astrocytes. The average peak amplitude of PRA however was significantly smaller ($p < 0.001$). Analogous to the altered rise rate, decay rate of EAAT-mediated sodium transients was slowed, the severity of impairment corresponded to the proximity to the lesion site: Both, sodium decay rate in PRA and in DRA was slowed, PRA, though, showed the most pronounced impairment of sodium recovery compared to DRA ($p < 0.001$). Data was statistically analysed by Student's t test (** $p < 0.01$; *** $p < 0.001$; *n.s.* > 0.05; Control: $n = 161$; $N = 12$; DRA: $n = 111$ and PRA: $n = 26$; $N = 7$). SBFI, sodium binding benzofuran isophthalate; SR-101, sulforhodamine 101; StrP, *stratum pyramidale*; StrR, *stratum radiatum*; Scale bar: 40 μm.
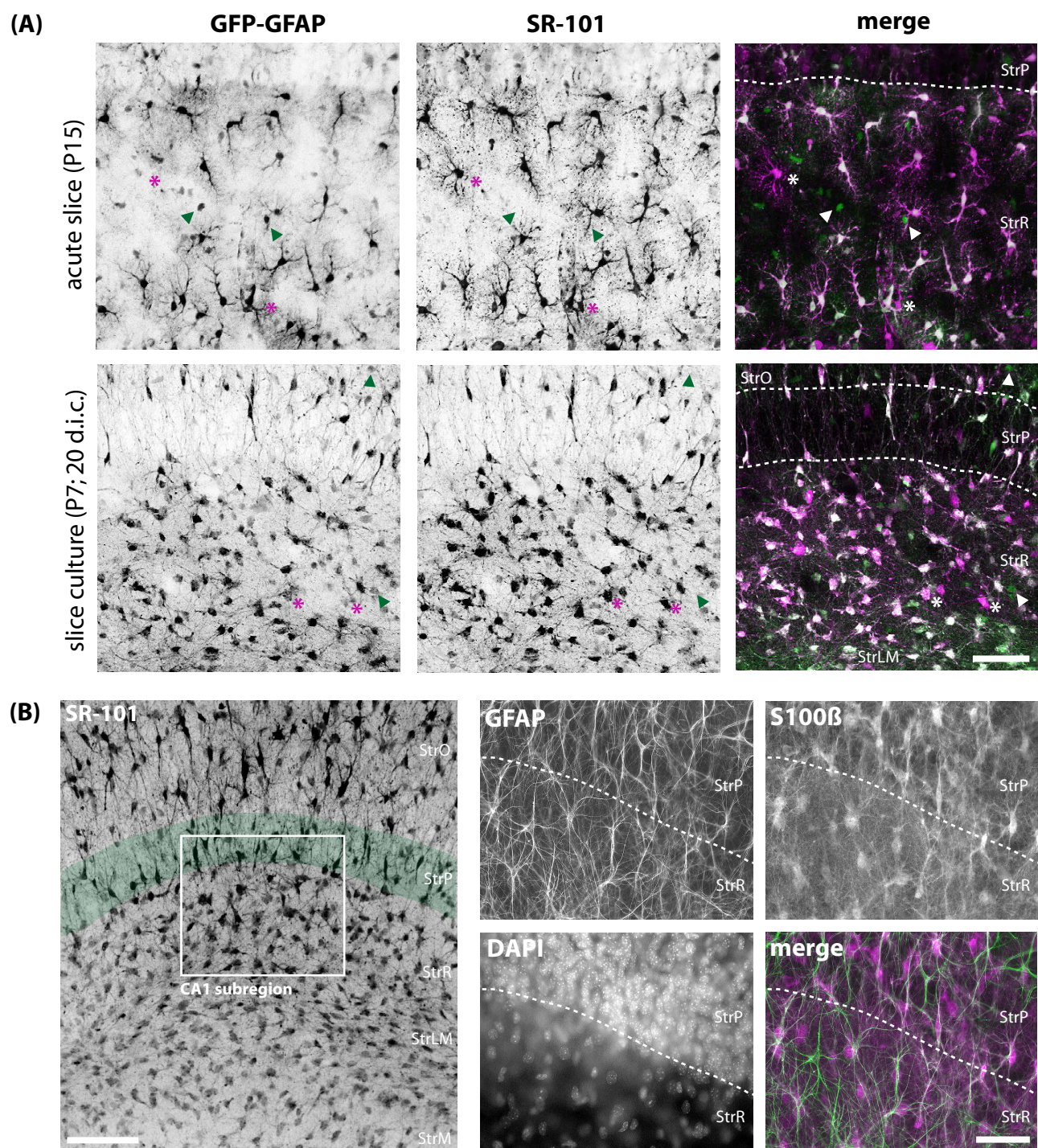
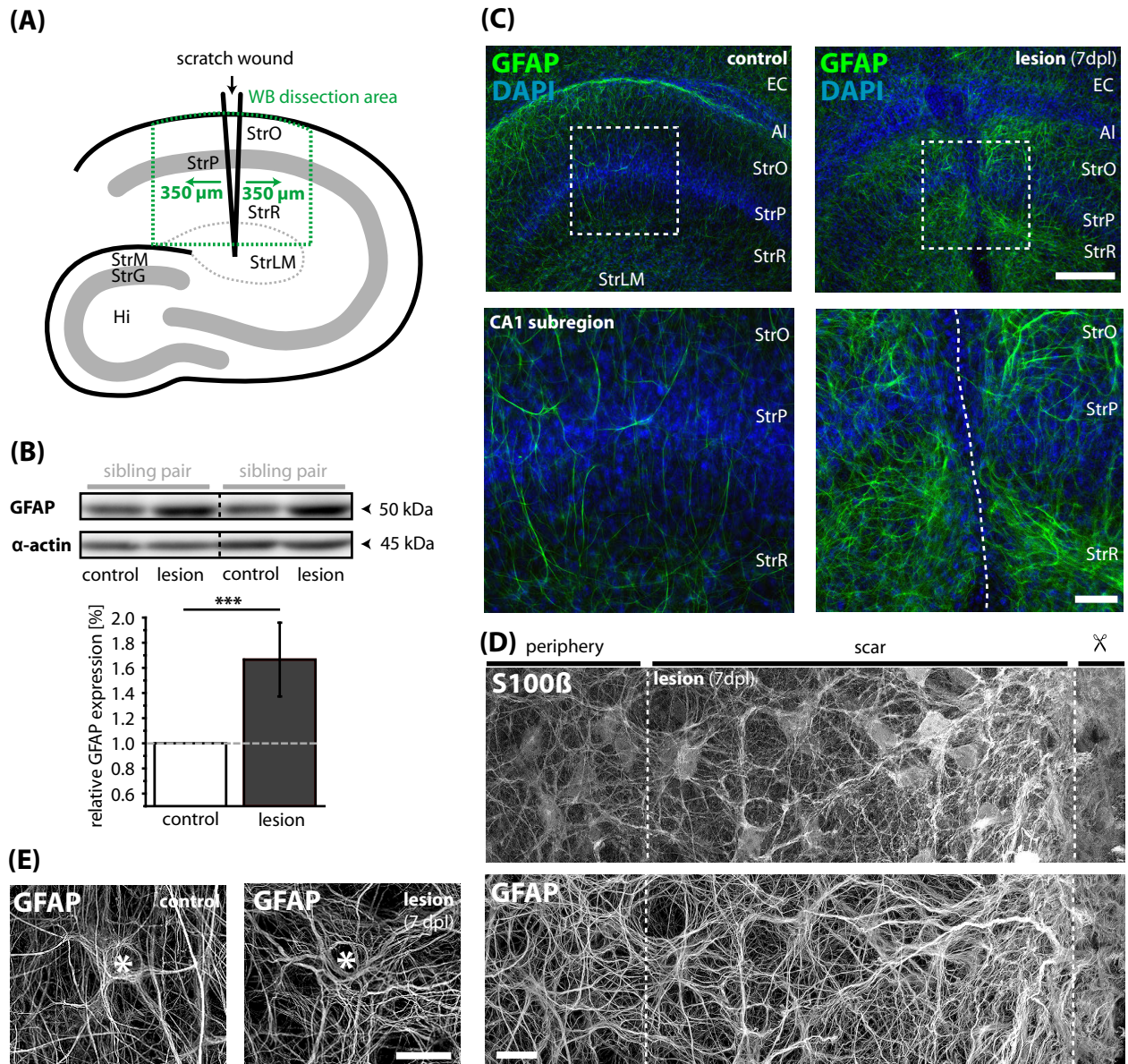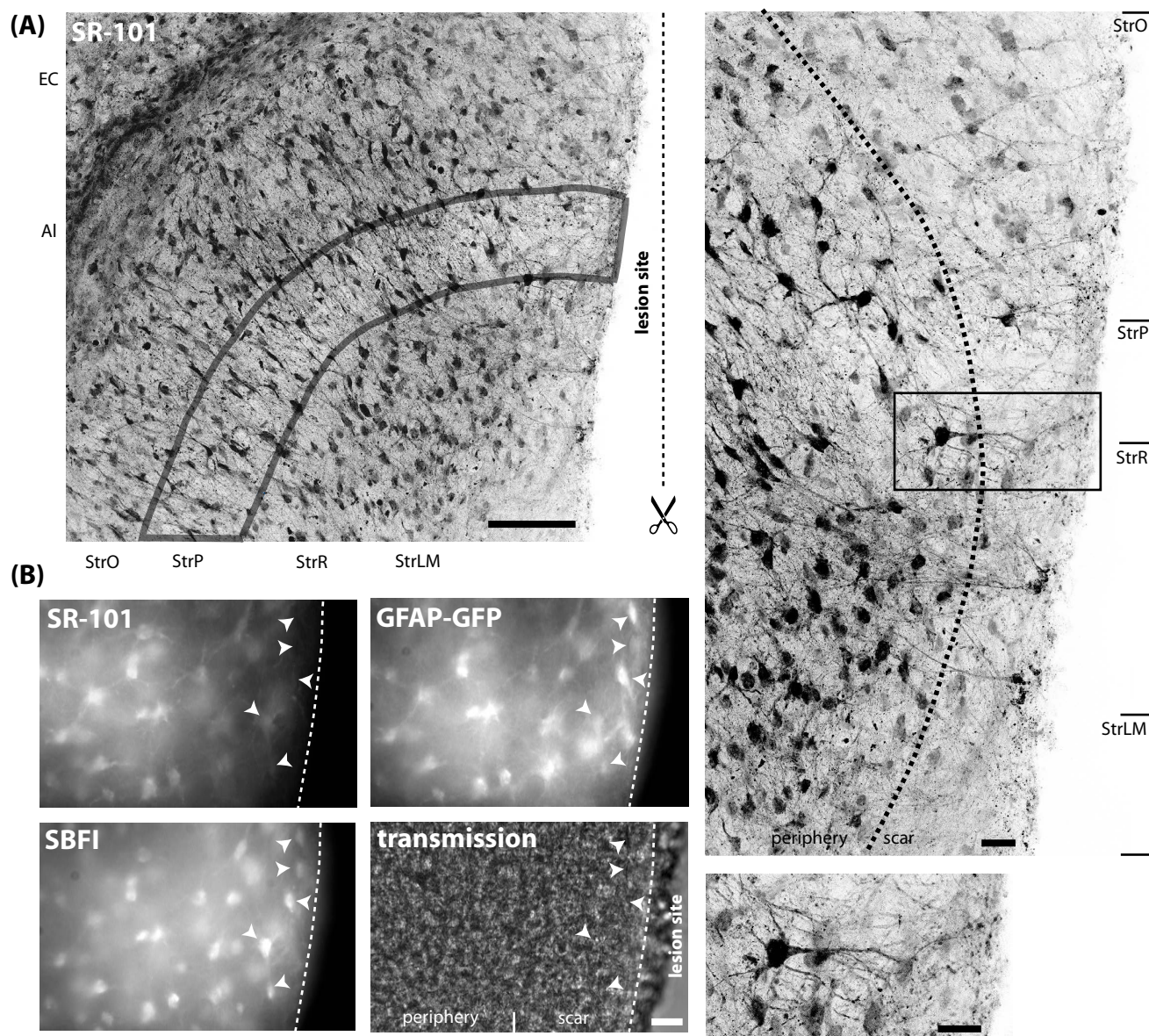**Fig. 1.** Schreiner, Stock, Langer, Kafitz & Rose

Fig. 2. Schreiner, Stock, Langer, Kafitz & Rose
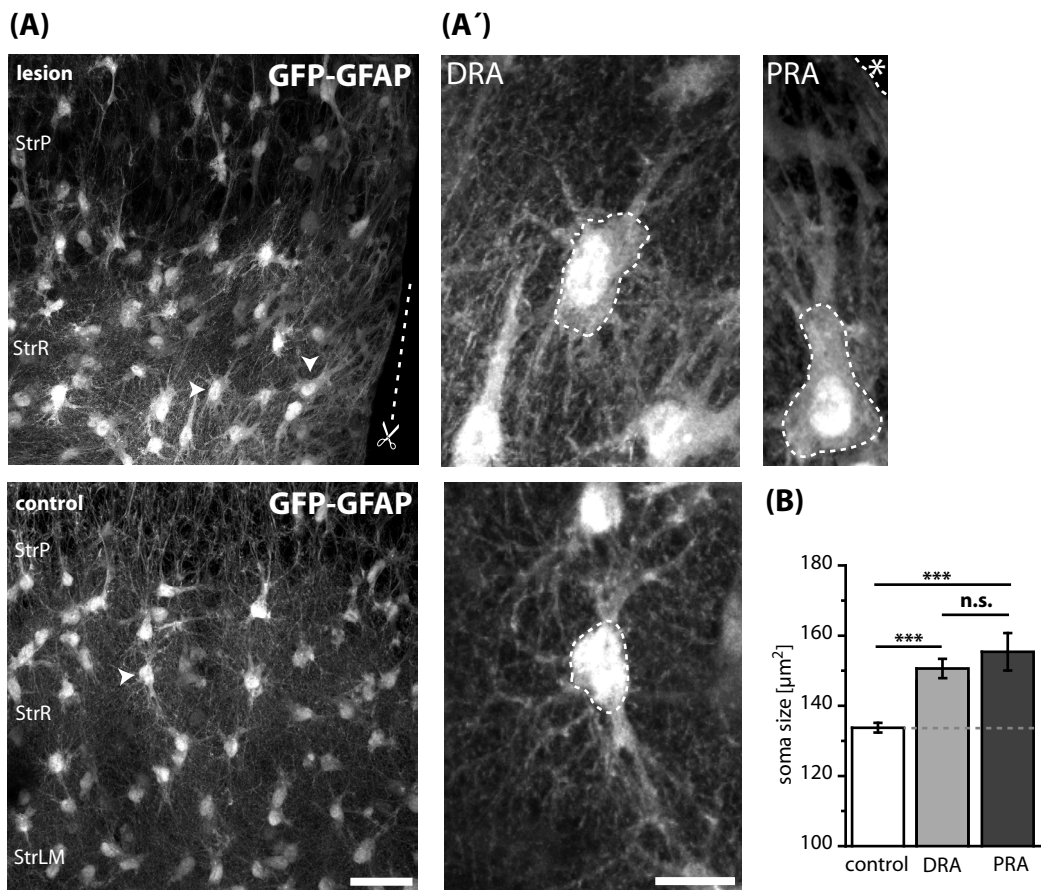
Fig. 3. Schreiner, Stock, Langer, Kafitz & Rose
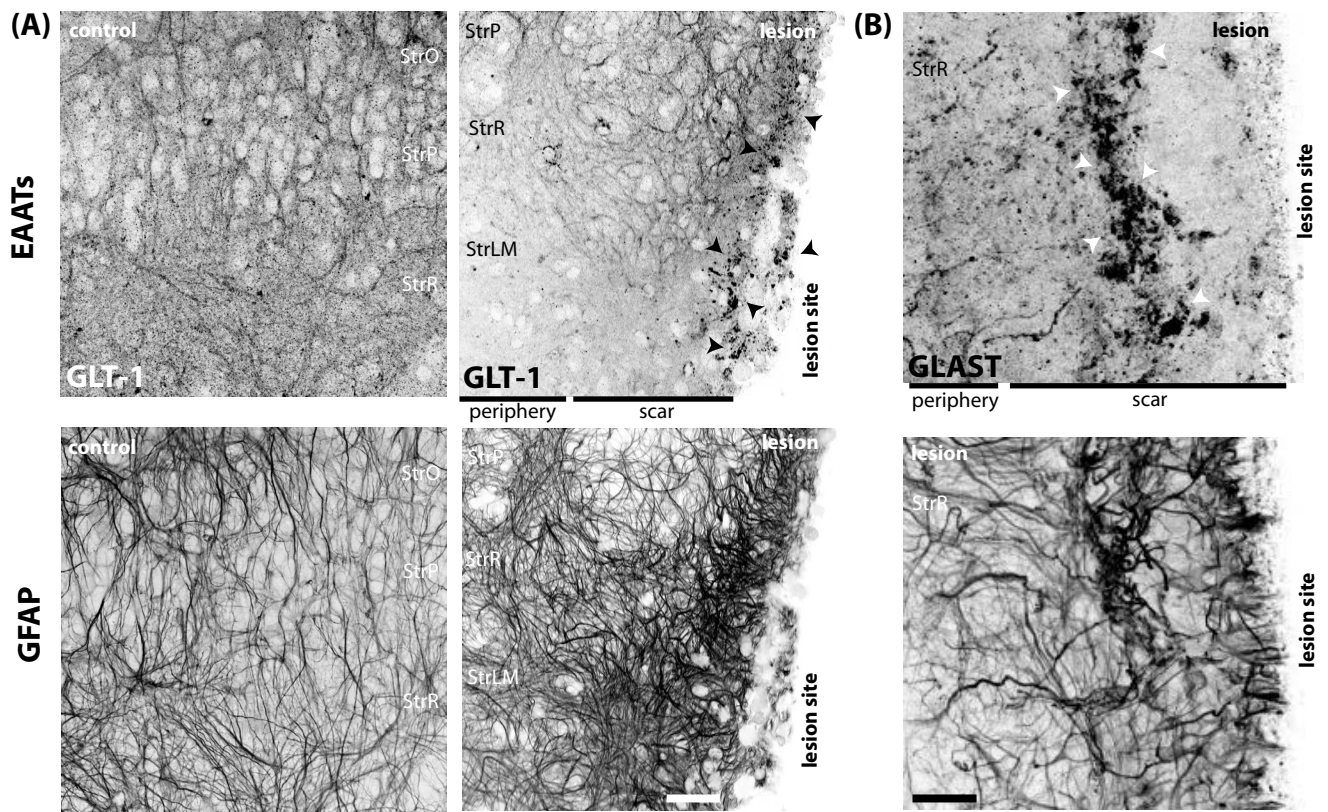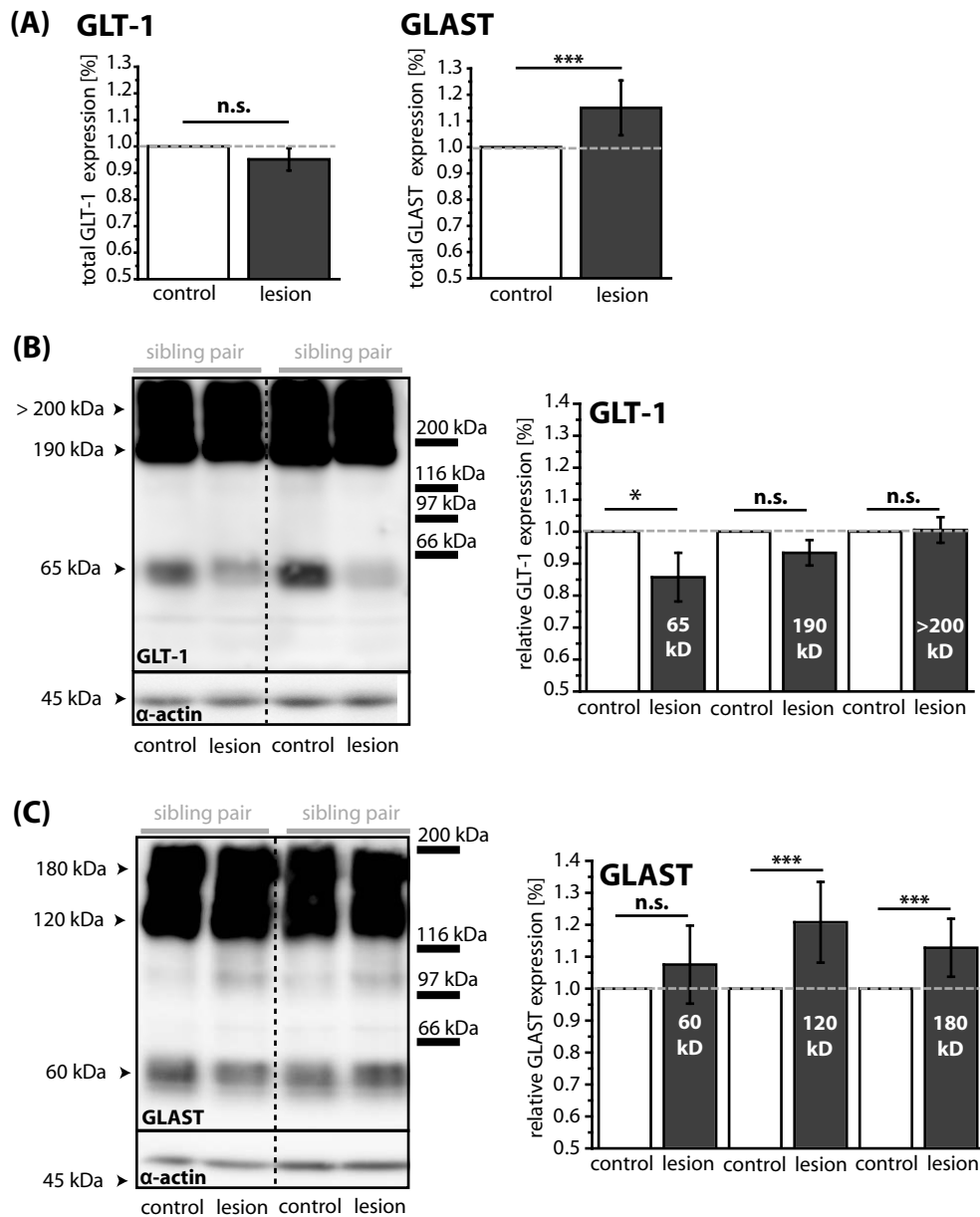
Fig. 4. Schreiner, Stock, Langer, Kafitz & Rose

(A)

EAATs

control · StrO · StrP · StrR · GLT-1

StrP · lesion · StrR · StrLM · GLT-1 · lesion site · periphery · scar

GFAP

control · StrO · StrP · StrR

StrP · lesion · StrR · StrLM · lesion site

(B)

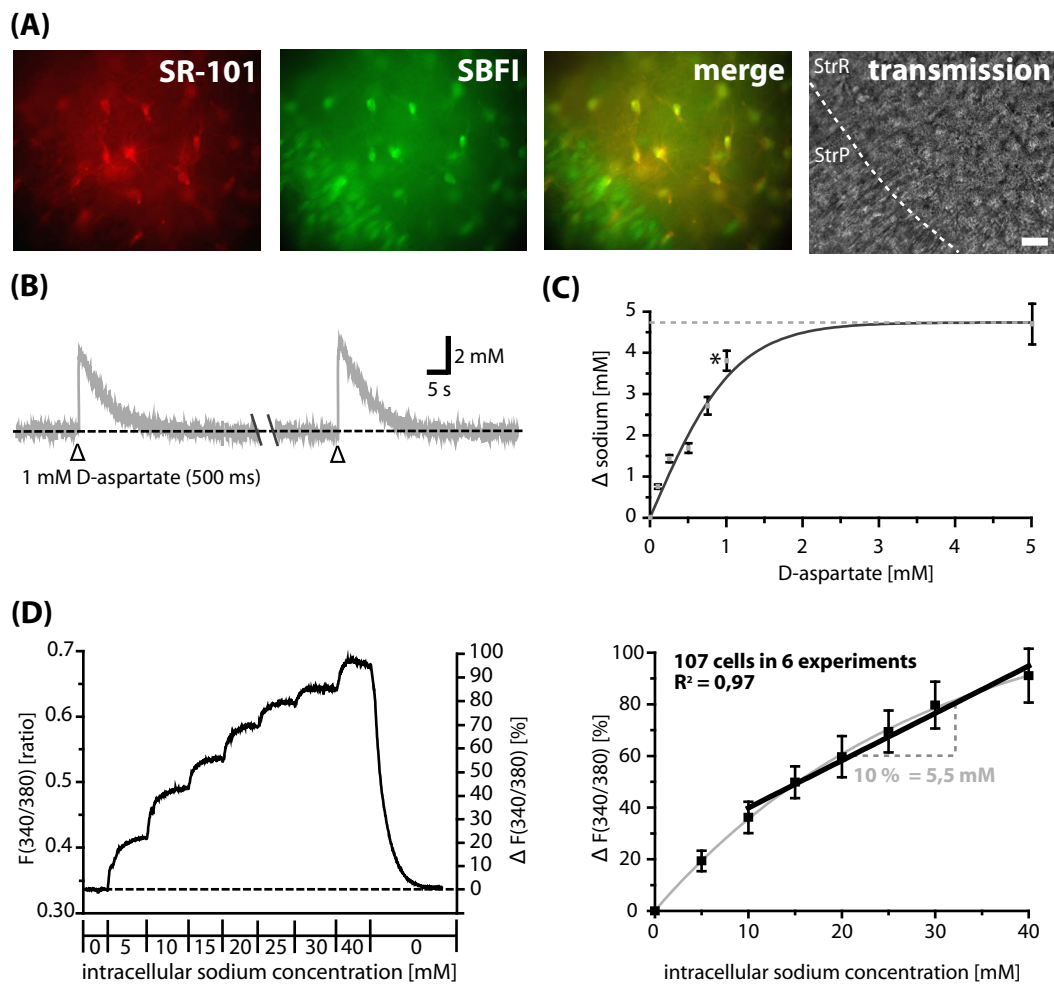StrR · lesion · GLAST · lesion site · periphery · scar

lesion · StrR · lesion site

Fig. 5. Schreiner, Stock, Langer, Kafitz & Rose

(A)

GLT-1

GLAST

(B)

(C)

Fig. 6. Schreiner, Stock, Langer, Kafitz & Rose

(A)

SR-101   SBFI   merge   StrR transmission

StrP

(B)

2 mM

5 s

1 mM D-aspartate (500 ms)

(C)

Δ sodium [mM]

D-aspartate [mM]

(D)

F(340/380) [ratio]

Δ F(340/380) [%]

intracellular sodium concentration [mM]

107 cells in 6 experiments
R² = 0,97
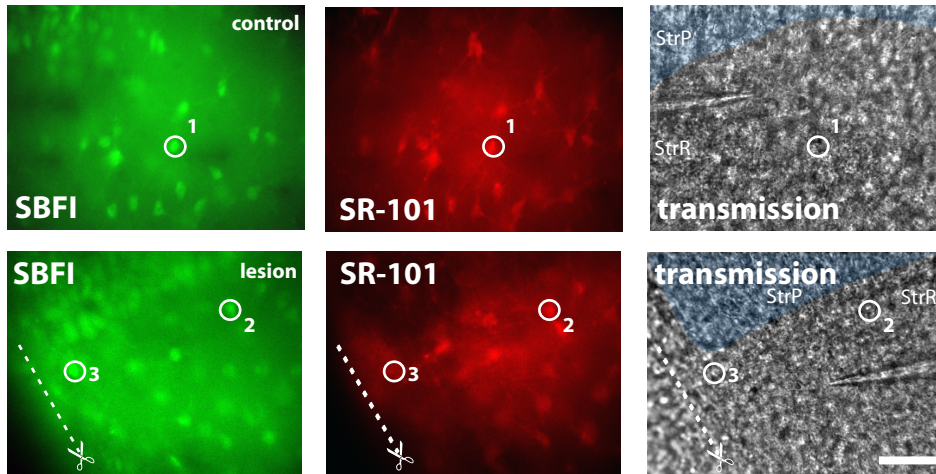
Δ F(340/380) [%]

10 % = 5,5 mM

intracellular sodium concentration [mM]
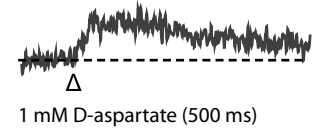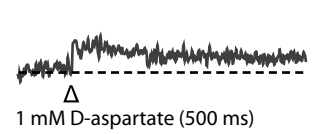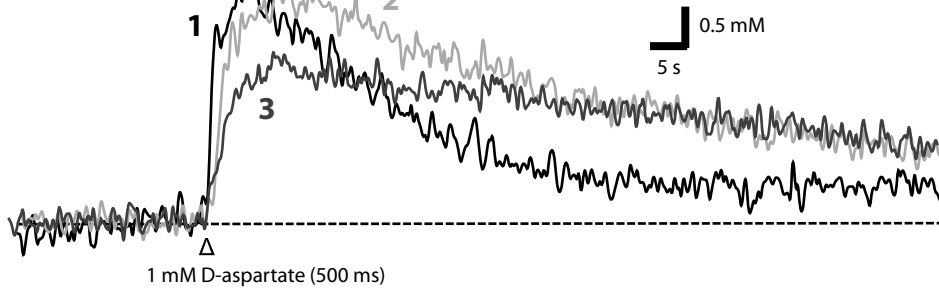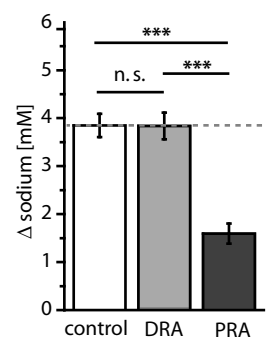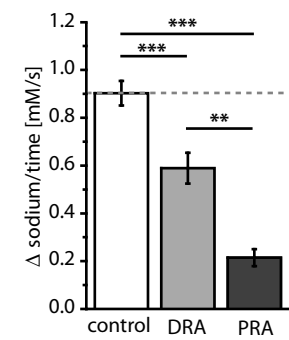
Fig. 7. Schreiner, Stock, Langer, Kafitz & Rose

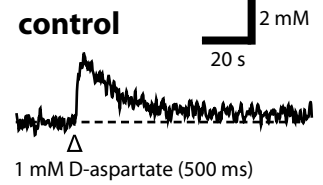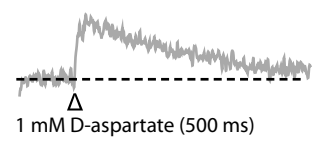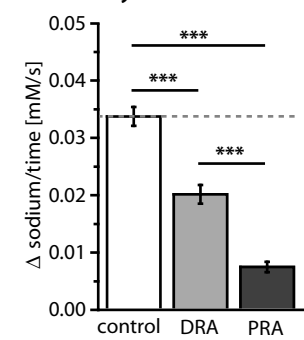**Fig. 8.** Schreiner, Stock, Langer, Kafitz & Rose

References

A

Abbott NJ, Rönnbäck L, Hansson E (2006) Astrocyte-endothelial interactions at the blood-brain barrier. *Nat Rev Neurosci.* 7(1):41-53.

Abele AE, Scholz KP, Scholz WK, Miller RJ (1990) Excitotoxicity induced by enhanced excitatory neurotransmission in cultured hippocampal pyramidal neurons. *Neuron*. 4(3):413-9.

Allaman I, Bélanger M, Magistretti PJ (2011) Astrocyte-neuron metabolic relationships: for better and for worse. *Trends Neurosci.* 34(2):76-87.

Alvarez-Buylla A, García-Verdugo JM, Tramontin AD (2001) A unified hypothesis on the lineage of neural stem cells. *Nat Rev Neurosci.* 2(4):287-93.

Amaral DG, Scharfman HE, Lavenex P (2007) The dentate gyrus: fundamental neuroanatomical organization (dentate gyrus for dummies). *Prog Brain Res.* 163:3-22.

Anderson CM, Swanson RA (2000) Astrocyte glutamate transport: review of properties, regulation, and physiological functions. *Glia.* 32(1):1-14.

Angulo MC, Le Meur K, Kozlov AS, Charpak S, Audinat E (2008) GABA, a forgotten gliotransmitter. *Prog Neurobiol.* 86(3):297-303

Ankarcrona M, Dypbukt JM, Bonfoco E, Zhivotovsky B, Orrenius S, Lipton SA, Nicotera P (1995) Glutamate-induced neuronal death: a succession of necrosis or apoptosis depending on mitochondrial function. *Neuron.* 15(4):961-73.

Appaix F, Girod S, Boisseau S, Römer J, Vial JC, Albrieux M, Maurin M, Depaulis A, Guillemain I, van der Sanden B (2012) Specific in vivo staining of astrocytes in the whole brain after intravenous injection of sulforhodamine dyes. *PLoS One.* 7(4):e35169.

Araque A, Parpura V, Sanzgiri RP, Haydon PG (1999) Tripartite synapses: glia, the unacknowledged partner. *Trends Neurosci.* 22(5):208-15.

Arriza JL, Fairman WA, Wadiche JI, Murdoch GH, Kavanaugh MP, Amara SG (1994) Functional comparisons of three glutamate transporter subtypes cloned from human motor cortex. *J Neurosci*. 14(9):5559-69.

B

Bak LK, Schousboe A, Waagepetersen HS (2006) The glutamate/GABA-glutamine cycle: aspects of transport, neurotransmitter homeostasis and ammonia transfer. *J Neurochem.* 98(3):641-53.

Baker DA, Xi ZX, Shen H, Swanson CJ, Kalivas PW (2002) The origin and neuronal function of in vivo nonsynaptic glutamate. *J Neurosci.* 22(20):9134-41.

Barres BA (2003) What is a glial cell? *Glia.* 43(1):4-5.

Barres BA (2008) The mystery and magic of glia: a perspective on their roles in health and disease. *Neuron.* 60(3):430-40.

Barros LF, Deitmer JW (2010) Glucose and lactate supply to the synapse. *Brain Res Rev.* 63(1-2):149-59.

Bass NH, Hess HH, Pope A, Thalheimer C (1971) Quantitative cytoarchitectonic distribution of neurons, glia, and DNa in rat cerebral cortex. *J Comp Neurol.* 143(4):481-90.

Bauer D, Haroutunian V, Meador-Woodruff JH, McCullumsmith RE (2010) Abnormal glycosylation of EAAT1 and EAAT2 in prefrontal cortex of elderly patients with schizophrenia. *Schizophr Res.* 117(1):92-8.

Bauer DE, Jackson JG, Genda EN, Montoya MM, Yudkoff M, Robinson MB (2012) The glutamate transporter, GLAST, participates in a macromolecular complex that supports glutamate metabolism. *Neurochem Int.* 61(4):566-74.

Baumann N, Pham-Dinh D (2001) Biology of oligodendrocyte and myelin in the mammalian central nervous system. *Physiol Rev.* 81(2):871-927.

Bélanger M, Yang J, Petit JM, Laroche T, Magistretti PJ, Allaman I (2011) Role of the glyoxalase system in astrocyte-mediated neuroprotection. *J Neurosci.* 31(50):18338-52.

Ben-Ari Y (2001) Developing networks play a similar melody. *Trends Neurosci.* 24(6):353-60.

Ben-Ari Y (2002) Excitatory actions of gaba during development: the nature of the nurture. *Nat Rev Neurosci.* (9):728-39.

Benediktsson AM, Marrs GS, Tu JC, Worley PF, Rothstein JD, Bergles DE, Dailey ME (2012) Neuronal activity regulates glutamate transporter dynamics in developing astrocytes. *Glia.* 60(2):175-88.

Bennay M, Langer J, Meier SD, Kafitz KW, Rose CR (2008) Sodium signals in cerebellar Purkinje neurons and Bergmann glial cells evoked by glutamatergic synaptic transmission. *Glia.* 56(10):1138-49.

Bennett MV, Contreras JE, Bukauskas FF, Sáez JC (2003) New roles for astrocytes: gap junction hemichannels have something to communicate. *Trends Neurosci.* 26(11):610-7.

Bernardinelli Y, Magistretti PJ, Chatton JY (2004) Astrocytes generate Na$^+$-mediated metabolic waves. *Proc Natl Acad Sci U S A.* 101(41):14937-42.

Bergles DE, Roberts JD, Somogyi P, Jahr CE (2000) Glutamatergic synapses on oligodendrocyte precursor cells in the hippocampus. *Nature.* 405(6783):187-91.

Bergles DE, Jabs R, Steinhäuser C (2010) Neuron-glia synapses in the brain. *Brain Res Rev.* 63(1-2):130-7.

Boudker O, Ryan RM, Yernool D, Shimamoto K, Gouaux E (2007) Coupling substrate and ion binding to extracellular gate of a sodium-dependent aspartate transporter. *Nature.* 445(7126):387-93.

Brown AM, Ransom BR (2007) Astrocyte glycogen and brain energy metabolism. Glia. 55(12):1263-71.

Buffo A, Rite I, Tripathi P, Lepier A, Colak D, Horn AP, Mori T, Götz M (2008) Origin and progeny of reactive gliosis: A source of multipotent cells in the injured brain. *Proc Natl Acad Sci U S A.* 105(9):3581-6.

Buffo A, Rolando C, Ceruti S (2010) Astrocytes in the damaged brain: molecular and cellular insights into their reactive response and healing potential. *Biochem Pharmacol.* 79(2):77-89.

Bushong EA, Martone ME, Jones YZ, Ellisman MH (2002) Protoplasmic astrocytes in CA1 stratum radiatum occupy separate anatomical domains. *J Neurosci.* 22(1):183-92.

Bushong EA, Martone ME, Ellisman MH (2004) Maturation of astrocyte morphology and the establishment of astrocyte domains during postnatal hippocampal development. Int J Dev Neurosci. 22(2):73-86.

Butt AM, Kiff J, Hubbard P, Berry M (2002) Synantocytes: new functions for novel NG2 expressing glia. *J Neurocytol.* 31(6-7):551-65.

C

Cahoy JD, Emery B, Kaushal A, Foo LC, Zamanian JL, Christopherson KS, Xing Y, Lubischer JL, Krieg PA, Krupenko SA, Thompson WJ, Barres BA (2008) A transcriptome database for astrocytes, neurons, and oligodendrocytes: a new resource for understanding brain development and function. *J Neurosci*. 28(1):264-78.

Camacho A, Massieu L (2006) Role of glutamate transporters in the clearance and release of glutamate during ischemia and its relation to neuronal death. *Arch Med Res*. 37(1):11-8.

Carmignoto G, Gómez-Gonzalo M (2010) The contribution of astrocyte signalling to neurovascular coupling. *Brain Res Rev*. 63(1-2):138-48.

Casado M, Bendahan A, Zafra F, Danbolt NC, Aragón C, Giménez C, Kanner BI (1993) Phosphorylation and modulation of brain glutamate transporters by protein kinase C. *J Biol Chem*. 268(36):27313-7.

Cavus I, Kasoff WS, Cassaday MP, Jacob R, Gueorguieva R, Sherwin RS, Krystal JH, Spencer DD, Abi-Saab WM (2005) Extracellular metabolites in the cortex and hippocampus of epileptic patients. *Ann Neurol*. 57(2):226-35.

Chatton JY, Marquet P, Magistretti PJ (2000) A quantitative analysis of L-glutamate-regulated Na^+ dynamics in mouse cortical astrocytes: implications for cellular bioenergetics. *Eur J Neurosci*. 12(11):3843-53.

Chatton JY, Pellerin L, Magistretti PJ (2003) GABA uptake into astrocytes is not associated with significant metabolic cost: implications for brain imaging of inhibitory transmission. *Proc Natl Acad Sci U S A*. 100(21):12456-61.

Chen JC, Hsu-Chou H, Lu JL, Chiang YC, Huang HM, Wang HL, Wu T, Liao JJ, Yeh TS (2005) Down-regulation of the glial glutamate transporter GLT-1 in rat hippocampus and striatum and its modulation by a group III metabotropic glutamate receptor antagonist following transient global forebrain ischemia. *Neuropharmacology*. 49(5):703-14.

Chen J, Tan Z, Zeng L, Zhang X, He Y, Gao W, Wu X, Li Y, Bu B, Wang W, Duan S (2012) Heterosynaptic long-term depression mediated by ATP released from astrocytes. *Glia*. in press

Chew SS, Johnson CS, Green CR, Danesh-Meyer HV (2010) Role of connexin43 in central nervous system injury. *Exp Neurol*. 225(2):250-61.

Choi S, Klingauf J, Tsien RW (2000) Postfusional regulation of cleft glutamate concentration during LTP at 'silent synapses'. *Nat Neurosci*. 3(4):330-6.

Cholet N, Pellerin L, Magistretti PJ, Hamel E (2002) Similar perisynaptic glial localization for the Na^+,K^+-ATPase alpha 2 subunit and the glutamate transporters GLAST and GLT-1 in the rat somatosensory cortex. *Cereb Cortex*. 12(5):515-25.

Chvátal A, Anderová M, Neprasová H, Prajerová I, Benesová J, Butenko O, Verkhratsky A (2008) Pathological potential of astroglia. *Physiol Res*. 57(Suppl 3):S101-10.

Clapham DE (2007) Calcium signaling. *Cell*. 131(6):1047-58.

Clements JD, Lester RA, Tong G, Jahr CE, Westbrook GL (1992) The time course of glutamate in the synaptic cleft. *Science*. 258(5087):1498-501.

Coco S, Calegari F, Pravettoni E, Pozzi D, Taverna E, Rosa P, Matteoli M, Verderio C (2003) Storage and release of ATP from astrocytes in culture. *J Biol Chem*. 278(2):1354-62

D

Daikhin Y, Yudkoff M (2000). Compartmentation of brain glutamate metabolism in neurons and glia. *J Nutr*. 130(4S):1026S-31S.

Danbolt NC (2001) Glutamate uptake. *Prog Neurobiol.* 65(1):1-105.

Deitmer JW, Rose CR (2010) Ion changes and signalling in perisynaptic glia. *Brain Res Rev.* 63(1-2):113-29.

Dienel GA, Cruz NF (2003) Neighborly interactions of metabolically-activated astrocytes in vivo. *Neurochem Int.* 43(4-5):339-54.

Djukic B, Casper KB, Philpot BD, Chin LS, McCarthy KD (2007) Conditional knock-out of Kir4.1 leads to glial membrane depolarization, inhibition of potassium and glutamate uptake, and enhanced short-term synaptic potentiation. *J Neurosci.* 27(42):11354-65.

Dringen R, Kussmaul L, Gutterer JM, Hirrlinger J, Hamprecht B (1999) The glutathione system of peroxide detoxification is less efficient in neurons than in astroglial cells. *J Neurochem.* 72(6):2523-30.

Drukarch B, Schepens E, Stoof JC, Langeveld CH, Van Muiswinkel FL (1998) Astrocyte-enhanced neuronal survival is mediated by scavenging of extracellular reactive oxygen species. *Free Radic Biol Med.* 25(2):217-20.

Dumas TC (2005) Late postnatal maturation of excitatory synaptic transmission permits adult-like expression of hippocampal-dependent behaviors. *Hippocampus.* 15(5):562-78.

E

Eddleston M, Mucke L (1993) Molecular profile of reactive astrocytes--implications for their role in neurologic disease. *Neuroscience.* 54(1):15-36.

Eichenbaum H (2000) A cortical-hippocampal system for declarative memory. *Nat Rev Neurosci.* 1(1):41-50.

Eng LF, Ghirnikar RS (1994) GFAP and astrogliosis. *Brain Pathol.* 4(3):229-37.

Eng LF, Ghirnikar RS, Lee YL (2000) Glial fibrillary acidic protein: GFAP-thirty-one years (1969-2000). *Neurochem Res.* 25(9-10):1439-51.

Eroglu C, Barres BA (2010) Regulation of synaptic connectivity by glia. *Nature.* 468(7321):223-31.

Eskandari S, Kreman M, Kavanaugh MP, Wright EM, Zampighi GA (2000) Pentameric assembly of a neuronal glutamate transporter. *Proc Natl Acad Sci U S A.* 97(15):8641-6.

Escartin C, Brouillet E, Gubellini P, Trioulier Y, Jacquard C, Smadja C, Knott GW, Kerkerian-Le Goff L, Déglon N, Hantraye P, Bonvento G (2006) Ciliary neurotrophic factor activates astrocytes, redistributes their glutamate transporters GLAST and GLT-1 to raft microdomains, and improves glutamate handling in vivo. *J Neurosci.* 26(22):5978-89.

Eulenburg V, Gomeza J (2010) Neurotransmitter transporters expressed in glial cells as regulators of synapse function. *Brain Res Rev.* 63(1-2):103-12.

Ezan P, André P, Cisternino S, Saubaméa B, Boulay AC, Doutremer S, Thomas MA, Quenech'du N, Giaume C, Cohen-Salmon M (2012) Deletion of astroglial connexins weakens the blood-brain barrier. *J Cereb Blood Flow Metab.* 32(8):1457-67.

F

Fairman WA, Vandenberg RJ, Arriza JL, Kavanaugh MP, Amara SG (1995) An excitatory amino-acid transporter with properties of a ligand-gated chloride channel. *Nature.* 375(6532):599-603.

Faissner A, Pyka M, Geissler M, Sobik T, Frischknecht R, Gundelfinger ED, Seidenbecher C (2010) Contributions of astrocytes to synapse formation and maturation - Potential functions of the perisynaptic extracellular matrix. *Brain Res Rev.* 63(1-2):26-38.

Fellin T, Pascual O, Gobbo S, Pozzan T, Haydon PG, Carmignoto G (2004) Neuronal synchrony mediated by astrocytic glutamate through activation of extrasynaptic NMDA receptors. *Neuron.* 43(5):729-43.

Fiacco TA, McCarthy KD (2006) Astrocyte calcium elevations: properties, propagation, and effects on brain signaling. *Glia.* 54(7):676-90.

Figley CR, Stroman PW (2011) The role(s) of astrocytes and astrocyte activity in neurometabolism, neurovascular coupling, and the production of functional neuroimaging signals. *Eur J Neurosci.* 33(4):577-88.

Filosa JA, Blanco VM (2007) Neurovascular coupling in the mammalian brain. *Exp Physiol.* 92(4):641-6.

Förster E, Zhao S, Frotscher M (2006) Laminating the hippocampus. *Nat Rev Neurosci.* 7(4):259-67.

Freeman MR (2010) Specification and morphogenesis of astrocytes. *Science.* 330(6005):774-8.

Fresu L, Dehpour A, Genazzani AA, Carafoli E, Guerini D (1999) Plasma membrane calcium ATPase isoforms in astrocytes. *Glia.* 28(2):150-5.

Furuta A, Rothstein JD, Martin LJ (1997) Glutamate transporter protein subtypes are expressed differentially during rat CNS development. *J Neurosci.* 17(21):8363-75.

G

Gécz J (2010) Glutamate receptors and learning and memory. *Nat Genet.* 42(11):925-6.

Gegelashvili G, Schousboe A (1997) High affinity glutamate transporters: regulation of expression and activity. *Mol Pharmacol.* 52(1):6-15.

Gegelashvili G, Dehnes Y, Danbolt NC, Schousboe A (2000) The high-affinity glutamate transporters GLT1, GLAST, and EAAT4 are regulated via different signalling mechanisms. *Neurochem Int.* 37(2-3):163-70.

Gemba T, Oshima T, Ninomiya M (1994) Glutamate efflux via the reversal of the sodium-dependent glutamate transporter caused by glycolytic inhibition in rat cultured astrocytes. *Neuroscience.* 63(3):789-95.

Genda EN, Jackson JG, Sheldon AL, Locke SF, Greco TM, O'Donnell JC, Spruce LA, Xiao R, Guo W, Putt M, Seeholzer S, Ischiropoulos H, Robinson MB (2011) Co-compartmentalization of the astroglial glutamate transporter, GLT-1, with glycolytic enzymes and mitochondria. *J Neurosci.* 31(50):18275-88.

Gendreau S, Voswinkel S, Torres-Salazar D, Lang N, Heidtmann H, Detro-Dassen S, Schmalzing G, Hidalgo P, Fahlke C (2004) A trimeric quaternary structure is conserved in bacterial and human glutamate transporters. *J Biol Chem.* 279(38):39505-12.

Genoud C, Quairiaux C, Steiner P, Hirling H, Welker E, Knott GW (2006) Plasticity of astrocytic coverage and glutamate transporter expression in adult mouse cortex. *PLoS Biol.* 4(11):e343.

Giaume C, McCarthy KD (1996) Control of gap-junctional communication in astrocytic networks. *Trends Neurosci.* 19(8):319-25.

Giaume C, Koulakoff A, Roux L, Holcman D, Rouach N (2010) Astroglial networks: a step further in neuroglial and gliovascular interactions. *Nat Rev Neurosci.* 11(2):87-99.

Gibbs ME, Hutchinson D, Hertz L (2008) Astrocytic involvement in learning and memory consolidation. *Neurosci Biobehav Rev.* 32(5):927-44.

Gilley JA, Kernie SG (2011) Excitatory amino acid transporter 2 and excitatory amino acid transporter 1 negatively regulate calcium-dependent proliferation of hippocampal neural progenitor cells and are persistently upregulated after injury. *Eur J Neurosci.* 34(11):1712-23.

Ginsberg SD, Martin LJ, Rothstein JD (1995) Regional deafferentation down-regulates subtypes of glutamate transporter proteins. *J Neurochem.* 65(6):2800-3.

Ginsberg SD, Rothstein JD, Price DL, Martin LJ (1996) Fimbria-fornix transections selectively down-regulate subtypes of glutamate transporter and glutamate receptor proteins in septum and hippocampus. *J Neurochem.* 67(3):1208-16.

Girouard H, Bonev AD, Hannah RM, Meredith A, Aldrich RW, Nelson MT (2010) Astrocytic endfoot Ca^{2+} and BK channels determine both arteriolar dilation and constriction. *Proc Natl Acad Sci U S A.* 107(8):3811-6.

González-González IM, García-Tardón N, Cubelos B, Giménez C, Zafra F (2008) The glutamate transporter GLT1b interacts with the scaffold protein PSD-95. *J Neurochem.* 105(5):1834-48.

González-González IM, García-Tardón N, Giménez C, Zafra F (2009) Splice variants of the glutamate transporter GLT1 form hetero-oligomers that interact with PSD-95 and NMDA receptors. *J Neurochem.* 110(1):264-74.

Gordon GR, Choi HB, Rungta RL, Ellis-Davies GC, MacVicar BA (2008) Brain metabolism dictates the polarity of astrocyte control over arterioles. *Nature.* 456(7223):745-9.

Gordon GR, Howarth C, MacVicar BA (2011) Bidirectional control of arteriole diameter by astrocytes. *Exp Physiol.* 96(4):393-9.

Grewer C, Watzke N, Rauen T, Bicho A (2003) Is the glutamate residue Glu-373 the proton acceptor of the excitatory amino acid carrier 1? *J Biol Chem.* 278(4):2585-92.

Grewer C, Rauen T (2005) Electrogenic glutamate transporters in the CNS: molecular mechanism, pre-steady-state kinetics, and their impact on synaptic signaling. *J Membr Biol.* 203(1):1-20.

Grewer C, Balani P, Weidenfeller C, Bartusel T, Tao Z, Rauen T (2005b) Individual subunits of the glutamate transporter EAAC1 homotrimer function independently of each other. *Biochemistry.* 44(35):11913-23.

Grewer C, Gameiro A, Zhang Z, Tao Z, Braams S, Rauen T (2008) Glutamate forward and reverse transport: from molecular mechanism to transporter-mediated release after ischemia. *IUBMB Life.* 60(9):609-19.

Grimaldi M (2006) Astrocytes refill intracellular Ca2+ stores in the absence of cytoplasmic [Ca2+] elevation: a functional rather than a structural ability. *J Neurosci Res.* 84(8):1738-49.

Grunewald M, Kanner BI (2000) The accessibility of a novel reentrant loop of the glutamate transporter GLT-1 is restricted by its substrate. *J Biol Chem.* 275(13):9684-9.

Gunnarson E, Zelenina M, Axehult G, Song Y, Bondar A, Krieger P, Brismar H, Zelenin S, Aperia A (2008) Identification of a molecular target for glutamate regulation of astrocyte water permeability. *Glia.* 15;56(6):587-96.

H

Haber M, Zhou L, Murai KK (2006) Cooperative astrocyte and dendritic spine dynamics at hippocampal excitatory synapses. *J Neurosci.* 26(35):8881-91.

Halassa MM, Fellin T, Haydon PG (2007) The tripartite synapse: roles for gliotransmission in health and disease. *Trends Mol Med.* 13(2):54-63.

Halassa MM, Fellin T, Haydon PG (2009) Tripartite synapses: roles for astrocytic purines in the control of synaptic physiology and behavior. *Neuropharmacology.* 57(4):343-6.

Halestrap AP, Price NT (1999) The proton-linked monocarboxylate transporter (MCT) family: structure, function and regulation. *Biochem J.* 343(Pt2):281-99.

Hansson E, Muyderman H, Leonova J, Allansson L, Sinclair J, Blomstrand F, Thorlin T, Nilsson M, Rönnbäck L (2000) Astroglia and glutamate in physiology and pathology: aspects on glutamate transport, glutamate-induced cell swelling and gap-junction communication. *Neurochem Int*. 37(2-3):317-29.

Harada T, Harada C, Watanabe M, Inoue Y, Sakagawa T, Nakayama N, Sasaki S, Okuyama S, Watase K, Wada K, Tanaka K (1998) Functions of the two glutamate transporters GLAST and GLT-1 in the retina. *Proc Natl Acad Sci U S A*. 95(8):4663-6.

Hartfuss E, Galli R, Heins N, Götz M (2001) Characterization of CNS precursor subtypes and radial glia. *Dev Biol*. 229(1):15-30.

Haugeto O, Ullensvang K, Levy LM, Chaudhry FA, Honoré T, Nielsen M, Lehre KP, Danbolt NC (1996) Brain glutamate transporter proteins form homomultimers. *J Biol Chem*. 271(44):27715-22.

Hawkins RA, Peterson DR, Viña JR (2002) The complementary membranes forming the blood-brain barrier. *IUBMB Life*. 54(3):101-7.

Haydon PG (2001) GLIA: listening and talking to the synapse. *Nat Rev Neurosci*. 2(3):185-93.

Haydon PG, Carmignoto G (2006) Astrocyte control of synaptic transmission and neurovascular coupling. *Physiol Rev*. 86(3):1009-31.

Henneberger C, Papouin T, Oliet SH, Rusakov DA (2010) Long-term potentiation depends on release of D-serine from astrocytes. *Nature*. 463(7278):232-6.

Herman MA, Jahr CE (2007) Extracellular glutamate concentration in hippocampal slice. *J Neurosci*. 27(36):9736-41.

Hertz L, Zielke HR (2004) Astrocytic control of glutamatergic activity: astrocytes as stars of the show. *Trends Neurosci*. 27(12):735-43.

Hirase H, Qian L, Barthó P, Buzsáki G (2004) Calcium dynamics of cortical astrocytic networks in vivo. *PLoS Biol*. 2(4):E96.

Hirrlinger J, Hülsmann S, Kirchhoff F (2004) Astroglial processes show spontaneous motility at active synaptic terminals in situ. *Eur J Neurosci*. 20(8):2235-9.

Höke A, Silver J (1994) Heterogeneity among astrocytes in reactive gliosis. *Perspect Dev Neurobiol*. 2(3):269-74.

Holmseth S, Scott HA, Real K, Lehre KP, Leergaard TB, Bjaalie JG, Danbolt NC (2009) The concentrations and distributions of three C-terminal variants of the GLT1 (EAAT2; slc1a2) glutamate transporter protein in rat brain tissue suggest differential regulation. *Neuroscience*. 162(4):1055-71.

Holthoff K, Witte OW (2000) Directed spatial potassium redistribution in rat neocortex. *Glia*. 29(3):288-92.

Honsek SD, Walz C, Kafitz KW, Rose CR (2012) Astrocyte calcium signals at Schaffer collateral to CA1 pyramidal cell synapses correlate with the number of activated synapses but not with synaptic strength. *Hippocampus*. 22(1):29-42.

Huang YH, Sinha SR, Tanaka K, Rothstein JD, Bergles DE (2004) Astrocyte glutamate transporters regulate metabotropic glutamate receptor-mediated excitation of hippocampal interneurons. *J Neurosci*. 24(19):4551-9.

Huggett J, Vaughan-Thomas A, Mason D (2000) The open reading frame of the Na^+-dependent glutamate transporter GLAST-1 is expressed in bone and a splice variant of this molecule is expressed in bone and brain. *FEBS Lett*. 485(1):13-8.

I

J

Jabs R, Pivneva T, Hüttmann K, Wyczynski A, Nolte C, Kettenmann H, Steinhäuser C (2005) Synaptic transmission onto hippocampal glial cells with hGFAP promoter activity. *J Cell Sci*. 118(Pt 16):3791-803.

Jiang J, Amara SG (2011) New views of glutamate transporter structure and function: advances and challenges. *Neuropharmacology*. 60(1):172-81.

Jing R, Wilhelmsson U, Goodwill W, Li L, Pan Y, Pekny M, Skalli O (2007) Synemin is expressed in reactive astrocytes in neurotrauma and interacts differentially with vimentin and GFAP intermediate filament networks. *J Cell Sci*. 120(Pt 7):1267-77.

K

Kacem K, Lacombe P, Seylaz J, Bonvento G (1998) Structural organization of the perivascular astrocyte endfeet and their relationship with the endothelial glucose transporter: a confocal microscopy study. *Glia*. 23(1):1-10.

Kafitz KW, Meier SD, Stephan J, Rose CR (2008) Developmental profile and properties of sulforhodamine 101-labeled glial cells in acute brain slices of rat hippocampus. *J Neurosci Methods*. 169(1):84-92.

Kanai Y, Hediger MA (1992) Primary structure and functional characterization of a high-affinity glutamate transporter. *Nature*. 360(6403):467-71.

Káradóttir R, Hamilton NB, Bakiri Y, Attwell D (2008) Spiking and nonspiking classes of oligodendrocyte precursor glia in CNS white matter. *Nat Neurosci*. 11(4):450-6.

Kettenmann H, Verkhratsky A (2008) Neuroglia: the 150 years after. *Trends Neurosci*. 31(12):653-9.

Kettenmann H, Hanisch UK, Noda M, Verkhratsky A (2011) Physiology of microglia. *Physiol Rev*. 91(2):461-553.

Kimelberg HK (2004) The problem of astrocyte identity. *Neurochem Int*. 45(2-3):191-202.

Kimelberg HK (2010) Functions of mature mammalian astrocytes: a current view. *Neuroscientist*. 16(1):79-106.

Kirischuk S, Kettenmann H, Verkhratsky A (2007) Membrane currents and cytoplasmic sodium transients generated by glutamate transport in Bergmann glial cells. *Pflugers Arch*. 454(2):245-52.

Kirischuk S, Parpura V, Verkhratsky A (2012) Sodium dynamics: another key to astroglial excitability? *Trends Neurosci*. 35(8):497-506.

Koch HP, Larsson HP (2005) Small-scale molecular motions accomplish glutamate uptake in human glutamate transporters. *J Neurosci*. 25(7):1730-6.

Koehler RC, Roman RJ, Harder DR (2009) Astrocytes and the regulation of cerebral blood flow. *Trends Neurosci*. 32(3):160-9.

Kofuji P, Newman EA (2004) Potassium buffering in the central nervous system. *Neuroscience*. 129(4):1045-56.

Kuga N, Sasaki T, Takahara Y, Matsuki N, Ikegaya Y (2011) Large-scale calcium waves traveling through astrocytic networks in vivo. *J Neurosci*. 31(7):2607-14.

Kugler P, Schleyer V (2004) Developmental expression of glutamate transporters and glutamate dehydrogenase in astrocytes of the postnatal rat hippocampus. *Hippocampus*. 14(8):975-85.

Kukley M, Capetillo-Zarate E, Dietrich D (2007) Vesicular glutamate release from axons in white matter. *Nat Neurosci*. 10(3):311-20.

Kunze A, Congreso MR, Hartmann C, Wallraff-Beck A, Hüttmann K, Bedner P, Requardt R, Seifert G, Redecker C, Willecke K, Hofmann A, Pfeifer A, Theis M, Steinhäuser C (2009) Connexin expression by radial glia-like cells is required for neurogenesis in the adult dentate gyrus. *Proc Natl Acad Sci U S A*. 106(27):11336-41.

L

Lamy CM, Chatton JY (2011) Optical probing of sodium dynamics in neurons and astrocytes. *Neuroimage.* 58(2):572-8.

van Landeghem FK, Weiss T, Oehmichen M, von Deimling A (2006) Decreased expression of glutamate transporters in astrocytes after human traumatic brain injury. *J Neurotrauma.* 23(10):1518-28.

Langer J, Rose CR (2009) Synaptically induced sodium signals in hippocampal astrocytes in situ. *J Physiol.* 587(Pt 24):5859-77.

Langer J, Stephan J, Theis M, Rose CR (2012) Gap junctions mediate intercellular spread of sodium between hippocampal astrocytes in situ. *Glia.* 60(2):239-52.

Lau A, Tymianski M (2010) Glutamate receptors, neurotoxicity and neurodegeneration. *Pflugers Arch.* 460(2):525-42.

Leary GP, Stone EF, Holley DC, Kavanaugh MP (2007) The glutamate and chloride permeation pathways are colocalized in individual neuronal glutamate transporter subunits. *J Neurosci.* 27(11):2938-42.

Lee A, Pow DV (2010) Astrocytes: Glutamate transport and alternate splicing of transporters. *Int J Biochem Cell Biol.* 42(12):1901-6.

Lee A, Anderson AR, Barnett AC, Chan A, Pow DV (2011) Expression of multiple glutamate transporter splice variants in the rodent testis. *Asian J Androl.* 13(2):254-65.

Lee A, Anderson AR, Beasley SJ, Barnett NL, Poronnik P, Pow DV (2012) A new splice variant of the glutamate-aspartate transporter: cloning and immunolocalization of GLAST1c in rat, pig and human brains. *J Chem Neuroanat.* 43(1):52-63.

Lerma J, Herranz AS, Herreras O, Abraira V, Martín del Río R (1986) In vivo determination of extracellular concentration of amino acids in the rat hippocampus. A method based on brain dialysis and computerized analysis. *Brain Res.* 384(1):145-55.

Levine JM, Card JP (1987) Light and electron microscopic localization of a cell surface antigen (NG2) in the rat cerebellum: association with smooth protoplasmic astrocytes. *J Neurosci.* 7(9):2711-20.

Li Z, Sheng M. Some assembly required: the development of neuronal synapses. *Nat Rev Mol Cell Biol.* 4(11):833-41.

Lin SC, Huck JH, Roberts JD, Macklin WB, Somogyi P, Bergles DE (2005) Climbing fiber innervation of NG2-expressing glia in the mammalian cerebellum. *Neuron.* 46(5):773-85.

Lisman JE, Raghavachari S, Tsien RW (2007) The sequence of events that underlie quantal transmission at central glutamatergic synapses. *Nat Rev Neurosci.* 8(8):597-609.

Loaiza A, Porras OH, Barros LF (2003) Glutamate triggers rapid glucose transport stimulation in astrocytes as evidenced by real-time confocal microscopy. *J Neurosci.* 23(19):7337-42.

Longuemare MC, Rose CR, Farrell K, Ransom BR, Waxman SG, Swanson RA (1999) K^+-induced reversal of astrocyte glutamate uptake is limited by compensatory changes in intracellular Na^+. *Neuroscience.* 93(1):285-92.

Lu YB, Iandiev I, Hollborn M, Körber N, Ulbricht E, Hirrlinger PG, Pannicke T, Wei EQ, Bringmann A, Wolburg H, Wilhelmsson U, Pekny M, Wiedemann P, Reichenbach A, Käs JA (2011) Reactive glial cells: increased stiffness correlates with increased intermediate filament expression. *FASEB J.* 25(2):624-31.

Luján R, Shigemoto R, López-Bendito G (2005) Glutamate and GABA receptor signalling in the developing brain. *Neuroscience*. 130(3):567-80.

M

Macnab LT, Williams SM, Pow DV (2006) Expression of the exon 3 skipping form of GLAST, GLAST1a, in brain and retina. *Neuroreport*. 17(18):1867-70.

Macnab LT, Pow DV (2007) Central nervous system expression of the exon 9 skipping form of the glutamate transporter GLAST.

Neuroreport. 18(8):741-5.

Madl JE, Burgesser K (1993) Adenosine triphosphate depletion reverses sodium-dependent, neuronal uptake of glutamate in rat hippocampal slices. *J Neurosci*. 13(10):4429-44.

Malhotra SK, Shnitka TK (2001) Diversity in Reactive Astrocytes. In: De Vellis JS (Ed.) *Neuroglia in the Aging Brain*. Humana Press Inc. Totowa, United States of America. pp. 17-33

Mathiisen TM, Lehre KP, Danbolt NC, Ottersen OP (2010) The perivascular astroglial sheath provides a complete covering of the brain microvessels: an electron microscopic 3D reconstruction. *Glia*. 58(9):1094-103.

Matsugami TR, Tanemura K, Mieda M, Nakatomi R, Yamada K, Kondo T, Ogawa M, Obata K, Watanabe M, Hashikawa T, Tanaka K (2006) Indispensability of the glutamate transporters GLAST and GLT1 to brain development. *Proc Natl Acad Sci U S A.* 103(32):12161-6.

Matyash V, Kettenmann H (2010) Heterogeneity in astrocyte morphology and physiology. *Brain Res Rev.* 63(1-2):2-10.

McCaslin AF, Chen BR, Radosevich AJ, Cauli B, Hillman EM (2011) In vivo 3D morphology of astrocyte-vasculature interactions in the somatosensory cortex: implications for neurovascular coupling. *J Cereb Blood Flow Metab*. 31(3):795-806.

Meeks JP, Mennerick S (2007) Astrocyte membrane responses and potassium accumulation during neuronal activity. *Hippocampus*. 17(11):1100-8.

Meldrum BS (2000) Glutamate as a neurotransmitter in the brain: review of physiology and pathology. *J Nutr*. 130(4S):1007S-15S.

Meier S, Bräuer AU, Heimrich B, Nitsch R, Savaskan NE (2004) Myelination in the hippocampus during development and following lesion. *Cell Mol Life Sci*. 61(9):1082-94.

Meier SD, Kovalchuk Y, Rose CR (2006) Properties of the new fluorescent Na+ indicator CoroNa Green: comparison with SBFI and confocal Na$^+$ imaging. *J Neurosci Methods*. 155(2):251-9.

Melzer N, Biela A, Fahlke C (2003) Glutamate modifies ion conduction and voltage-dependent gating of excitatory amino acid transporter-associated anion channels. *J Biol Chem*. 278(50):50112-9.

Middeldorp J, Hol EM (2011) GFAP in health and disease. *Prog Neurobiol*. 93(3):421-43.

Minta A, Tsien RY (1989) Fluorescent indicators for cytosolic sodium. *J Biol Chem.* 264(32):19449-57.

Mitani A, Tanaka K (2003) Functional changes of glial glutamate transporter GLT-1 during ischemia: an in vivo study in the hippocampal CA1 of normal mice and mutant mice lacking GLT-1. *J Neurosci*. 23(18):7176-82.

Moretto MB, Arteni NS, Lavinsky D, Netto CA, Rocha JB, Souza DO, Wofchuk S (2005) Hypoxic-ischemic insult decreases glutamate uptake by hippocampal slices from neonatal rats: prevention by guanosine. *Exp Neurol.* 195(2):400-6.

N

Nagelhus EA, Mathiisen TM, Ottersen OP (2004) Aquaporin-4 in the central nervous system: cellular and subcellular distribution and coexpression with KIR4.1. *Neuroscience*. 129(4):905-13.

Nakagawa T, Otsubo Y, Yatani Y, Shirakawa H, Kaneko S (2008) Mechanisms of substrate transport-induced clustering of a glial glutamate transporter GLT-1 in astroglial-neuronal cultures. *Eur J Neurosci*. 28(9):1719-30.

Navarrete M, Perea G, Fernandez de Sevilla D, Gómez-Gonzalo M, Núñez A, Martín ED, Araque A (2012) Astrocytes mediate in vivo cholinergic-induced synaptic plasticity. *PLoS Biol*. 10(2):e1001259.

Nedergaard M, Takano T, Hansen AJ (2002) Beyond the role of glutamate as a neurotransmitter. *Nat Rev Neurosci*. 3(9):748-55.

Nedergaard M, Ransom B, Goldman SA (2003) New roles for astrocytes: redefining the functional architecture of the brain. *Trends Neurosci*. 26(10):523-30.

Nedergaard M, Rodríguez JJ, Verkhratsky A (2010) Glial calcium and diseases of the nervous system. *Cell Calcium*. 47(2):140-9.

Neves G, Cooke SF, Bliss TV (2008) Synaptic plasticity, memory and the hippocampus: a neural network approach to causality. *Nat Rev Neurosci*. 9(1):65-75.

Nimmerjahn A, Kirchhoff F, Kerr JN, Helmchen F (2004) Sulforhodamine 101 as a specific marker of astroglia in the neocortex in vivo. *Nat Methods*. 1(1):31-7.

Nimmerjahn A, Helmchen F (2012) In vivo labeling of cortical astrocytes with sulforhodamine 101 (SR101). *Cold Spring Harb Protoc*. 2012(3):326-34.

Nishiyama A, Komitova M, Suzuki R, Zhu X (2009) Polydendrocytes (NG2 cells): multifunctional cells with lineage plasticity. *Nat Rev Neurosci*. 10(1):9-22.

Nyitrai G, Kékesi KA, Juhász G (2006) Extracellular level of GABA and Glu: in vivo microdialysis-HPLC measurements. *Curr Top Med Chem*. 6(10):935-40.

O

Oberheim NA, Wang X, Goldman S, Nedergaard M (2006) Astrocytic complexity distinguishes the human brain. *Trends Neurosci*. 29(10):547-53.

Oberheim NA, Tian GF, Han X, Peng W, Takano T, Ransom B, Nedergaard M (2008) Loss of astrocytic domain organization in the epileptic brain. *J Neurosci*. 28(13):3264-76.

Oberheim NA, Takano T, Han X, He W, Lin JH, Wang F, Xu Q, Wyatt JD, Pilcher W, Ojemann JG, Ransom BR, Goldman SA, Nedergaard M (2009) Uniquely hominid features of adult human astrocytes. *J Neurosci*. 29(10):3276-87.

Ogata K, Kosaka T (2002) Structural and quantitative analysis of astrocytes in the mouse hippocampus. *Neuroscience*. 113(1):221-33.

Ogawa S, Lee TM, Kay AR, Tank DW (1990) Brain magnetic resonance imaging with contrast dependent on blood oxygenation. *Proc Natl Acad Sci U S A*. 87(24):9868-72.

Oliet SH, Mothet JP (2006) Molecular determinants of D-serine-mediated gliotransmission: from release to function. *Glia*. 54(7):726-37.

Olsen ML, Sontheimer H (2008) Functional implications for Kir4.1 channels in glial biology: from K^+ buffering to cell differentiation. *J Neurochem*. 107(3):589-601.

Østby I, Øyehaug L, Einevoll GT, Nagelhus EA, Plahte E, Zeuthen T, Lloyd CM, Ottersen OP, Omholt SW (2009) Astrocytic mechanisms explaining neural-activity-induced shrinkage of extraneuronal space. *PLoS Comput Biol.* 5(1):e1000272.

P

Panatier A, Vallée J, Haber M, Murai KK, Lacaille JC, Robitaille R (2011) Astrocytes are endogenous regulators of basal transmission at central synapses. *Cell.* 146(5):785-98.

Parpura V, Basarsky TA, Liu F, Jeftinija K, Jeftinija S, Haydon PG (1994) Glutamate-mediated astrocyte-neuron signalling. *Nature.* 369(6483):744-7.

Parpura V, Zorec R (2010) Gliotransmission: Exocytotic release from astrocytes. *Brain Res Rev.* 63(1-2):83-92.

Peacey E, Miller CC, Dunlop J, Rattray M (2009) The four major N- and C-terminal splice variants of the excitatory amino acid transporter GLT-1 form cell surface homomeric and heteromeric assemblies. *Mol Pharmacol.* 75(5):1062-73.

Pellerin L, Magistretti PJ (1994) Glutamate uptake into astrocytes stimulates aerobic glycolysis: a mechanism coupling neuronal activity to glucose utilization. *Proc Natl Acad Sci U S A.* 91(22):10625-9.

Pellerin L, Pellegri G, Bittar PG, Charnay Y, Bouras C, Martin JL, Stella N, Magistretti PJ (1998) Evidence supporting the existence of an activity-dependent astrocyte-neuron lactate shuttle. *Dev Neurosci.* 20(4-5):291-9.

Pellerin L, Bouzier-Sore AK, Aubert A, Serres S, Merle M, Costalat R, Magistretti PJ (2007) Activity-dependent regulation of energy metabolism by astrocytes: an update. *Glia.* 55(12):1251-62.

Pellerin L, Magistretti PJ (2012) Sweet sixteen for ANLS. *J Cereb Blood Flow Metab.* 32(7):1152-66.

Perea G, Araque A (2007) Astrocytes potentiate transmitter release at single hippocampal synapses. *Science.* 317(5841):1083-6.

Perea G, Navarrete M, Araque A (2009) Tripartite synapses: astrocytes process and control synaptic information. *Trends Neurosci.* 32(8):421-31.

Perea G, Araque A (2010) GLIA modulates synaptic transmission. *Brain Res Rev.* 63(1-2):93-102.

Peters OA, Palay SL, Webster HF (1991) In: Peters OA, Palay SL, Webster HF (Eds.) *The fine structure of the nervous system: Neurons and their supporting cells.* Oxford University Press. New York, United States of America. 3rd edition, p. 161

Peters A (2004) A fourth type of neuroglial cell in the adult central nervous system. *J Neurocytol.* 33(3):345-57.

Petzold GC, Albeanu DF, Sato TF, Murthy VN (2008) Coupling of neural activity to blood flow in olfactory glomeruli is mediated by astrocytic pathways. *Neuron.* 58(6):897-910.

Petzold GC, Murthy VN (2011) Role of astrocytes in neurovascular coupling. *Neuron.* 71(5):782-97.

Pfrieger FW (2002) Role of glia in synapse development. *Curr Opin Neurobiol.* 12(5):486-90.

Phillis JW, Ren J, O'Regan MH (2000) Transporter reversal as a mechanism of glutamate release from the ischemic rat cerebral cortex: studies with DL-threo-beta-benzyloxyaspartate. *Brain Res.* 868(1):105-12.

Pines G, Danbolt NC, Bjørås M, Zhang Y, Bendahan A, Eide L, Koepsell H, Storm-Mathisen J, Seeberg E, Kanner BI (1992) Cloning and expression of a rat brain L-glutamate transporter. *Nature.* 360(6403):464-7.

Pines G, Zhang Y, Kanner BI (1995) Glutamate 404 is involved in the substrate discrimination of GLT-1, a (Na^+ + K^+)-coupled glutamate transporter from rat brain. *J Biol Chem.* 270(29):17093-7.

Poitry-Yamate CL, Vutskits L, Rauen T (2002) Neuronal-induced and glutamate-dependent activation of glial glutamate transporter function. *J Neurochem.* 82(4):987-97.

Porras OH, Ruminot I, Loaiza A, Barros LF (2008) Na^+-Ca^{2+} cosignaling in the stimulation of the glucose transporter GLUT1 in cultured astrocytes. *Glia.* 56(1):59-68.

Q

R

Rao KV, Panickar KS, Jayakumar AR, Norenberg MD (2005) Astrocytes protect neurons from ammonia toxicity. *Neurochem Res.* 30(10):1311-8.

Rauen T, Wiessner M, Sullivan R, Lee A, Pow DV (2004) A new GLT1 splice variant: cloning and immunolocalization of GLT1c in the mammalian retina and brain. *Neurochem Int.* 45(7):1095-106.

Reichenbach A, Derouiche A, Grosche J, Hanani M (2004) Structural associations of glia with the various compartments of neurons. In: Hatton GI, Parpura V (Eds.) *Glial Neuronal Signaling*. Kluwers Academic Publishers. Norwell, United States of America. pp. 53–97.

Reichenbach A, Derouiche A, Kirchhoff F (2010) Morphology and dynamics of perisynaptic glia. *Brain Res Rev.* 63(1-2):11-25.

Reyes N, Ginter C, Boudker O (2009) Transport mechanism of a bacterial homologue of glutamate transporters. *Nature.* 462(7275):880-5.

Ridet JL, Malhotra SK, Privat A, Gage FH (1997) Reactive astrocytes: cellular and molecular cues to biological function. *Trends Neurosci.* 20(12):570-7.

Robel S, Berninger B, Götz M (2011) The stem cell potential of glia: lessons from reactive gliosis. *Nat Rev Neurosci.* 12(2):88-104.

Rossi DJ, Oshima T, Attwell D (2000) Glutamate release in severe brain ischaemia is mainly by reversed uptake. *Nature.* 403(6767):316-21.

Rose CR, Ransom BR (1996) Intracellular sodium homeostasis in rat hippocampal astrocytes. *J Physiol.* 491(Pt2):291-305.

Rose CR (1997) Intracellular Na^+ Regulation in Neurons and Glia: Functional Implications. *Neuroscientist.* 3(2):85-88.

Rose EM, Koo JC, Antflick JE, Ahmed SM, Angers S, Hampson DR (2009) Glutamate transporter coupling to Na,K-ATPase. *J Neurosci.* 29(25):8143-55.

Rothstein JD, Dykes-Hoberg M, Pardo CA, Bristol LA, Jin L, Kuncl RW, Kanai Y, Hediger MA, Wang Y, Schielke JP, Welty DF (1996) Knockout of glutamate transporters reveals a major role for astroglial transport in excitotoxicity and clearance of glutamate. *Neuron.* 16(3):675-86.

Rothstein JD, Patel S, Regan MR, Haenggeli C, Huang YH, Bergles DE, Jin L, Dykes Hoberg M, Vidensky S, Chung DS, Toan SV, Bruijn LI, Su ZZ, Gupta P, Fisher PB (2005) Beta-lactam antibiotics offer neuroprotection by increasing glutamate transporter expression. *Nature.* 433(7021):73-7.

Rouach N, Koulakoff A, Abudara V, Willecke K, Giaume C (2008) Astroglial metabolic networks sustain hippocampal synaptic transmission. *Science.* 322(5907):1551-5.

S

Sauvageot CM, Stiles CD (2002) Molecular mechanisms controlling cortical gliogenesis. *Curr Opin Neurobiol*. 12(3):244-9.

Scemes E, Giaume C (2006) Astrocyte calcium waves: what they are and what they do. *Glia*. 54(7):716-25.

Scemes E, Spray DC, Meda P (2009) Connexins, pannexins, innexins: novel roles of "hemi-channels". *Pflugers Arch*. 457(6):1207-26.

Schlag BD, Vondrasek JR, Munir M, Kalandadze A, Zelenaia OA, Rothstein JD, Robinson MB (1998) Regulation of the glial Na$^+$-dependent glutamate transporters by cyclic AMP analogs and neurons. *Mol Pharmacol*. 53(3):355-69.

Schools GP, Zhou M, Kimelberg HK (2006) Development of gap junctions in hippocampal astrocytes: evidence that whole cell electrophysiological phenotype is an intrinsic property of the individual cell. *J Neurophysiol*. 96(3):1383-92.

Schousboe A, Sonnewald U, Civenni G, Gegelashvili G (1997) Role of astrocytes in glutamate homeostasis. Implications for excitotoxicity. *Adv Exp Med Biol*. 429:195-206.

Schousboe A, Waagepetersen HS (2005) Role of astrocytes in glutamate homeostasis: implications for excitotoxicity. *Neurotox Res*. 8(3-4):221-5.

Schreiner AE, Rose CR (2012) Quantitative imaging of intracellular sodium. In: Méndez-Vilas A (Ed.). *Current microscopy contributions to advances in science and technology*. Formatex Research Centre. Badajoz, Spain. *in press*

Scott HA, Gebhardt FM, Mitrovic AD, Vandenberg RJ, Dodd PR (2011) Glutamate transporter variants reduce glutamate uptake in Alzheimer's disease. *Neurobiol Aging*. 32(3):553.e1-11.

Seal RP, Amara SG (1998) A reentrant loop domain in the glutamate carrier EAAT1 participates in substrate binding and translocation. *Neuron*. 21(6):1487-98.

Seki Y, Feustel PJ, Keller RW Jr, Tranmer BI, Kimelberg HK (1999) Inhibition of ischemia-induced glutamate release in rat striatum by dihydrokinate and an anion channel blocker. *Stroke*. 30(2):433-40.

Sherwood CC, Stimpson CD, Raghanti MA, Wildman DE, Uddin M, Grossman LI, Goodman M, Redmond JC, Bonar CJ, Erwin JM, Hof PR (2006) Evolution of increased glia-neuron ratios in the human frontal cortex. *Proc Natl Acad Sci U S A*. 103(37):13606-11.

Shibata T, Yamada K, Watanabe M, Ikenaka K, Wada K, Tanaka K, Inoue Y (1997) Glutamate transporter GLAST is expressed in the radial glia-astrocyte lineage of developing mouse spinal cord. *J Neurosci*. 17(23):9212-9.

Simard M, Nedergaard M (2004) The neurobiology of glia in the context of water and ion homeostasis. *Neuroscience*. 129(4):877-96.

Simon C, Götz M, Dimou L (2011) Progenitors in the adult cerebral cortex: cell cycle properties and regulation by physiological stimuli and injury. *Glia*. 59(6):869-81.

Sofroniew MV (2009) Molecular dissection of reactive astrogliosis and glial scar formation. *Trends Neurosci*. 32(12):638-47.

Sofroniew MV, Vinters HV (2010) Astrocytes: biology and pathology. *Acta Neuropathol*. 119(1):7-35.

Spruston N (2008) Pyramidal neurons: dendritic structure and synaptic integration. *Nat Rev Neurosci*. 9(3):206-21.

Storck T, Schulte S, Hofmann K, Stoffel W (1992) Structure, expression, and functional analysis of a Na(+)-dependent glutamate/aspartate transporter from rat brain. *Proc Natl Acad Sci U S A.* 89(22):10955-9.

van Strien NM, Cappaert NL, Witter MP (2009) The anatomy of memory: an interactive overview of the parahippocampal-hippocampal network. *Nat Rev Neurosci.* 10(4):272-82.

Sullivan SM, Macnab LT, Björkman ST, Colditz PB, Pow DV (2007) GLAST1b, the exon-9 skipping form of the glutamate-aspartate transporter EAAT1 is a sensitive marker of neuronal dysfunction in the hypoxic brain. *Neuroscience.* 149(2):434-45.

Suzuki A, Stern SA, Bozdagi O, Huntley GW, Walker RH, Magistretti PJ, Alberini CM (2011) Astrocyte-neuron lactate transport is required for long-term memory formation. *Cell.* 144(5):810-23.

T

Takano T, Tian GF, Peng W, Lou N, Libionka W, Han X, Nedergaard M (2006) Astrocyte-mediated control of cerebral blood flow. Nat Neurosci. 9(2):260-7.

Tanaka K, Watase K, Manabe T, Yamada K, Watanabe M, Takahashi K, Iwama H, Nishikawa T, Ichihara N, Kikuchi T, Okuyama S, Kawashima N, Hori S, Takimoto M, Wada K (1997) Epilepsy and exacerbation of brain injury in mice lacking the glutamate transporter GLT-1. *Science.* 276(5319):1699-702.

Tanaka J, Toku K, Zhang B, Ishihara K, Sakanaka M, Maeda N (1999) Astrocytes prevent neuronal death induced by reactive oxygen and nitrogen species. *Glia.* 28(2):85-96.

Theriault E, Frankenstein UN, Hertzberg EL, Nagy JI (1997) Connexin43 and astrocytic gap junctions in the rat spinal cord after acute compression injury. *J Comp Neurol.* 382(2):199-214.

Tian G, Lai L, Guo H, Lin Y, Butchbach ME, Chang Y, Lin CL (2007) Translational control of glial glutamate transporter EAAT2 expression. *J Biol Chem.* 282(3):1727-37.

Trotter J, Karram K, Nishiyama A (2010) NG2 cells: Properties, progeny and origin. *Brain Res Rev.* 63(1-2):72-82.

Tsai PS, Kaufhold JP, Blinder P, Friedman B, Drew PJ, Karten HJ, Lyden PD, Kleinfeld D (2009) Correlations of neuronal and microvascular densities in murine cortex revealed by direct counting and colocalization of nuclei and vessels. *J Neurosci.* 29(46):14553-70.

Tzingounis AV, Wadiche JI (2007) Glutamate transporters: confining runaway excitation by shaping synaptic transmission. *Nat Rev Neurosci.* 8(12):935-47.

U

Ueda Y, Doi T, Tsuru N, Tokumaru J, Mitsuyama Y (2002) Expression of glutamate transporters and ionotropic glutamate receptors in GLAST knockout mice. *Brain Res Mol Brain Res.* 104(2):120-6.

Ullian EM, Christopherson KS, Barres BA (2004) Role for glia in synaptogenesis. *Glia.* 47(3):209-16.

Unichenko P, Myakhar O, Kirischuk S (2012) Intracellular Na+ concentration influences short-term plasticity of glutamate transporter-mediated currents in neocortical astrocytes. *Glia.* 60(4):605-14.

Utsunomiya-Tate N, Endou H, Kanai Y (1997) Tissue specific variants of glutamate transporter GLT-1. *FEBS Lett.* 416(3):312-6.

V

Vallejo-Illarramendi A, Domercq M, Matute C (2005) A novel alternative splicing form of excitatory amino acid transporter 1 is a negative regulator of glutamate uptake. *J Neurochem.* 95(2):341-8.

Vannucci SJ, Maher F, Simpson IA (1997) Glucose transporter proteins in brain: delivery of glucose to neurons and glia. *Glia.* 21(1):2-21.

Verkhratsky A (2010) Physiology of neuronal-glial networking. *Neurochem Int.* 57(4):332-43.

Verkhratsky A, Rodríguez JJ, Parpura V (2012) Calcium signalling in astroglia. *Mol Cell Endocrinol.* 353(1-2):45-56.

Volterra A, Meldolesi J (2005) Astrocytes, from brain glue to communication elements: the revolution continues. *Nat Rev Neurosci.* 6(8):626-40.

Voutsinos-Porche B, Bonvento G, Tanaka K, Steiner P, Welker E, Chatton JY, Magistretti PJ, Pellerin L (2003) Glial glutamate transporters mediate a functional metabolic crosstalk between neurons and astrocytes in the mouse developing cortex. *Neuron.* 37(2):275-86.

Voutsinos-Porche B, Knott G, Tanaka K, Quairiaux C, Welker E, Bonvento G (2003b) Glial glutamate transporters and maturation of the mouse somatosensory cortex. *Cereb Cortex.* 13(10):1110-21.

W

Wadiche JI, Amara SG, Kavanaugh MP (1995) Ion fluxes associated with excitatory amino acid transport. *Neuron.* 15(3):721-8.

Walz W (2000) Role of astrocytes in the clearance of excess extracellular potassium. *Neurochem Int.* 36(4-5):291-300.

Wang DD, Bordey A (2008) The astrocyte odyssey. *Prog Neurobiol.* 86(4):342-67.

Watase K, Hashimoto K, Kano M, Yamada K, Watanabe M, Inoue Y, Okuyama S, Sakagawa T, Ogawa S, Kawashima N, Hori S, Takimoto M, Wada K, Tanaka K (1998) Motor discoordination and increased susceptibility to cerebellar injury in GLAST mutant mice. *Eur J Neurosci.* 10(3):976-88.

Wilhelmsson U, Li L, Pekna M, Berthold CH, Blom S, Eliasson C, Renner O, Bushong E, Ellisman M, Morgan TE, Pekny M (2004) Absence of glial fibrillary acidic protein and vimentin prevents hypertrophy of astrocytic processes and improves post-traumatic regeneration. *J Neurosci.* 24(21):5016-21.

Wilhelmsson U, Bushong EA, Price DL, Smarr BL, Phung V, Terada M, Ellisman MH, Pekny M (2006) Redefining the concept of reactive astrocytes as cells that remain within their unique domains upon reaction to injury. *Proc Natl Acad Sci U S A.* 103(46):17513-8.

Witcher MR, Kirov SA, Harris KM (2007) Plasticity of perisynaptic astroglia during synaptogenesis in the mature rat hippocampus. *Glia.* 55(1):13-23.

X

Y

Yang Y, Ge W, Chen Y, Zhang Z, Shen W, Wu C, Poo M, Duan S (2003) Contribution of astrocytes to hippocampal long-term potentiation through release of D-serine. *Proc Natl Acad Sci U S A.* 100(25):15194-9.

Yang CZ, Zhao R, Dong Y, Chen XQ, Yu AC (2008) Astrocyte and neuron intone through glutamate. *Neurochem Res.* 33(12):2480-6.

Yang Y, Gozen O, Watkins A, Lorenzini I, Lepore A, Gao Y, Vidensky S, Brennan J, Poulsen D, Won Park J, Li Jeon N, Robinson MB, Rothstein JD (2009) Presynaptic regulation of astroglial excitatory neurotransmitter transporter GLT1. *Neuron.* 61(6):880-94.

Yang Y, Gozen O, Vidensky S, Robinson MB, Rothstein JD (2010) Epigenetic regulation of neuron-dependent induction of astroglial synaptic protein GLT1. *Glia*. 58(3):277-86.

Yang Y, Vidensky S, Jin L, Jie C, Lorenzini I, Frankl M, Rothstein JD (2011) Molecular comparison of GLT1^{+} and ALDH1L1[+] astrocytes in vivo in astroglial reporter mice. *Glia*. 59(2):200-7.

Yernool D, Boudker O, Folta-Stogniew E, Gouaux E (2003) Trimeric subunit stoichiometry of the glutamate transporters from Bacillus caldotenax and Bacillus stearothermophilus. *Biochemistry*. 42(44):12981-8.

Yernool D, Boudker O, Jin Y, Gouaux E (2004) Structure of a glutamate transporter homologue from Pyrococcus horikoshii. *Nature*. 431(7010):811-8.

Z

Zamanian JL, Xu L, Foo LC, Nouri N, Zhou L, Giffard RG, Barres BA (2012) Genomic analysis of reactive astrogliosis. *J Neurosci*. 32(18):6391-410.

Zelenina M (2010) Regulation of brain aquaporins. *Neurochem Int*. 57(4):468-88.

Zeng XN, Sun XL, Gao L, Fan Y, Ding JH, Hu G (2007) Aquaporin-4 deficiency down-regulates glutamate uptake and GLT-1 expression in astrocytes. *Mol Cell Neurosci*. 34(1):34-9.

Zhang S, Boyd J, Delaney K, Murphy TH (2005) Rapid reversible changes in dendritic spine structure in vivo gated by the degree of ischemia. *J Neurosci*. 25(22):5333-8.

Zhang Y, Barres BA (2010) Astrocyte heterogeneity: an underappreciated topic in neurobiology. *Curr Opin Neurobiol*. 20(5):588-94.

Zhou J, Sutherland ML (2004) Glutamate transporter cluster formation in astrocytic processes regulates glutamate uptake activity. *J Neurosci*. 24(28):6301-6.

Zhou M, Schools GP, Kimelberg HK (2006) Development of GLAST(+) astrocytes and NG2(+) glia in rat hippocampus CA1: mature astrocytes are electrophysiologically passive. *J Neurophysiol*. 95(1):134-43.

Ziskin JL, Nishiyama A, Rubio M, Fukaya M, Bergles DE (2007) Vesicular release of glutamate from unmyelinated axons in white matter. *Nat Neurosci*. 10(3):321-30.

Zonta M, Angulo MC, Gobbo S, Rosengarten B, Hossmann KA, Pozzan T, Carmignoto G (2003) Neuron-to-astrocyte signaling is central to the dynamic control of brain microcirculation. *Nat Neurosci*. 6(1):43-50.

Acknowledgements

- In the first instance I gratefully acknowledge **Prof. Dr. Christine Rose** for great support and excellent supervision during all stages of this thesis. I appreciated her scientific enthusiasm, all the encouragement and our professional discussions a lot. I´m thankful for the opportunity to spend my years as doctoral candidate in her laboratory.

- I would like to take the opportunity to thank **Prof. Dr. Willbold** for offering to evaluate this thesis and the DFG for supporting the projects included.

- **Peter**, your sharp and systematic mind has impressed me most among all scientists I got to know in the last years. I hope many students can benefit from your excellent scientific teaching.

- Particularly, I want to thank **Simone** for her excellent expertise and for her first introducing me to general laboratory work.

- **Julia**, it was so great to spend all these years with you "on the dark side" of the lab. Thank you for your technical advice and our scientific discussions, but also for sharing daily anger and joy and with me.

- My first steps in the laboratory were accompanied by **Silke** and **Karl**, who provided excellent theoretical and technical support. I really appreciated your help.

- **Christian** and **Claudia K.**, thank you both so much for so many helpful discussions and your continuous encouragement.

- I further would like to thank **Marion**, **Tanja** and **Claudia R.** for ensuring frictionless daily lab operations and for providing assistance, whenever needed.

- **Lennart** and **Dana**, I really appreciated your supervision. I was incredibly lucky to work together with such bright and diligent students.

- Finally, I would like to express my gratitude to all former and present colleagues that were not mentioned by name for their help and their contribution to a great working atmosphere.

- ❖ Personally I owe this work my beloved husband **David** who has always supported and honored me, my ideas and my ideals.

- ❖ **Lukas**, **Simon** and **Rachel**, you have saved me from fading away while "living" science.

Author´s Declaration

I confirm that this work submitted for assessment is my own and is expressed in my own words. Any uses made within it of the works of other authors in any form (e.g. ideas, equations, figures, text, tables) are properly acknowledged at the point of their use. A full list of the references employed has been included. The dissertation has not been presented to any other University for examination.

Duesseldorf, 14.11.2012   Alexandra Schreiner

Erklärung

Hiermit versichere ich, dass ich die vorliegende Arbeit selbständig angefertigt und keine anderen Hilfsmittel und Quellen verwendet habe, als die erlaubten. Alle genutzten Quellen und Hilfsmittel sind vollständig angegeben und die Stellen der Arbeit (einschließlich Tabellen, Karten und Abbildungen), die anderen im Wortlaut oder im Sinn nach entnommen sind, habe ich in jedem Einzelfall als Entlehnung kenntlich gemacht. Eine vollständige Liste der Quellenangaben ist beigefügt. Diese Arbeit wurde weder vollständig noch in Teilen einem anderen Prüfungsamt zur Erlangung eines akademischen Grades vorgelegt.
Die von mir vorgelegte Dissertation ist von Prof. C. R. Rose betreut worden.

Düsseldorf, den 14.11.2012   Alexandra Schreiner

Curriculum Vitae

Alexandra Elisabeth Schreiner, née Rduch

Ostwall 144, 47798 Krefeld

Personal Information

Born on 10th August 1984 in Katowice, Poland

General Education

1991-2004   Elementary School and Grammar School, Krefeld, Germany.

2004   General university entrance degree (major class: biology and mathematics)

Abitur

Academic Education

2008-2009   Heinrich-Heine-University, Duesseldorf, Germany

Diploma, Biology

2009-2012   Heinrich-Heine-University, Duesseldorf, Germany

Ph.D. student, Biology

Research & Professional Experience

2008-2009   Heinrich-Heine-University, Duesseldorf, Germany

Diploma student (supervisors: Christine R. Rose & Karl W. Kafitz)*, Neurobiology*

2008   Heinrich-Heine-University, Duesseldorf, Germany

Student assistant, Neurobiology

2009-2012   Heinrich-Heine-University, Duesseldorf, Germany

Ph.D. student/doctoral researcher (supervisor: Christine R. Rose)*, Neurobiology*

Düsseldorf, 14.11.2012

Erratum

page 30:

(QUELLEN; Grewer et al., 2008) **has to be replaced by** (Mitani & Tanaka, 2003; Weller et al., 2008; Grewer et al., 2008; Liao et al., 2009).

page 141:

To add: <u>Liao G</u>, <u>Zhou M</u>, <u>Cheung S</u>, <u>Galeano J</u>, <u>Nguyen N</u>, <u>Baudry M</u>, <u>Bi X</u> (2009) Reduced early hypoxic/ischemic brain damage is associated with increased GLT-1 levels in mice expressing mutant (P301L) human tau. B*rain Res*. 1247:159-70.

page 148:

To add: <u>Weller ML</u>, <u>Stone IM</u>, <u>Goss A</u>, <u>Rau T</u>, <u>Rova C</u>, <u>Poulsen DJ (2008)</u> Selective overexpression of excitatory amino acid transporter 2 (EAAT2) in astrocytes enhances neuroprotection from moderate but not severe hypoxia-ischemia. *Neuroscience*. 155(4):1204-11.